**University of Alberta**

# Interaction Buckling Failure of Stiffened Steel Plates

by

Chi Lui Emily Wang ©

A thesis submitted to the Faculty of Graduate Studies and Research in partial fulfilment of the requirements for the degree of Master of Science

in

Structural Engineering

Department of Civil and Environmental Engineering

Edmonton, Alberta

Fall 2005

Library and
Archives Canada

Published Heritage
Branch

395 Wellington Street
Ottawa ON K1A 0N4
Canada

Bibliothèque et
Archives Canada

Direction du
Patrimoine de l'édition

395, rue Wellington
Ottawa ON K1A 0N4
Canada

*Your file Votre référence*
*ISBN: 0-494-09308-0*
*Our file Notre référence*
*ISBN: 0-494-09308-0*

NOTICE:
The author has granted a non-exclusive license allowing Library and Archives Canada to reproduce, publish, archive, preserve, conserve, communicate to the public by telecommunication or on the Internet, loan, distribute and sell theses worldwide, for commercial or non-commercial purposes, in microform, paper, electronic and/or any other formats.

The author retains copyright ownership and moral rights in this thesis. Neither the thesis nor substantial extracts from it may be printed or otherwise reproduced without the author's permission.

AVIS:
L'auteur a accordé une licence non exclusive permettant à la Bibliothèque et Archives Canada de reproduire, publier, archiver, sauvegarder, conserver, transmettre au public par télécommunication ou par l'Internet, prêter, distribuer et vendre des thèses partout dans le monde, à des fins commerciales ou autres, sur support microforme, papier, électronique et/ou autres formats.

L'auteur conserve la propriété du droit d'auteur et des droits moraux qui protège cette thèse. Ni la thèse ni des extraits substantiels de celle-ci ne doivent être imprimés ou autrement reproduits sans son autorisation.

---

In compliance with the Canadian Privacy Act some supporting forms may have been removed from this thesis.

While these forms may be included in the document page count, their removal does not represent any loss of content from the thesis.

Conformément à la loi canadienne sur la protection de la vie privée, quelques formulaires secondaires ont été enlevés de cette thèse.

Bien que ces formulaires aient inclus dans la pagination, il n'y aura aucun contenu manquant.

Canada

# Abstract

The buckling behaviour of four full-scale stiffened plates with longitudinal T-stiffener was investigated experimentally and analytically. The specimens were designed according to the set of non-dimensional geometric parameters confirmed analytically to result in interaction buckling failure. The primary objective of this study was to achieve interaction buckling under uniaxial compression at different load eccentricities. Initial imperfections were measured for all specimens and longitudinal residual stresses were measured on a duplicate specimen. The tests confirmed the existence of interaction buckling.

The finite element model used in this study was validated by testing a series of full-scale stiffened plates. The numerical analysis indicated that the model was capable to predict the capacity and failure modes of the specimens.

An assessment on current DNV (Det Norske Veritas), API (American Petroleum Institute) and S136-01/S16-01 design guidelines predicted inconsistent buckling capacities for the test specimens. However, DNV predicted the failure mode of the specimens accurately.

# Acknowledgement

The financial support of the Natural Science and Engineering Research Council (NSERC) is gratefully acknowledged. Without the support of this institution, this research would not have been possible.

I would like to thank my supervisors Dr. G. Y. Grondin and Dr. A. E. Elwi for their guidance throughout this project. Thanks also to fellow graduate students Imtiaz Sheikh and Amy Yip for their guidance and assistance. I would also like to thank Richard Helfrich and Larry Burden of the I.F. Morrison Structural Laboratory for their much valued assistance.

Most importantly I would like to thank the Lord Jesus, in whom I trust, and my family and friends for their love and support. Thank you Kalvin for your unconditional love and patience. Special thanks to Aunt Estella, without her I will not be where I am now.

# Table of Contents

1. Introduction

1.1 General ........ 1
1.2 Statement of the Problem ........ 2
1.3 Objectives and Scope of Work ........ 3
1.4 Organization of Thesis ........ 4

2. Literature Review

2.1 Introduction ........ 6
2.2 Summary of Recent Studies by Sheikh, Grondin and Elwi (2000, 2001) ........ 7
2.3 Applications of Stiffened Steel Plate in Civil Engineering Structures ........ 13
  2.3.1 Stiffened Steel Plates in Box Girder Bridge ........ 13
  2.3.2 Columns and Piers ........ 15
  2.3.3 Cold-Formed Steel Members ........ 16
2.4 Initial Imperfections and Residual Stresses ........ 18
2.5 Experimental Investigations ........ 20
2.6 Numerical and Parametric Investigations ........ 25
2.7 Summary ........ 26

3. Experimental Program

3.1 Introduction ........ 33
3.2 Test Specimens ........ 33
  3.2.1 Test Specimen Selection Procedures ........ 34
  3.2.2 Preliminary Finite Element Analysis ........ 35
    3.2.2.1 Elements, Mesh and Initial Imperfections ........ 35
    3.2.2.2 Material Model ........ 36
    3.2.2.3 Residual Stresses ........ 37
    3.2.2.4 Boundary Conditions ........ 38
    3.2.2.5 Solution Strategy ........ 39
  3.2.3 Final Test Specimens ........ 40
3.3 Test Set-Up ........ 41
  3.3.1 End Supports ........ 42
  3.3.2 Lateral Restraints System ........ 43
  3.3.3 Instrumentation and Data Acquisition ........ 43
3.4 Testing Procedure ........ 44
3.5 Initial Imperfection Measurements ........ 45
  3.5.1 Plate and the Flange Imperfections ........ 46
  3.5.2 Web Imperfections ........ 47
3.6 Residual Stress Measurements ........ 47
  3.6.1 Measurement Technique ........ 47
  3.6.2 Preparation of Test Specimen ........ 48
3.7 Tension Coupon Tests ........ 49

4. Experimental Results
4.1 General ........ 73
4.2 Material Properties ........ 73
4.3 Initial Imperfections ........ 74
4.4 Residual Stresses ........ 75
4.5 Test Results ........ 75
4.5.1 Specimen SSP2 ........ 76
4.5.2 Specimen SSP3 ........ 77
4.5.3 Specimen SSP4 ........ 78
4.5.4 Specimen SSP1 ........ 79

5. Prediction of Test Results
5.1 General ........ 101
5.2 Finite Element Analysis ........ 101
5.2.1 Material Model ........ 101
5.2.2 Initial Imperfections and Residual Stresses ........ 102
5.2.3 Comparison between of Finite Element Analysis and Experimental Results ........ 102
5.2.4 Assessment of the Effect of Load Eccentricity ........ 105
5.3 Design Guidelines ........ 107
5.3.1 Det Norske Veritas DNV-RP-C201 (2002) ........ 107
5.3.2 American Petroleum Institute Bulletin 2V (2000) ........ 108
5.3.3 CSA S136-01 (2002)/S16-01 (2002) ........ 110
5.3.4 Comparison with Design Practice ........ 112

6. Summary, Conclusions and Recommendations
6.1 Summary ........ 128
6.2 Conclusions ........ 131
6.3 Recommendations ........ 133

List of References ........ 134

Appendix A - Ancillary Test Results ........ 142

Appendix B - Results of Initial Imperfection Measurements ........ 148

Appendix C - Experimental Strain Gauge Results ........ 161

Appendix D - Measured Displacements ........ 169

Appendix E - Summary and Recommendations of DNV-RP-C201, October 2002 ........ 175

# List of Tables

Table 2.1 Parameters Leading to Interaction Buckling Mode Observed by Sheikh *et al.* (2001) .......... 28

Table 2.2 Maximum Plate Imperfections and Compressive Residual Stresses .......... 29

Table 2.3 Maximum Imperfections in Stiffener for $\lambda_0^1 > 0.6$ .......... 29

Table 3.1 Trial Specimens and Corresponding β-Values .......... 51

Table 3.2 Material Properties for Preliminary Finite Element Model .......... 51

Table 3.3 Measured Dimensions of Test Specimens and Corresponding β-Values .......... 52

Table 3.4 Eccentricity of the Applied Axial Load .......... 53

Table 4.1 Material Properties .......... 81

Table 4.2 Summary of Measured Initial Imperfections .......... 82

Table 4.3 Comparison of Measured Initial Imperfections with the Classification Proposed by Smith *et al.* (1991) .......... 83

Table 4.4 Summary of Test Results .......... 83

Table 5.1 Comparison between Test Results and Finite Element Analysis Results .......... 114

Table 5.2 True Stresses and True Plastic Strains .......... 114

Table 5.3 Eccentricity Study on SSP2 and SSP4 .......... 115

Table 5.4 Comparison between Design Practice Predictions and Test Results .......... 116

Table A.1 Tension Coupon Test Results .......... 143

Table B.1 Measured Initial Imperfection Data for Specimen SSP1 .......... 150

Table B.2 Measured Initial Imperfection Data for Specimen SSP2 .......... 152

Table B.3 Measured Initial Imperfection Data for Specimen SSP3 .......... 154

Table B.4 Measured Initial Imperfection Data for Specimen SSP4 .......... 156

# List of Figures

Figure 1.1 Typical Buckling Modes ........................................ 5

Figure 2.1 Load Deformation Responses for Common Buckling Mode in Stiffened Steel Plates ........................................ 30

Figure 2.2 Typical Load versus Deformation Response for Interaction Buckling Failure and Stiffener Tripping Failure ........................................ 30

Figure 2.3 Observed Failure Modes under Uniaxial Compression of Sheikh *et al.* (2001) ........................................ 31

Figure 2.4 Typical Initial Imperfection-'Hungry Horse' Shape ........................................ 32

Figure 2.5 Typical Residual Stress Pattern in Stiffened Steel Plate with T Stiffener ........................................ 32

Figure 3.1 Stiffened Steel Plate Dimensions ........................................ 54

Figure 3.2 β-Values for Preliminary Analysis (Shaded Area) ........................................ 54

Figure 3.3 Typical Mesh ........................................ 55

Figure 3.4 Preliminary Analysis Load versus Deformation Response Curves ........................................ 56

Figure 3.5 Schematic of Test Setup ........................................ 57

Figure 3.6 Schematic of Boundary Conditions ........................................ 58

Figure 3.7 Top and Bottom Boundary Conditions ........................................ 59

Figure 3.8 Required Degrees of Freedom on a Finite Element Model ........................................ 60

Figure 3.9 Edge Restraint Apparatus ........................................ 61

Figure 3.10 Plate Edge Restraining System Demonstration ........................................ 62

Figure 3.11 Instrumentation ........................................ 63

Figure 3.12 Positions of Strain Gauges on Specimen SSP2 ........................................ 64

Figure 3.13 Support Structure for the Edge Restraints ........................................ 65

Figure 3.14 Layout of the Vertical Transducers for Initial Imperfections Measurement ........................................ 66

Figure 3.15 Measurement Setup for Flange and Plate Initial Imperfection ........................................ 67

Figure 3.16 Plexiglass Frame for Measuring Initial Imperfections in Web .......... 68
Figure 3.17 Location of Residual Stress Measurements .......... 69
Figure 3.18 Residual Stress Strips Layout .......... 70
Figure 3.19 Bam-Setzdehnungsmesser Mechanical Extensometer for Residual Stress Measurements .......... 71
Figure 3.20 Residual Stress Strips after Sectioning .......... 71
Figure 3.21 Material Coupon dimensions .......... 72
Figure 4.1 Typical Stress versus Strain Curve .......... 84
Figure 4.2 Stress versus Strain Curve for the 7.9 mm Plate .......... 84
Figure 4.3 Measured Initial Imperfections in SSP4 .......... 85
Figure 4.4 Residual Stresses in Specimen .......... 86
Figure 4.5 Out-of-plane Deformations of SSP2 Plate at Different Axial Displacements .......... 87
Figure 4.6 SSP2 After Stiffener Tripping .......... 88
Figure 4.7 Axial Load versus End Rotations for SSP2 .......... 89
Figure 4.8 Load versus Axial Deformation Curve for Specimen SSP2 .......... 89
Figure 4.9 Load versus Axial Deformation Curve for Specimen SSP3 .......... 90
Figure 4.10 Out-of-plane Deformations of SSP3 Plate at Different Axial Displacements .......... 91
Figure 4.11 Deformed Shape of SSP3 .......... 92
Figure 4.12 Axial Load versus End Rotations for SSP3 .......... 93
Figure 4.13 Load versus Axial Deformation Curve for Specimen SSP4 .......... 93
Figure 4.14 Out-of-plane Deformations of SSP4 Plate at Different Axial Displacements .......... 94
Figure 4.15 Deformed Shape of SSP4 .......... 95
Figure 4.16 Axial Load versus End Rotations for SSP4 .......... 96
Figure 4.17 Load versus Axial Deformation Curve for Specimen SSP1 .......... 96
Figure 4.18 Out-of-plane Deformations of SSP1 Plate at Different Axial Displacements .......... 97
Figure 4.19 (a) Deformed Shape of SSP1 during Testing .......... 98

Figure 4.19 (b) SSP1 after Testing .......................................... 99
Figure 4.20 Axial Load versus End Rotations for SSP1 .......................... 100
Figure 5.1 True Stress versus True Strain Curve for the 4.8 mm Plate ......... 117
Figure 5.2 Finite Element Mesh with Initial Imperfections of Test Specimen SSP4 .......................................................... 117
Figure 5.3 Residual Stresses in Specimen for Finite Element Analysis ......... 118
Figure 5.4 Deformed Shape of SSP1 at Various Stages of Loading ......... 119
Figure 5.5 Deformed Shape of SSP2 at Various Stages of Loading ......... 120
Figure 5.6 Deformed Shape of SSP3 at Various Stages of Loading ......... 121
Figure 5.7 Deformed Shape of SSP4 at Various Stages of Loading ......... 122
Figure 5.8 Axial Load versus Axial Deformation Curve for Specimen SSP1 .......................................................... 123
Figure 5.9 Axial Load versus Axial Deformation Curve for Specimen SSP2 .......................................................... 123
Figure 5.10 Axial Load versus Axial Deformation Curve for Specimen SSP3 .......................................................... 124
Figure 5.11 Axial Load versus Axial Deformation Curve for Specimen SSP4 .......................................................... 124
Figure 5.12 Deformed Shape of SSP2 at Various Stages of Loading (load applied at Centroid .......................................................... 125
Figure 5.13 Eccentricity Studies on Specimen SSP2 .............................. 126
Figure 5.14 Eccentricity Studies on Specimen SSP4 .............................. 126
Figure 5.15 Effective Width Comparisons between 1995 and 2002 Edition of DNV .......................................................... 127
Figure A.1 Stress versus Strain Curves for the 3.0 mm Plate .................... 144
Figure A.2 Stress versus Strain Curves for the 3.4 mm Plate .................... 144
Figure A.3 Stress versus Strain Curves for the 4.8 mm Plate .................... 145
Figure A.4 Stress versus Strain Curves for the 6.3 mm Plate .................... 145
Figure A.5 Stress versus Strain Curves for the 7.9 mm Plate .................... 146
Figure A.6 Stress versus Strain Curves for the 9.5 mm Plate .................... 146
Figure A.7 Stress versus Strain Curves for the 12.7 mm Plate .................. 147

Figure B.1 Measured Initial Imperfections in SSP1 .................................. 158
Figure B.2 Measured Initial Imperfections in SSP2 .................................. 159
Figure B.3 Measured Initial Imperfections in SSP3 .................................. 160
Figure C.1 Location of Strain Gauges on Test Specimen at Mid-span ......... 162
Figure C.2 Axial Load versus Strain Curve at Mid-span of SSP1 ......... 163
Figure C.3 Axial Load versus Strain Curve at Mid-span of SSP2 ......... 164
Figure C.4 Axial Load versus Strain Curve at Mid-span of SSP3 ......... 166
Figure C.5 Axial Load versus Strain Curve at Mid-span of SSP4 ......... 167
Figure D.1 Location of LVDT on Test Specimens .................................. 170
Figure D.2 Out-of-plane Deformations for the Plate in SSP1 ..................... 171
Figure D.3 Out-of-plane Deformations for the Plate in SSP2 ..................... 172
Figure D.4 Out-of-plane Deformations for the Plate in SSP3 ..................... 173
Figure D.5 Out-of-plane Deformations for the Plate in SSP4 ..................... 174

# List of Symbols

| | |
|---|---|
| $A_s$ | area of stiffener |
| $A_p$ | area of plate |
| $b$ | fictitious effective width or plate width |
| $b_p$ | width of stiffened steel plate taken as the stiffener spacing |
| $b_f$ | stiffener flange width |
| d | depth of section |
| $E$ | modulus of elasticity |
| $f_{cr}$ | elastic local buckling stress |
| $f_{max}$ | ultimate stress at edge of plate |
| $f_y$ | yield strength |
| $f_{yp}$ | yield strength of plate material |
| $f_{ys}$ | yield strength of stiffener material |
| $f_r$ | magnitude of the maximum compressive residual stress in the plate |
| $f_r$ | the residual stress |
| $h_w$ | stiffener web height |
| $k$ | buckling coefficient |
| L | length |
| $L_a$ | mean gauge length before sectioning |
| $L_b$ | mean gauge length after sectioning |
| $L_u$ | length of stiffened panel |
| $P_c$ | peak load capacity of the stiffened plate |
| $P_y$ | yield capacity of the stiffened plate |
| $M_a$ | applied bending moment |
| $M_p$ | plastic moment capacity of stiffened panel |
| $r_o$ | radius of gyration of the entire section |
| $r_z$ | torsional radius of gyration of stiffener about its centroid |
| $t$ | plate thickness |
| $t_f$ | stiffener flange thickness |
| $t_p$ | plate thickness |

| | |
|---|---|
| $t_w$ | stiffener web thickness |
| $T$ | fictitious temperature distribution |
| $U_1$ | axial shortening of the stiffened plate |
| $w$ | plate width |
| $\alpha_T$ | coefficient of thermal expansion. |
| $\beta$ | a coefficient |

$\beta_1 = \frac{b_p}{t_p}\sqrt{f_{yp}/E}$ = plate transverse slenderness

$\beta_2 = \frac{h_w}{t_w}\sqrt{f_{ys}/E}$ = stiffener web slenderness

$\beta_3 = \frac{b_f}{t_f}\sqrt{f_{ys}/E}$ = stiffener flange slenderness

$\beta_4 = \dfrac{\frac{L_u}{r_z}\sqrt{f_{ys}/E}}{\frac{b_p}{t_p}\sqrt{f_{yp}/E}}$ = ratio of torsional slenderness of stiffener to plate transverse slenderness

$\beta_5 = \frac{A_s}{A_p}$ = stiffener to plate area ratio

$\beta_6 = k * \beta_1^2$ = initial plate imperfections

$\beta_7 = \delta_s / L_u$ = initial stiffener imperfections

$\beta_8 = \frac{f_r}{f_{yp}}$ = residual stresses

$\beta_9 = \frac{M_a}{M_p}$ = applied to plastic moment ratio

$\beta_{10} = \frac{P_c}{P_y}$ = peak to yield load ratio

| | |
|---|---|
| $\beta_{11} = \dfrac{U_1}{L_u}$ | = axial shortening of stiffened panel |
| $\delta_p$ | maximum initial imperfection in the plate |
| $\delta_s$ | maximum initial imperfection in the stiffener |
| $\lambda_o$ | slenderness of stiffener |
| $\sigma_r/\sigma_{res}$ | residual stress magnitude |
| $\sigma_y$ | yield strength of material |
| $\nu$ | Poisson's ratio |

# 1 Introduction

## 1.1 General

Stiffened steel plate panels of ship structures are generally made of steel plates stiffened with parallel steel stiffeners that span between bulkheads. Therefore, the system is composed of repetitive panels with continuous longitudinal edge conditions. A representative panel consists of a stiffener and the tributary plate. The plate width is the distance in between centrelines of adjacent stiffeners. Aside from loading and end conditions, the aspect ratio of the panels and the stiffener and plate geometric and material properties are the other primary factors that control the behaviour of the system.

Stiffened steel plate panels have been widely used as primary components for many structural systems such as box-girders, aircraft, ships, and offshore structures. The simplicity in fabrication and their high strength-to-weight ratio make these stiffened plates attractive. Even though a stiffened steel panel represents only a small fraction of the total weight of a structure, it has substantial contribution to its strength and stability. In a box girder, the bottom flange is subjected to compressive stresses under the action of dead, live and erection loads above continuous supports. The deck and bottom shell of ship hulls experience bending compressive stresses due to sagging and hogging bending moments (Alagusundaramoorthy *et al.*, 1999). Under these loading conditions, four largely recognized forms of instabilities are found in stiffened plates (Murray, 1973; Bonello *et al.*, 1993; Hu, 1993; Grondin *et al.*, 1999; Sheikh *et al.*, 2000): plate induced overall buckling (PI), stiffener induced overall buckling (SI), stiffener tripping (ST) and plate buckling (PB).

Overall buckling is often referred to as 'Euler buckling' or 'Flexural buckling', can take the form of plate-induced or stiffener-induced failure. As demonstrated in Figure 1.1(a), plate-induced (PI) failure shows the panel deflecting away from the plate.

In stiffener-induced (SI) failure, shown in Figure 1.1(b), the panel deflects towards the plate, and is associated with yielding in compression in the flange of the stiffener.

Lateral torsional buckling of the stiffener (also called tripping) consists of twisting of the stiffener about its line of attachment with the plate, illustrated in Figure 1.1(c). This occurs when the stiffeners of a panel have high flexural rigidity and low torsional rigidity (Danielson *et al.*, 1990). Failure caused by stiffener tripping (ST) is more critical than plate buckling failure because it is associated with a sudden collapse. As observed by Louca and Harding (1996), one of the main aspects of tripping failure is the rapid drop in load capacity that occurs because of the loss of stiffener rigidity.

The local buckling of stiffened steel plates can either be plate buckling (PB) between the stiffeners or stiffeners buckling. The former results in a transfer of load onto the stiffeners; as a result the stiffeners may fail by flexural buckling. This failure mode may happen under in-plane loading only, distributed lateral loads alone or in combination with in-plane loading, i.e. under any loading condition. The resulting loss of effectiveness due to plate buckling is normally allowed for in design recommendations by the adoption of an effective width, assumed to act along with the stiffeners (Shanmugam and Archokiasamy, 1996). The finite element model shown in Figure 1.1(d) illustrates the plate buckling failure mode.

## 1.2 Statement of the Problem

Although the behaviour of stiffened steel plate has been studied over the past 30 years, some of the stability aspects are still not well understood. In a recent parametric study by Sheikh *et al.* (2001), a buckling failure mode consisting of interaction between plate buckling and overall buckling was observed under both axial compression and combined axial compression and bending but predominantly found in the former loading condition. Sheikh *et al.* (2001) identified a group of scale independent dimensionless variables (β) that describe the strength and behaviour of stiffened steel plates. These parameters are related to geometry, material properties and loading condition of the stiffened panel. Under the applied load, the specifically designed panels would fail in plate buckling followed by plate-induced overall buckling in the post-buckling regime. This failure behaviour showed an abrupt loss of load carrying capacity similar to that observed with stiffener tripping. Although this buckling behaviour is not documented in any other literatures, many have recognized the existence of combinations of buckling modes as listed in Section 1.1. The severity of the post-buckling behaviour is not recognized in design standards.

Because this behaviour was found through finite element analysis, many questions remain unanswered such as whether this form of behaviour really exists and how sensitive is it to changes in panel parameters. Thus, there is a need to conduct experiments to reveal the possible existence and the true nature of interaction buckling.

## 1.3 Objectives and Scope of Work

The primary objective of the work reported in the following is to experimentally verify the existence of interaction buckling in stiffened steel plate under uniaxial compression. In addition, there are a number of secondary objectives:

- to understand the nature of interaction buckling,
- to investigate the buckling and post-buckling strength of large scale test specimens,
- to investigate the sensitivity of specimens to eccentric loading conditions,
- to verify and compare the $\beta$-values of the test specimens with the proposed ranges in Sheikh *et al.* (2001),
- to assess the ability of the finite element method to predict the pre- and post-buckling strength and behaviour, and
- to review and evaluate current design guidelines.

In this research, the scope of work includes:

- design and preparation four geometrically different stiffened steel plate panels, with longitudinal T-stiffeners;
- measurement of initial imperfections and residual stresses in the test specimens;
- physical compression tests of four test specimens;

- finite element analysis with the actual dimensions, material properties, initial imperfections and residual stresses obtained from the test specimens, and
- assessment the current design practice.

In order to fully understand the phenomenon and to determine the causes of interaction buckling, it is necessary to examine the effect of geometric parameters of the panel on this particular failure mode. However, this is beyond the scope of this study.

## 1.4 Organization of Thesis

This thesis consists of six chapters. Chapter 2 presents a brief summary of the literature on both the experimental and analytical investigations of stiffened steel plates; emphasis is on the work of Sheikh *et al.* (2000, 2001) and references related to civil engineering structures. Chapter 3 describes the preliminary analysis used to design the test specimens, the test set up, the necessary instrumentation, and the test procedures as well as other supporting tests required for the completion of the testing program. A summary of the test results is presented in Chapter 4 along with observations made during testing. In Chapter 5, the results of the experimental program are compared with the predictions from the finite element analysis and a few current guidelines: Det Norske Veritas (DNV, 2002), American Petroleum Institute (API, 2000), and a combination of the North American Cold-formed Steel Specification CSA-S136-01 (2002) and Limit States Design of Steel Structures CSA-S16-01 (2001). Finally, conclusions are presented in Chapter 6, followed by recommendations for future tests.

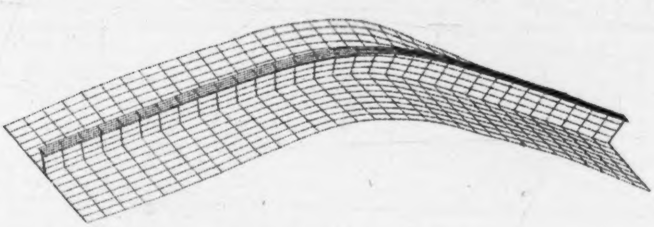

(a) Plate Induced Overall Buckling (PI)

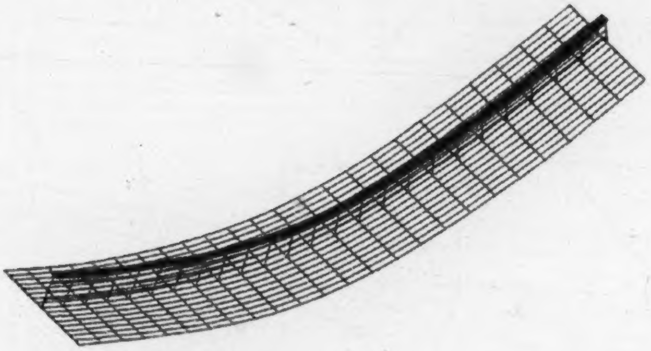

(b) Stiffener Induced Overall Buckling (SI)

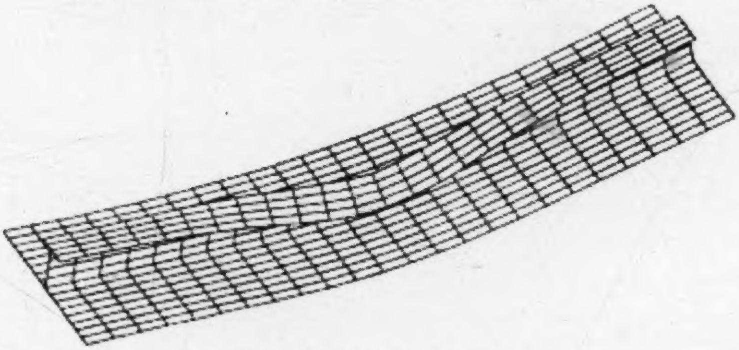

(c) Stiffener Tripping (ST)

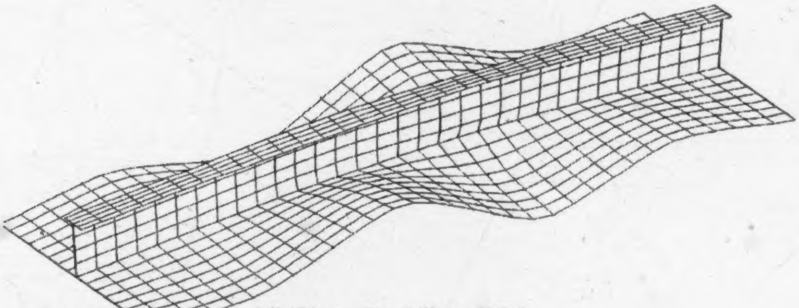

(d) Plate Buckling (PB)

Figure 1.1 Typical Buckling Modes

# 2 Literature Review

## 2.1 Introduction

According to Troitsky (1976), the development of stiffened steel plates was probably based on the observation of existing forms of nature. From an engineering point of view, manipulating the distribution of material in a structural member is the most efficient way to resist stress and deformation economically. The use of stiffened plates began in the nineteenth and early twentieth century, mainly in the construction of steel bridges, hulls of ships and aircraft applications.

In the last three decades, extensive experimental, numerical and statistical studies have been conducted on the buckling behaviour and ultimate load carrying capacity of stiffened steel plate panels with longitudinal stiffeners. Despite a large number of researchers involved, the behaviour of stiffened steel plates has only been investigated to a certain extent. The earlier research work concentrated on the buckling behaviour of stiffened steel plates under uniaxial compression (Murray, 1973; Ghavami, 1994). Recently, researchers have become interested in panels subjected to combined loading conditions, such as biaxial compressive loads, or combined in-plane compression and bending due to lateral pressure. As mentioned in the previous chapter, this study focuses on the specific aspects of the buckling and post-buckling behaviour of steel plate with longitudinal tee stiffeners under uniaxial compression.

Since the Canadian Standard Association CSA-S16-01 offers limited design guidance on the design of stiffened steel plates, designers opt for using other guidelines as design aid. The American Petroleum Institute (API) and Det Norske Veritas (DNV) are two of the well-developed design guidelines in North America and Europe. However, these guidelines are generally conservative. Comparisons of their predictions with analytical and experimental research results can be found in Balaz and Murray (1992), Ostapenko (1989), Grondin *et al.* (1999) and Sheikh *et al.* (2000).

The work of Sheikh *et al.* (2000, 2001) is summarized in the following. The chapter, then, reviews studies of stiffened steel plate employed in civil structures as well as the design approach of cold-formed steel members. Recent experimental studies and numerical analyses on stiffened steel plate are outlined at the end of this chapter. A detailed review of other literature is presented by Sheikh *et al.* (2001).

## 2.2 Summary of Recent Studies of Sheikh, Grondin and Elwi (2000, 2001)

In recent years an ongoing study of the buckling of stiffened steel plates has been underway at the University of Alberta. The study presented in this thesis is the most recent contribution and is a follow up on the numerical parametric study carried out by Sheikh *et al.* (2001) as part of that research program. The parametric study was performed on steel plates stiffened with tee-shape stiffener under two loading conditions: uniaxial compression, and combined uniaxial compression and bending to cause compression on the stiffener side of the plate. The authors used a finite element model proposed by Grondin *et al.* (1998). Taking advantage of the symmetry of stiffened plates, only one panel, i.e. a proportion of the plate of width $b_p$ with the stiffener centred on the plate strip, was modelled. Continuous boundary conditions along the plate longitudinal edges were provided. That finite element model was validated using the results of full-scale tests conducted by Murray (1973) and Grondin *et al.* (1998). The purpose of the Sheikh *et al.* (2001) study was to identify those parameters that may dominate the strength and modes of failure of stiffened steel plates (as noted in Section 1.1). The load versus deformation responses for the typical failure modes of stiffened steel plates are illustrated in Figure 2.1. Emphasis was placed on the conditions that would lead to the stiffener tripping failure. The study focused on the behaviour in the inelastic range of material response and the effect of plate–stiffener interaction.

Four types of parameters that characterised the behaviour of stiffened steel plates were investigated, namely, geometric properties, elastic properties as well as loading and deformation parameters. The primary physical parameters:

| | |
|---|---|
| $b_p$ | width of stiffened steel plate taken as the stiffener spacing |
| $t_p$ | plate thickness |

| | |
|---|---|
| $h_w$ | stiffener web height |
| $t_w$ | stiffener web thickness |
| $b_f$ | stiffener flange width |
| $t_f$ | stiffener flange thickness |
| $L_u$ | length of stiffened panel |
| $f_{yp}$ | yield strength of plate material |
| $f_{ys}$ | yield strength of stiffener material |
| $f_r$ | magnitude of the maximum compressive residual stress in the plate |
| $E$ | Modulus of elasticity |
| $\nu$ | Poisson's ratio |
| $\delta_p$ | maximum initial imperfection in the plate |
| $\delta_s$ | maximum initial imperfection in the stiffener |
| $U_l$ | axial shortening of the stiffened plate |
| $P_c$ | peak load capacity of the stiffened plate |
| $M_a$ | applied bending moment |

The authors identified a group of scale independent dimensionless variables. The parameters were validated by conducting a series of analyses where the scale of the specimen was changed without changing the value of the dimensionless parameters. The proposed dimensionless parameters are:

$$\beta_1 = \frac{b_p}{t_p}\sqrt{f_{yp}/E}$$ (Plate transverse slenderness);

$$\beta_2 = \frac{h_w}{t_w}\sqrt{f_{ys}/E}$$ (Stiffener web slenderness);

$$\beta_3 = \frac{b_f}{t_f}\sqrt{f_{ys}/E}$$ (Stiffener flange slenderness);

$$\beta_4 = \frac{\frac{L_u}{r_z}\sqrt{f_{ys}/E}}{\frac{b_p}{t_p}\sqrt{f_{yp}/E}}$$ (Ratio of torsional slenderness of stiffener to plate transverse slenderness, $\beta_1$)

$\beta_5 \quad = \quad \dfrac{A_s}{A_p}$ (Stiffener to plate area ratio);

$\beta_6 \quad = \quad k\,\beta_1^{\,2}$ (Initial plate imperfections);

$\beta_7 \quad = \quad \delta_s / L_u$ (Initial stiffener imperfections);

$\beta_8 \quad = \quad \dfrac{f_r}{f_{yp}}$ (Residual stresses);

$\beta_9 \quad = \quad \dfrac{M_a}{M_p}$ (Applied to plastic moment ratio);

$\beta_{10} \quad = \quad \dfrac{P_c}{P_y}$ (Peak to yield load ratio);

$\beta_{11} \quad = \quad \dfrac{U_1}{L_u}$ (Axial shortening of stiffened panel).

where $r_z$ is the torsional radius of gyration of a stiffener about its centroid, $A_s$ and $A_p$ are the cross sectional areas of stiffener and plate, respectively, $k$ is a constant that depends on severity of the initial imperfection magnitude in the plate, $M_p$ is the plastic moment capacity of a stiffened panel and $P_y$ is the yield capacity of the stiffened plate. The rest of the variables are defined earlier in this section.

The first nine parameters are input parameters while $\beta_{10}$ is an output and $\beta_{11}$ is a controlling parameter for monitoring the response of the stiffened plates. In order to further reduce the amount of finite element modelling, the authors restricted the ranges of $\beta_1$ to $\beta_5$ to values established from the findings of various researchers. The so-called "average" magnitude of initial imperfection proposed by Smith *et al.* (1991) was assigned to both the plate and stiffener components ($\beta_6 = 0.1\ \beta_1^2$ and $\beta_7 = 0.0015$). A residual stress pattern with a "severe" magnitude corresponding to $\beta_8 = 0.3$ was used in this investigation. The least stable stiffener geometric configuration (i.e. slender web and stocky flange) was investigated under two loading conditions, uniaxial compression ($\beta_9 = 0.0$) and combined uniaxial compression and bending ($\beta_9 = 0.2$), to ensure the failure outcome. The value of 0.2 corresponded to a bending moment equal to 20 % of the plastic moment capacity of the stiffened panel cross-section applied so as to increase the compressive stresses in the stiffener. The final input parametric matrix is shown below. Other values, not defined below, were also investigated to refine the boundaries between various buckling modes.

$$\begin{array}{ccccccccccccccccc}
\beta_1 & - & \beta_2 & - & \beta_3 & - & \beta_4 & - & \beta_5 & - & \beta_6 & - & \beta_7 & - & \beta_8 & - & \beta_9 \\
\begin{bmatrix}0.70\\1.28\\2.00\\2.70\end{bmatrix} & - & \begin{bmatrix}1.50\\1.05\\0.60\end{bmatrix} & - & \begin{bmatrix}1.125\\0.750\\0.375\end{bmatrix} & - & \begin{bmatrix}0.50\\1.00\\1.50\\2.00\end{bmatrix} & - & \begin{bmatrix}0.300\\0.150\\0.075\end{bmatrix} & - & (average) & - & (average) & - & (severe) & - & \begin{bmatrix}0.0\\0.2\end{bmatrix}
\end{array}$$

The above parametric matrix would require 864 analysis runs to perform a full factorial design. To further reduce the number of runs, $\beta_1$ and $\beta_4$ were selected as the primary parameters and the other geometric parameters were varied to study their effects. The selection of the primary parameters was based on their influence on buckling mode found from the literature review by Sheikh *et al.* (2001). Through finite element models, $\beta_1$ was found to be responsible for change of failure mode from plate buckling to overall buckling. And $\beta_4$ was found to be the primary parameter controlling the stiffener tripping failure mode.

Under the combined compression and bending case, stiffened steel plate were first loaded by a bending moment that caused the stiffener flange to go into flexural compression, followed by a gradual application of axial compression up to a nominal axial strain of 0.01. Three types of failure modes were observed: (1) predominately stiffener tripping, (2) several plate buckling, and (3) a few cases of interaction mode referred to as “dual failure mode” in the work of Sheikh *et al.* (2001).

The effect of $\beta_1$ and $\beta_4$ was again significant. The capacity of stiffened steel plate and failure mode were unaffected by a change in $\beta_2$, $\beta_3$ and $\beta_5$ values under the combined load case. However, it was found that with the same $\beta$–values, the failure mode shifted from overall buckling, and in some cases from plate buckling to stiffener tripping with the application of an initial bending moment to cause flexural compression in the stiffener flange. In addition, the strength of the specimens that failed by stiffener tripping decreased when subjected to the combined action of bending and axial compression. However, the strength of stiffened plates failing by plate buckling increased with the application of initial moments.

Of all the dimensionless parameters investigated, the plate transverse flexural slenderness ratio ($\beta_1$) was found to be the most dominant parameter affecting the strength and behaviour of stiffened steel plates for all failure modes. For torsionally stiff plates (small $\beta_4$), as $\beta_1$ increased, the ultimate strength decreased and the failure mode changed from plate-induced overall buckling to plate buckling. The post-buckling response became increasingly unstable as $\beta_1$ increased. The influence of $\beta_4$ and $\beta_5$ to the strength of the stiffened plate failing by either plate buckling or overall buckling was found to be negligible under uniaxial compression. A decrease in both the peak strength and post-buckling response for stiffener tripping and plate buckling failure modes was observed with a decrease in stiffener to plate area ratio.

Interaction buckling characterises a mode of failure that initiates with plate buckling then switches to plate-induced overall buckling in the post-buckling range. The interaction buckling response diagram was divided into four segments (see Figure 2.2.): an initial pre-buckling segment (OA), a first stable post-buckling segment (AB), an unstable post-buckling segment (BC) and a second stable post-buckling segment (CD). Plate buckling was observed at point A. The unstable post-buckling segment corresponds to the onset of plate induced overall buckling taking over plate buckling. It was also found that interaction buckling has a stable post-buckling phase (CD) at a load level significantly lower than the plate post-buckling stage because significant reduction in plate contribution to panel stiffness would have taken place during segment AB. Although the individual buckling modes involved in interaction buckling were considered stable failure behaviours, interaction buckling results in a rapid decrease in the load carrying capacity in the post-buckling regime.

Before the onset of plate buckling (point A), the compressive stresses in the stiffener are small. As deformations increase in the post-buckling range, the tensile stresses starts to develop in the stiffener; at point B, the onset of plate induced overall buckling occurs. The formation of a plastic hinge then develops at mid-length at point C. In the second stable post-buckling segment, the second buckling is characterized by the rotation of the plastic hinge.

According to Sheikh *et al.* (2001), the most critical condition for interaction buckling mode occurs when overall buckling overtakes inelastic plate buckling at, or immediately after, the peak load under uniaxial compression. This results in an axial load versus deformation response as catastrophic as that of a stiffener tripping failure. Material yielding was not found in this critical condition.

The authors reported that interaction buckling was affected primarily by the plate slenderness ratio ($\beta_1$), the stiffener to plate area ratio ($\beta_5$) and, to some extent, the ratio of stiffener torsional slenderness to plate transverse flexural slenderness ($\beta_4$). The possible dependency on $\beta_4$ could result from the fact that $\beta_4$ is increased by increasing the length of the stiffened plate panel, thus making the panel more susceptible to overall buckling. Figure 2.3 clearly shows that the interaction buckling mode is associated with higher values of $\beta_1$ and lower values of $\beta_5$. The failure mode shifted from plate buckling to interaction buckling with a decrease in stiffener to plate area ratio ($\beta_5$). A study of the effect of unloading cycle on interaction buckling response after the peak load showed that there was almost no difference in the load versus deformation response. Assessment of the sensitivity of stiffened steel plates to eccentricity was not studied. A detail list of $\beta$-values combinations at which interaction buckling was observed is shown in Table 2.1.

Sheikh *et al.* (2001) studied two design guidelines that offer the most comprehensive approach for the design of stiffened steel plates: API (1987) and DNV (1995). After comparing with the finite element analysis results, they found that the guidelines were unable to predict the same failure modes with any consistency for both uniaxial compression and combined compression and bending cases.

For the case of uniaxial compression, it was found that both guidelines predicted the strength of stiffened plates failing by plate-induced overall buckling and plate buckling modes reasonably accurately. The DNV guideline showed good accuracy in the prediction of the capacity of plate-induced overall buckling behaviour while the API guideline was unconservative in its prediction. Less accurate results were obtained from the DNV guideline in the prediction of the plate buckling capacity but the predictions from the API were mainly conservative. However, both guidelines had poor predictions for the interaction buckling failure mode under uniaxial compression and the combined load case. For stiffener tripping failure, the DNV guideline provided inconsistent and unconservative predictions whereas the API guideline seems to be more accurate but unreliable as reflected by a large standard deviation in the test-to-predicted values. It was suggested by Sheikh *et al.* that both guidelines needed to be improved.

## 2.3 Applications of Stiffened Steel Plate in Civil Engineering Structures

The aircraft industry concentrates on stiffened plates with lighter materials, such as aluminium. In contrast, most naval and structural applications employ relatively heavy steel plates and steel stiffeners. Nonetheless, most of the applications of stiffened plate are areas where high strength-to-weight ratio is important. Even though a stiffened steel panel represents only a small fraction of the total weight of structures such as box-girder bridges, ships, and marine structures, it has a substantial contribution to the strength and stability. During the 1970s, numerous investigations of the behaviour of stiffened plates were carried out in the context of box girder bridge applications. From the mid 1980s until now, studies of the behaviour of ship or offshore structural components has become more popular.

### 2.3.1 Stiffened Steel Plates in Box Girder Bridges

Steel box girder bridges gained acceptance worldwide because of their aesthetic advantages, efficient utilization of structural steel, suitability for curve alignment, resistance to corrosion and low maintenance (Lally and Wolchuk, 1976). In a steel box girder bridge, the bottom flange and webs are steel plates that may be stiffened or unstiffened, and the deck may be an orthotropic steel plate or a composite reinforced concrete slab. The high strength, but relatively lightweight, stiffeners provide the flexibility for the designer.

The collapse of box girder bridges during construction stimulated extensive research work on the behaviour of stiffened steel elements since the 1970s (Shanmugam and Arockiasamy, 1996). Since then, recommendations have been made as a result of the experimental and theoretical investigations for design and fabrication of these structural elements in bridges.

A typical box girder flange may encounter longitudinal stresses associated with overall bending moment and axial force in the box, in-plane flange plate shear stresses due partly to applied torsion, local bending stresses caused by wheel loading, and other in-plane transverse stresses caused by cross-sectional distortion of the box and in-plane bending of support diaphragms (Chatterhee and Dowling, 1976). As a result of the above loading conditions, three instability problems may arise: overall instability of the cross section, web buckling and compression flange buckling. The last instability situation is the most relevant to a stiffened plate subjected to uniform compression. In the negative moment regions of continuous steel box girder bridges the bottom flange plate is subjected to uniform compressive stresses due to the flexural component of loading as well as warping stresses caused by the distortional component of loading. According to ASCE and AASHTO (1971), if the flexural compressive stresses are increased by 10% to account for the warping stresses, the flange can be safely treated as a stiffened plate subjected to uniform compression.

In modern highway construction, bridge engineers are required to cope with an increasing demand for wider and longer-span superstructures. Introduced after the Second World War, orthotropic steel deck systems have been widely used to reduce the weight of the cross-sectional areas and the depth of the girders, which corresponds to a reduction of the number of main girders and a relatively cost-effective design (Roik, 1976; Chen and Yang, 2002).

The orthotropic bridge deck generally consists of flat, thin steel plate, stiffened by a series of closely spaced longitudinal stiffeners orthogonal to the floor beams (or transverse stiffeners). As the stiffeners and floor beams have uneven rigidity, elastic behaviour is different in each of these two directions. Because of the orthogonal physical difference as well as their difference in elastic properties between the stiffeners and floor beams, the whole system becomes known as orthotropic (Troitsky, 1968).

An orthotropic steel deck plate stiffened by welded longitudinal stiffeners is assumed to act as a flexural member under wheel loads. However, the deck plates in the positive moment areas of cable-stayed bridge and girder-type bridge are primarily subjected to flexural compressive stress under traffic load.

The longitudinal stiffeners are often designed with an open section, i.e. as rolled flats, bulb profiles, angles or tees. Thus, most of the tests on box girders cover such forms of longitudinal stiffeners. In recent investigations researchers have found that closed section stiffeners offer numerous advantages over the open sections from both structural and economic point of view (Roik, 1976; Chen and Yang, 2002). Because of their high torsional stiffness, closed section stiffeners elastically restrain the plate sub-panels, and hence boost the corresponding ultimate stress. In experimental tests on box girders with triangular stiffeners, Dubas (1976) demonstrated that closed-section stiffeners allow a greater spacing between the stiffeners due to their own width. In addition, their high bending stiffness allows a greater spacing of the transverse stiffeners accompanied by a corresponding reduction of the labour-intensive intersections. A slight increase in fabrication cost is involved because of the process of cold forming of the required section shape. In addition, the detailing of transverse joints for closed stiffeners is more complex than that for open section stiffeners. This usually requires an extra transition piece for the necessary adjustments. Chen and Yang (2002) examined the elastic behaviour of 30 full-scale orthotropic steel decks with U-shaped stiffeners under axial compressive force.

### 2.3.2 Columns and Piers

Stiffened steel plate can also be found in box-beams, structural columns and bridge piers. In columns and piers, the stiffened plates experience load excitation due to wind and/or seismic load. Steel bridge piers are usually perforated to allow accessibility for maintenance. However, the presence of manholes and door openings can substantially reduce the strength and ductility of a pier since the cross-sectional area is reduced and stresses may concentrate in its vicinity (Fujii, 2002). During an earthquake, a stiffened plate with a hole is not only subjected to cyclic axial forces when used as a flange, but also subjected to a combination of in-plane bending moments and shear forces when located in a web. In the Great Hanshin-Awaji Earthquake Disaster of 1995, local buckling at manholes triggered buckling failure in many steel bridge piers. Fujii (2002) carried out an analytical examination of the behaviour of a perforated stiffened plate subjected to cyclic axial forces.

### 2.3.3 Cold-Formed Steel Members

The design of cold-formed steel members provides some background information on the understanding of stiffened steel plate. Interaction buckling occurs with a combination of two failure modes. The stiffened steel plate first reaches plate buckling failure, a type of local buckling behaviour, and then fails by overall buckling. In the design of hot rolled structural members, local buckling is usually prevented by using stockier cross-sections or by using web stiffeners where necessary. The former approach limits the width to thickness ratio to certain values to prevent local buckling. In contrast, the design of cold-formed steel member considers the post-buckling strength as the design capacity instead of the stress at local buckling. In cold-formed steel structures, individual members are usually thin and their width-to-thickness ratios are usually large. These members usually buckle locally at a stress level lower than the yield strength of steel when they are subjected to axial compression. After local buckling, the plate undergoes a redistribution of stress, which allows the plate to carry additional compressive load. Sometimes, the member may have post-buckling strength several times larger than the initial local buckling stress. This is especially true for members with relatively large width-to-thickness ratios.

The post-buckling strength is determined by means of the effective width approach first introduced by Von Karman et *al.* (1932). Under uniaxial compression, a rectangular plate experiences uniform stress distribution prior to local buckling. The elastic local buckling stress can be obtained from:

$$f_{cr} = k\frac{\pi^2 E}{12\left(1-\nu^2\right)\left(w/t\right)^2} \tag{2-1}$$

where,

$E$ = Young's modulus

$\nu$ = Poisson's ratio

$w$ = plate width

$t$ = plate thickness

$k$ = plate buckling coefficient which depends on $L/w$ ratio, boundary conditions, and stress distribution.

After buckling, a portion of the buckling load at the centre strip transfers to the edge portion of the plate. As a result, a non-uniform stress distribution is developed. The redistribution of stress continues until the stress at the edge reaches the yield point of the steel and the plate begins to fail. Instead of considering the non-uniform distribution of stress over the entire width of the plate, the effective width approach assumes that the total load is carried only by a fictitious effective width, $b$, subjected to a uniformly distributed stress equal to the edge stress $f_{max}$. This ultimate stress, $f_{max}$, is usually taken as the yield strength, i.e., $f_{max} = f_y$. Replacing the buckling stress and the plate width with the yield strength and the effective width, respectively, Equation (2-1) becomes:

$$f_{\max} = f_y = k\frac{\pi^2 E}{12\left(1-\nu^2\right)\left(b/t\right)^2} \tag{2-2}$$

By rearranging the equation, the effective width $b$ can be defined as

$$b = \sqrt{\frac{\pi^2 E\, k\, t^2}{12\left(1-\nu^2\right) f_y}} \tag{2-3}$$

Depending on the boundary conditions, the buckling stresses vary. For the case of simply supported plate on all sides, k = 4 while for plate fixed along the unloaded edges and simply supported along the loaded edges k = 6.97 (Yu, 1990).

In hot-rolled steel structure design, the width to thickness ratio is limited to certain values to prevent local buckling. This is not true for most cold-formed sections. In contrast to column buckling, a buckled compressed plate has considerable reserve capacity, particularly if the buckling stress is low.

## 2.4 Initial Imperfections and Residual Stresses

Other than the geometry of the stiffened plate and the type of loading, the failure modes described in Section 1.2 depend heavily on factors that may or may not be controllable by the designer. They are the initial imperfections and residual stresses arising from the welding process, as well as damage and corrosion sustained during normal and/or abnormal operating conditions. The latter will not be addressed here since they are highly dependent on many unpredictable variables such as sudden impacts or incidental changes in surrounding environment.

Extensive statistical analysis of actual measurements of the magnitude and distribution of post-welding distortions and residual stresses of stiffened steel plates were conducted by Faulker (1976), Carlsen and Czujko (1978), and Smith *et al.* (1991). Carlsen and Czujko observed a typical 'hungry horse' shape of initial imperfection in full-scale stiffened plate panels (Figure 2.4) with the plate on the compression side and a half-sine wave along the width of the panel. This typical shape was found to have the same load-deflection curve with initial imperfection patterns of three half-sine waves along the length of the plate and a half-sine wave across the width of the panel. They also found that the distribution of initial imperfection could affect the strength of the stiffened plate as well as its buckling mode. The typical 'hungry horse' shape was also found by Smith *et al.* (1991) to be the dominant initial imperfection distribution in their study.

Smith *et al.* (1991) proposed three levels of initial imperfections and residual stresses, namely, average, slight and severe, corresponding to the mean, 3 percentile and 97 percentile values of maximum post-welding distortion. The magnitude of each group, tabulated in Table 2.2 and Table 2.3, was obtained from a survey of as-built stiffened plates. The distortion magnitudes in the plate were found to be proportional to the square root of plate transverse flexural slenderness, $\beta_1$ ($\beta_1 = \frac{b_p}{t_p}\sqrt{f_{yp}/E}$ , where $b_p$, $t_p$, $f_y$ and $E$ are as defined above). The range on the maximum imperfections in stiffener is listed in Table 2.2, where $\lambda_0$ denotes as the slenderness of stiffener acting with its associated plating. In contrast, a linear relationship was proposed by Carlsen and Czujko.

Faulkner (1976) examined the statistical variation of residual welding stresses and the strength data for a wide range of slenderness on nominally identical models. Residual stress patterns were as expected with low compression stresses in the plate regions away from the stiffeners and high tensile stresses near the plate-stiffener junction. The presence of residual stresses was found to reduce the compressive strength by as much as 20 %. He recognised that both overall buckling mode and stiffener tripping mode can involve a complicated interaction with plate buckling actions.

Grondin *et al.* (1998) studied the magnitude and distribution of the longitudinal residual stresses resulting from welding of the stiffener to the plate. A typical residual stress distribution pattern is proposed in Figure 2.5 from the measurement of full-scale stiffened plates. This pattern agrees with the description proposed by Faulkner. High tensile stresses approaching the yield strength of the material were measured near the weld between the plate and the stiffener. Compressive stresses that were less than 20 % of the yield strength were measured near the free edges of the plate and at the stiffener flange-web junction. Compressive stresses of less than 30 % of the yield strength were measured in the rest of the section. In the parametric study of Grondin *et al.* (1999), the magnitude and distribution of initial imperfections were found to have a significant influence on the capacity of stiffened plates failing by plate buckling but minimal effect on overall buckling failure. Residual stresses were also found to have a significant influence on the strength of stiffened plates that failed by plate buckling. Moreover, the stiffened plate strength was found to be reduced in direct proportion to the magnitude of the applied compressive residual stresses in the plate for plate slenderness, $\beta$ (same definition as the above), of values greater than 1.7. However, when yielding set in before buckling, the effect of compressive residual stresses gradually diminished.

Most earlier analytical studies and design methods considered the influence of initial imperfections for the plating between stiffeners, but only a few included the initial imperfection effects for the stiffener. Based on the approximate relationships established by Grondin *et al.*, initial imperfections and residual stresses should be incorporated in finite element models in order to truly understand the buckling and post-buckling strengths of stiffened plates.

## 2.5 Experimental Investigations

Over five decades a large body of experimental evidence has accumulated on the elastic behaviour of small scale-aeronautic quality stiffened plates. Full-scale experimental studies of stiffened steel plate fabricated from hot rolled steel plate are relatively scarce. With the help of computational models, researcher can study the buckling and post-buckling behaviour of stiffened steel plates up to failure. The results are then compared with the experimental results, and reasonable agreements are obtained in most of these studies. Hence, many of the analytical studies adopt the experimental work of others to verify their finite element models or design equations.

The test programs by Murray (1973), Ghavami (1994), Hu *et al.* (1997) and Pan and Louca (1999) are some of the experimental studies that were used by others to verify their finite element models. Full-scale stiffened steel panels were tested under uniaxial compression, and under combined compression and bending. Two failure modes were observed in all these studies: stiffener tripping and plate buckling. Detailed literature reviews of these studies are presented in Sheikh *et al.* (2001). Pan and Louca (1999) also investigated the response of stiffened panel with bulb flat type stiffener. Murray, and Pan and Louca did not measure the actual residual stresses and initial imperfections in their test programs.

Faulkner (1976) studied the ultimate strength of 65 longitudinally stiffened, approximately 1/6 to 1/4 scale of mild steel ship panels, under uniaxial compression. The plate thickness and stiffener slenderness parameters of the specimens ranged from 20 to 120. Except for two specimens, all specimens incorporated five stiffeners. The stiffeners were mostly T-shaped stiffeners with some flat bars. The specimens were simply supported on the loaded edges and free along the unloaded edges. Several panels were loaded eccentrically at one-third of the distance between the centroid and the equal area axis, away from the former. This was an attempt to account for the shift of neutral axis caused by progressive yielding of the cross-section. Most specimens were loaded at the initial neutral axis. Two primary modes of failure were observed, namely, overall buckling (both plate induced and stiffener induced) and stiffener tripping. However, the most common failure mode was overall buckling triggered by inelastic plate buckling. The author did not report any axial load versus overall deformation response and only some of the failure modes of the specimens were reported. Faulkner only measured the maximum initial imperfection of the plate and the stiffener.

Shanmugam and Arockiasamy (1996) conducted experimental and analytical investigations of the behaviour and ultimate strength of stiffened plates under the combined action of lateral and in-plane load. A series of 10 stiffened plate specimens with two different plate slenderness ratios (b/t = 65 and 101) were tested to failure under different lateral and in-plane load combinations. Each panel consisted of a base plate, four longitudinal stiffeners and three transverse stiffeners with thick end plates attached. They were fabricated from mild-steel sheets of different thicknesses. All component plates were hydraulically shear-cut to the required dimensions. Relatively large values of plate slenderness were chosen for the base plate and stiffeners were kept stocky in order to avoid the premature failure of stiffeners and to ensure initiation of the failure by local buckling of base plates. Simply supported on all sides, the specimens were subjected to a predetermined level of in-plane load, which was maintained constant, and then to a gradually increasing lateral load until failure. Each specimen was analysed using an elasto-plastic finite element model to determine the ultimate load-carrying capacity and the analysis results were compared to those obtained experimentally. In addition, some large-scale specimens of stiffened plates reported by Shanmugam and Arockiasamy (1996) were also analysed numerically. No initial imperfection measurements were reported for the test specimens. Imperfection corresponding to b/1000, b being the panel width between the stiffeners of the test specimens, was assumed to allow for the possible imperfection due to out-of-straightness and welding.

Grondin *et al.* (1998) carried out large-scale tests on twelve identical single stiffened steel plate specimens under axial compression and combined compression and lateral loads. Each specimen was 2000 mm long and consisted of a 500 x 10 mm plate stiffened with a WT 125 x 12.5 stiffener.

The specimens were all fitted with welded end plates and were loaded through a half cylindrical bearing. This loaded edge configuration was proven to be sufficient and reliable by a preliminary finite element analysis. Considerable attention was given to the unloaded edges boundary restraint in a preliminary finite element analysis because they only tested single stiffened steel plate specimens. The unloaded edge boundary restraints were designed to simulate the continuous support in a continuous stiffened steel plate panel. The specimens were loaded under three conditions. The first group was tested in various configurations under lateral loads and axial loads. The second group was initially loaded with a lateral load sufficient to impose permanent deformations in the plate then unloaded and reloaded with an axial load. The last group of test specimens consisted of plates damaged by removing parts of the web or flanges at the mid-span to simulate corrosion and then tested under axial load.

These analyses examined the behaviour of a stiffened plate for three different conditions of restraint at the longitudinal edge: fully-restrained, totally unrestrained and a model with varying discrete restraints along each unloaded edge. The authors found that under axial compression there was no difference in the stiffened plate behaviour when at least five discrete point restraints were provided and the stiffener flange was initially in compression. However, when the stiffener flange was initially in tension, the behaviour in the region of the peak load softened and the ultimate load value dropped if the boundary condition were anything less than the continuous restraint. The authors concluded that five discrete rotational restraints were sufficient to simulate the continuous boundary condition along the unloaded edges.

The longitudinal restraints along the unloaded edge were custom built to provide freedom only to the longitudinal displacement, lateral out-of-plane displacement and out-of-plane flexural rotation. This restraint system will be described in details in Chapter 3.

Initial imperfections were reported for all the specimens. An additional specimen was fabricated for the residual stresses measurement. The method of sectioning was used to measure the residual stresses for one complete cross-section and for three partial cross-sections. The measured residual stresses distribution is described in Figure 2.5. All specimens, except one of the damaged specimen, exhibited one of two basic buckling failure modes, plate buckling or stiffener tripping.

Alagusundaramoorthy *et al.* (1999) experimentally investigated the effect of different cutouts as well as reinforcement around cutouts on the collapse capacity of stiffened panels. Eighteen stiffened steel plates with simply supported boundary conditions were tested up to collapse under uniaxial compression. Each stiffened panel was composed of four longitudinal flat bar stiffeners, with thickness of 4 mm or 5 mm. The specimens were divided into four categories: six panels without any cutout in the plate, six panels with a square cutout, four panels with a rectangular cutout, and two panels with a reinforced rectangular cutout. Initial geometric imperfections of the plate, stiffener and overall panel were measured for all specimens before testing. During the tests, overall axial deformations, out-of-plane deflections and strains along the midsection of the panels were monitored.

The specimens failed either by plate-induced overall buckling or stiffener-induced overall buckling. It was found that the presence of cutouts significantly reduced the panel's strength by 20 % to 46 %, especially for the case of rectangular cutouts. With the reinforcement around the rectangular cutout, the panel had appreciable increase in strength, especially for plate initiated failure, but less for stiffener initiated failure. In the case of stiffener-induced failure, one of the stiffeners first failed by stiffener yielding, which started to shed load to the adjacent stiffeners. This trigged progressive failure of adjacent stiffeners and resulted in a very sudden collapse of the specimen.

Budweg and Shin (1987) investigated experimentally the static and dynamic responses of a specifically designed aluminium stiffened flat plate subjected to hydrostatic pressure and underwater shock. They studied the tripping failure of a rectangular flat plate stiffened by a machined longitudinal narrow-flanged T-stiffener. In the static test, only strain and deflection data were collected as the water pressure increased from 0 kPa to 2410 kPa. The specimen was loaded up to a deflection of four times the plate thickness where it experienced elastic tripping. It was noted that a deflection of more than four times the plate thickness would be required to initiate inelastic tripping in the specimen. The dynamic part of the experimental program simulated and captured the response of the stiffened plate of a submarine under the detonation of an explosive charge (UNDerwater Explosion, UNDEX, shock responses). The test panel was securely bolted into an air-back chamber with the stiffener in contact with the water pressure. To simulate an underwater explosion, steel cables were used to suspend the entire set up under water. In the test, three-quarters of the test plate was blown away from the test panel. The specimen underwent initial stage of inelastic tripping of the stiffener, which was at a point before the collapse of the stiffener. Because the stiffener only experienced the initial stage of inelastic tripping, only the web was observed to begin buckling at the point of the attachment to the flange but the stiffener remained vertical, i.e. the stiffener had not rotated out of the vertical plane, and no total collapse of the stiffener was observed. Nevertheless, extreme deformation of up to seven plate thicknesses was recorded.

Zha and Moan (2001) investigated the ultimate strength of twenty-five aluminium plates with flat bar stiffeners that failed by a torsional buckling. The paper included experimental results, finite element modelling and comparison with codes. The study accounted for residual stresses and initial imperfections as well as the deterioration of mechanical strength in the heat-affected zones (HAZ). The aluminium alloy stiffened panels included various heights of flat bar and various thicknesses of plate and stiffener. The stiffened panels were simply supported along the loaded edges while free along the others. Most panels failed by stiffener tripping when the compressive axial load reached beyond 60 % to 70 % of their ultimate loads. Only two specimens failed by interaction of torsional buckling of stiffeners with local buckling of the plate panel.

### 2.6 Numerical and Parametric Investigations

Common analytical work involves complicated theoretical equations or numerical parametric studies. The studies on closed form analysis and design equations are beyond the scope of this study. Numerical parametric studies can be divided into two techniques, namely, the finite difference method and the finite element method. Again, much of this work (Hu, 1993; Grondin *et al.*, 1999, and Pan and Louca, 1999) is described by Sheikh *et al.* (2001). Therefore, only a few studies outside of their review are described below.

Ostapenko and Chu (1986) conducted a study on stiffener tripping of stiffened plates with symmetrical stiffeners and asymmetrical stiffeners under axial compression and end moments. They compared the test results from Smith (1975) (tee stiffener) and Horne (1976) (angle stiffener) with a number of approaches. For the former test, the Adamchak method was found to give better estimate of the tripping stress because it considered the effect of the plate restraint varying along the member. The General Dynamics Design Guidelines gave realistic results with a faster and simpler approach. The Faulkner interim solution, however, was unconservative, since its upper limit in predicting the tripping stress is arbitrarily assigned. For the angle stiffener tests, the Guidelines did not consider the length of the stiffener and was only valid when the slenderness ratio of the column was low. The Argyris method, an iteration approach to determine the minimum critical load, provided fairly accurate predictions.

Continuing the above research, Ostapenko (1989) investigated the tripping behaviour and strength of asymmetrical plate stiffeners. Two neighbouring stiffeners were considered as a typical unit from a wide stiffened plate. The analytical study, using differential equations or energy formulation, involved the use of ten deformation functions, three per stiffener and four for the plate. Distortion of the stiffener cross-section, initial imperfections and buckling of the plate were considered but not the effect of residual stresses and large deformation. An effective plate width was used to account for the post-buckling strength of the plate. The stiffened plate was analysed under three different load cases: axial load, and combination of axial load with lateral loading towards the plate or towards the stiffener.

A comparison was made between the strengths of tee and angle stiffeners when they had flanges of the same size. Under axial compression, an angle stiffener was observed to resist tripping better than a tee stiffener when the slenderness ratio ($L/r_o$) was in a lower range. With increasing slenderness ratio, the situation reversed, the overall axial strength of panels with tee stiffeners became higher than that of panels with angle stiffeners. In the elastic range, plate buckling and overall buckling were the predominant buckling modes for asymmetrical stiffeners. Ostapenko reports that the buckling mode was affected by the plate slenderness ratio (b/t), slenderness ratio of the entire section ($L/r_o$) and the stiffener depth to plate width ratio (d/b). A sequential combination of all or some of the buckling modes in Section 1.2 was observed. For the asymmetrical section under axial compression, the overall buckling mode involved the interaction of the tripping and the overall buckling modes.

Under load combinations, lateral loading was found to have an insignificant effect on the tripping strength for symmetrical (tee) stiffeners but it had an adverse effect on angle stiffeners due to bi-axial bending. Depending on the direction of the applied lateral load, the stiffener swayed in different directions. For transverse loading towards the plate, the stiffener tended to rotate counter-clockwise whereas loading towards the stiffener caused the stiffener to rotate clockwise. Furthermore, the ultimate capacity gradually decreased with an increasing imperfection.

## 2.7 Summary

The buckling and post-buckling behaviour under axial compression and combined load cases on stiffened steel plates have been studied experimentally, numerically and statistically. Full-scale experimentation is scarcely found because of the difficulties associated with such tests. The stiffened plate geometry is generally found to be the primary governing factor for the buckling strength and failure mode. Many researchers accounted for the effect of post-welding distortions since they could lower the strength and could alter the failure mode of stiffened plates. A few measurement surveys have been conducted on the initial imperfections and residual stresses of stiffened plate. Thus, measurement on these post-welding distortions can broaden the data and validate the relationships proposed by Carlsen and Czujko (1978) and Smith *et al.* (1991). Among the work reviewed above, only Faulkner (1976) and Ostapenko and Chu (1986) have discussed the concurrent or sequential combinations of different buckling modes.

Most importantly, only Sheikh *et al.* (2002) have revealed the interaction buckling behaviour predominantly under axial compression, characterized by plate buckling overtaken by plate-induced overall buckling. The abrupt collapse behaviour of interaction buckling similar to that of stiffener tripping has raised concerns. Because of the lack of experimental work as well as many unknowns related to interaction buckling failure, this literature review concludes that there is a need for additional experimental work to investigate the post-buckling behaviour of stiffened steel plates failing by interaction buckling.

Table 2.1 Parameters Leading to Interaction Buckling Mode Observed by Sheikh *et al.* (2001)

| **Uniaxial Compression ($\beta_2 = 1.500$, $\beta_3 = 0.375$, $\beta_9 = 0.0$)** | | |
|---|---|---|
| $\beta_5$ | $\beta_1$ | $\beta_4$ |
| 0.30 | 2.70 | 1.50 |
| | | 2.00 |
| 0.15 | 1.28 | 1.50 |
| | | 2.00 |
| | 2.00 | 1.00 |
| | | 1.50 |
| | | 2.00 |
| | 2.70 | 1.00 |
| | | 1.50 |
| | | 2.00 |
| 0.075 | 1.28 | 1.00 |
| | | 1.50 |
| | | 2.00 |
| | 2.00 | 0.50 |
| | | 1.00 |
| | | 1.50 |
| | | 2.00 |
| | 2.70 | 0.50 |
| | | 1.00 |
| | | 1.50 |
| | | 2.00 |
| **Combined Compression and Bending ($\beta_2 = 0.60$, $\beta_3 = 0.75$, $\beta_9 = 0.2$)** | | |
| $\beta_5$ | $\beta_1$ | $\beta_4$ |
| 0.15 | 2.00 | 1.00 |
| | 2.70 | 1.00 |
| 0.075 | 2.00 | 1.00 |
| | 2.70 | 1.00 |

Table 2.2 Maximum Plate Imperfections and Compressive Residual Stresses

(Source: Smith *et al*., 1991)

| **Level** | **Maximum Initial Imperfection in Plate ($\frac{\delta_{p\max}}{t_p}$)** | **Residual Compressive Stresses in Plate ($\frac{\sigma_{res}}{\sigma_y}$)** |
|---|---|---|
| **Slight** | $0.025\beta_1^2$ | 0.05 |
| **Average** | $0.1\ \beta_1^2$ | 0.15 |
| **Severe** | $0.3\ \beta_1^2$ | 0.3 |

Table 2.3 Maximum Imperfections in Stiffener for $\lambda_0^1 > 0.6$

(Source: Smith *et al*., 1991)

| **Level** | **Maximum Initial Imperfection in Stiffener ($\frac{\delta_{s\max}}{l_u}$)** |
|---|---|
| **Slight** | 0.00025 |
| **Average** | 0.0015 |
| **Severe** | 0.0046 |

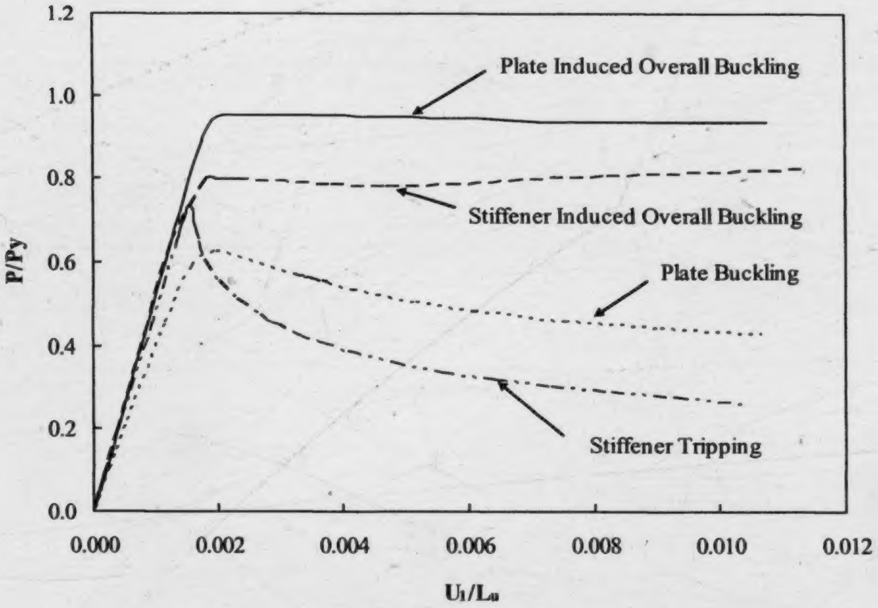

Figure 2.1 Load Deformation Responses for Common Buckling Mode in Stiffened Steel Plates (Source: Sheikh *et al.*, 2001)

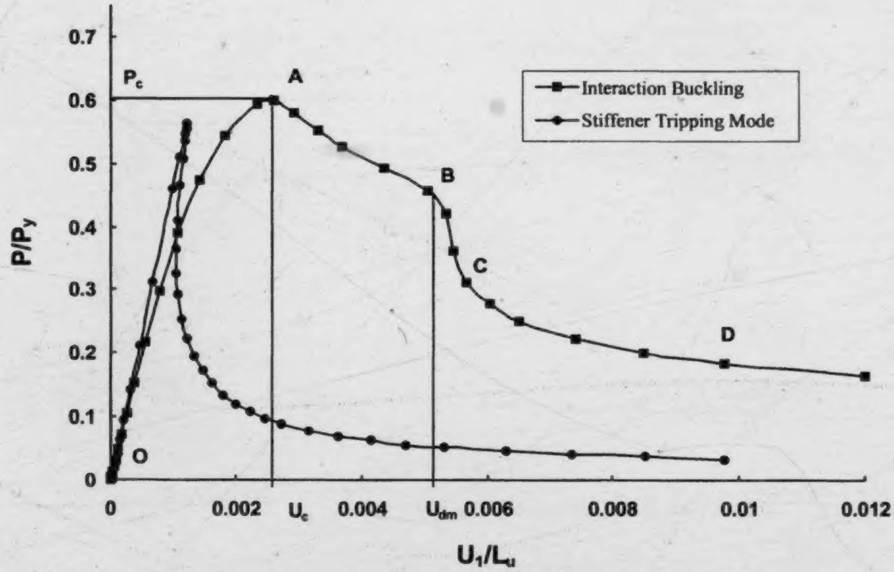

Figure 2.2 Typical Load versus Deformation Response for Interaction Buckling Failure and Stiffener Tripping Failure (Source: Sheikh *et al.*, 2001)

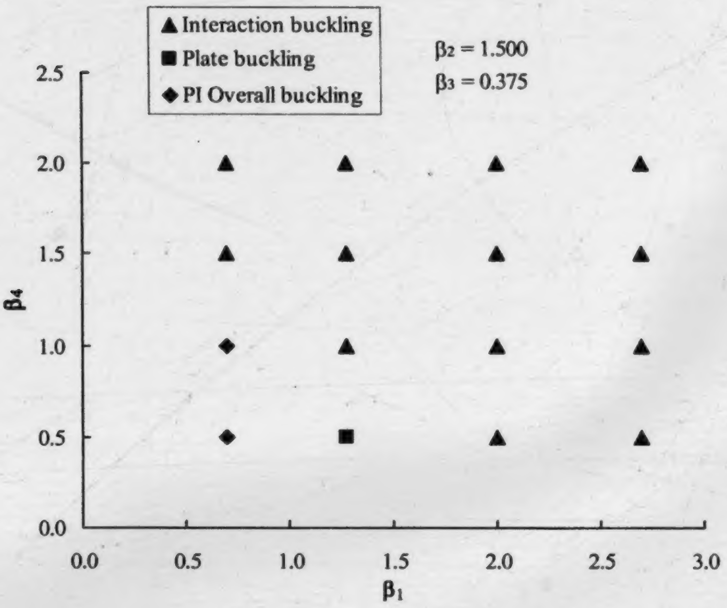

(a) $\beta_5 = 0.075$

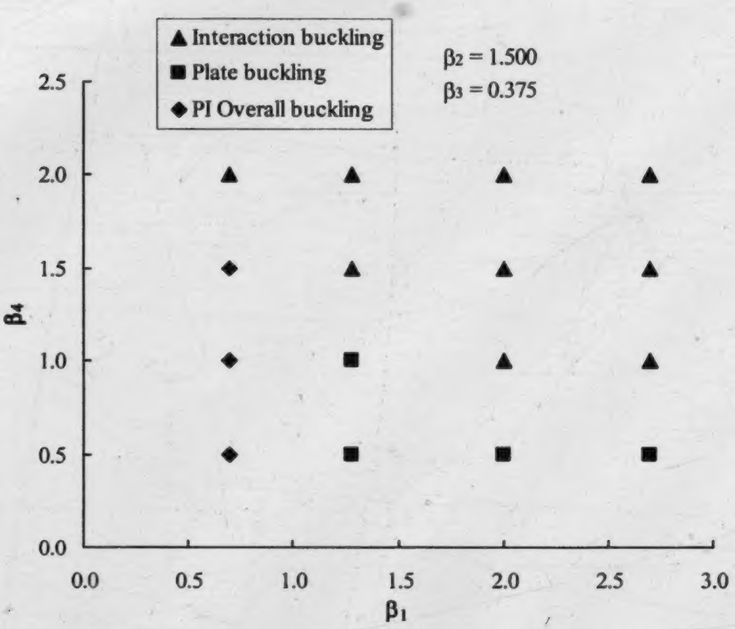

(b) $\beta_5 = 0.150$

**Figure 2.3 Observed Failure Modes under Uniaxial Compression of Sheikh *et al.* (2001)**

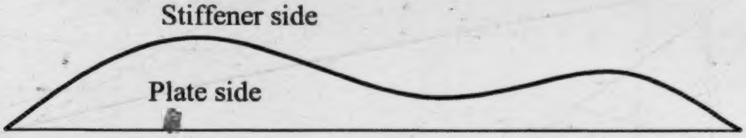
Stiffener side
Plate side

Figure 2.4 Typical Initial Imperfection-'Hungry Horse' Shape (Source: Carlsen and Czujko, 1978)

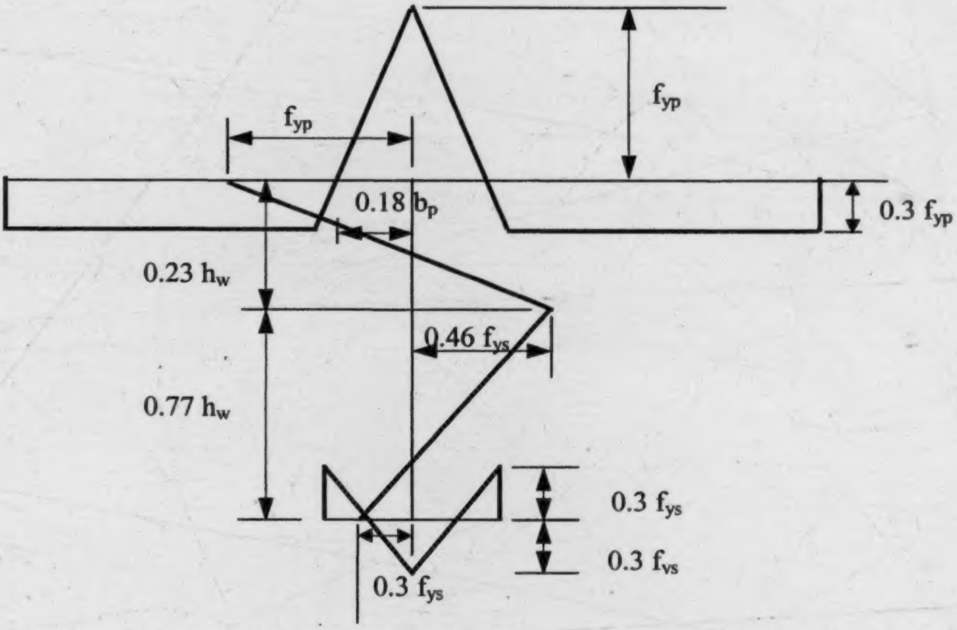
$f_{yp}$
$f_{yp}$
0.18 $b_p$
0.3 $f_{yp}$
0.23 $h_w$
0.46 $f_{ys}$
0.77 $h_w$
0.3 $f_{ys}$
0.3 $f_{ys}$
0.3 $f_{ys}$

Figure 2.5 Typical Residual Stress Pattern in Stiffened Steel Plate with T Stiffener (Source: Grondin *et al.*, 1999 and Sheikh *et al.*, 2001)

# 3 Experimental Program

## 3.1 Introduction

The purpose of the experimental program was to verify the existence of interaction buckling in steel plates stiffened with tee stiffeners and loaded in uniaxial compression. This test program focused on the buckling sequence and the effect of load eccentricity on the failure mode. The buckling capacity and the post-buckling behaviour and capacity were observed and recorded for each specimen.

A review of the literature indicated that, other than for geometric parameters, initial imperfections and residual stresses are the two primary factors that affect the failure behaviour of stiffened steel plates. Therefore, initial imperfections and residual stresses were measured. The mechanical material properties of each specimen were also determined from tension coupon tests. These ancillary tests enabled comparison between the results from the experiment, the finite element analysis and the predictions from common design guides.

## 3.2 Test Specimens

Five stiffened steel plate specimens were fabricated by a local steel fabricator using standard fabrication procedures. As mentioned in Chapter 2, there is a wide range of stiffened steel plate specimens reported in the literature, from a single stiffened steel plate to a full panel with up to five stiffeners. However, the differences are insignificant as long as adequate boundary conditions are implemented (Grondin *et al.* 1999). Therefore, this experimental program tested only a single stiffened steel plate element to reduce the size of the specimens as well as the cost of fabrication. The stiffened steel plate test program consisted of four simple stiffened plates with different dimensions. An extra specimen (SSP1) was duplicated for the residual stresses measurement. Similar to the specimens used in Grondin *et al.* (1998), steel plates stiffened with T-shape stiffeners were fabricated for this investigation; except that these stiffeners were composed of two flat plates welded together instead of a single hot rolled WT section. This was required in order to satisfy the proposed β-value combinations by Sheikh *et al.* (2001) for the study of interaction buckling behaviour and its post-buckling behaviour.

The nomenclature and dimensions of each component of the test specimens are illustrated in Figure 3.1. These components are denoted as flange (top flange), web, and plate (bottom flange).

### 3.2.1 Test Specimen Selection Procedures

A typical configuration of a stiffened steel plate panel consists of a flat plate with equally spaced longitudinal stiffeners spanning between girders or floor beams. In order to test only one bay of the stiffened panel, namely a portion of the plate width $b_p$ with a stiffener centred on the plate strip, a boundary condition was applied along the unloaded edges to simulate a continuous assembly of these stiffened plate panels and to take advantage of its symmetry. As discussed in the literature review, Grondin *et al.* (1998) have successfully designed a boundary restraint system that can simulate the boundary conditions in a single panel of a multi-panel stiffened steel plate. Therefore, this restraint system was selected for this testing program. The unloaded edge boundary restraint system consists of five discrete restraints that prevent rotation about the edge of the test specimens but allow out-of-plane displacements and rotation about the transverse axis. In order to use this existing restraint system, the length and the plate thickness of the test specimens were restricted within the system allowance. To simplify the specimen selection, the test specimens were 2000 mm long, similar to the specimens tested by Grondin *et al.* (1998). Although the test specimens of Grondin *et al.* (1998) had a plate thickness of 10 mm, the maximum nominal plate thickness that the clamp could physically accommodate was 12.7 mm. Thus, the nominal plate thicknesses of 10 mm and 12.7 mm were selected for determining the possible specimen cross-sections.

Assuming the mechanical properties of all the specimen components were identical, the geometry of the specimen would be the primary factor controlling the β-values. In order to study the interaction buckling behaviour, the geometries of the test specimens were developed from β-values that fall within the range of β-values proposed by Sheikh *et al.* (2001), as detailed in Section 2.2. Since the authors only found a few cases of interaction buckling with $\beta_5 = 0.300$, the trial specimens would be established only from the combinations of β-values with $\beta_5$ of 0.15 and 0.075 as shown in Figure 3.2. These $\beta_5$ values were thought more likely to prompt interaction buckling failure. Trial specimens, of each plate thickness, were developed from the combinations of β-values within the shaded areas of Figure 3.2. A series of trial specimens were produced under the assumption that all the components in the stiffened steel plates had the same static yield strength of 420 MPa (i.e. $f_{yp} = f_{ys}$), and a Young's modulus of 200 000 MPa. Although a large number of geometry combinations resulted from the recommended β-values, the ones with unreasonable dimensions were eliminated. The remainder were chosen to be studied in the preliminary finite element analysis.

### 3.2.2 Preliminary Finite Element Analysis

In order to verify the interaction buckling mode by tests on large scale specimens, the purpose of the preliminary analysis was to test the trial specimens and subsequently narrow them to a series of test specimens that would fail in this failure mode. The single stiffened steel plate model was tested with five discrete restraints along its longitudinal edges, which were proven to be successful in simulating a continuous boundary condition of a single panel within a multi-panel stiffened panel by Grondin *et al.* (1998). This analysis was conducted with the compression load applied at the centroid of the plate, although the tests were later conducted with a small load eccentricity as discussed later in Section 3.2.2.4. The mechanical properties of the model with the adopted nominal dimensions of the trial specimens as listed in Table 3.1 are shown in Table 3.2, with "average" level of initial imperfections proposed by Smith *et al.* (1991), and residual stresses distribution and magnitude measured from Grondin *et al.* (1998).

#### 3.2.2.1 Elements, Mesh and Initial Imperfections

The finite element program ABAQUS Version 5.6 was used in the finite element analysis. The stiffened plate specimens were modelled by using four-node shell element (S4R). It is a four-node, doubly curved shell element that accounts for finite membrane strains and allows for changes in element thickness. Each node of the shell element has six degrees of freedom (three displacement components and three rotation components). Figure 3.3 shows a finite element mesh of a typical specimen which consisted of a total of 576 S4R shell elements, 384 elements in the plate and 96 elements in both the web and the flange.

Following the parametric studies done by Sheikh *et al.* (2001), an "average" level of initial imperfections proposed by Smith *et al.* (1991) (Table 2.1 and Table 2.2) was applied to the models for both the imperfections in the plate and the stiffener. The so-called "average" magnitude of imperfection corresponds to a value of $\beta_6$ equal to $0.1\beta_1^2$ in the plate and $\beta_7$ equal to 0.0015 in the stiffener. Since the assumed imperfection on the stiffener only depended on the length of the specimen, the maximum initial imperfections for the web and the flange were the same for all the trial specimens. The maximum magnitudes of initial imperfection for the specimen are presented in Table 3.1. The distribution of initial imperfections in the plate was based on four half sine waves along the length and two quarter-sine wave across the width. The distribution of initial imperfections in the stiffener was defined by a single half sine wave along the length at stiffener flange to web junction, with a parabolic variation along the web height as detailed in Sheikh *et al.* (2001).

#### 3.2.2.2 Material Model

Metal plasticity of the specimen was modelled using an elastic-plastic constitutive model incorporating a von Mises yield surface and an isotropic strain-hardening flow rule. Because of the possible large deformations and finite strains during the analysis, the input stress-strain relationship was defined by the true stress-true strain values. A modulus of elasticity of 200 000 MPa was used for all the specimens. The static yield strength used for each component of the trial specimens as well as a description of the true stress-true strain curve adopted for the analysis are listed in Table 3.2. The proposed static yield strengths were the measured values obtained from the tests of Grondin *et al.* (1998).

#### 3.2.2.3 Residual Stresses

Only the longitudinal stresses were introduced to the model because the transverse residual stresses were expected to be relatively small and non-influential in the behaviour of the test specimens. The residual stress pattern reported by Grondin *et al.* (1998) was adopted for the preliminary analyses.

The introduction of residual stresses in the model causes a distortion in the specimen, which must be considered when investigating the effect of initial imperfections. Therefore, the residual stresses were applied in two stages. First initial strains were imposed in the form of a temperature distribution that resulted in initial residual stresses in the specimens. This involved the use of orthotropic temperature material property that had zero thermal expansion coefficients in directions 2 and 3 (transverse directions), for modelling the longitudinal initial strains only. A set of strains equivalent to the magnitude but opposite to the measured strains was introduced to the model with the assumed initial imperfections mentioned in Section 3.2.2.1. The initial strains introduced initial stresses, upon which an iterative process was carried out in order to establish equilibrium at the end of the first stage. The resulting displacements were then superimposed on the assumed initial imperfections generating a new deformed, stress-free mesh. Initial strains corresponding to the residual strains were then applied on the newly generated model. By the end of the first load step, the model had incorporated the assumed magnitude and distribution of the initial imperfections and the residual stresses. This two-stage method was developed by Roman and Elwi (1987) for applying residual stresses in stiffened cylinders. A similar procedure was also performed by a number of researchers (Chen *et al.*, 1993; Hu *et al.*, 1993; and Grondin *et al.*, 1998). The two-step method accounted for the deformations introduced by the residual stresses in the definition of the initial imperfections. Based on the findings of Sheikh *et al.* (2000), the one-step method generally results in a conservative prediction compared to that from the two-step method. The application of the one-step method was found to give a lower peak strength and softer post-buckling response for plate-buckling failure mode, which is sufficient for design purpose. However, since the analytical results will be compared with the experimental results, the two-step method was applied.

The fictitious temperature distribution, *T*, was derived from the measured residual stress distribution as follows,

$$T = -\frac{f_r}{\alpha_T E} \tag{3-1}$$

where $f_r$ is the residual stress, *E* is the modulus of elasticity and $\alpha_T$ is the coefficient of thermal expansion. Since the fictitious temperature distribution is material independent from the modulus of elasticity, the same set of temperature distribution was applied to the other analyses.

#### 3.2.2.4 Boundary Conditions

Two sets of boundary conditions were considered for this analysis. The longitudinal unloaded edges were clamped with the restraint fixtures. The loaded ends were required to rotate locally while remaining plane.

Additional end bearing plates welded onto the ends of the specimens were recommended by Grondin *et al.* (1998) to simulate the connections between the stiffened plate with bulkheads or floor beams; which are stiff in their own planes but are flexible in the out-of-plane direction. This stiff pin-ended support condition was modelled with a rigid frame composed of rigid three-dimensional beam elements, B31 from the ABAQUS library (HKS, 1997b), aligned along the specimen ends. These beam elements used a separate set of nodes from those forming the specimen ends. The two sets of nodes were constrained to simulate a welded connection. These stiff end frames in the analysis ensured uniform load distribution over the cross-section. To model degrees of freedom at the reaction end of the specimen, the geometric centroid of end cross-section was restrained along the longitudinal axis (1-axis) and rotational movements about all axes. On the loaded end, only three degrees of freedom remained for its geometric centroid, namely the translation along the longitudinal axis (1-axis) and the rotations about the other two axes (2- and 3-axis). End rotation was constrained to take place at some distance from the ends of the specimen to simulate the test conditions that used bearings to allow rotation at 84.2 mm from the ends of specimen SSP2 and 89.6 mm from the ends of specimen SSP1, SSP3 and SSP4.

Ideally, the rotation about the longitudinal axis was suppressed at all the nodes along the unloaded edges to simulate full continuity in a stiffened plate panel. Yet, it would be impractical to weld each specimen onto the restraint frame in the experimental study. Grondin *et al.* (1998) investigated the behaviour of stiffened plate for three different boundary restraint conditions along each longitudinal unloaded edge: continuous edge restrained, totally unrestrained and a model that uses five discrete restraints. The fully restrained case is the ideal situation where a typical stiffened plate unit is linked to the other stiffened plate units and/or welded to floor beam or bulkhead. The investigation by Grondin *et al.* concluded that the use of five discrete restraints could capture the same behaviour as for a continuous edge restraint, with only a slight reduction in the ultimate load. Based on this, the experimental set up in this study adopted the five discrete restraints boundary conditions. As a result, the longitudinal edge restraint system used in the test of Grondin *et al.* (1998) was reused for the experimental program.

In order to model the effect of the discrete restraint devices, short rigid beam elements were attached to the centre of each clamp restraint. These rigid beams can be found along the unloaded edges as stick element in Figure 3.3. Besides, the bending stiffness of the two plate elements adjacent to each short beam element was increased by an order of magnitude, and was assumed to be linearly elastic to simulate the stiffness of the clamping elements. The rotational restraint was applied by constraining the translation along the 2-axis (transverse to the plate) at the tip of each short beam. This allowed for accurate modelling of a rotational constraint about an axis tangential to the edge of the plate. This is considered to be more realistic than a direct restraint of the rotation about the 1-axis (the longitudinal axis of the plate).

#### 3.2.2.5 Solution Strategy

During the tests, the load-deformation responses of the specimens were monitored through stroke control on the axial shortening of the specimens in order to cover the pre-buckling and post-buckling behaviour of the specimens. In the analysis, the modified Riks method in ABAQUS was used to capture the non-linear effects of geometry and material response as well as the softening behaviour of the specimens, well into the post-buckling range.

The modified Riks method, also known as the arc length method, uses the load magnitude and the displacements as unknowns, and controls the increments (arc lengths) taken along the load versus displacement response. Since the Riks algorithm treats both loads and displacements as unknowns, termination of a Riks loading step will not occur at a predetermined load or displacement. Instead, the Riks step will terminate at the first solution that satisfies the user-defined step termination criterion. This criterion can be a maximum load, a maximum displacement at a given degree of freedom, or a maximum number of increments within a load step. Since this study only dealt with the uniaxial compression case, a maximum of 1 percent nominal strain value was used as the incremental Riks procedure to obtain the peak behaviour and strength.

### 3.2.3 Final Test Specimens

A plot of the response diagrams from the preliminary analysis is shown in Figure 3.4. The test specimens were selected based on the desired interaction buckling behaviour in the load versus deformation response, namely, a sudden loss of capacity after overall buckling. In addition to the selection of the test specimens, it was also observed that a slight change to the web thickness had little effect on the behaviour of the specimen (comparison between trial specimen 2 and 3). However, increasing the plate thickness not only increased the capacity of the specimen, but also made it less ductile.

The measured dimensions of the selected test specimens are listed in Table 3.3 along with the corresponding β-values and the proposed values from Sheikh *et al.* (2001). Because of the limited selection of plate thicknesses and some fabrication restrictions on plate width, the actual β-values of the specimens were slightly different from the β-values initially selected in the preliminary analysis. SSP1 and SSP4 have a plate thickness of 12.7 mm whereas SSP2 and SSP3 have a plate thickness of 10.0 mm. A 16 mm thick end plate was welded to the loaded ends of the test specimens to ensure a uniform load distribution during testing.

Specimen SSP1 was chosen because it had a ductile post-buckling behaviour. This would allow more time to observe the change in behaviour during testing. Among the final test specimens, specimen SSP2 was specifically chosen because of its unique load versus axial deformation response. This specimen belongs to the most critical case of interaction buckling which is also mentioned in the work of Sheikh *et al.* (2001). In this case, the overall buckling overtakes plate buckling at, or immediately after, attaining the peak load. More importantly, the load versus axial deformation response of this type usually behaves in the same manner as stiffener tripping. Hence, specimen SSP2 was chosen for verifying this critical behaviour. In order to differentiate the two failure modes in the analysis, one must study the incremental deformed shape of the specimen at each stage of the analysis. The geometry for SSP3 and SSP4 was designed from the same set of recommended β-values as shown in Table 3.3. Based on a smaller plate thickness, SSP3 is scaled down version of SSP4. The intent of choosing SSP3 and SSP4 with such a proportion was to study the scale effect on buckling behaviour.

These specimens were supposed to be fabricated from CSA G40.21-94 350W hot rolled steel plates. However, the actual yield strength of the material, as presented in Chapter 4, indicates that the material used for the fabrication of the test specimens did not meet the grade requirements for a few of the test specimens. Prior to testing, another set of finite element analyses were performed with the measured geometries of each specimen. The analyses confirmed that the specimens would fail by interaction buckling mode when they were loaded at their centroid.

## 3.3 Test Set-Up

The tests were conducted in the I. F. Morrison Structural Laboratory at the University of Alberta. A schematic of the test setup is shown in Figure 3.5. The specimens were placed in the upright position with edge restraint clamps equally spaced along the unloaded edges. Axial compressive loads were applied through a MTS 6000 universal testing machine at the top of the specimen. Considerable attention was given to the boundary conditions of the test set-up since these conditions have a direct influence on the failure behaviour of the specimens. Further details of the test setup are described below.

### 3.3.1 End Supports

To simulate the boundary conditions of a single stiffened plate in a multi-stiffened panel in the experiment, a similar approach as Grondin *et al.* (1998) was adopted. Each specimen was equipped with fully welded end bearing plates to ensure that the end cross-section would remain plane. Knife edge supports were provided to simulate inflection points along the length of a panel.

A schematic of the end boundary conditions is presented in Figure 3.6. On the top support, the MTS testing machine loaded the specimen through a distributing beam resting on a series of knife-edges. An additional end plate was placed between the 16 mm thick specimen end plate and the knife-edges to provide extra stiffness to the welded end plate. This also provided extra space for the seating of the knife-edges. An identical set up was used for the bottom end support as shown in Figure 3.7. Plaster of Paris was spread in two locations to ensure uniform contact while loading: 1) between the knife-edge and the additional end plate, and 2) between the additional end plate and the specimen end plate. This boundary arrangement simulated a pinned end condition which is free to rotate, free from horizontal reactions through friction forces, and stiff in-plane and free out-of–plane similar to the welded connections between the stiffener and the floor beam.

Initially, it was intended to load the specimens at their centroid. In the first test, specimen SSP2 was inadvertently loaded off its Centroid with a eccentricity towards its stiffener, which caused failure of SSP2 by stiffener tripping. To explore further the effect of eccentricity on the buckling behaviour, the knife-edge was then placed at various distances from the centroidal axis of the remaining specimens, as listed in Table 3.4. The eccentricity is shown as negative towards the plate and positive towards the stiffener.

### 3.3.2 Lateral Restraints System

Since the test specimens were single stiffened steel plates, the boundary conditions along the unloaded edges must simulate the interaction between a single unit with its co-existing stiffened steel plates in a full panel replicating the degrees of freedom at the plate connection between each single stiffened steel plate element. Among the six degrees of freedom, the restraint system was required to restrict three degrees of freedom (lateral in-plane displacement, tangential rotation along the edge and in-plane rotation) while leaving the others free. Figure 3.8 illustrates this concept on a deformed stiffened steel plate finite element model. Each stick represents a discrete restraint.

The edge restraining system designed in the work of Grondin *et al.* (1998) was used for this experimental program. The design concept and degrees of freedom of the fixture are illustrated in Figure 3.9 (a), while Figure 3.9 (b) shows a schematic of a restraint. The grip fixture was mounted on a bearing shaft, which was inserted into an angular spherical bearing, allowing rotation about the 2-axis. This fixture rested on a square platform (carriage B) that contained sets of linear motion bearings on the bottom of each corner. The linear motion bearings allowed carriage B to travel on the bearing shafts, mounted on carriage A, with freedom of translation along the 3-axis. Carriage A also had sets of linear motion bearings on its bottom, and was free to slide along the 1-axis via the two bottom shafts. This restraining system, thus, fully accounts for the essential restrained degrees of freedom while serving the purpose of a continuous boundary condition. A picture of the plate edge restraining system during SSP1 testing is shown in Figure 3.10. As plate buckling occurred, the edge restraints rotated along with the buckles and slid along the 1- and 3-axes to follow the deformed configuration of SSP1.

### 3.3.3 Instrumentation and Data Acquisition

The instrumentation used is summarized in Figure 3.11. It consisted of 17 displacement transducers for measuring axial shortening, lateral deflection at the side of plate opposite to the stiffener, and torsional displacement of the stiffener. The last two measurements were intended to monitor possible plate buckling behaviour and stiffener tripping, respectively. Two rotation meters (instruments A and B) were attached at the end plates, which provided indication of symmetry of the set-up and the direction of the buckling behaviour. Eleven strain gauges (see Section 1-1 in Figure 3.11) were mounted at the mid-length of each specimen to measure the axial strains and to identify any potential material yielding. There was no strain gauge on the bottom left corner of SSP2 flange because of a sudden enlargement on the weld. Figure 3.12 shows the locations of the strain gauges at the front and back of specimen SSP2. A record of the axial load was provided by the MTS universal testing machine along with the overall stroke of the entire set up. This stroke (axial deformation) measurement was not used in the development of the load versus deformation curves because it might include the softening of the set-up. Therefore, an additional linear variable displacement transducer (LVDT) was positioned at the point of loading between the additional end plates in order to measure the axial deformation of the specimen alone (see location of instrument C). Two load cells were placed beneath the bottom end support to check the axial force equilibrium and to detect any effect of friction from the restraint system. Having two load cells instead of one in the set up assured a stable base during the buckling of the specimens. All the instrumentations were calibrated prior to testing. Data from the instrumentation was monitored and acquired through LabVIEW® software.

## 3.4 Testing Procedure

Prior to testing, preparation involved obtaining actual specimen dimensions, initial imperfections measurement, mounting strain gauges on each specimen, calibrating the instrumentation, setting up the restraining frames onto the W shape columns, aligning the test set up, and setting up end supports. Proper aligning of the test set up was critical. The alignment must have the following,

- the restraining frame-columns formed a H with the specimens;
- carriage B of each restraint was placed in the middle of the bearing shaft allowing for leeway in the 3 direction for buckling movement;
- the five discrete restraints were set at 375 mm apart with the middle restraint at the mid length of each specimen; and

- the point of loading on the specimen was aligned with the centre of the MTS machine.

After the alignment was completed, the columns (with the restraining system attached) were fastened to a strong floor as shown in Figure 3.13. The bottom support was set in between the restraining frames. The specimen was then positioned on top of the bottom boundary set up with the plate edge restraints clamped on the unloaded edge of the specimen. Lastly, the top boundary support was placed on the specimen as well as the instrumentation.

During testing, the axial load was applied through displacement control, which permitted tracking of the post-buckling response. The specimen was first loaded to 100 kN and then unloaded to minimize the effect of sitting of the test set up and to detect any abnormalities. The deformation of the specimen was observed throughout the test to monitor the presence of plate buckling and overall buckling behaviour. After the second plateau, the test was continued until the specimen reached approximately 15 mm of axial deformation.

In order to efficiently facilitate the replacement of test specimens, 127 x 178 x 4.76 mm HSS spacers were utilized to accommodate the various plate widths of the specimens as shown in Figure 3.13. One or two of these HSS were inserted in between the column and the restraint frame at quarter length. The remaining gaps were then filled with flat plates or shims.

### 3.5 Initial Imperfection Measurements

After measuring the cross sectional dimensions, the initial out-of-plane geometrical imperfections were mapped for all the components of each specimen. The measuring process for each specimen was divided into two parts: the horizontal components (flange and plate) and the web. Different measuring devices and set ups were required for the horizontal components and the web. Only one side of each element was measured since it was assumed that the thickness of each component was constant along the length of the specimen.

### 3.5.1 Plate and the Flange Imperfections

In order to measure the geometric imperfections of the horizontal components, a reference plane was first established. A sheet of 32 mm thick plexiglass was laid on top of three hemispheres to avoid the unevenness of the floor. Four adjustable bolts were used to support a rigid steel frame that was positioned above the plexiglass sheet. Steel balls were inserted between the adjustable bolt and the steel frame to provide a point contact. This rigid rectangular steel frame acted as a track for the vertical transducers. A total of nine LVDTs were fixed on an angle, which slid along the steel frame for each measurement. The layout of the transducers is illustrated in Figure 3.14. The spacing of the transducers was set to accommodate all four specimens. Smaller transducers were used for the flange because of the limited accessibility. Before taking any measurements, two steel blocks were positioned below the small transducers to simulate the stiffener, and to reach the small transducers. After the frame was levelled longitudinally and laterally with the adjustable bolts, three readings were taken to develop the flat plane. The plexiglass was then removed and replaced with a specimen.

The test specimen was placed with its flange facing up as shown in Figure 3.15. The rectangular frame was situated on the flange of the specimen and the adjustable bolts. The steel frame was levelled repeatedly before taking each measurement. The transducer rack was dragged along the steel frame and stopped at constant intervals for each measurement. Six longitudinal readings were taken along the plate and three readings along the flange at each interval. Readings were recorded along the length at every 125 mm for SSP1, 120 mm for SSP2, and 150 mm intervals for the remaining two specimens along their full length. Three sets of imperfection measurements were recorded for each specimen. All the data were recorded by the computerized FLUKE data acquisition system.

### 3.5.2 Web Imperfections

Instead of using displacement transducers, a digital dial gauge was used to measure the imperfections on the web. A plexiglass frame was custom built for the digital dial gauge to simplify the measuring process, as shown in Figure 3.16. This frame was built at 90° angle that helped detect the sweep of the web element in the 1-direction and 3-direction. At each location, the digital dial gauge was pressed against the plexiglass, which was the reference surface for the dial gauge. Readings were recorded at the same intervals as the previous section for each specimen. Again, three sets of data were taken with a difference among the readings not exceeding ±0.1 mm.

## 3.6 Residual Stress Measurements

Residual stresses are induced in steel structural members during manufacturing. The first source of residual stress is induced from the non-uniform cooling after the hot rolling process of steel products. Other source of residual stresses from fabrication: cutting, welding, and cold forming. Therefore, residual stresses measurements of the test specimens are important.

The residual thermal and cold-work stresses can be divided into longitudinal and transverse stresses. However, this study only emphasizes the longitudinal residual stresses, especially those caused by welding because it has a pronounced influence on the stiffened steel plate. The residual stresses in longitudinal direction vary with respect to the width and thickness of the plate members. Hence, the following measurements assumed that the residual stresses through the plate thickness are uniform.

### 3.6.1 Measurement Technique

The method of sectioning was chosen for the residual stresses measurement. The technique and procedure followed closely to that reported by two references: Tebedge, Alpsten and Tall (1971), and Essa and Kennedy (1993). Since the method is destructive, the specimen can no longer be used after testing. The process of sectioning the test specimens causes a relaxation in stress and a corresponding strain. The relaxation in stress is then obtained by applying Hooke's Law. Two assumptions are made when this method is used: the transverse residual stresses are negligible and the cutting process causes no significant residual strain.

### 3.6.2 Preparation of Test Specimen

As mentioned in Section 3.2, an extra specimen was fabricated to the same specifications as specimen SSP1 to establish representative residual stresses profile for the finite element analysis. There was evidence of heat straightening being applied on the specimen; therefore, the test location selected was away from these heat-treated areas. The location of the test section is shown in Figure 3.17. The specimen is at least twice the depth away from the end plates to avoid the influence of end effects on the magnitude and distribution of the residual stresses. Evidence of cold work and transverse crack in the mill scale were not identified on the specimen.

A pattern of strips and the width of each strip are shown in Figure 3.18. Lines defining the strips were scribed on both sides of all elements of the cross section, except the flange. The width of the strips was selected according to the usual residual stress gradient pattern and the dimensions of the specimen. The two widths used in the layout were 6 mm and 12 mm. Although the gauge length was only 100 mm long, each strip was 200 mm long to provide sufficient clamping area during the cutting process.

As soon as the sections were scribed, 1.6 mm gauge holes were defined at 100 mm on centre using a template punch at the top and bottom of each strip, except at the flange-web junction and the web-plate junction. These junctions had three gauge lengths on the welds and on the flat portion. Steel balls were placed into the gauge holes. Since this measurement used a Bam-Setzdehnungsmesser mechanical extensometer (see Figure 3.19), these steel balls were required with this type of gauge as gauge marks. To ensure the steel ball remained in the holes during sectioning, a small amount of epoxy was deposited into the holes before placing the steel balls. The use of steel balls helped improve the accuracy of the measurements and made repeatable readings possible. In addition, it avoided giving unreliable readings at gauge holes at the edges or at corners due to different alignment and human errors from taking stable readings.

Gauge length measurements along the gauge length were taken with the above mechanical extensometer, before and after sectioning. Top and bottom readings were recorded for all strips except those that could not be accessed. To eliminate the possibility of erroneous data, the temperature changes during measurement were also monitored before and after each set of readings. This was done by taking measurements on a reference bar periodically during the measurements. The sectioning process was performed with a band saw along the defined sectioning lines. The specimen was clamped against the band saw table to avoid significant bowing of the strips. After sectioning, no ball separation was evident but slight lateral bending was notable at strips near the tip of the plate. A total of 99 strips were cut as displayed in Figure 3.20.

For each gauge length, five sets of readings were taken before and after sectioning with their deviations limited to ±0.003 mm. Residual strain released by sectioning is calculated as the change in the gauge length after longitudinal sectioning divided by the original gauge length (Equation 3-2). Residual stresses were then calculated based on the modulus of elasticity determined from tension coupon tests. An elongation of a strip after sectioning indicates that a compressive residual stress has been released by sectioning while shortening of a strip results from the release of tensile residual stress.

$$\sigma_r = \left(\frac{L_b - L_a}{L_b}\right)E \tag{3-2}$$

where, $\sigma_r =$ residual stress magnitude (tension is positive)

$L_b =$ mean gauge length before sectioning

$L_a =$ mean gauge length after sectioning

$E =$ modulus of elasticity

### 3.7 Tension Coupon Tests

Standard tension coupon tests were performed to obtain the mechanical material properties of each component of the test specimens. Seven sets of three coupons (a total of 21) were prepared from the extra materials cut from the stock of material used in the specimens. All coupon specimens were oriented in the rolling direction. After cutting from the parent plate, the tension coupons were milled to a reduced section as shown in

Figure 3.21. The dimensions of the coupon were designed in accordance with the specification in ASTM A370 (2002) except for the grip length, which was lengthened to 100 mm. The gauge section was 12.5 mm in width and 50 mm in length. The cross sectional areas of the coupons were measured prior to testing.

The tests were conducted in a MTS 1000 testing machine under displacement control. A 50 mm gauge length extensometer was clipped onto the tension coupons for strain measurement. The rupture strain was obtained based on the change of the distance between the two punched marks, spaced at 50 mm. The machine ran at displacement control at 0.15 mm/min in the elastic range and 1.5 mm/min in the strain hardening range. Axial load, axial deformation and extensometer strain readings were recorded at constant intervals throughout the tests. For each coupon, static readings were taken at yielding and ultimate peak portions. The final gauge length was measured after rupture in order to obtain the strain at rupture.

Table 3.1 Trial Specimens and Corresponding β-Values

| **Trial Speicimen** | **1** | **2** | **3** | **4** | **5** | **6** | **7** | **8** | **9** | **10** | **11** |
|---|---|---|---|---|---|---|---|---|---|---|---|
| **$t_p$ (mm)** | 11.5 | 12.0 | 12.0 | 9.7 | 10.0 | 11.5 | 12.0 | 10 | 9.7 | 10 | 11.5 |
| **$t_w$ (mm)** | 4.3 | 4.0 | 4.5 | 2.5 | 2.5 | 3.7 | 3.5 | 3.5 | 3.1 | 3.0 | 2.6 |
| **$t_f$ (mm)** | 8.4 | 8.0 | 8.0 | 5.0 | 5.0 | 7.2 | 7.0 | 7.0 | 6.1 | 6.0 | 5.1 |
| **$h_w$ (mm)** | 139 | 140 | 140 | 83.1 | 85.0 | 120 | 120 | 120 | 101 | 100 | 84.8 |
| **$b_p$ (mm)** | 678 | 680 | 680 | 572 | 570 | 502 | 500 | 500 | 423 | 420 | 502 |
| **$b_f$ (mm)** | 68.6 | 70.0 | 70.0 | 40.9 | 40.0 | 59.1 | 60.0 | 60.0 | 50.0 | 50.0 | 41.8 |
| **L (mm)** | 2000 | 2000 | 2000 | 2000 | 2000 | 2000 | 2000 | 2000 | 2000 | 2000 | 2000 |
| **$\beta_1$** | 2.70 | 2.60 | 2.60 | 2.70 | 2.61 | 2.00 | 1.91 | 2.29 | 2.00 | 1.92 | 2.00 |
| **$\beta_2$** | 1.50 | 1.60 | 1.43 | 1.50 | 1.56 | 1.50 | 1.57 | 1.57 | 1.50 | 1.53 | 1.54 |
| **$\beta_3$** | 0.375 | 0.401 | 0.401 | 0.375 | 0.367 | 0.375 | 0.393 | 0.393 | 0.375 | 0.382 | 0.375 |
| **$\beta_4$** | 0.70 | 0.72 | 0.72 | 1.17 | 1.18 | 1.09 | 1.14 | 0.95 | 1.29 | 1.36 | 2.00 |
| **$\beta_5$** | 0.15 | 0.14 | 0.15 | 0.075 | 0.072 | 0.15 | 0.14 | 0.17 | 0.15 | 0.14 | 0.075 |
| **$\delta_p$ max** | 4.6 | 4.5 | 4.5 | 3.9 | 3.8 | 2.5 | 2.4 | 2.9 | 2.1 | 2.0 | 2.5 |
| **$\delta_w$ max** | 2.3 | | | | | | | | | | |
| **$\delta_f$ max** | 1.1 | | | | | | | | | | |

*** β-values based on Fy = 420 MPa.**

Table 3.2 Material Properties for Preliminary Finite Element Model

| **Part** | **$\sigma_1$ (MPa)** | **$\varepsilon_1$ (%)** | **$\sigma_2$ (MPa)** | **$\varepsilon_2$ (%)** |
|---|---|---|---|---|
| **Plate** | 425 | 0 | 525 | 1 |
| **Flange** | 395 | 0 | 495 | 1 |
| **Web** | 411 | 0 | 511 | 1 |

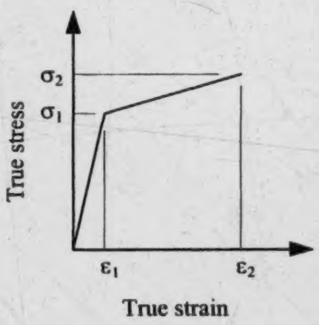

Table 3.3 Measured Dimensions of Test Specimens and Corresponding β-Values

| **Specimen** | **SSP1** | | **SSP2** | | **SSP3** | | **SSP4** | |
|---|---|---|---|---|---|---|---|---|
| **$t_p$ (mm)** | 12.8 | | 9.5 | | 9.3 | | 12.6 | |
| **$t_w$ (mm)** | 4.7 | | 2.9 | | 2.9 | | 3.2 | |
| **$t_f$ (mm)** | 7.8 | | 6.2 | | 6.2 | | 7.8 | |
| **$h_w$ (mm)** | 151 | | 88.4 | | 101 | | 126 | |
| **$b_p$ (mm)** | 799 | | 569 | | 420 | | 500 | |
| **$b_f$ (mm)** | 75.1 | | 38.2 | | 50.9 | | 63.4 | |
| **L (mm)** | 2000 | | 2000 | | 2000 | | 2000 | |
| **β Parameters** | **Proposed Value[1]** | **Actual Value** | **Proposed Value** | **Actual Value** | **Proposed Value** | **Actual Value** | **Proposed Value** | **Actual Value** |
| $\beta_1$ | 2.7 | 2.6 | 2.7 | 2.3 | 2.0 | 1.7 | 2.0 | 1.7 |
| $\beta_2$ | 1.5 | 1.4 | 1.5 | 1.2 | 1.5 | 1.3 | 1.5 | 1.6 |
| $\beta_3$ | 0.375 | 0.41 | 0.375 | 0.24 | 0.375 | 0.32 | 0.375 | 0.34 |
| $\beta_4$ | — | 0.6 | — | 1.1 | — | 1.3 | — | 1.2 |
| $\beta_5$ | 0.15 | 0.13 | 0.75 | 0.09 | 0.15 | 0.16 | 0.15 | 0.14 |
| $\beta_6$ | —[2] | 1.0 | — | 1.0 | — | 1.0 | — | 1.0 |
| $\beta_7$ | — | 0.82 | — | 0.89 | — | 1.1 | — | 1.2 |
| $\beta_8$ | — | 2.5 | — | 3.5 | — | 4.8 | — | 4.0 |

[1] Analytical β-values from Sheikh *et al.* (2001)

[2] $\beta_6$, $\beta_7$, and $\beta_8$ are the initial imperfections and residual stresses ratios. They were calculated from actual specimen imperfections; therefore, no proposed β-values are available.

Table 3.4 Eccentricity of the Applied Axial Load

| **Specimen** | **Centroid Location[1] (mm)** | **Eccentricity[2] (mm)** |
|---|---|---|
| **SSP1** | 19.6 | -10 |
| **SSP2** | 10.7 | 3 |
| **SSP3** | 15.9 | -5 |
| **SSP4** | 19.5 | -5 |

[1] Distance from the plate extreme fibre to the centroid.

[2] Eccentricity measured from centroidal axis to the location of loading (positive towards the flange and negative towards the plate).

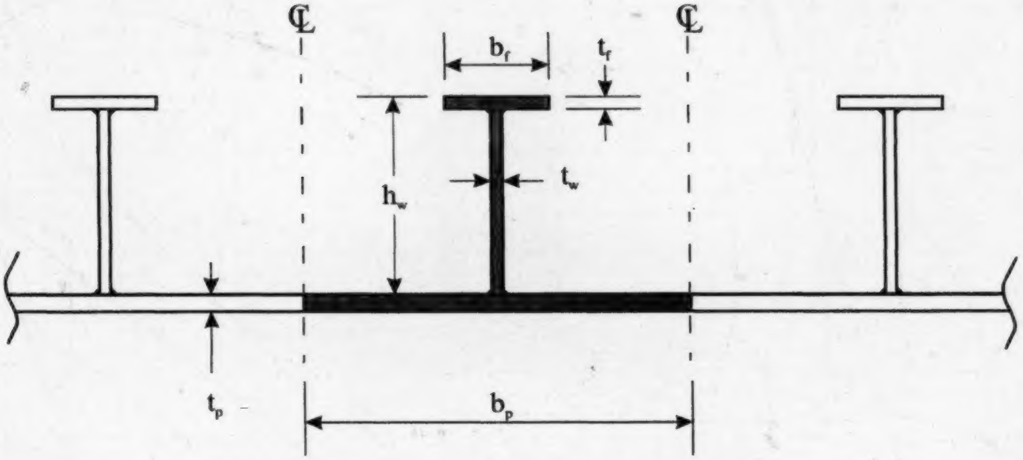
℄
℄
$b_f$
$t_f$
$h_w$
$t_w$
$t_p$
$b_p$

Figure 3.1 Stiffened Steel Plate Dimensions

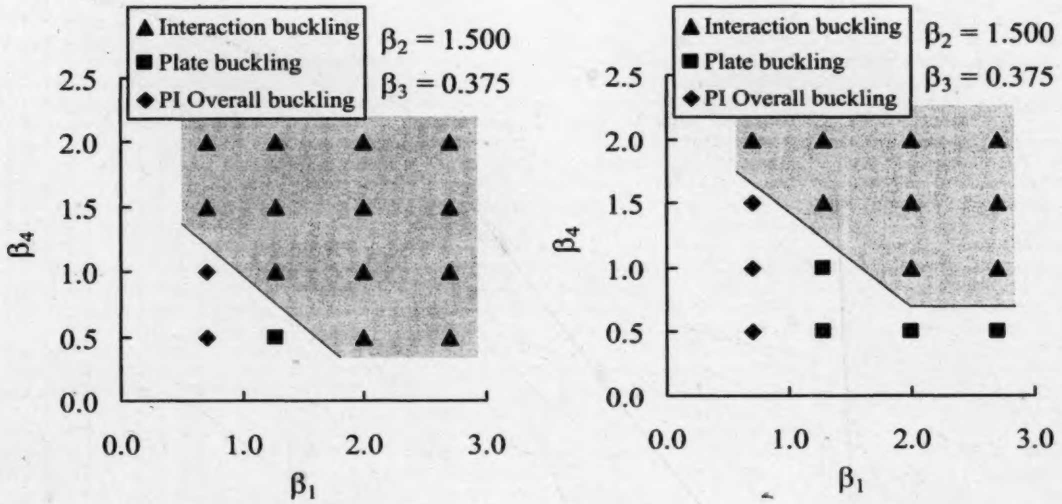

($\beta_5 = 0.075$)

($\beta_5 = 0.150$)

Figure 3.2 β-Values for Preliminary Analysis (Shaded Area)

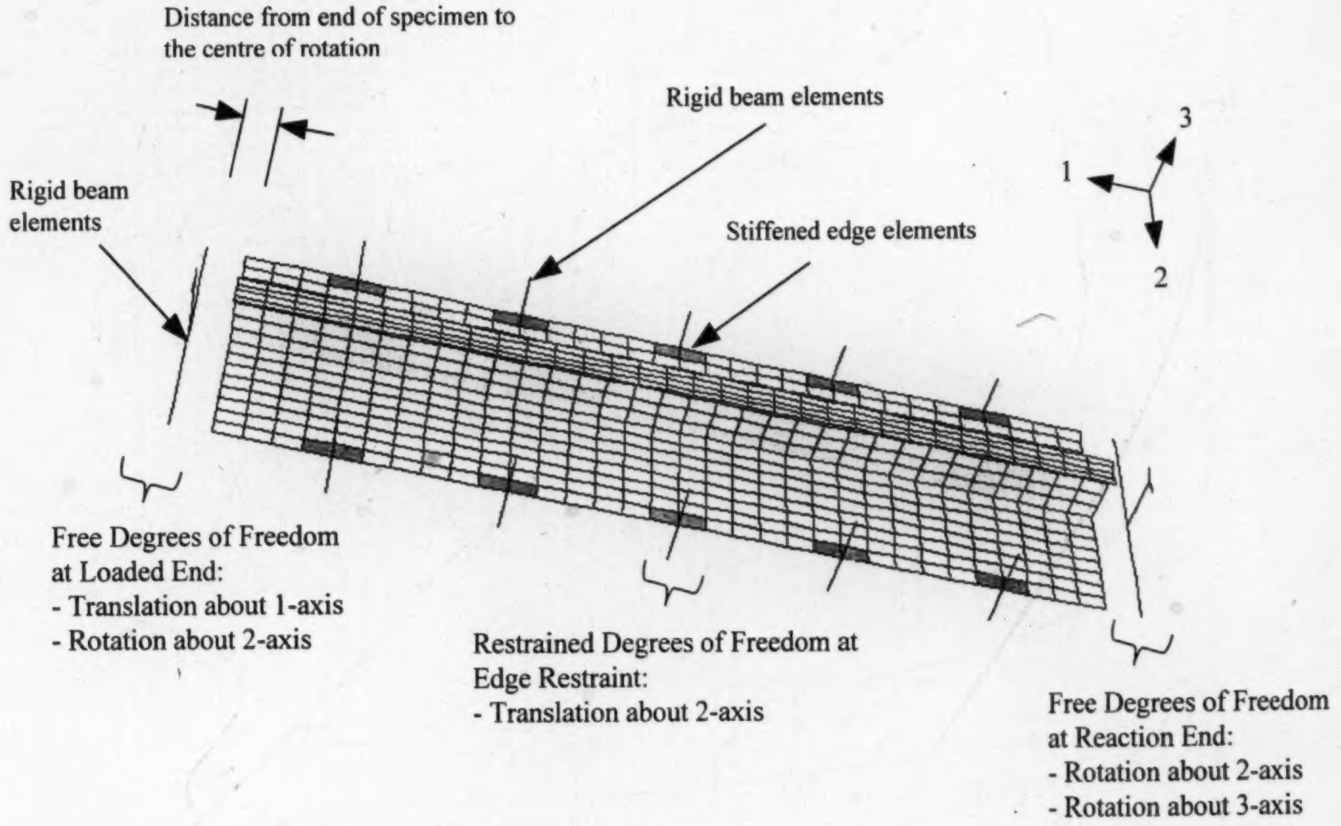
Distance from end of specimen to the centre of rotation
Rigid beam elements
3
1
2
Rigid beam elements
Stiffened edge elements
Free Degrees of Freedom at Loaded End:
- Translation about 1-axis
- Rotation about 2-axis
Restrained Degrees of Freedom at Edge Restraint:
- Translation about 2-axis
Free Degrees of Freedom at Reaction End:
- Rotation about 2-axis
- Rotation about 3-axis

Figure 3.3 Typical Mesh

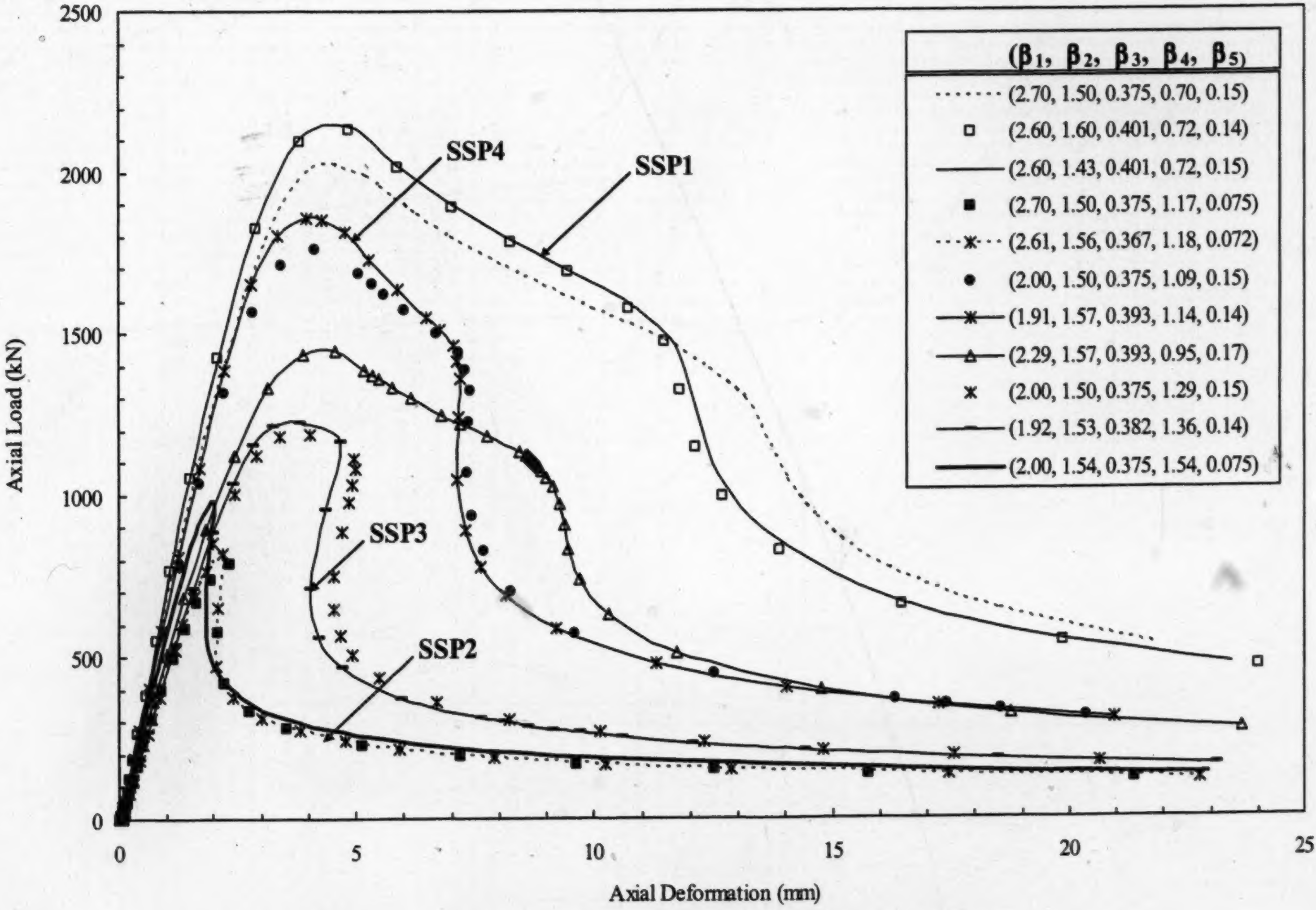

Figure 3.4 Preliminary Analysis Load versus Deformation Response Curves

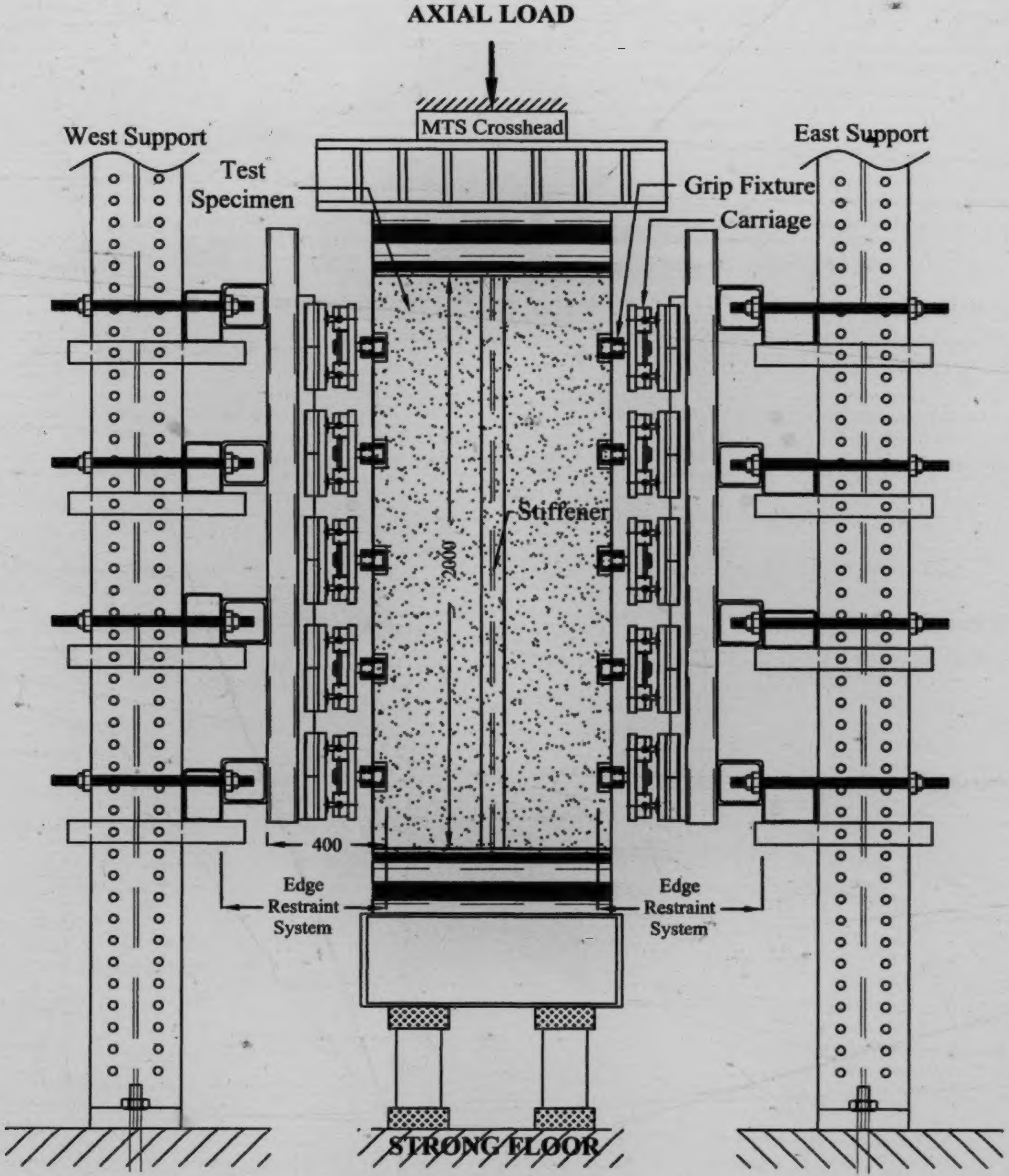
AXIAL LOAD
MTS Crosshead
West Support
East Support
Test Specimen
Grip Fixture
Carriage
Stiffener
2000
400
Edge Restraint System
Edge Restraint System
STRONG FLOOR

Figure 3.5 Schematic of Test Setup

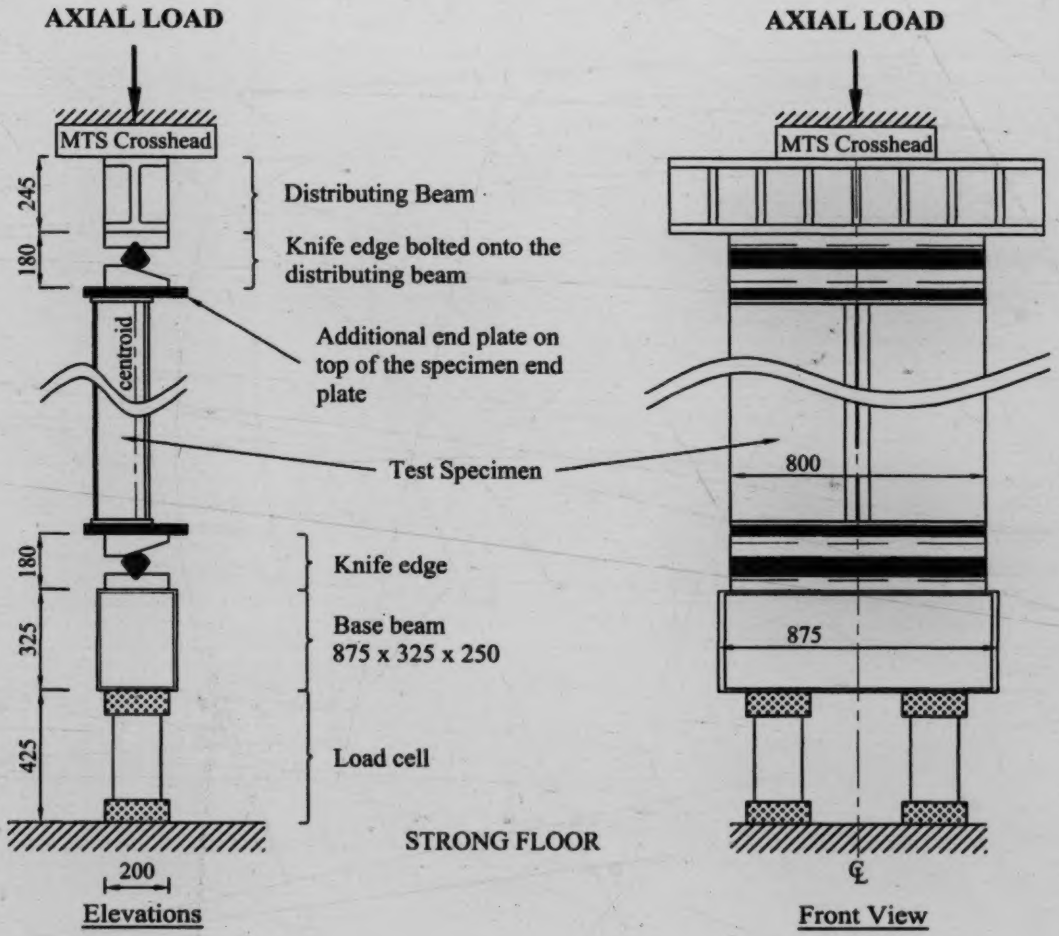
AXIAL LOAD
AXIAL LOAD
MTS Crosshead
MTS Crosshead
245
180
Distributing Beam
Knife edge bolted onto the distributing beam
centroid
Additional end plate on top of the specimen end plate
Test Specimen
800
180
Knife edge
325
Base beam 875 x 325 x 250
875
425
Load cell
STRONG FLOOR
200
℄
Elevations
Front View

Figure 3.6 Schematic of Boundary Conditions

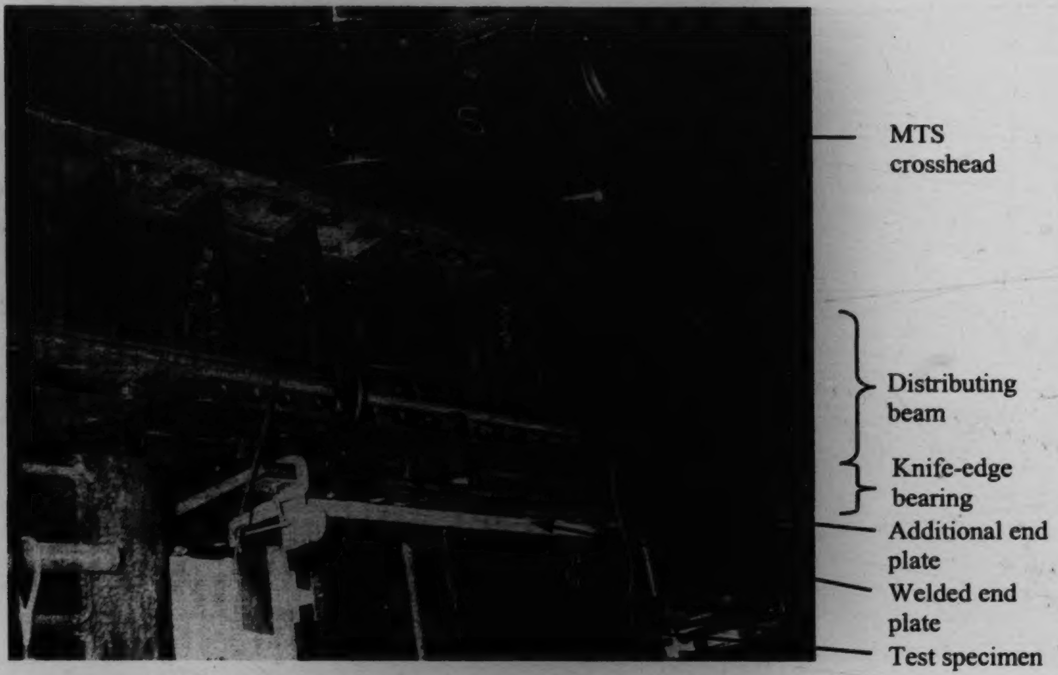
MTS crosshead
Distributing beam
Knife-edge bearing
Additional end plate
Welded end plate
Test specimen

(a) Top Boundary Condition

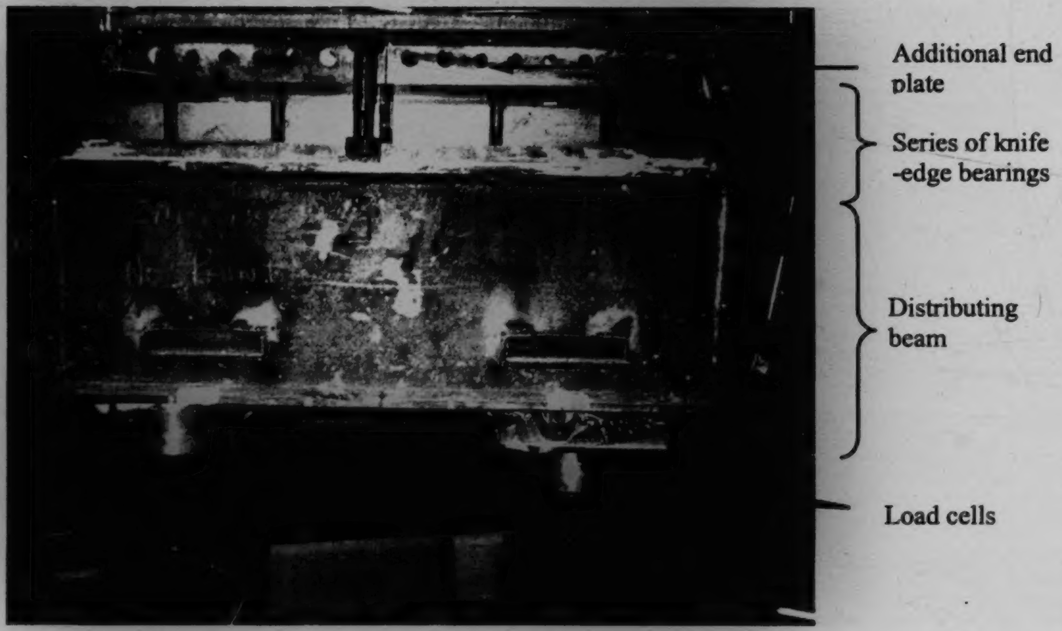
Additional end plate
Series of knife -edge bearings
Distributing beam
Load cells

(b) Bottom Boundary Condition

Figure 3.7 Top and Bottom Boundary Conditions

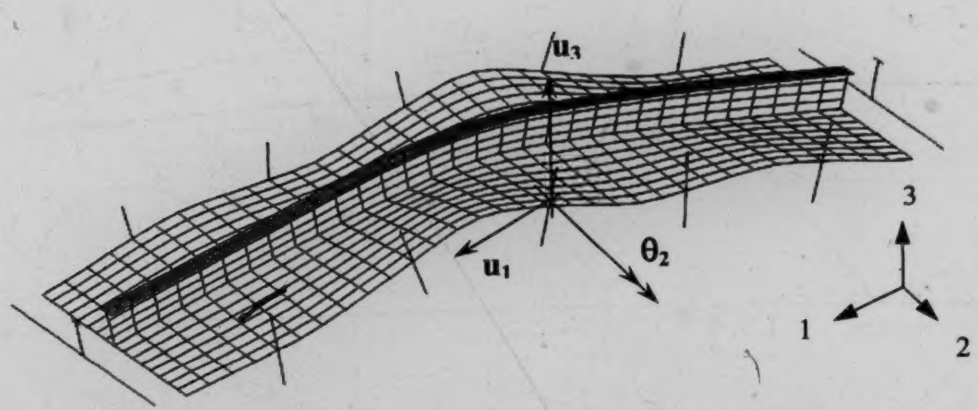

Figure 3.8 Required Degrees of Freedom for the Finite Element Model

(Refer to Figure 3.3 for boundary conditions details)

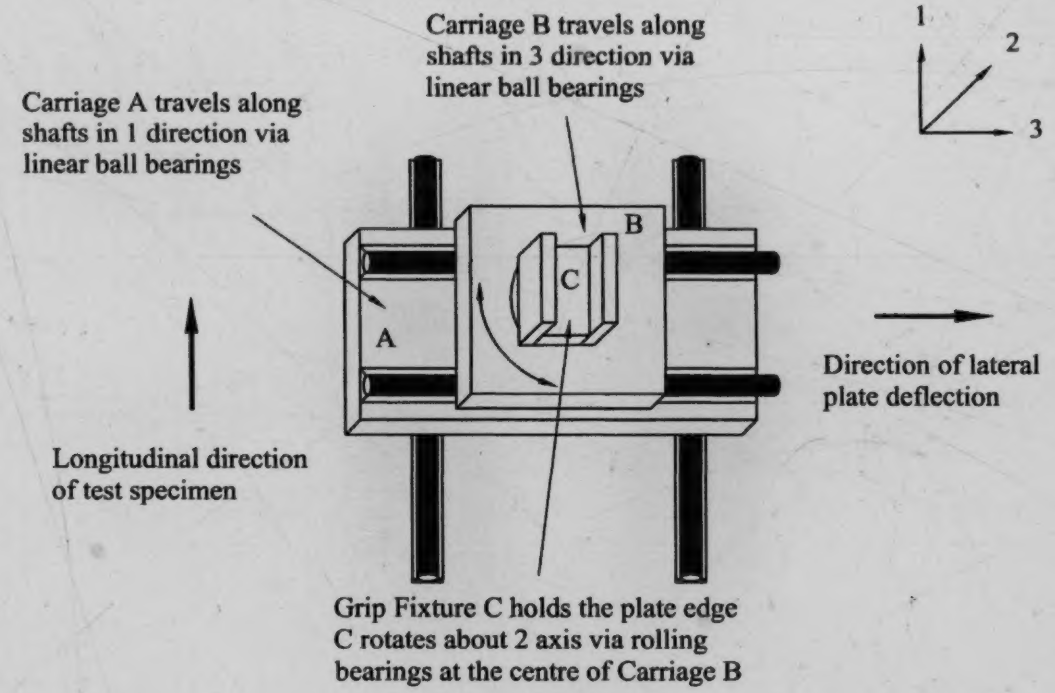
Carriage B travels along shafts in 3 direction via linear ball bearings
1
2
3
Carriage A travels along shafts in 1 direction via linear ball bearings
B
C
A
Direction of lateral plate deflection
Longitudinal direction of test specimen
Grip Fixture C holds the plate edge C rotates about 2 axis via rolling bearings at the centre of Carriage B

(a) Illustration of the Concept

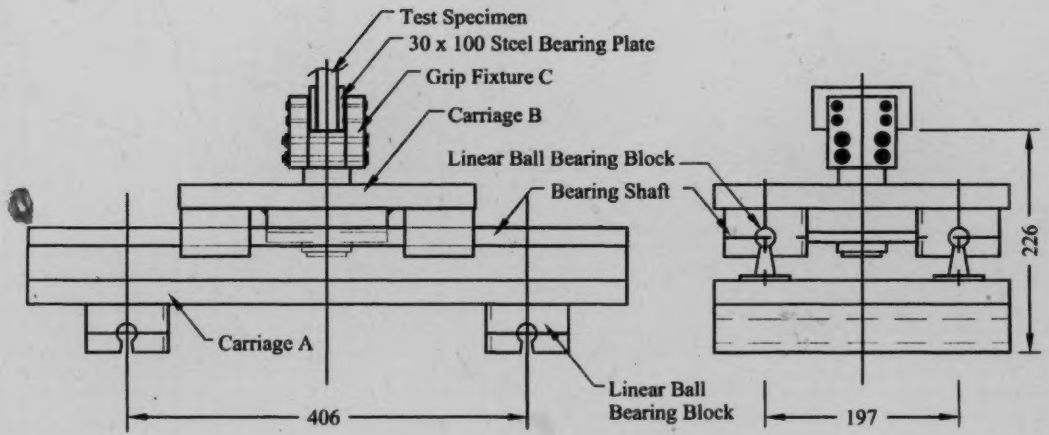
Test Specimen
30 x 100 Steel Bearing Plate
Grip Fixture C
Carriage B
Linear Ball Bearing Block
Bearing Shaft
Carriage A
Linear Ball Bearing Block
406
197
226

(b) Details of the Restraints

Figure 3.9 Edge Restraint Apparatus

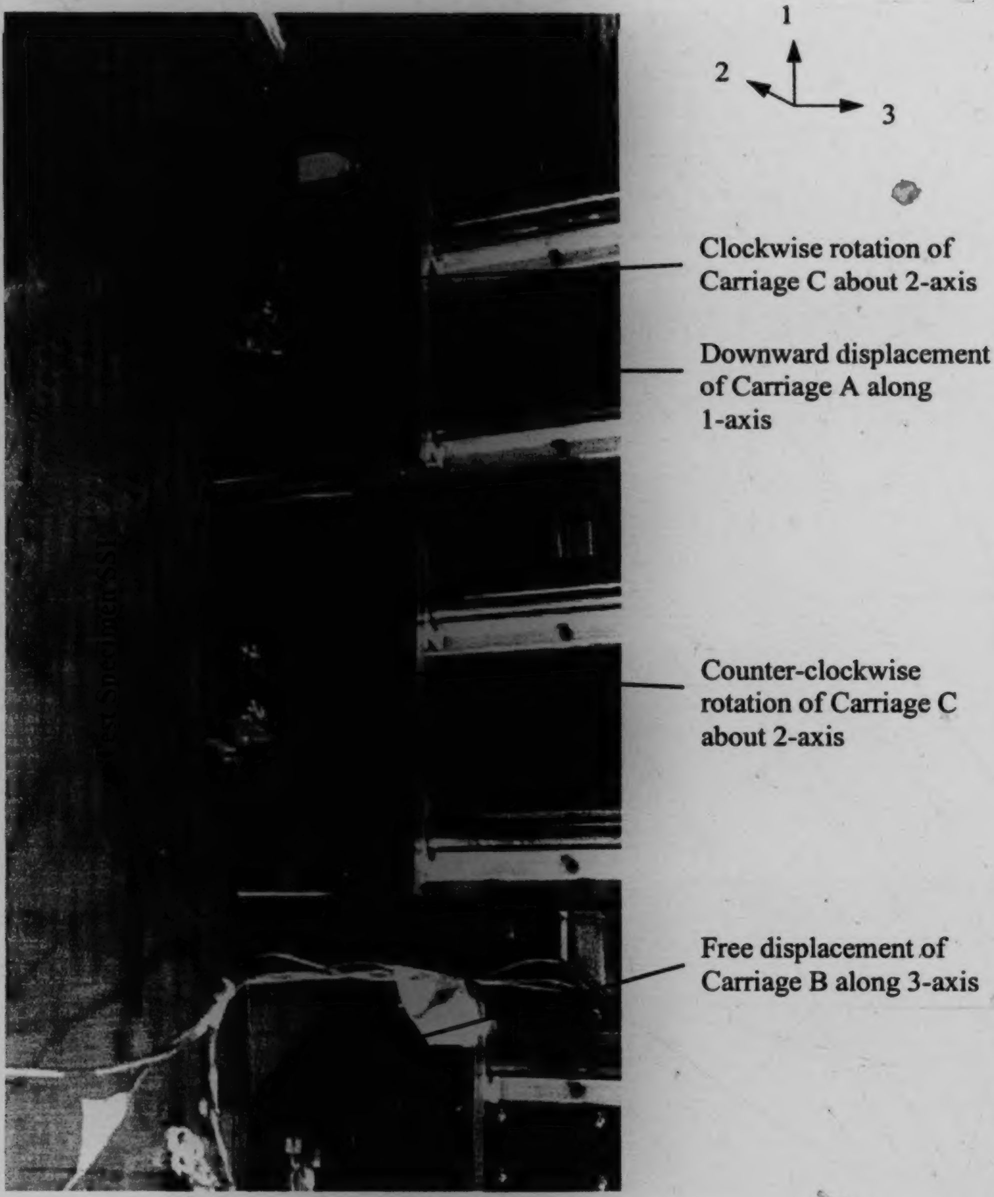

Clockwise rotation of Carriage C about 2-axis

Downward displacement of Carriage A along 1-axis

Counter-clockwise rotation of Carriage C about 2-axis

Free displacement of Carriage B along 3-axis

Figure 3.10 Plate Edge Restraining System Demonstration

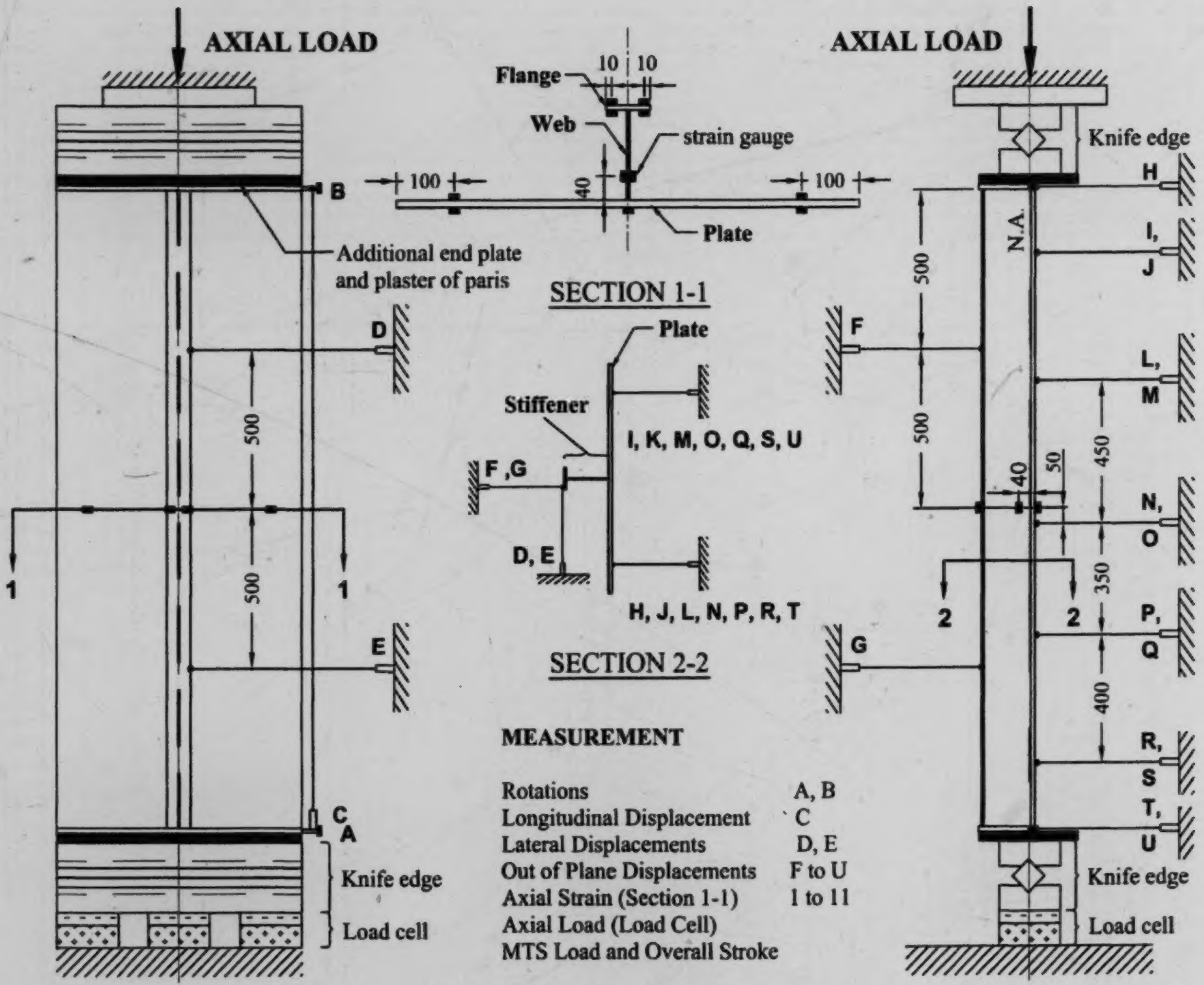
AXIAL LOAD
AXIAL LOAD
Flange
10
10
Web
strain gauge
100
100
40
Plate
B
Additional end plate
and plaster of paris
SECTION 1-1
Plate
Stiffener
I, K, M, O, Q, S, U
F ,G
D, E
H, J, L, N, P, R, T
SECTION 2-2
D
E
500
500
1
1
C
A
Knife edge
Load cell
Knife edge
H
I,
J
L,
M
N,
O
P,
Q
R,
S
T,
U
N.A.
F
G
500
500
40
50
450
350
400
2
2
Knife edge
Load cell

**MEASUREMENT**

| | |
|---|---|
| Rotations | A, B |
| Longitudinal Displacement | C |
| Lateral Displacements | D, E |
| Out of Plane Displacements | F to U |
| Axial Strain (Section 1-1) | 1 to 11 |
| Axial Load (Load Cell) | |
| MTS Load and Overall Stroke | |

Figure 3.11 Instrumentation

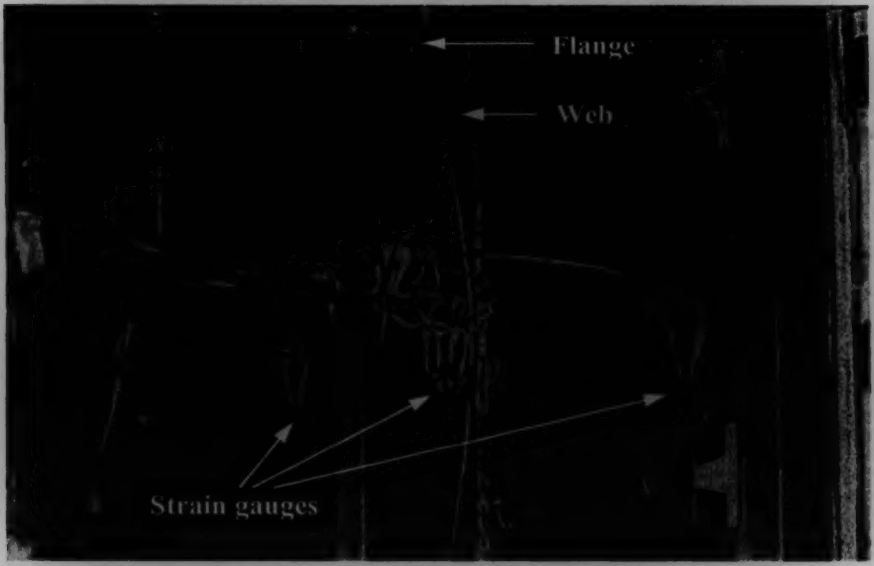
Flange
Web
Strain gauges

(a) Front View

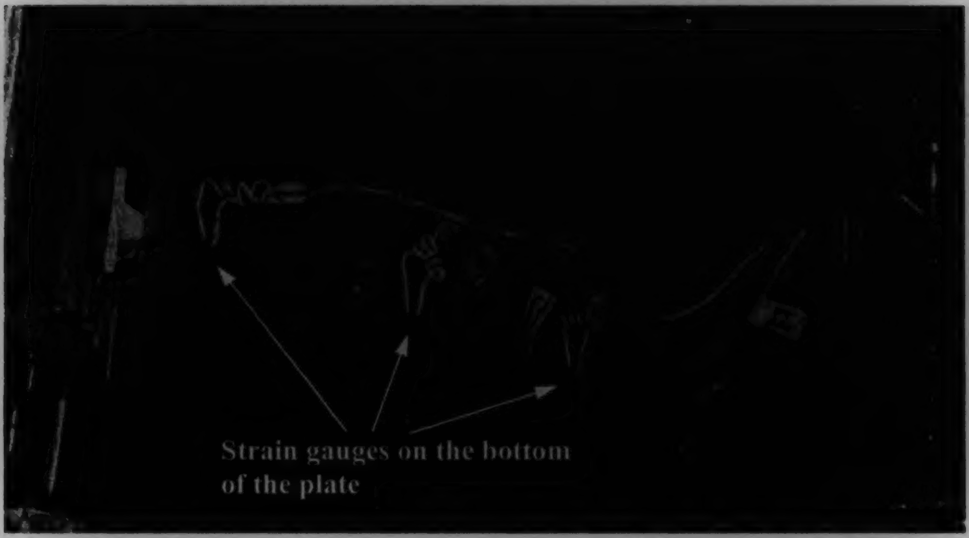
Strain gauges on the bottom of the plate

(b) Rear View

Figure 3.12 Positions of Strain Gauges on Specimen SSP2

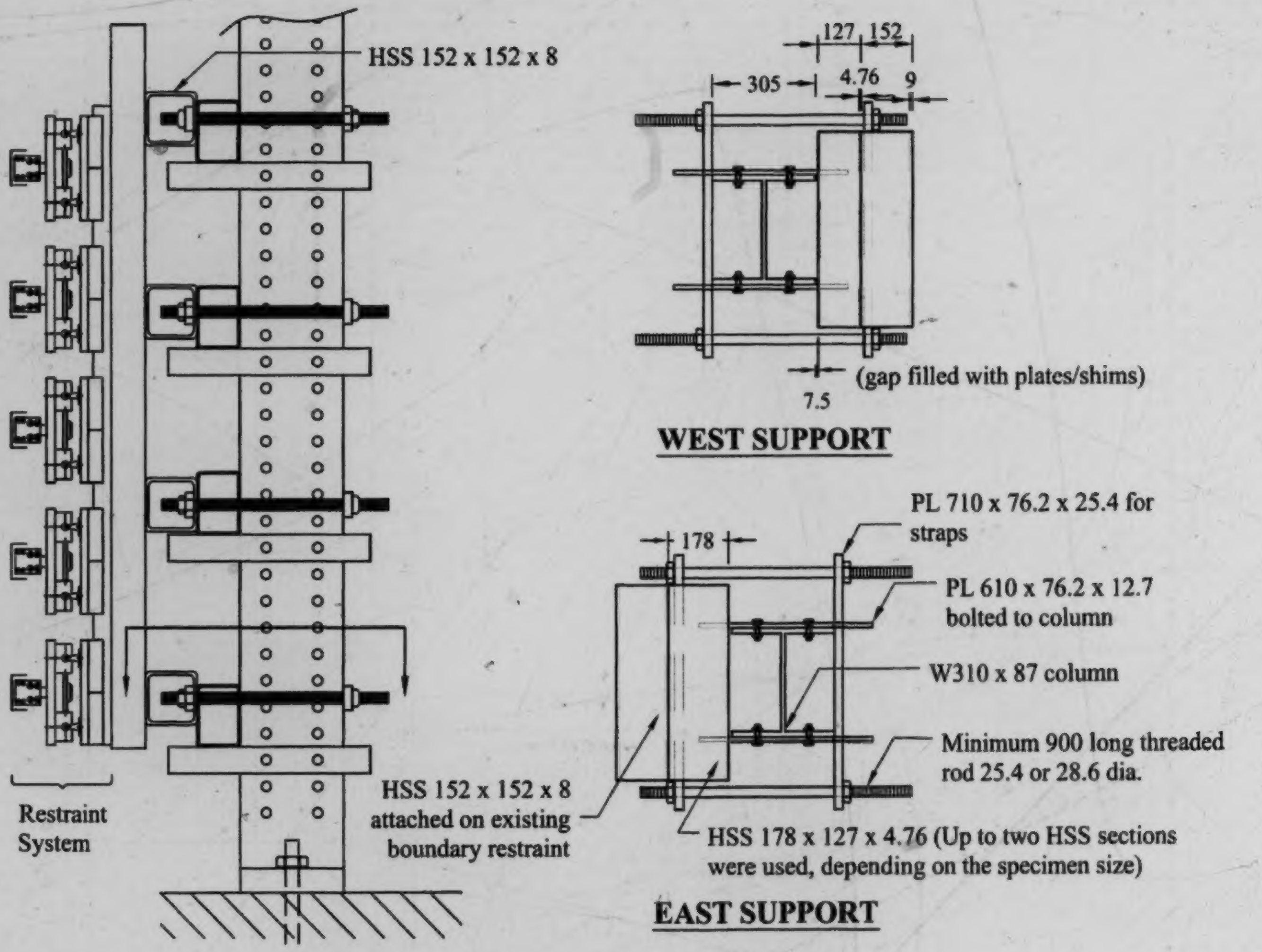
HSS 152 x 152 x 8
Restraint System
HSS 152 x 152 x 8 attached on existing boundary restraint
127
152
305
4.76
9
7.5
(gap filled with plates/shims)
WEST SUPPORT
178
PL 710 x 76.2 x 25.4 for straps
PL 610 x 76.2 x 12.7 bolted to column
W310 x 87 column
Minimum 900 long threaded rod 25.4 or 28.6 dia.
HSS 178 x 127 x 4.76 (Up to two HSS sections were used, depending on the specimen size)
EAST SUPPORT

Figure 3.13 Support Structures for the Edge Restraints

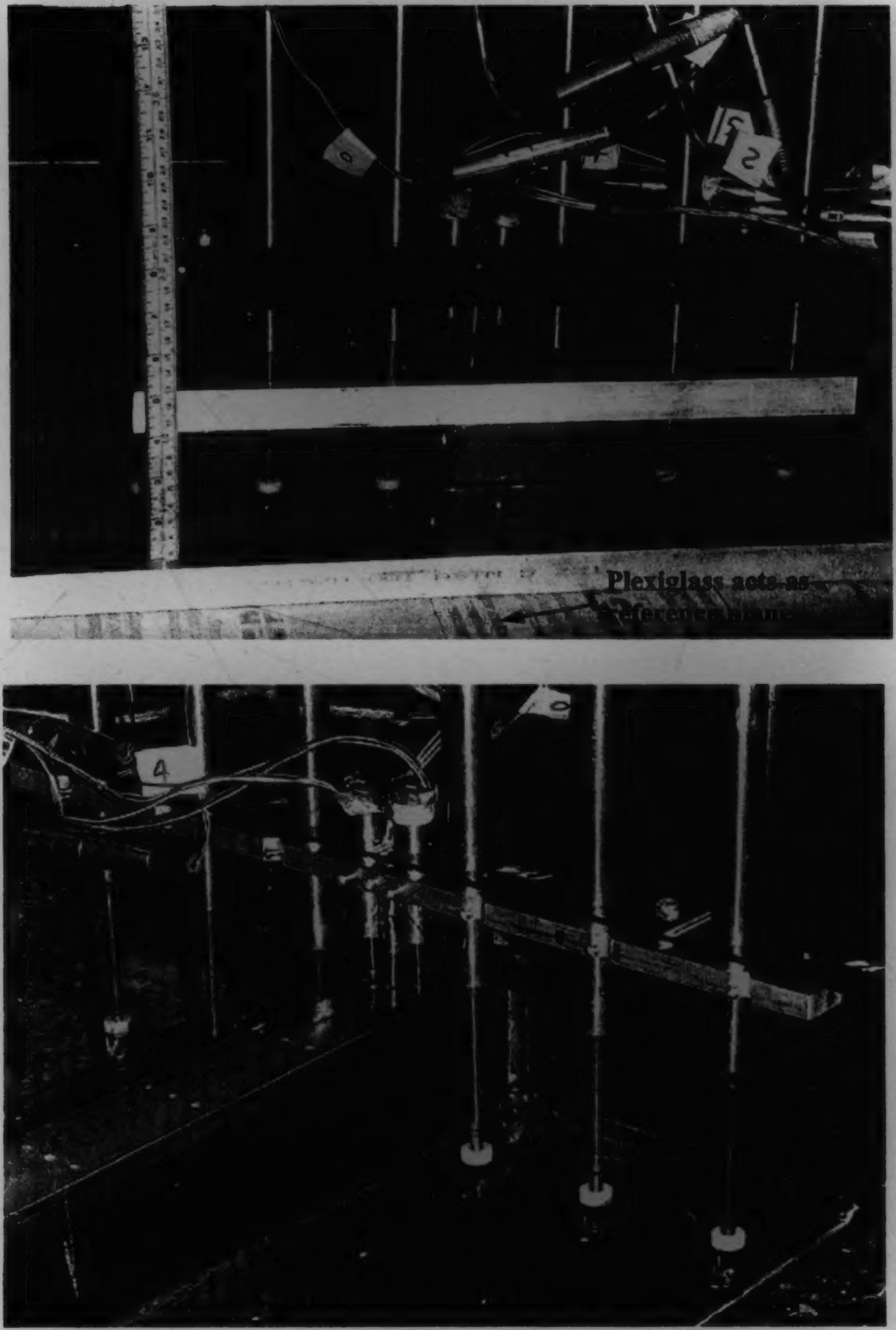
0
1
2
3
Plexiglass acts as
reference plane
4
0

Figure 3.14 Layout of the Vertical Transducers for Initial Imperfections measurement

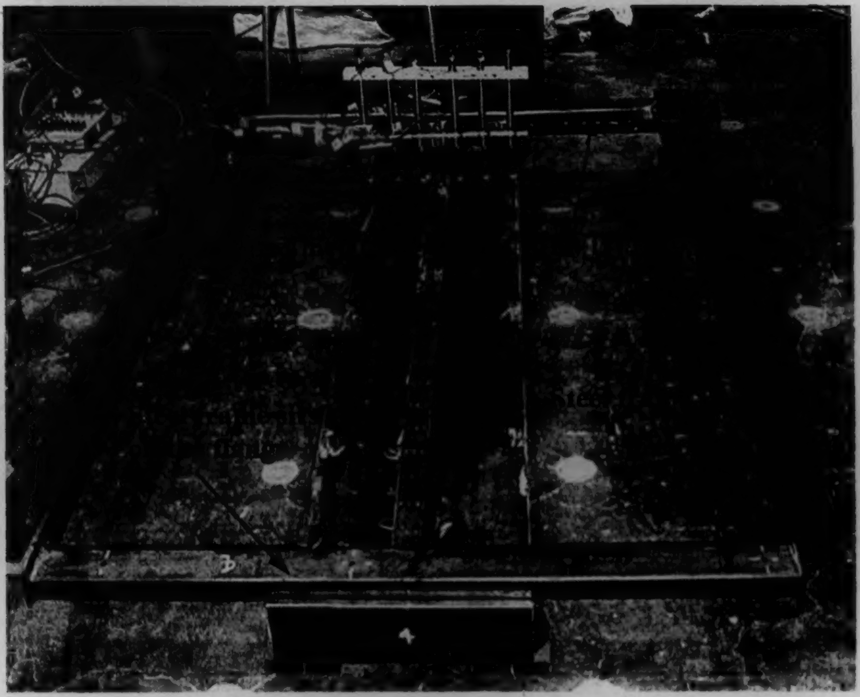

Figure 3.15 Measurement Setup for Flange and Plate Initial Imperfection

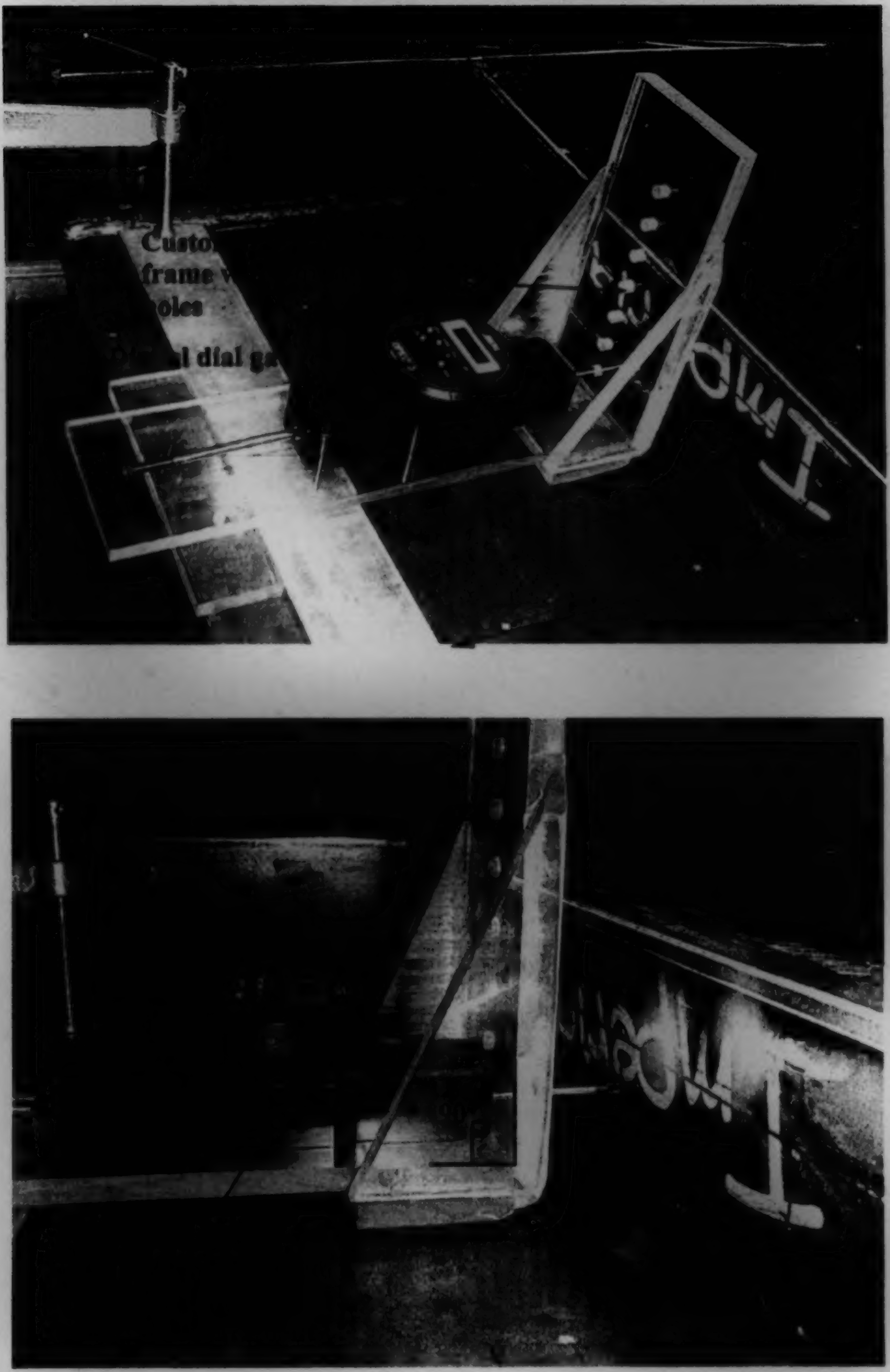
Custo
frame w
holes
al dial ga

Figure 3.16 Plexiglass Frame for Measuring Initial Imperfections in the Web

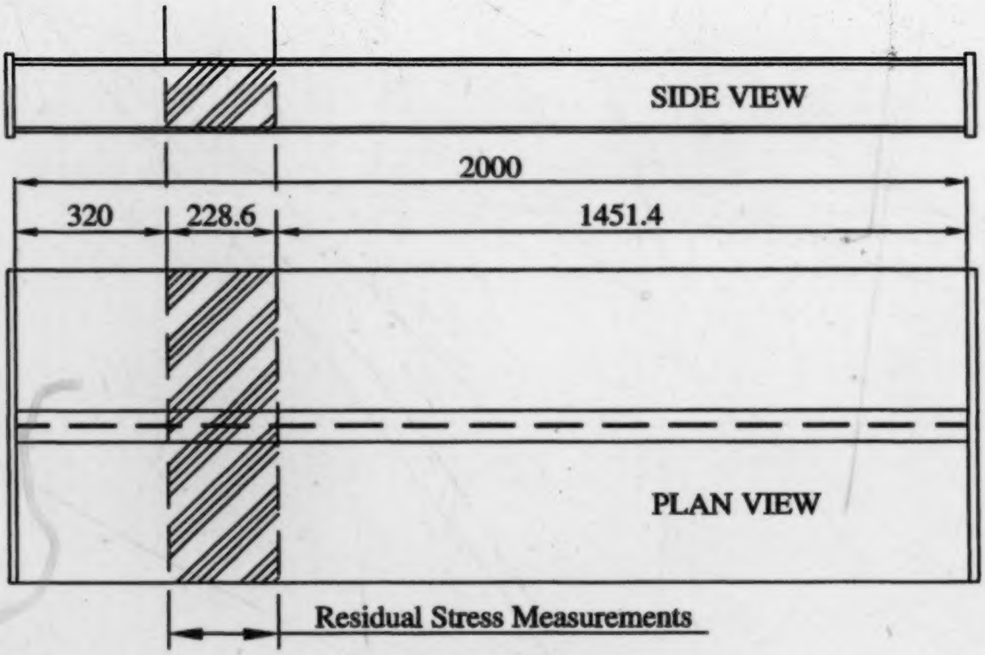
SIDE VIEW
2000
320
228.6
1451.4
PLAN VIEW
Residual Stress Measurements

Figure 3.17 Location of Residual Stress Measurements

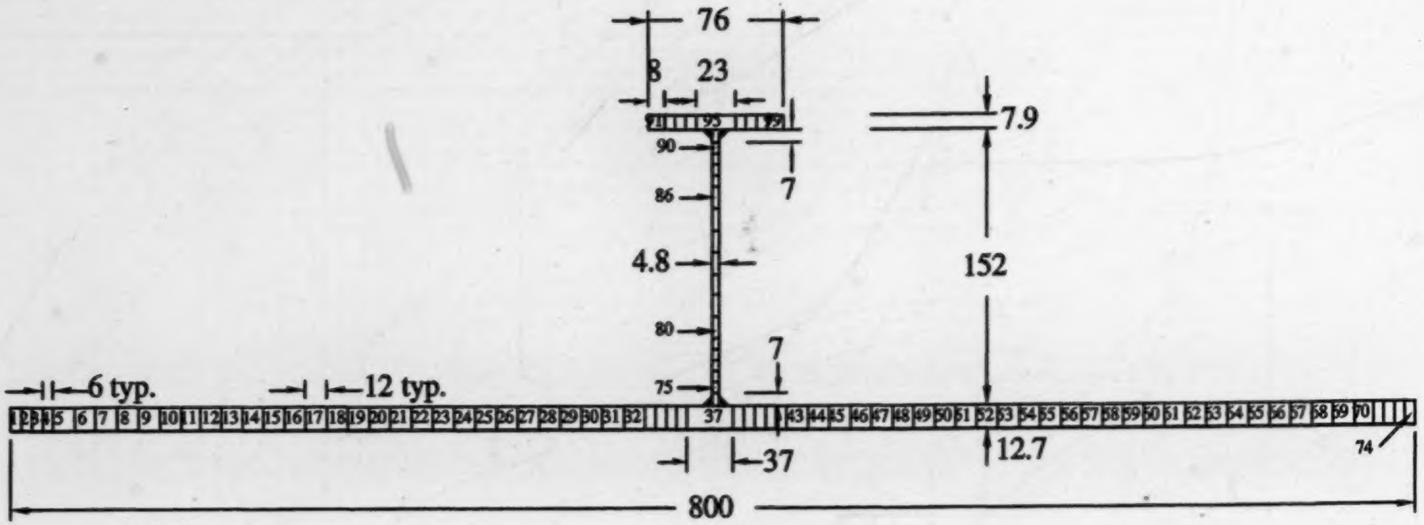
76
8
23
7.9
7
90
86
4.8
152
80
7
75
6 typ.
12 typ.
37
37
12.7
74
800

Figure 3.18 Residual Stress Strips Layout

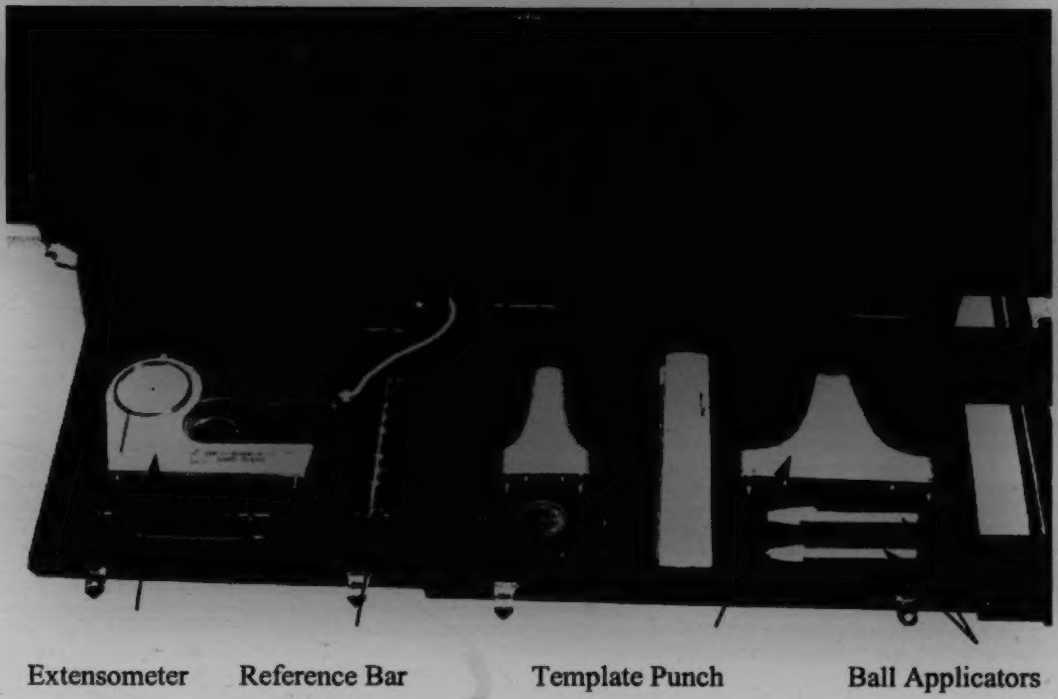
Extensometer
Reference Bar
Template Punch
Ball Applicators

Figure 3.19 Bam-Setzdehnugsmesser Mechanical Extensometer for Residual Stress Measurements

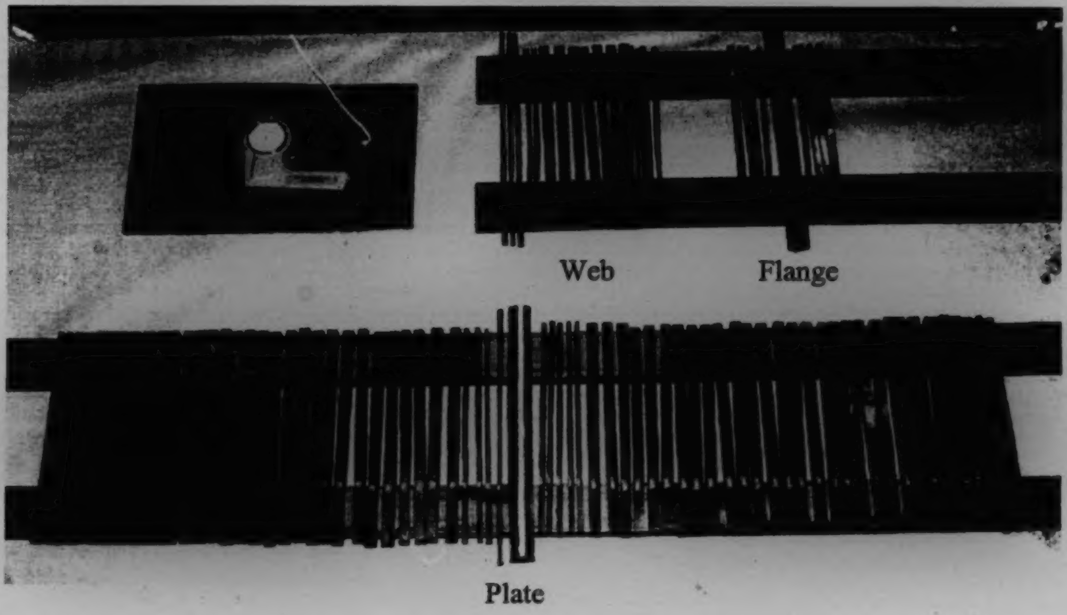
Web
Flange
Plate

Figure 3.20 Residual Stress Strips after Sectioning

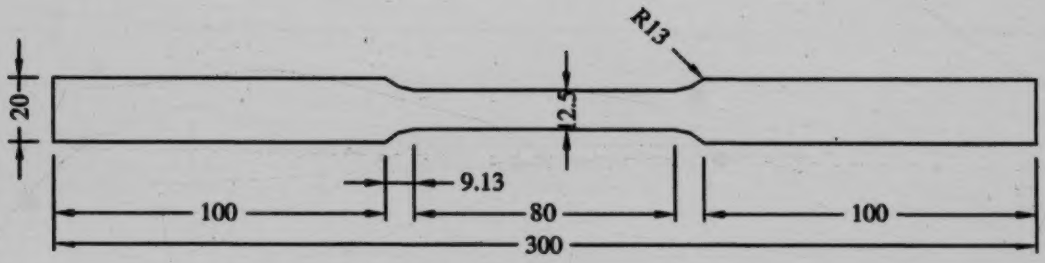
R13
20
12.5
9.13
100
80
100
300

Figure 3.21 Material Coupon Dimensions

**(Refer to Table 3.3 for the various thickness of plates used in the test specimens)**

# 4 Experimental Results

## 4.1 General

Compression tests on four large-scale stiffened steel plate panels with tee stiffeners were performed as described in Chapter 3. This chapter describes the data collected and the observations made during the tests. The restraint system from the experimental study of Grondin *et al.* (1999) was used in this research. There were concerns about damaging the edge restraint fixtures due to the fact that the plate thickness of specimen SSP1 presented in Chapter 3 was thicker than that of the plate specimens tested by Grondin *et al.* (1999). Although the safety factor on the bearings was sufficiently large to accommodate the larger plate thickness, to be on the safe side, the test program started with the specimens with smaller plate thickness in the following sequence: SSP2, SSP3, SSP4 and SSP1.

## 4.2 Material Properties

Elastic modulus, static and dynamic yield stresses, strain hardening modulus, static and dynamic ultimate stresses, strain at ultimate stress, and rupture strain are given in Table 4.1. The values in Table 4.1 are the mean values of three coupons cut from each plate. These results are modified into true stress and true strain for the finite element analysis in Chapter 5.

A typical stress-strain curve (6.3 mm plate) is shown in Figure 4.1. The strain hardening modulus, $E_{sh}$, was obtained from the initial slope of the stress-strain curve at the start of the strain hardening as illustrated in Figure 4.1. The stress-strain curve for the 7.9 mm plate (Figure 4.2) is different from the rest because it does not have a well defined yield plateau. Hence, the yield strength of the 7.9 mm plate was determined by the 0.2 percent offset method on the static stress-strain curve, which was obtained by stopping the testing machine and maintaining the strain constant until the load had stabilised. Because of the nature of the 7.9 mm plate, its strain hardening modulus was determined from the slope of the curve just beyond the dynamic yield. A detailed summary and stress versus strain diagrams for each coupon test are presented in Appendix A.

The coupon test results confirmed that most plates were made of hot-rolled steel. Variation of less than 3 percent from the nominal 200 000 MPa elastic modulus were found among the coupons. Of all the steel plates, the 3.0 mm plate had the lowest static yield strength at 200 MPa, which is far from the static yield strength of typical 300W steel. On the other hand, the 3.4 mm plate has a mean static yield strength of 283 MPa. Due to the unavailability of mill certificates, confirmation of steel grade with the fabricator was inconclusive.

### 4.3 Initial Imperfections

The initial out-of-plane imperfections of the test specimens were measured before testing. These measurements included the initial imperfections of the plate, web, and flange. The measured initial imperfections were incorporated in the finite element analysis to provide a better representation of the actual test specimens in the analysis. Using the commercial mapping software Surfer version 8.0 Surface Mapping System, the measured initial imperfection data were mapped onto the finite element mesh for each test specimen. These plots of initial imperfections in the plate, web and flange of specimen SSP4 are shown in Figure 4.3. The initial imperfections of the other test specimens are presented in Appendix B. A summary of the measured initial imperfections is tabulated in Table 4.2. The maximum out-of-straightness ($u_1$) of all the test specimens was approximately 3.2 mm. The absolute maximum out-of-plane imperfections were 9 mm and 6.8 mm for the plate ($u_2$) and the flange ($u_3$) respectively. The absolute maximum out-of-straightness of the web ($u_4$) was 2.2 mm at the web-to-plate junction and 6 mm ($u_5$) at the web-to-flange junction.

An examination of the measured initial imperfections indicates larger plate distortion near the ends and along the stiffener-to-plate junctions. Table 4.3 presents a comparison between the maximum plate initial imperfection, $\delta_{pmax}$, divided by the plate thickness, $t_p$, with the three levels of initial imperfections proposed by Smith *et al.* (1991). The comparison shows that all the plates, except for SSP2, had initial imperfections between average and severe. The initial imperfections in SSP2 are relatively small and just exceed the level classified as "slight" by Smith *et al.*

## 4.4 Residual Stresses

Residual stresses were measured in a test specimen fabricated to the same specifications as specimen SSP1. The residual stresses shown in Figure 4.4 were calculated using the mean modulus of elasticity from the plate, web and flange coupon test data, namely, 204 000 MPa, 202 000 MPa and 196 000 MPa. Tensile residual strains in excess of the yield strain were measured at the plate-to-web and flange-to-web junctions and along the flame cut edges of the plate due to higher strength of the weld. Compressive residual stresses of less than 20 % of the yield strength were measured in the plate and the web but about 50 % of yield were observed in the flange. Unlike the residual stress pattern in Figure 2.2, the measured residual stresses were more irregular.

In order to assure the accuracy of the measurement, one must look at the equilibrium of the residual stresses distribution; which is done by calculating the integral of the residual stresses over the entire cross-section. The ratio of unbalanced axial force over yield strength of the cross-section is 2.8 %. The ratio of the unbalanced moment to yield moment of the cross-section is 0.8 %. Ideally these ratios should be zero but the obtained values are considered small and within the accuracy of the method used to measure the residual stresses. Therefore, equilibrium is satisfied and the measurements are valid.

## 4.5 Test Results

Four stiffened steel plate panels were tested under axial load with a small eccentricity as described in Chapter 3. The data collected during the uniaxial compression tests are described in this section. A comparison of the test results with the finite element analysis and the design practices is presented in Chapter 5.

Interaction buckling and stiffener tripping were the two modes of failure observed in the tests. A summary of the failure load and the observed failure mode for each test specimen is presented in Table 4.4. Specimen SSP1 had the highest capacity as expected since it was the largest of the four specimens. Except for SSP2, all specimens were tested with a small load eccentricity towards the plate to avoid stiffener tripping failure. Specimen SSP2 was inadvertently loaded with an eccentricity of 3 mm towards the flange, which was the primary cause of the stiffener tripping failure in SSP2. The following test results are presented in the sequence of the testing order. Test specimen SSP2 was tested first, followed by SSP3, SSP4, and SSP1.

### 4.5.1 Specimen SSP2

Under an increasing axial load, the specimen gradually bent towards the stiffener, and eventually failed by stiffener tripping. The plot of the out-of-plane deformations of the plate, shown in Figure 4.5, provides a history of the buckling behaviour of the specimen. Unlike plate buckling behaviour, both east and west sides of the plate bent towards the stiffener as the load increased. Once the specimen reached its failure load, tripping of the stiffener occurred, which resulted in a sudden drop in load carrying capacity. A straight edge was held against the specimen (see Figure 4.6) after the failure of the test specimen, to assess the extent of local distortion of the stiffener resulting from rotation of the stiffener about the stiffener-to-plate junction. SSP2 was the only specimen that failed in this mode. As mentioned earlier, this failure mode was unexpected because the preliminary finite element analysis in Chapter 3 had predicted that SSP2 would fail by interaction buckling. This finding is discussed in the next chapter.

Figure 4.7 shows the axial load versus out-of-plane rotation at the top and bottom ends of the specimen. A small sketch on the top left corner of the figure indicates the buckling direction of the specimen. This plot confirms that the specimen was loaded symmetrically.

Test specimen SSP2 failed by stiffener tripping, followed by a sudden loss of capacity, as illustrated in the load versus axial deformation curve shown in Figure 4.8.

The response diagram shows the relationship between the axial load provided by the MTS machine and the axial displacement of the specimen in the 1-direction ($u_1$) of SSP2. The plot is consistent with the stiffener tripping failure mode introduced in Chapter 1 and Chapter 2. Yielding of the stiffener was detected at the mid-span of the specimen by the strain gauges before the peak load. The collapse of the specimen was so sudden that the data acquisition system was unable to capture the behaviour during the drop. Upon unloading, the specimen did not follow a path parallel to its elastic regime; instead, a path with shallower slope was taken. Note that no indication of plate yielding was found in the mid-span of SSP2

Figure 4.8 also compares the load applied to the test specimen, as measured by the testing machine at the top of the specimen, to the reaction force measured by two load cells at the base. The excellent agreement between the MTS load and the reaction forces measured with load cells indicate that no significant vertical friction existed in the edge restraint devices.

### 4.5.2 Specimen SSP3

For a better understanding of the failure behaviour of SSP3, the axial load versus axial deformation of the specimen (Figure 4.9) is divided into four segments: an initial pre-buckling segment (OA), a first stable post-buckling segment (AB), an unstable post-buckling segment (BC) and a second stable post-buckling segment (CD). In the pre-buckling segment (OA), initial imperfections were amplified when loading was first applied (Figure 4.10). As the buckling capacity was approached, the plate gradually changed shape to adopt its lowest energy shape. The plot also reveals two half-sine waves along the specimen. Point A on the load versus deformation curve corresponds to the onset of plate bucking. This can be defined by an initiation of diverging behaviour observed in the strain gauge results (Appendix C) and out-of-plane deformations as measured by LVDT's (Appendix D). The location of point A was determined from the LVDT data at approximately 1100 kN. This is very close to the peak load (1160 kN) reached at an axial deformation of 4.4 mm. Within the first stable segment, the amplitude of the plate buckles continued to enlarge at a faster pace as point A was approached.

Local yielding in the plate was found at mid-span according to the strain gauge results, immediately after point A. Yielding of the flange was detected just before point B. Meanwhile, the load carrying capacity gradually decreased then reached a turning point (point B), at which the specimen experienced an abrupt loss in capacity. At this point, overall buckling overcame the plate buckling mode while the specimen bent instantaneously towards the plate with a loud bang. This tremendous energy release overcame the elastic buckling waves developed in the plate buckling mode. As a result, the waves became almost unnoticeable after the overall buckling failure. The change in the plate configuration is well illustrated in Figure 4.10, as one compares the difference between the sets of out-of-plane reading at an axial deformation of 4.4 mm and at 6.2 mm (point C). By the end of the test, large permanent deformations were observed as shown in Figure 4.11. Since the stiffener was on the tension side of the specimen, SSP3 failed by plate-induced overall buckling, following the plate buckling mode. Unlike the typical plate buckling failure mode, interaction buckling has dramatically reduced the post-buckling capacity of the specimen. A reduction of more than 70 % of the peak load was observed in the unstable post-buckling segment (BC). The failure behaviour of specimen SSP3 was consistent with the general understanding of interaction buckling as described in Section 1.2. The axial load versus end rotation curves for each end of the test specimen showed symmetrical behaviour of the test specimen (see Figure 4.12).

### 4.5.3 Specimen SSP4

As expected, specimen SSP4 also exhibited the characteristic response of an interaction buckling failure. Its response was similar to that of SSP3 since SSP4 was designed from the same set of β-values. Figure 4.13 indicates that the load versus axial deformation behaviour for SSP4 is very similar to that of SSP3 (Figure 4.9). As shown in Figure 4.14, initial imperfections along the specimen were amplified before the lowest buckling mode shape was adopted. Two half-sine waves were observed as the axial load approached the peak load. According to the Appendix C and Appendix D, point A in Figure 4.13 is located at 1840 kN, which is just before a peak load of 1940 kN. With a thicker plate, SSP4 was capable of achieving a higher capacity than SSP3. No drastic snap through action was observed at point B. The drop in capacity of SSP4 was relatively quiet and slow. Unlike SSP3, small amplitude plate buckling waves remained visible along the plate edge of SSP4 after the drop in capacity, as shown in Figure 4.15. The differences could be caused by the stockier plate and the plastically deformed buckling waves along the plate edges. Because of these two factors, it is suspected that higher energy was required to alter the wave direction, which resulted in a much gradual response. At the start of the second stable post-buckling regime (point C), SSP4 was able to retain about 35 % of its peak strength. Again, perfect symmetry was found in the end rotation response (see Figure 4.16).

### 4.5.4 Specimen SSP1

Compared to SSP3 and SSP4, specimen SSP1 had the most stable and ductile post-buckling response (see Figure 4.17). SSP1 only exhibited one half-sine wave along its length, (Figure 4.18). Flaking of mill-scale was visible as the magnitude of the plate buckle waves increased. It was a good indication of plate yielding after plate buckling started. There was no abrupt drop in load carrying capacity. Although the specimen had undergone large axial deformation, the buckling waves remained largely visible at the end of the test, as shown in Figure 4.19.

Even though SSP1 failed by interaction buckling, the failure behaviour of the specimen was much more stable than observed for SSP3 and SSP4. Moreover, point A (corresponding to plate buckling) and point B (corresponding to onset of overall buckling) cannot be clearly located on the load versus deformation curve presented in Figure 4.17. According to the behaviour of SSP3 and SSP4, point A is located in the vicinity of the peak load and before the yielding of the plate while point B is typically found at the onset of a sudden drop in capacity. However, the peak load for SSP1 was observed well after plate yielding according to the strain measurements. There was no obvious sharp drop in buckling capacity. Thus, the determination of points A and B must be defined from the observations in Appendix C and Appendix D. Based on the indication from the strain gauge results and the out-of-plane deformation measurements, point A should be positioned at 1400 kN. Point A is much lower than point B as compared to the behaviour observed in SSP3 and SSP4. However, plate buckling behaviour and yielding of the plate was indeed detected at 1400 kN. Point B is found to be at the peak load, 1940 kN, since reversal of stress was identified in the strain gauge results, which indicates overall buckling of the plate.

After plate yielding occurred, some of the load started to be distributed to the stiffener as the load increased. Because SSP1 had a stockier stiffener than SSP4, this enabled the specimen to sustain more load before and during overall buckling took place.

A comparison between the responses of other failure modes illustrated in Figure 2.3 can also verify that SSP1 indeed failed by interaction buckling. According to these load versus axial deformation curves, typical overall buckling mode indicates a stable post-buckling response while plate buckling results in a slight loss in strength. Although buckling towards the plate was observed, SSP1 did not fail by plate-induced overall buckling alone because it has a significant load reduction in the post-buckling range. In addition, this drop in load carrying capacity of SSP1 went further than a typical plate buckling mode. Beyond point B, the load slowly dropped to almost 40 % of the peak. This is a significant reduction in strength compared to the slight drop typically observed from plate buckling. Combining the evidences in the observation and the load-deformation response, it can be concluded that specimen SSP1 failed by interaction buckling.

As shown in Figure 4.20, SSP1 experienced some lack of symmetry starting from the start of the testing. This may be because the top and bottom supports were not aligned and the initial imperfections existed in the specimen. In addition, the crest of the one half-sine wave buckling shape was further up from the mid-span of the specimen, as shown in the Figure 4.18. This also caused more rotation at the top end than at the bottom end.

Table 4.1 Material Properties

| Plate Imperial Designation | Measured Plate Thickness (mm) | Modulus of Elasticity, E (MPa) | Static Yield Strength, $\sigma_{sy}$ (MPa) | Dynamic Yield Strength, $\sigma_{dy}$ (MPa) | Strain Hardening Modulus, $E_{sh}$[1] (MPa) | Static Ultimate Strength, $\sigma_{su}$ (MPa) | Dynamic Ultimate Strength, $\sigma_{du}$ (MPa) | Ultimate Strain (%) | Rupture Strain (%) |
|---|---|---|---|---|---|---|---|---|---|
| **11 Ga** | **3.0** | 206000 | 200 | 215 | 1390 | 317 | 336 | 24.2 | 46.0 |
| **10 Ga** | **3.4** | 191000 | 284 | 297 | 1380 | 357 | 380 | 18.8 | 39.1 |
| **3/16"** | **4.8** | 202000 | 300 | 319 | 1880 | 441 | 467 | 22.2 | 33.2 |
| **1/4"** | **6.3** | 199000 | 330 | 346 | 2410 | 477 | 510 | 20.7 | 35.6 |
| **5/16"** | **7.9** | 196000 | 287[2] | 299 | 4234 | 440 | 469 | 20.0 | 40.2 |
| **3/8"** | **9.5** | 199000 | 402 | 419 | 1420 | 476 | 505 | 17.7 | 38.8 |
| **1/2"** | **12.7** | 204000 | 340 | 354 | 2350 | 475 | 501 | 17.8 | 43.9 |

[1] The strain hardening modulus is illustrated in Figure 4.1 and Figure 4.2 for 7.9 mm plate.

[2] The static and dynamic yield strengths of 7.9 mm plate are determined by the 0.2 % offset method because it did not exhibit a yield plateau (see Figure 4.2).

Table 4.2 Summary of Measured Initial Imperfections

| Specimen | $u_1$ (mm) | $u_2$ (mm) | $u_3$ (mm) | $u_4$ (mm) | $u_5$ (mm) |
|---|---|---|---|---|---|
| **SSP1** | -0.4 to 1.3 | -9 to 3.4 | -1.1 to 4.6 | -0.7 to 1.4 | -6 to 0.1 |
| **SSP2** | 2.4 | 2.4 | 2.6 | 1.9 | 4.1 |
| **SSP3** | 3.2 | 4.5 | 6.8 | 2.2 | 4.0 |
| **SSP4** | 0.6 | 3.7 | 3.1 | 1.3 | 2.1 |

Note: $u_1$ = out-of-straightness of the specimen
$u_2$ = absolute maximum out-of-plane deflection of plate
$u_3$ = absolute maximum out-of-plane deflection of flange
$u_4$ = absolute maximum in-plane off-centre deflection of the web
$u_5$ = absolute maximum in-plane off-centre deflection of the flange

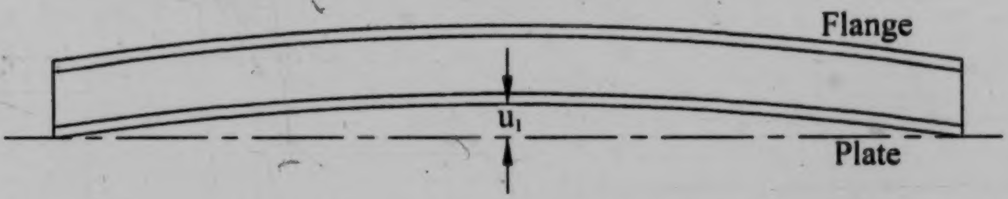

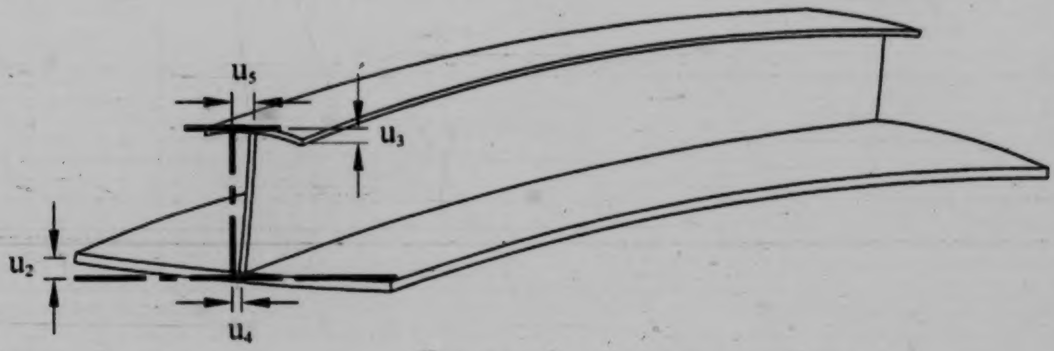

Table 4.3 Comparison of measured initial imperfections with the classification proposed by Smith *et al.* (1991)

| Specimen | Measured $(\frac{\delta_{p_{max}}}{t_p})$ | Plate transverse slenderness, $\beta_1$* | Maximum initial imperfection level by Smith *et al.* (1991) | | |
|---|---|---|---|---|---|
| | | | Slight (= $0.025\beta_1^2$) | Average (= $0.1\beta_1^2$) | Severe (= $0.3\beta_1^2$) |
| **SSP1** | 0.71 | 2.56 | 0.16 | 0.65 | 1.96 |
| **SSP2** | 0.25 | 2.70 | 0.18 | 0.73 | 2.19 |
| **SSP3** | 0.48 | 2.02 | 0.10 | 0.41 | 1.23 |
| **SSP4** | 0.29 | 1.62 | 0.07 | 0.26 | 0.78 |

* $\beta_1$ = Plate transverse slenderness as defined in Section 2.2

Table 4.4 Summary of Test Results

| Specimen | Maximum Axial Load (kN) | Buckling Mode |
|---|---|---|
| **SSP1** | 1940 | Interaction Buckling |
| **SSP2** | 680 | Stiffener Tripping |
| **SSP3** | 1160 | Interaction Buckling |
| **SSP4** | 1890 | Interaction Buckling |

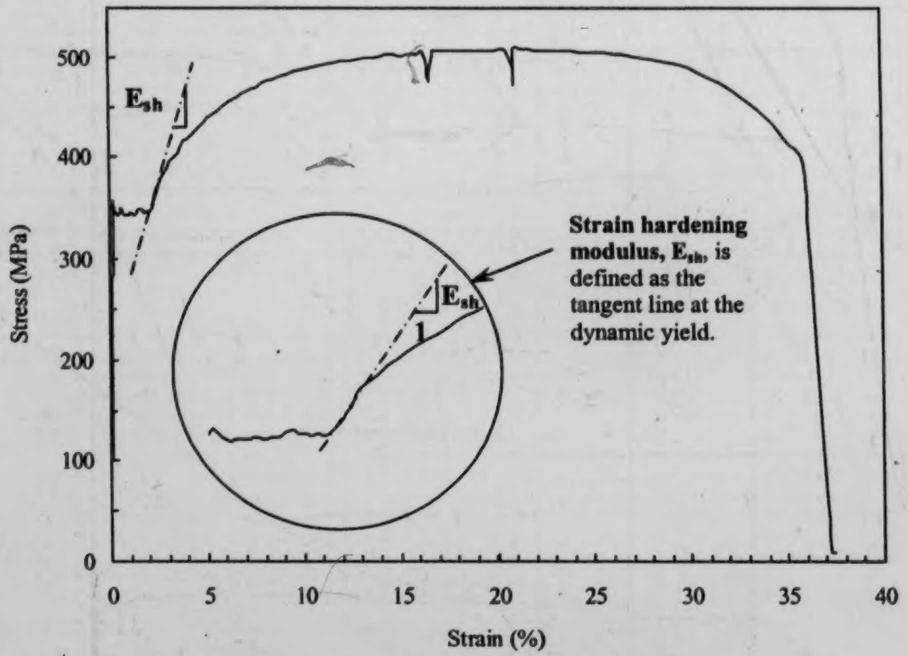

Figure 4.1 Typical Stress versus Strain Curve

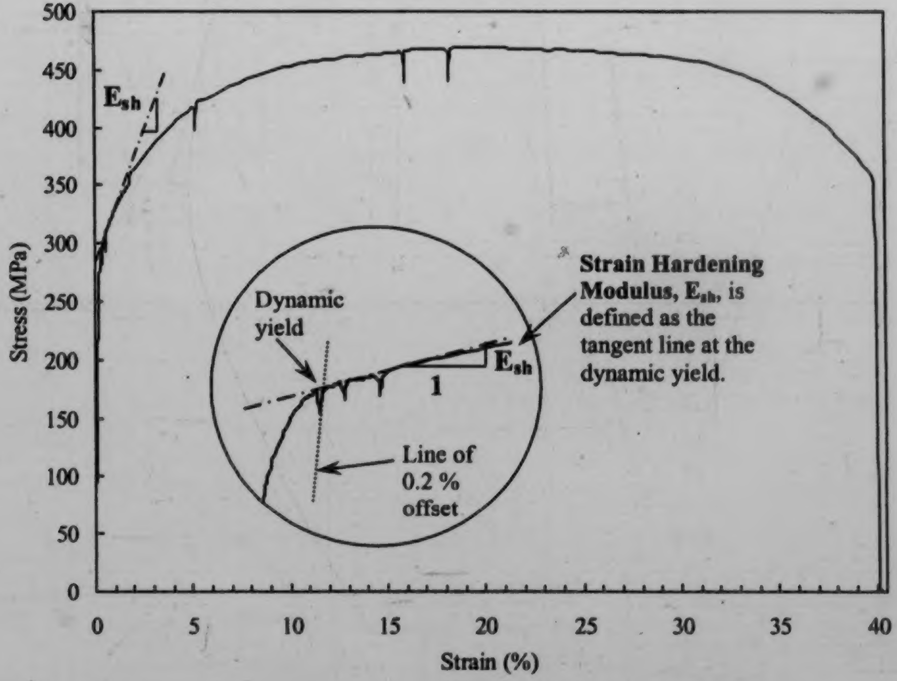

Figure 4.2 Stress versus Strain Curve for 7.9 mm Plate

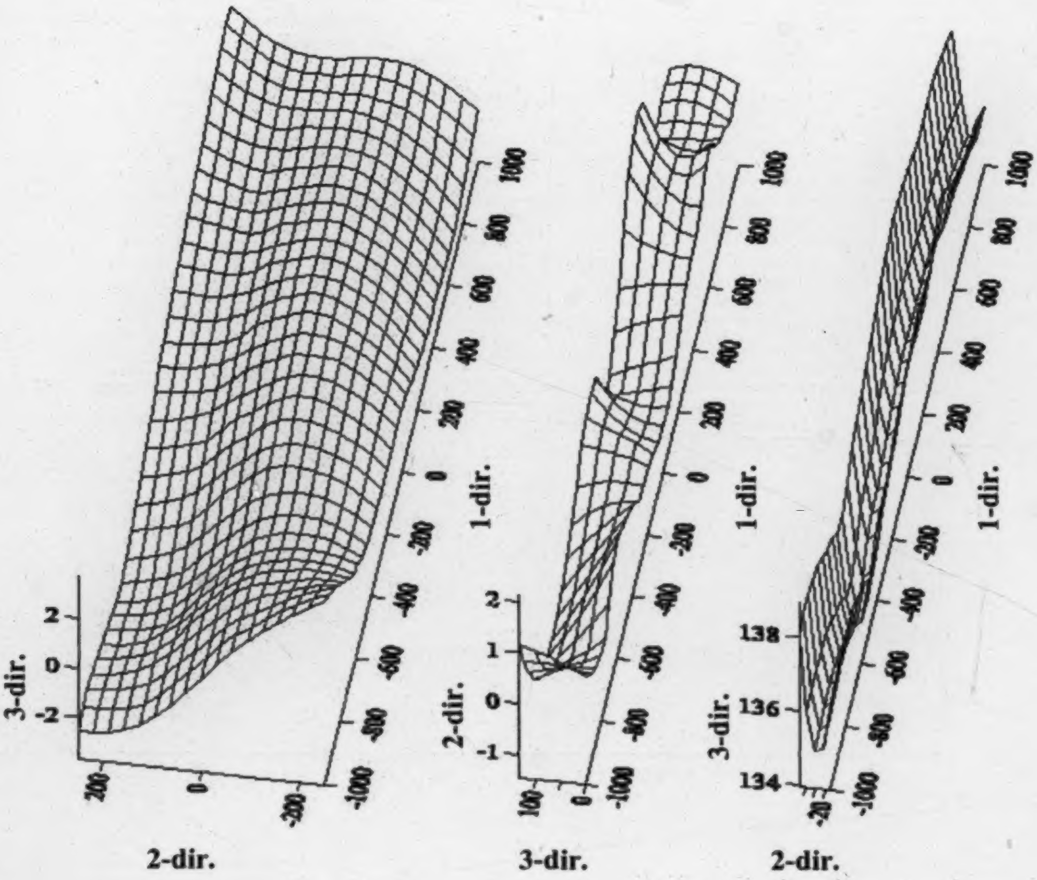

(a) Plate

(b) Web

(c) Flange

Figure 4.3 Measured Initial Imperfections in SSP4

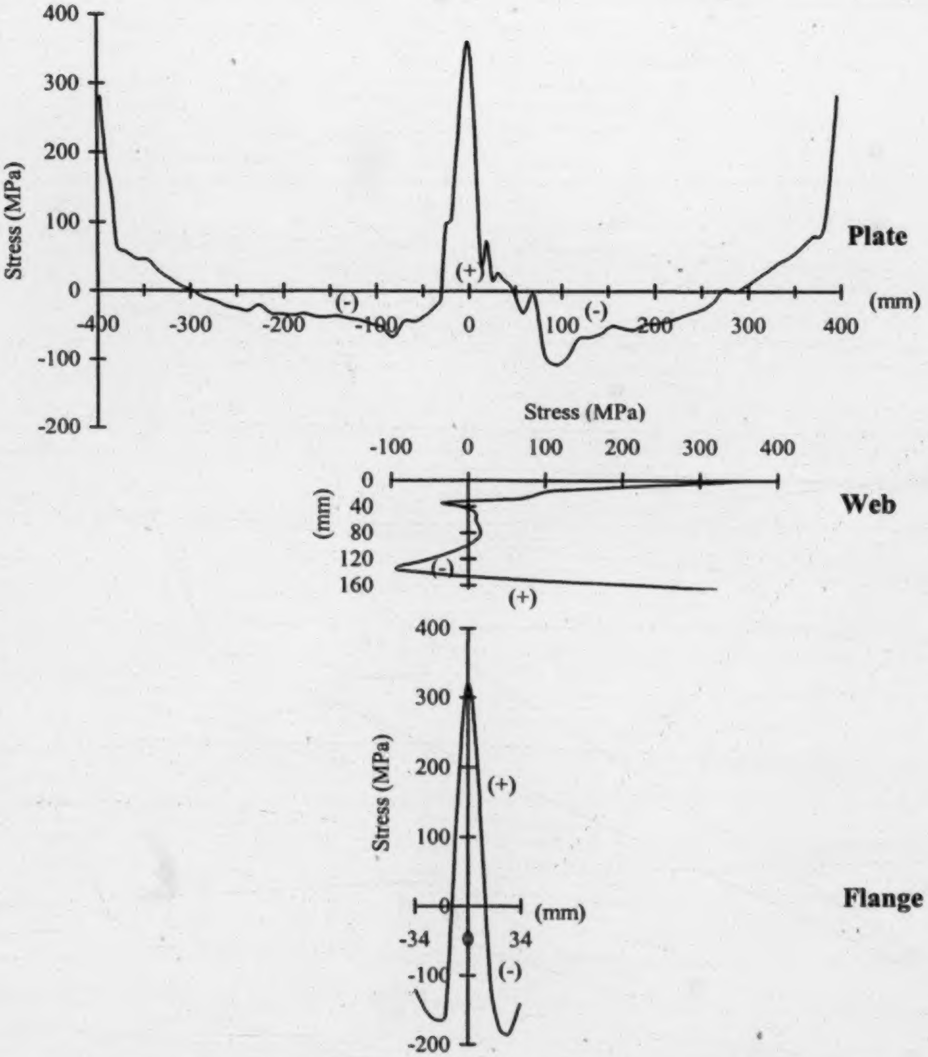

| | | | $\left(\sigma_r / \sigma_y\right)$ |
|---|---|---|---|
| Maximum tensile residual stress | | | |
| at flange-to-web weld = | 320 | MPa | 1.1 |
| at plate-to-web weld = | 360 | MPa | 1.1 |
| at plate edge = | 320 | MPa | 0.94 |
| Average compression stress | | | |
| in plate = | 41 | MPa | 0.12 |
| in web = | 48 | MPa | 0.16 |
| in flange = | 150 | MPa | 0.51 |

Figure 4.4 Residual Stresses in Specimen

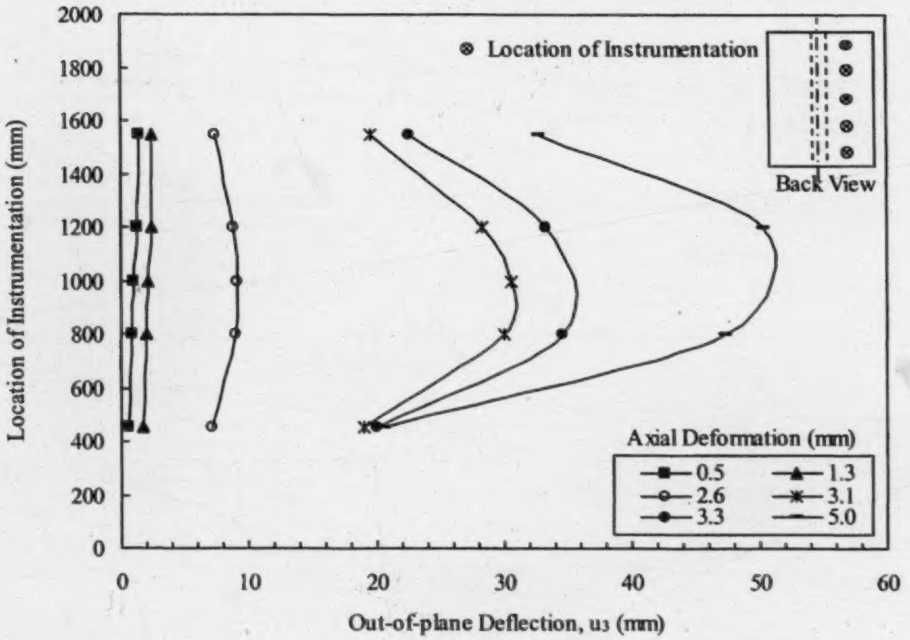

(a) East Side

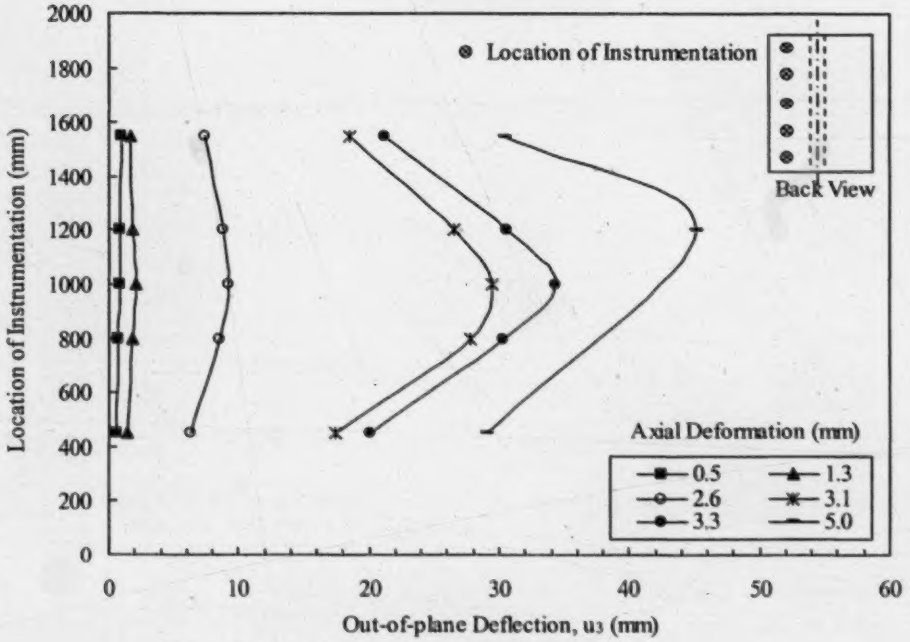

(b) West Side

Figure 4.5 Out-of-plane Deformations of SSP2 Plate at Different Axial Displacements

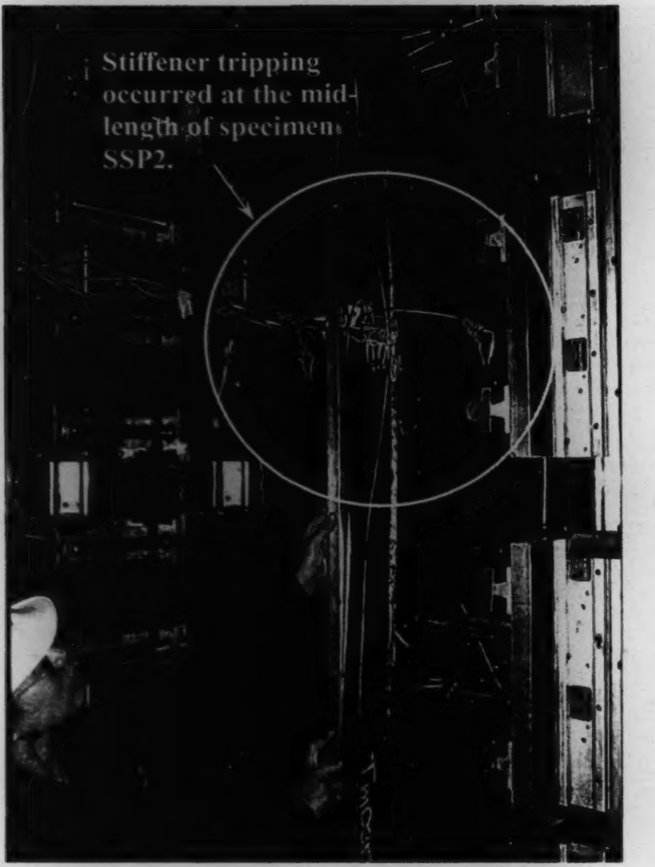
Stiffener tripping occurred at the mid-length of specimen SSP2.

Figure 4.6 SSP2 after Stiffener Tripping

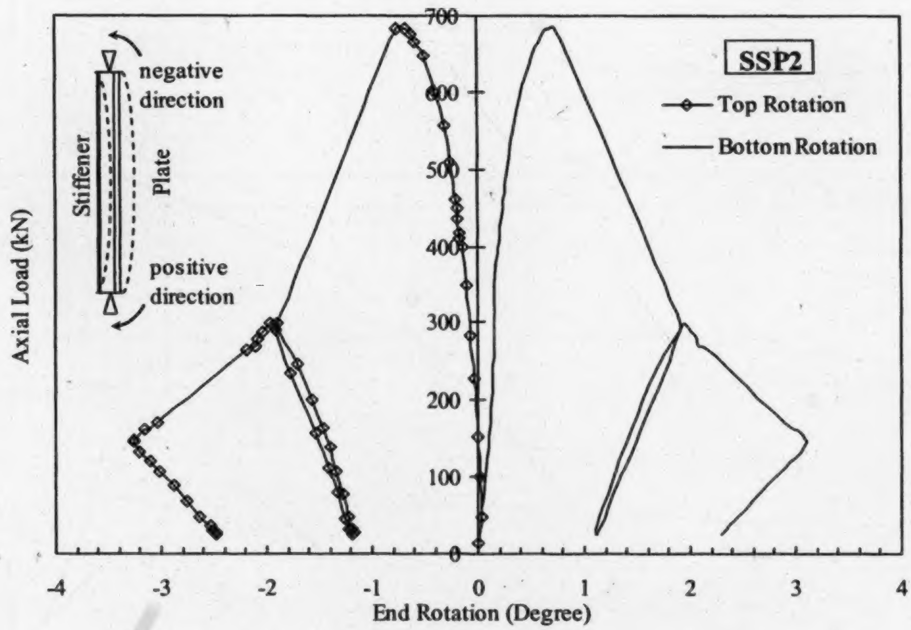

Figure 4.7 Axial Load versus End Rotations for SSP2

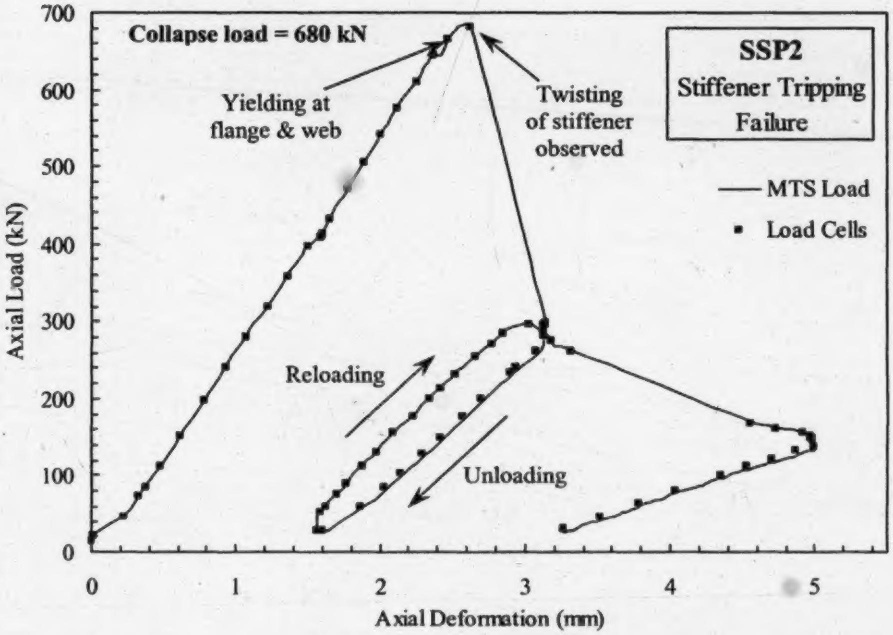

Figure 4.8 Load versus Axial Deformation Curve for Specimen SSP2

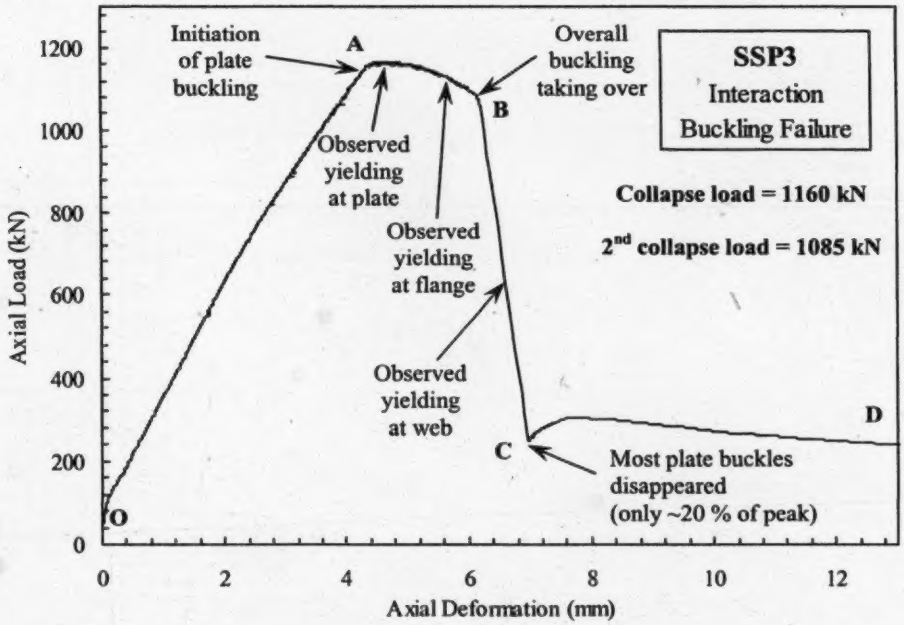

Figure 4.9 Load versus Axial Deformation Curve for Specimen SSP3

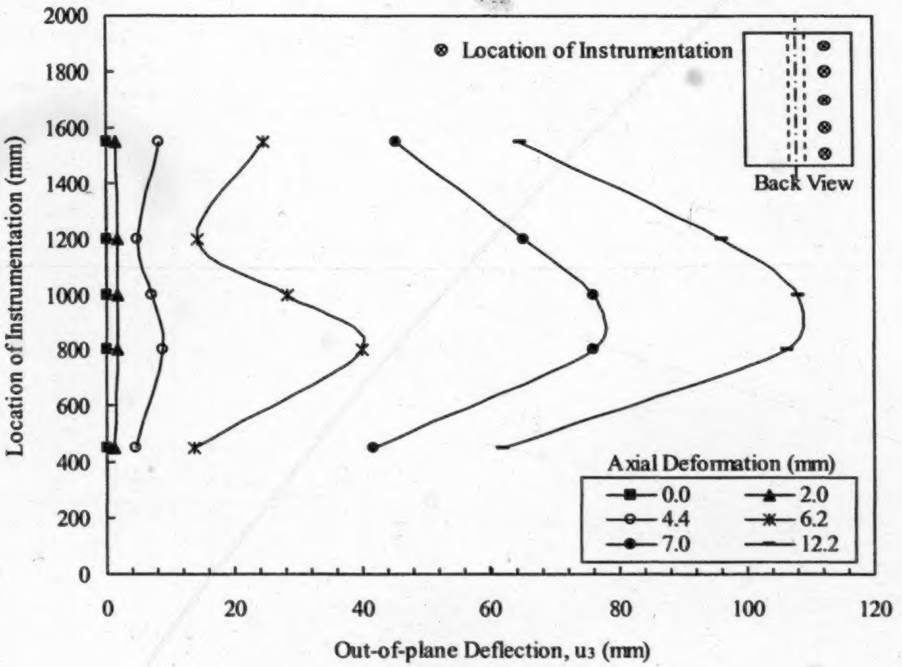

(a) East Side

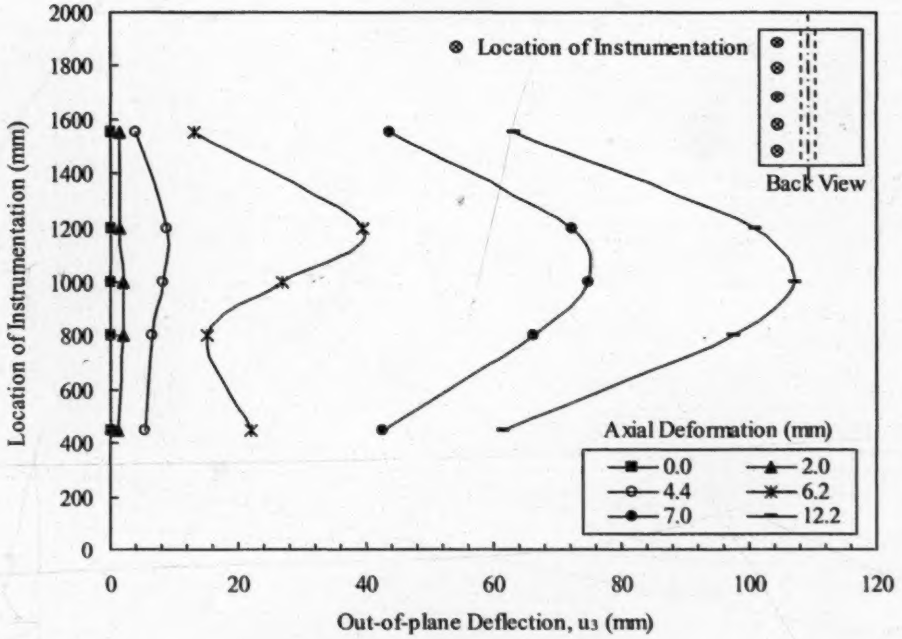

(b) West Side

**Figure 4.10 Out-of-plane Deformations of SSP3 Plate at Different Axial Displacements**

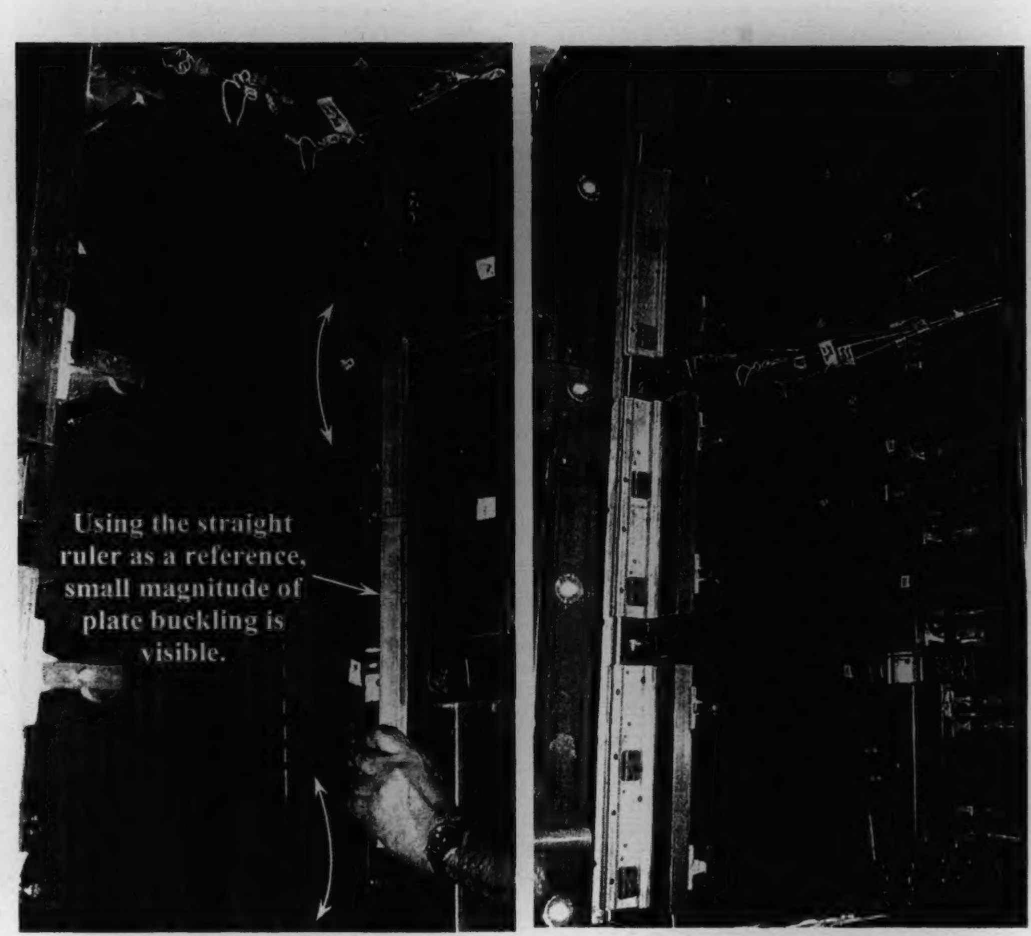
Using the straight ruler as a reference, small magnitude of plate buckling is visible.

(a) During plate buckling (b) During overall buckling

Figure 4.11 Deformed Shape of SSP3

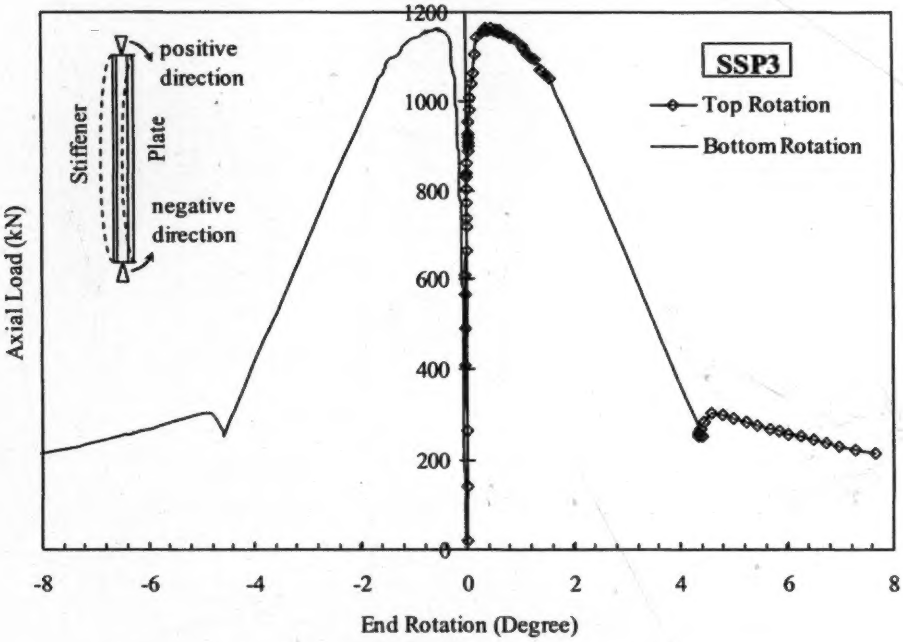

Figure 4.12 Axial Load versus End Rotations for SSP3

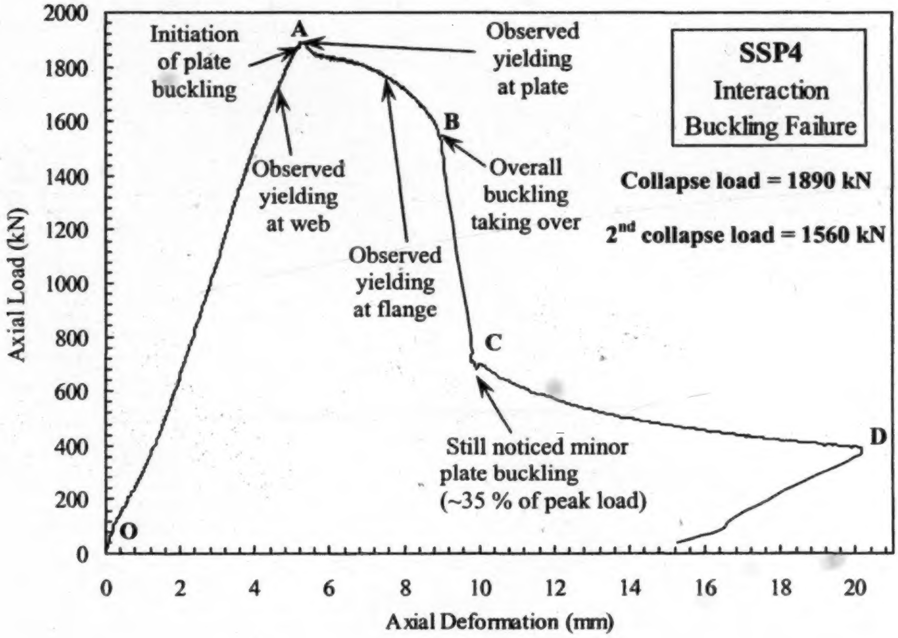

Figure 4.13 Load versus Axial Deformation Curve for Specimen SSP4

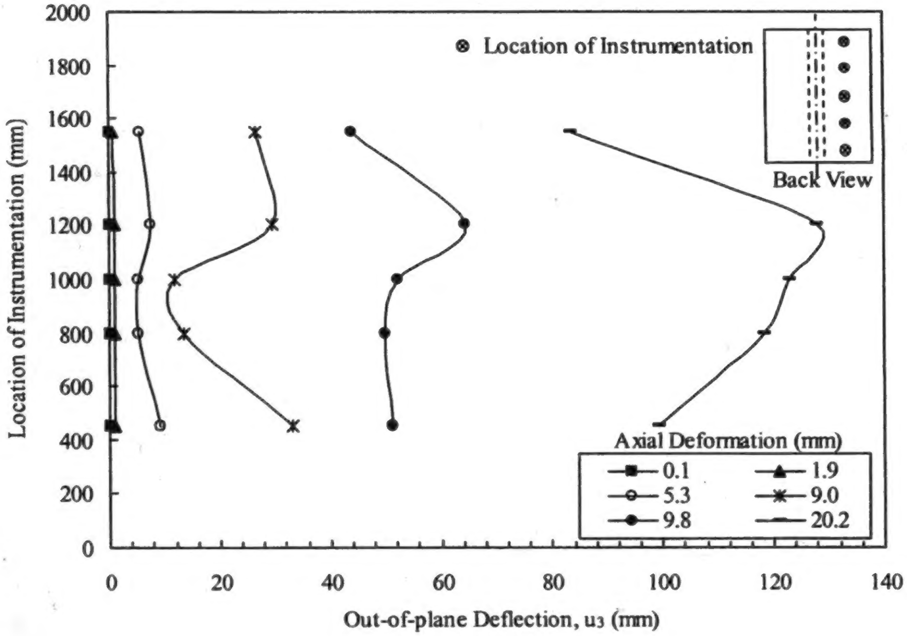

(a) East Side

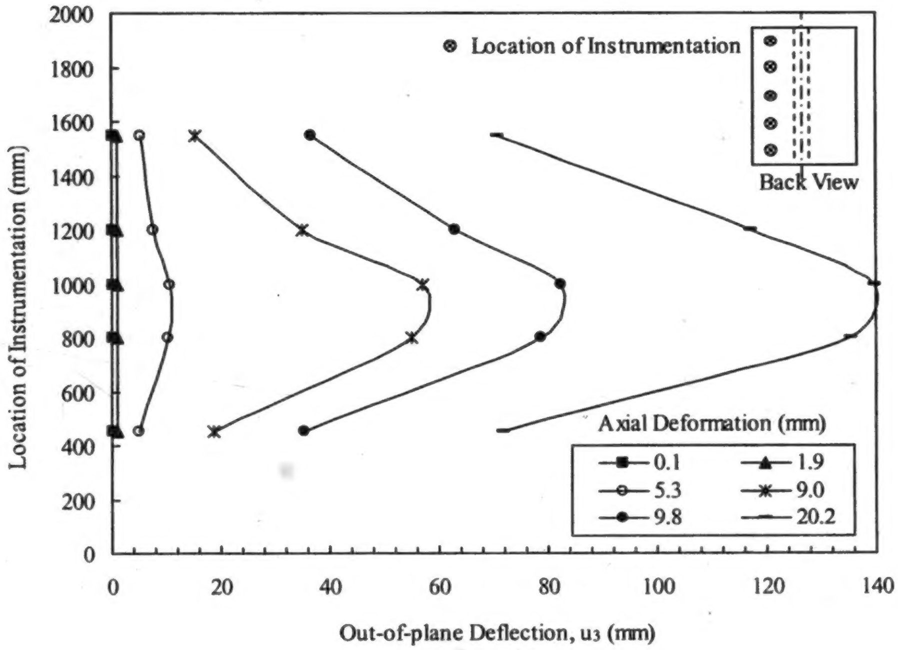

(b) West Side

Figure 4.14 Out-of-plane Deformations of SSP4 Plate at Different Axial Displacements

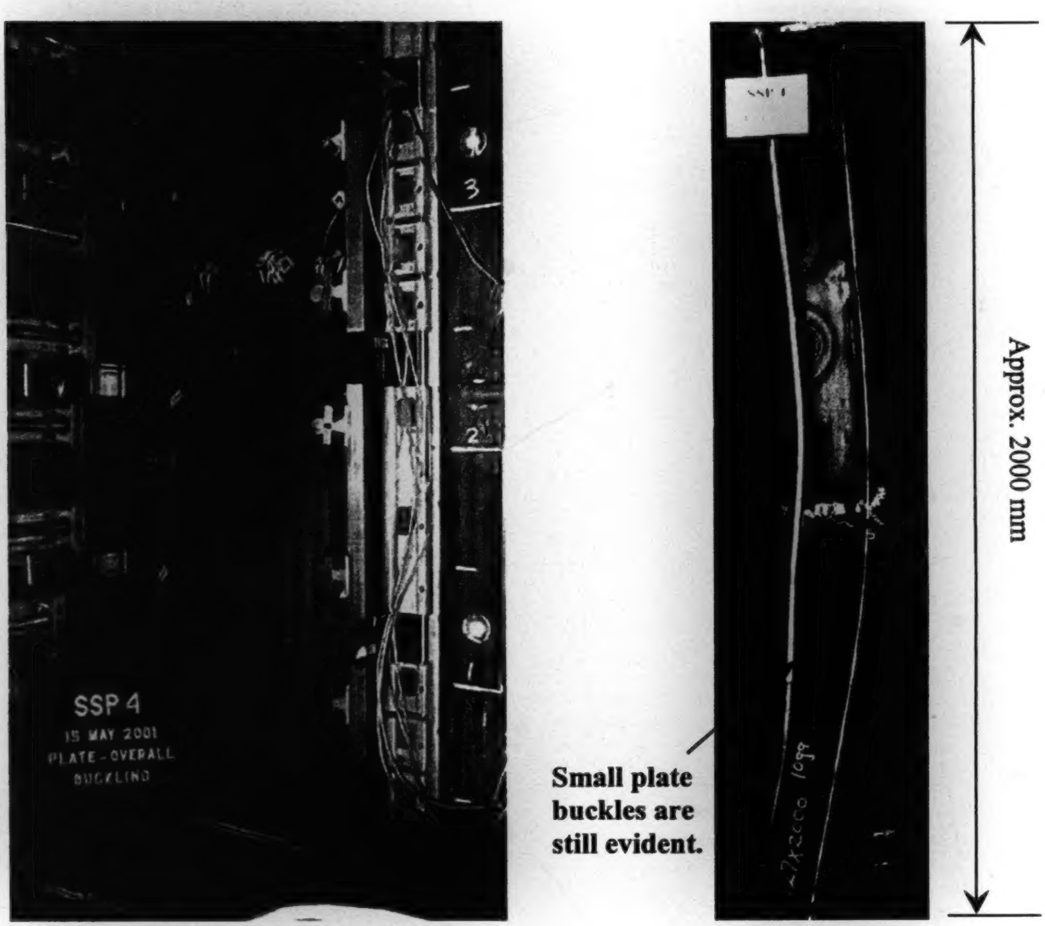
SSP 4
15 MAY 2001
PLATE - OVERALL
BUCKLING
3
2
1

Small plate buckles are still evident.

Approx. 2000 mm

(a) End of Test

(b) Side View

Figure 4.15 Deformed Shape of SSP4

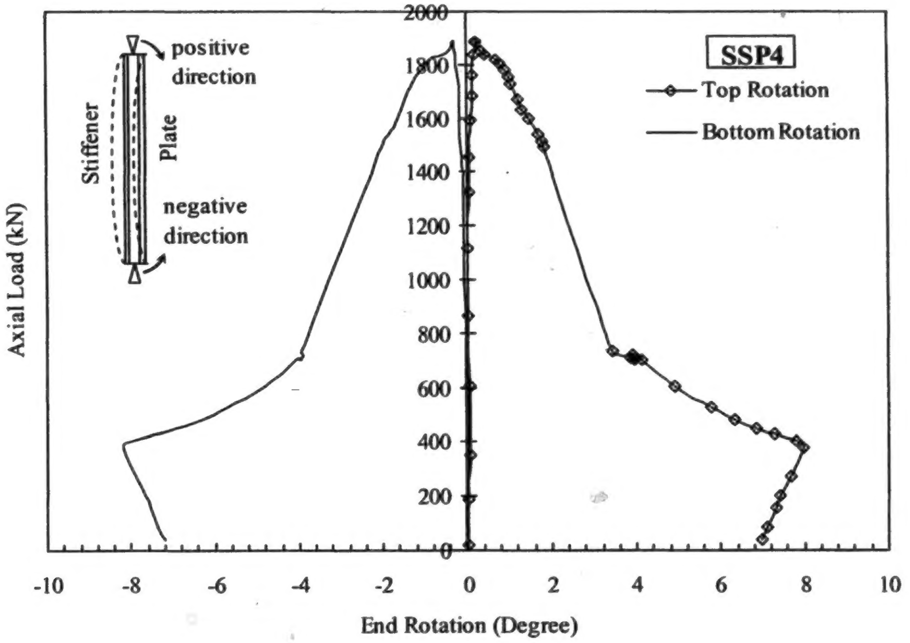

Figure 4.16 Axial Load versus End Rotations for SSP4

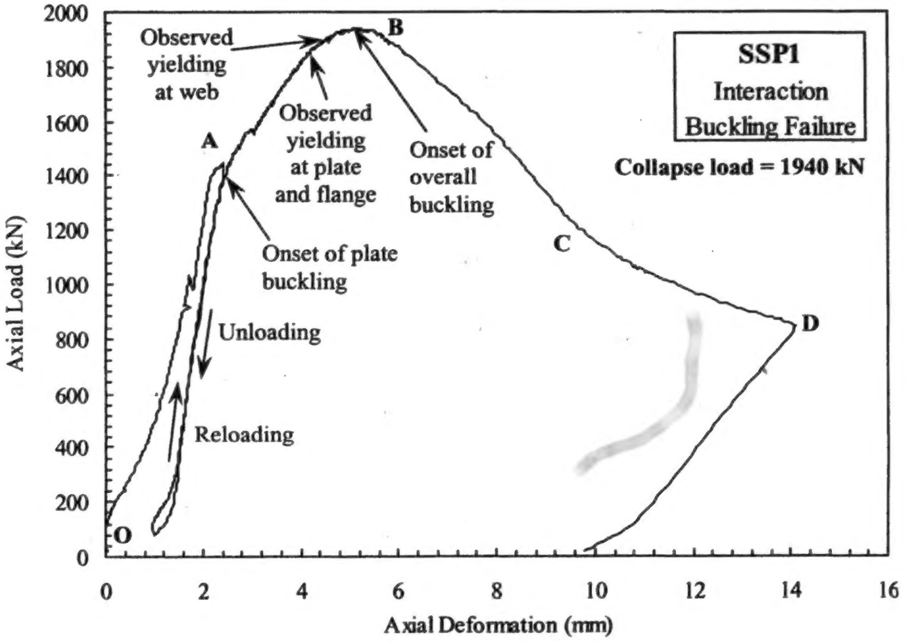

Figure 4.17 Load versus Axial Deformation Curve for Specimen SSP1

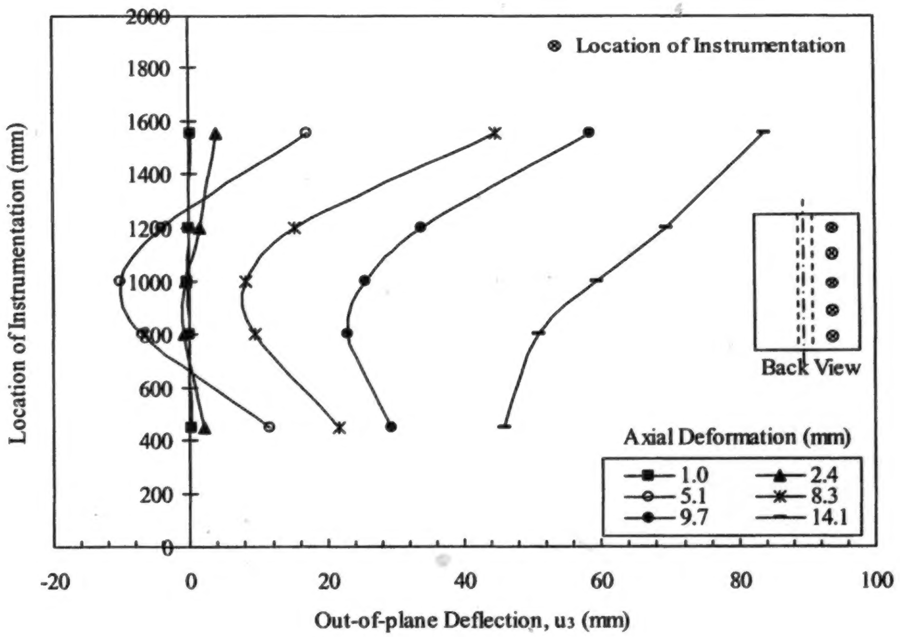

(a) East Side

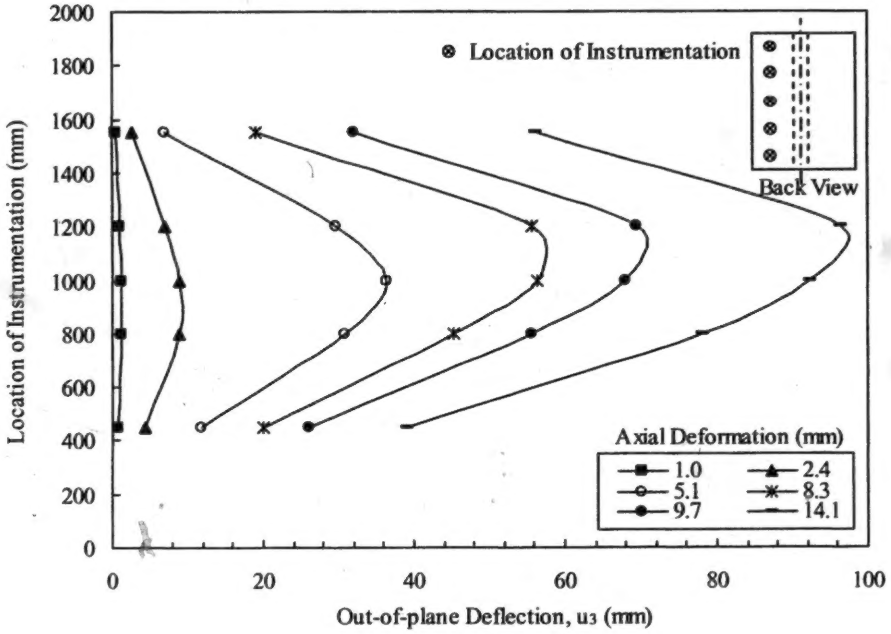

(b) West Side

Figure 4.18 Out-of-plane Deformations of SSP1 Plate at Different Axial Displacements

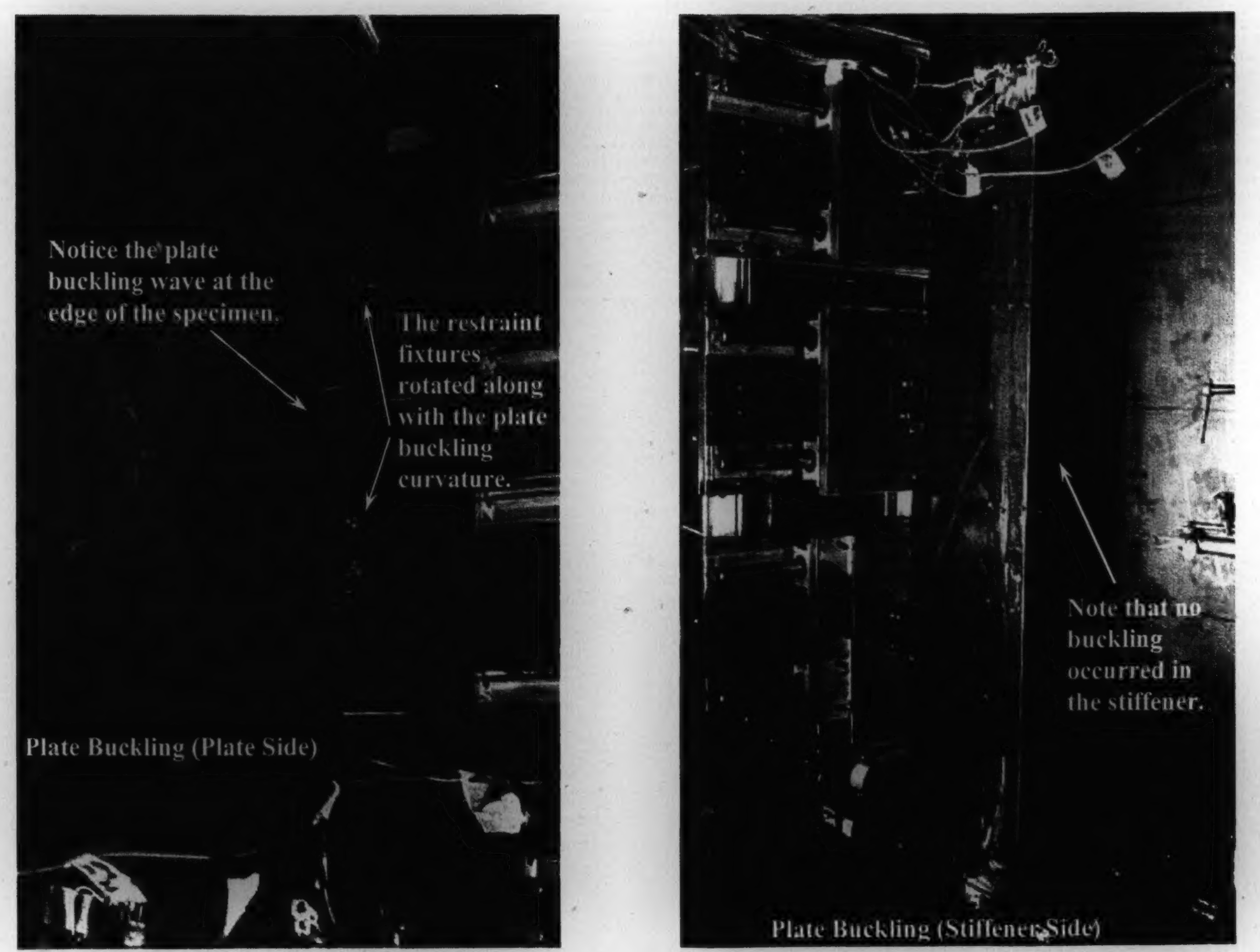
Notice the plate
buckling wave at the
edge of the specimen.
The restraint
fixtures
rotated along
with the plate
buckling
curvature.
Plate Buckling (Plate Side)
Note that no
buckling
occurred in
the stiffener.
Plate Buckling (Stiffener Side)

Figure 4.19 (a) Deformed Shape of SSP1 during Testing

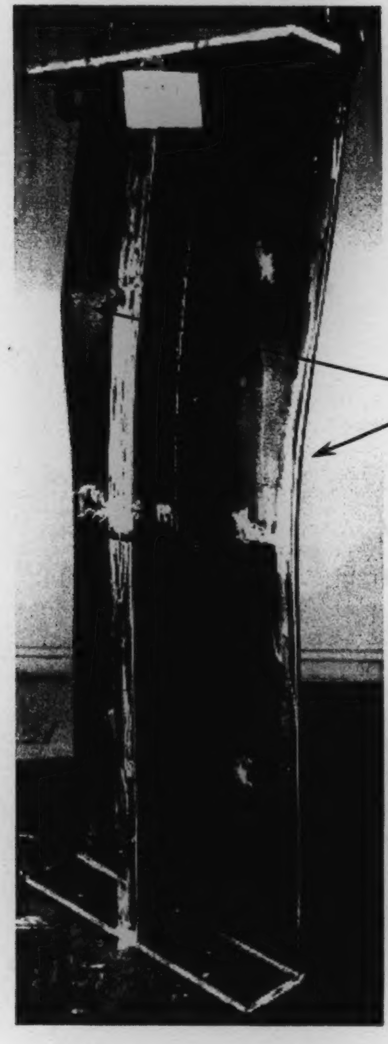

Plate buckling waves still remained visible after the test was completed

Figure 4.19(b) SSP1 after Testing

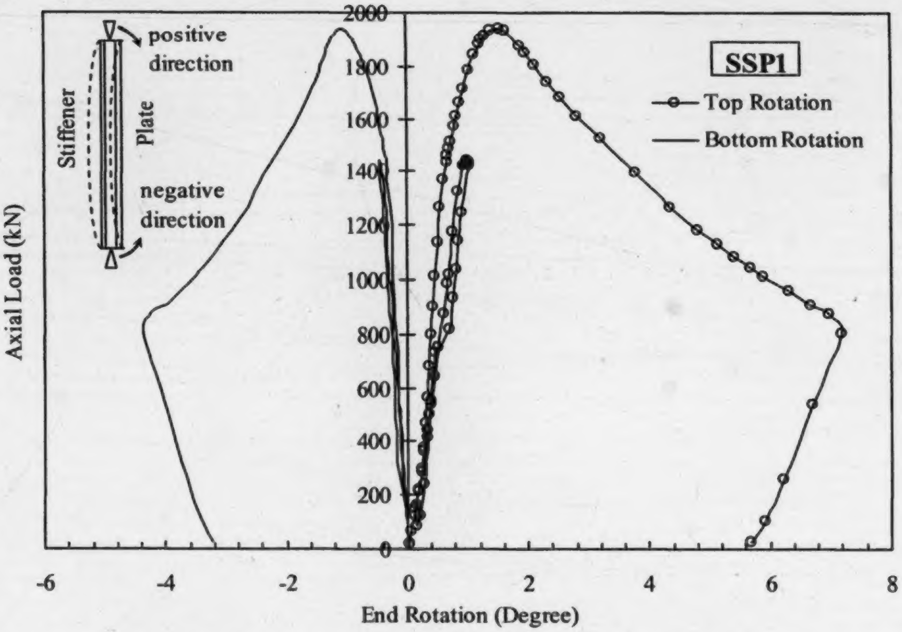

Figure 4.20 Axial Load versus End Rotations for SSP1

# 5 Prediction of Test Results

## 5.1 General

This chapter presents a comparison between the test results presented in Chapter 4 and the predictions from the finite element analysis and various current design equations. This exercise was carried to further validate the finite element model.

## 5.2 Finite Element Analysis

A series of finite element analyses similar to the preliminary analyses in Chapter 3 were performed for each one of the test specimens using the measured specimen dimensions, material properties, initial imperfections and residual stresses. Since the test specimens were loaded with a small eccentricity, the corresponding eccentricity for each specimen was incorporated into the finite element analysis as listed in the second column of Table 5.1. A comparison between the finite element analysis results and the experimental results is presented along with an investigation of the sensitivity of stiffened plates to load eccentricity.

### 5.2.1 Material Model

The true stress-strain relationship was obtained from the coupon test results presented in Section 4.2. True stress and true strain were obtained using the following expressions,

True Stress: $\sigma_{true} = \sigma_{nom}(1 + \varepsilon_{nom})$ (5-1)

True Strain: $\varepsilon_{true} = \ln(1 + \varepsilon_{nom})$ (5-2)

True Plastic Strain: $\varepsilon_{true,pl} = \ln(1 + \varepsilon_{nom}) - (\sigma_{true} / E)$ (5-3)

where $\sigma_{nom}$ and $\varepsilon_{nom}$ are the engineering stress and engineering strain obtained from the tension coupon tests. A comparison between the true stress versus true strain curve obtained for the 4.8 mm steel plate and the true stress versus true strain curve used for the finite element analysis is demonstrated in Figure 5.1. The stress versus strain curves used in the finite element analysis were formed by a series of straight line segments defined in

Table 5.2 where $\sigma_t$ are the true stress values, obtained using Equation (5-1), and $\varepsilon_{pl}$ are the true plastic strains obtained from Equation (5-3).

### 5.2.2 Initial Imperfections and Residual Stresses

The measured initial imperfections were incorporated into the finite element mesh when the mesh geometry was defined. Since the initial imperfection measurements were not performed on the same grid as the finite element mesh, a mapping process, based on an inverse distance weighted least squares method was carried out using the commercial program Surfer 8.0® Surface Mapping System. A sample of the measured initial imperfections for specimen SSP4, magnified 200 times, is shown in Figure 5.2.

Following the procedures outlined in Section 3.2.2.3, the measured residual stress pattern shown in Figure 4.4 were applied to the finite element model as initial strains in the form of a temperature distribution as the first load step. Equilibrium was established at the end of this load step. The measured residual stresses, the nodal input for the first load step, and the element stresses obtained from the finite element analysis are presented in Figure 5.3. Good agreement between the measured and the modelled residual stresses is observed. Although residual stresses were measured only in one specimen, a similar residual stress pattern was adopted for all four finite element models.

### 5.2.3 Comparison between Finite Element Analysis and Experimental Results

A summary of the test results and the finite element analysis results is presented in Table 5.1 for each test specimen. The table shows the predicted peak strengths and failure modes as well as the test-to-predicted ratio. The ability of the model to predict the failure mode of the test specimens is consistent with the findings of Grondin *et al.* (1998), even for interaction buckling failure. Two types of failure modes were observed in the analyses, namely, stiffener tripping and interaction buckling. SSP2 was the only specimen that failed by stiffener tripping.

The deformed shapes shown in Figures 5.4 to 5.7 captured the behaviour of the test specimens. In the case of interaction buckling failure, plate buckling was first observed, followed by plate-induced overall buckling. With a narrower plate width, SSP3 had smaller plate buckles but more waves along its plate element. In contrast, larger waves were observed in SSP1 and SSP4 but with fewer waves along their plate length. As discussed in Section 3.2.3, specimen SSP2 belongs to the most critical case with a geometry that is highly susceptible to both interaction buckling and stiffener tripping. The preliminary analysis presented in Chapter 3 was conducted on a specimen with a thinner web than that of the fabricated specimen and was loaded at its centroid. During testing, specimen SSP2 was the only specimen loaded with an eccentricity towards its stiffener. Because of the difference in geometry between the analysis model and the test specimen and the load eccentricity, the stress distribution in the test specimen was substantially different from that of the preliminary analysis. Subsequently, the eccentric load weakened the stiffener and SSP2 failed by stiffener tripping.

Although the numerical model successfully predicted the failure modes, none of the load versus axial shortening responses from the model closely matched that of the tests. Comparisons between the axial load versus deformation curves of the experiment and the finite element analysis are presented in Figures 5.8 to 5.11. Except for the unloading curve of SSP1, the stiffness of the test specimens from the tests are 23 % to 57 % smaller than predicted by the finite element analysis.

Attempts have been made to explain the large discrepancy between the observed and predicted stiffness. Malfunction of the LVDT was first suspected as the source of error since it directly measured the axial deflection of the specimens. However, the LVDT was calibrated before the test and no problems were found. In addition, a dial gauge was set up before the reloading of SSP1 and the dial gauge measurements were consistent with the LVDT measurements. Therefore, equipment malfunction was ruled out. Flaking and cracking of the plaster placed between the test specimens end plate and bearings was observed during the tests. Since axial deformation measurements were performed between the two end bearings, crushing of the plaster would be another source of shortening. It is expected that the plaster would crack at the same rate and display approximately the same modulus of elasticity for all specimens. In order to test this theory, the measured displacements in specimen SSP2 were corrected to match the finite element predictions and the same corrections were applied to SSP3 and SSP4. However, it was found that the adjustment required for SSP2 was excessive for the other specimens. For example, SSP2 had a combined plaster thickness of approximately 3 mm but SSP3 only had 2 mm. At the peak load (700 kN) of SSP2, a difference of 1.4 mm axial deformation was recorded between the finite element analysis and the test results. A stiffness adjustment factor of $6.67\text{x}10^{-4}$ mm of axial reduction/kN · mm of plaster can be obtained. Applying this factor to the results of SSP3 with the adjustment from the thickness of the plaster ($1.33\text{x}10^{-3}$ mm/kN), the revised axial deformation versus axial deformation curve for the test result would have a greater stiffness than the finite element analysis. Thus, the plaster cannot be the only source of discrepancy between the analysis results and the test results. Separation of the specimen end plate and the bottom bearing plate was also observed during the tests. This, however, could not explain the extensive axial shortening in the specimen. It is because the separate of the end plates could only counteract the reduction in the axial shortening of the specimen. Lastly, the stiffness from the analysis results was compared to the calculated stiffness from the measured properties of the test specimens. It was found that the stiffness from the analysis is close to the calculated value. Therefore, the finite element analysis seems to be reliable. None of the above truly explains the cause of the discrepancy. Uncertainties still remain in the amount of axial deflection recorded. Because of the discrepancy between the test and the analysis displacements, the following focuses mainly on the ultimate load and the post-buckling behaviour.

Table 5.1 indicates that the finite element analysis was able to predict the test capacity very well, except for specimen SSP1. The test-to-predicted ratios for specimen SSP2, SSP3 and SSP4 are similar to the findings in Grondin *et al.* (1998). Despite the relatively large error in the prediction for SSP1, the average predicted capacity was within ± 5 percent of the test results with a coefficient of variation of 0.13.

A typical interaction buckling response is characterized by plate buckling, usually near the peak load, followed by overall buckling just before a sudden drop in load carrying capacity. Despite the differences between the measured and predicted displacements discussed above, the finite element model is able to capture the general post buckling behaviour of the test specimens; the analysis predicted the observed stiffener tripping behaviour for SSP2 and the interaction buckling behaviour for the remaining specimens, as outlined in sections 1.1 and 2.2. The analysis results for SSP2, shown in Figure 5.9, indicate a sudden loss in load carrying capacity immediately after the peak load. This behaviour is consistent with the test.

The predicted failure mode for SSP3 is interaction buckling, which is consistent with the observed failure mode (see Figure 5.10). During the test, the peak capacity occurred at about 4.4 mm axial deformation and the load dropped at about 6.2 mm. This loss of capacity was observed within 0.4 mm of the peak capacity in the finite element analysis.

Better agreement between the test result and the finite element analysis was found in specimen SSP4 than SSP3. The post buckling behaviour of SSP4 remained ductile but the overall buckling capacity was lower than the one observed in the test. The analysis predicts a more sudden loss of capacity than observed in the test.

Specimen SSP1 was expected to reach a peak strength 29 percent higher than observed. As discussed in Section 4.5.4, the test results indicated a somewhat different post-buckling behaviour than a typical interaction buckling behaviour, i.e. a lower plate buckling strength. However this was not captured in the analysis.

### 5.2.4 Assessment of the Effect of Load Eccentricity

The analysis results presented in the previous sections have indicated that the finite element model can predict reliably the failure mode and the peak capacity but not the stiffness. Therefore, the model will be used to explore the effect of load eccentricity. In addition to the actual load eccentricity used in the experimental study, other eccentricities were investigated to determine the effect of eccentricity on the strength and behaviour of stiffened steel plates as indicated in Table 5.3. The eccentricity is taken as negative towards the plate and positive towards the stiffener.

Eccentricities ranging from 0 mm to 3.4 mm (test condition) were investigated for specimen SSP2. It can be recalled that the preliminary analysis predicted that test specimen SSP2 would fail by interaction buckling. A deformed shape of specimen SSP2 at various stages loaded at its centroid is illustrated in Figure 5.12. According to the deformed configurations, plate buckling occurred first, followed by plate induced overall buckling. This indicates that if specimen SSP2 had been loaded concentrically it would have failed by interaction buckling. Within the range of eccentricities investigated, it was found that the failure mode changed from interaction buckling to stiffener tripping when the eccentricity exceeded 1 mm.

A similar investigation was performed on specimen SSP4, with eccentricities ranging from 10 mm towards the plate to 5 mm towards the stiffener. Again, two types of failure modes were observed as the load eccentricity was varied. Interaction buckling is observed when the load eccentricity is negative and stiffener tripping governs for the concentric load case and positive load eccentricities.

The load versus axial deformation relationships for various load eccentricities are plotted in Figures 5.13 and 5.14 for SSP2 and SSP4, respectively. The load responses obtained from the test specimens are also included in the diagrams for comparison (3.4 mm for SSP2 and -5 mm for SSP4). It is observed that as the eccentricity moves towards the stiffener, the eccentric load increases the stress in the stiffener, which increases the possibility of failure by stiffener tripping. Another interesting detail is found in the post buckling stage on the response diagram. As shown in Figure 5.14, SSP4 response changes from more ductile stiffener tripping failure to abrupt behaviour. Similar reduction in ductility is found as SSP4 is loaded closer to the plate.

The investigation of the effect of load eccentricity on the strength and behaviour of test specimens SSP2 and SSP4 indicates that both test specimens are very sensitive to the load eccentricity. Given the sensitivity of these two specimens to load eccentricity and the accuracy with which load eccentricity can be measured in the tests, the observed discrepancy between the test and predicted load carrying capacities could be explained.

## 5.3 Design Guidelines

Both the 1995 version of the Det Norske Veritas (DNV) and the 1987 version of the American Petroleum Institute (API) design guidelines were chosen in the study by Sheikh *et al.* (2001) to predict the failure behaviour of stiffened plates loaded in uniaxial compression and combined compression and bending. A later version of these two guidelines (DNV, 2002; and API, 2000) are evaluated in this study along with a combination of the Canadian Standard Association cold-formed steel design standard (CSA-S136-01, 2002) and limit states design of steel structures (CSA-S16.1-01, 2002). Since the tests were performed under uniaxial compression plus bending, a brief summary of the design provisions relevant to combined uniaxial compression and bending is presented below.

### 5.3.1 Det Norske Veritas DNV-RP-C201 (2002)

A detailed review of the DNV guideline is presented in Appendix E. A single longitudinal stiffener with an associated width of plating is considered to be representative of a multiple panel stiffened plate. Although DNV consider built-up sections in the design calculations, stiffened plate panels built from two or more different materials (hybrid panels) are not addressed. Therefore, assumptions were made upon the yield strength and modulus of elasticity in the DNV equations. These assumptions are relatively conservative and are stated in Appendix E.

For the design of plate panels with multiple longitudinal stiffeners, the DNV guideline considers three types of failure modes, namely, interaction between plate buckling and plate-induced overall buckling, interaction between plate buckling and stiffener-induced overall buckling, and interaction between stiffener tripping and overall buckling. The proposed design calculations are divided into two loading cases: lateral pressure on the plate side and lateral pressure on the stiffener side. The 2002 edition of DNV adopts the same effective width as CSA-S136-01 to account for the loss of plate strength due to plate buckling under uniaxial compression. A comparison between the effective slenderness ratio, ${}^{b_e}\!/_{t_p}$ , used in the 1995 edition and the 2002 edition of the DNV guideline are shown in Figure 5.15. Under uniaxial compression, the 1995 effective width approach yields a smaller effective width than the 2002 version for plate-induced overall buckling. In contrast, the effective width is generally decreased if using the 2002 edition of DNV for stiffener-induced overall buckling condition.

### 5.3.2 American Petroleum Institute (API) Bulletin 2V (2000)

In the 2000 edition of the API design guideline, the ultimate limit state for the design of uniaxially stiffened panels under axial compression considers a section with single stiffener acting with its attached plating. Similar to DNV, the API guideline does not consider hybrid sections. Therefore, to be consistent with DNV, material properties for the flange were assumed for all elements of SSP2 and the calculations for the remaining specimens were based on the plate material properties.

The beam-column interaction equation proposed by API is given as

$$\frac{P}{P_u} + B_1 \frac{M}{M_u} \leq 1.0 \qquad (5\text{-}4)$$

where

$P$ = axial load (Applied load for this study)

$M$ = end moment which is taken as the product of the axial load and the measured eccentricity

$M_u$ = maximum moment that can be resisted by the member in the absence of axial loads. This is taken as the plastic moment of the entire cross-section for transverse axis bending. However, to be consistent with the other approach, yield moment with respect to the extreme fibre of the flange was assumed for SSP2 and the opposite was used for the rest of the specimens.

$P_u$ = ultimate axial load of the column given by the product of the ultimate design stress and the measured cross-sectional area ($f_u A$)

$$B_1 = \frac{C_m}{1 - P/P_E} \geq 1.0 \quad \text{(moment amplification factor)} \qquad (5\text{-}5)$$

$$C_m = 0.6 + 0.4\frac{M_1}{M_2} \geq 0.4 \qquad (5\text{-}6)$$

For equal end moments with single curvature, the ratio of the smaller to larger end-moments in the plane of bending, $M_1/M_2$, is +1; which results in $C_m = 1.0$. Finally:

$$P_E = \frac{\pi^2 EI}{(KL)^2} \qquad (5\text{-}7)$$

where $I$ is the moment of inertia of the cross-section, $L$ is the unsupported column length and $K$ is taken as 1.0 for pinned end boundary condition.

The ultimate design stress, $f_u$, of the stiffened plate is defined by a modified plate slenderness ratio, $\bar{\lambda}$, that considers the interaction between the stiffeners within the stiffened panel. The ultimate strength curves adopted by API reflect the influence of residual stresses, initial geometric imperfections and inelastic behaviour. For multiple stiffened plates under pure compression, the ultimate stress takes the following form:

$$\frac{f_u}{f_y} = \begin{cases} 1.0, & \bar{\lambda} \leq 0.5 \\ 1.5 - \bar{\lambda}, & 0.5 < \bar{\lambda} \leq 1.0 \\ 0.5/\bar{\lambda}, & \bar{\lambda} > 1.0 \end{cases} \qquad (5\text{-}8)$$

where $\bar{\lambda}$ is the slenderness parameter, defined as:

$$\bar{\lambda} = \left(\frac{b}{t}\right)\sqrt{\frac{F_y\, 12\left(1 - \nu^2\right)}{E\pi^2 k}} \qquad (5\text{-}9)$$

where $b$ and $t$ are the measured plate width and plate thickness, respectively (i.e. $b = b_p$, $t = t_p$); $f_y = F_y$ is taken as the yield strength of the plate; E is the modulus of elasticity of the plate and $\nu$ is Poisson's ratio for steel (0.3). As the number of stiffeners on a plate increases, the buckling coefficient, $k$, approaches zero and the critical stress for the plate reaches the yield strength. In this study only one stiffener was used with a plate of width $b_p$, making the buckling coefficient, $k$, equal to 4.0.

### 5.3.3 CSA S136-01 (2002)/S16-01 (2002)

S136-01 is selected for this study because it considers interaction between plate buckling and overall buckling. It uses an effective width concept to account for the loss in plate effectiveness as a result of plate buckling. An advantage of the effective width calculations in S136-01 is that it allows the user to incorporate the actual material properties of the panel elements in the equations and evaluates all elements in a section. DNV only considers the effective width of the plate but S136 considers the web and the flange as well. It is therefore implicit in the DNV guideline that the slenderness of the stiffener plate elements will be sufficiently small to enable the stiffener elements to reach yield before local buckling. The effective width method is summarized as follow:

$$b = \begin{cases} w & when \quad \lambda \le 0.673 \\ \rho w & when \quad \lambda > 0.673 \end{cases} \tag{5-10}$$

where

$b$ = effective width

$w$ = flat width (measured plate width and web height of the test specimens)

$$\rho = \frac{\left(1 - 0.22/\lambda\right)}{\lambda} \tag{5-11}$$

The slenderness parameter $\lambda$ used in Equation (5-11) is similar to $\bar{\lambda}$ in Equation (5-9); however, the plate buckling coefficient, $k$, depends on the boundary conditions and stress distribution. A value of 4.0 is used for a plate simply supported all around. This is a conservative value for a web plate since it is assumed that the flange plate does not provide any rotational restraint. For unstiffened element, such as flange plates, $k$ is taken as 0.43.

Since CSA-S136-01 is specially designed for cold-formed sections, the column curve adopted in the standard is based on the material properties, initial imperfections and residual stresses commonly found in cold-formed sections. Therefore, the interaction equation for beam-column built with hot rolled steel sections adopted by CSA-S16-01 is used.

Typically, it is necessary to determine the classification of the test specimen in order to calculate the flexural capacity of a beam-column. Since the measured plate slenderness ratios for the test specimens exceed the limit for Class 2 sections given in CSA-S16-01, the proposed interaction equation for Class 3 is chosen.

$$\frac{C_f}{C_r} + \frac{U_{1x} M_f}{M_r} \leq 1.0 \qquad (5\text{-}12)$$

where

$C_f$ = factored axial load

$$C_r = AF_y\left(1+\lambda^{2n}\right)^{-1/n} \quad \text{(axial compression resistance with n = 1.34)} \qquad (5\text{-}13)$$

$$\lambda = \frac{KL}{r}\sqrt{\frac{F_y}{\pi^2 E}} \quad \text{(non-dimensional slenderness parameter with K = 1.0)} \qquad (5\text{-}14)$$

$r$ = radius of gyration

$M_f$ = factored moment caused by the measured eccentricity

$M_r$ = yield moment based on yielding at the extreme fibre of the section ($S\,Fy$) at pure bending

$U_{1x}$ = factor accounting for the second order effect of the axial force acting on the deformed member (P-δ effect). This is equivalent to $B_1$ of Equation (5-5)

The above calculations are based on an effective cross-section. The material properties of the flange are taken for SSP2, and those of the plate are used for the other test specimens. It should be noted that Equation (5-12) makes use of a factored axial load resistance, $C_r$, and moment resistance, $M_r$, to reflect the fact that the actual strength could be smaller than the expected strength based on nominal material properties. In the work presented below, however, the actual resistance, based on measured material properties, will be used. Similarly, the factored applied force effects, $C_f$ and $M_f$ represent the combined axial load and moment resistance of the beam-column when Equation (5-12) reaches a value of 1.0.

The moment resistance in Equation (5-12) is different from that in the DNV guideline. The former considers a moment that would produce a yield stress in the extreme fibre of the section. However, the yield moment in the DNV guideline is based on the stress in the extreme plate fibre of the effective section. This implies that the DNV guideline allows the stress in the stiffener to go beyond its yield strength while the extreme fibre on the plate side is at yield as the moment is applied. CSA-S16-01 limits the maximum stress in a section to the yield strength. For the test specimens used in this test program, the stress in the stiffener did not exceed yield because the applied moment was small relative to the axial load under the combined loading. Therefore, yielding of the stiffener was not a concern, and the interaction equation proposed by DNV is still valid but less conservative than S16-01.

### 5.3.4 Comparison with Design Practice

A comparison between the design equations presented above and the experimental results is presented in Table 5.4. The table presents the peak strength predicted by each guideline and a comparison between the test peak strength and the predicted peak strength. The predicted peak capacities were obtained by setting the interaction equations to 1.0. As mentioned in Section 5.3.1, the DNV guideline is the only guideline that predicts the peak strength for three failure modes: plate-induced overall buckling (PI), stiffener-induced overall buckling (SI) and stiffener tripping (ST). However, only the critical load for the governing failure mode (i.e. the one giving the minimum peak strength) in the DNV guideline is presented in the table. The results suggest that the DNV guideline is capable of predicting the failure mode of the test specimens since the predicted failure modes by the DNV guideline match the test failure modes.

The test-to-predicted ratio in the table gives a good indication of the accuracy of the design guidelines. Table 5.4 separates the comparison among the tests (SSP1, SSP3 and SSP4) failed by interaction buckling mode from the test (SSP2) failed by stiffener tripping. It is because each guideline considers differently between the different failure modes. The ratio reveals that, in most part, the guidelines are quite conservative with most of the test-to-predicted ratios greater than 1.0, except the strength estimate for SSP1 using the combined CSA-S136 CSA-S16 approach. Except for specimen SSP2, the DNV guideline and CSA-S136 / CSA-S16 provide similar test capacity predictions. It is because they are based on similar effective width and column curves. In general, there is no particular trend in the predictions of interaction bucking failure. Among all the specimens, SSP4 has the most consistent estimate from all guidelines. On the other hand, poor predictions are generally observed for SSP3.

For interaction buckling, the combination of the effective width used in CSA-S136 and the column curve from CSA-S16 provides the lowest mean test-to-predicted ratio, 1.22, but API shows the least variation with a coefficient of variation of 0.07. In the prediction of stiffener tripping, DNV is the most conservative compared to the other guidelines with a test to predicted ratio of 1.90. The guidelines have improved since the work of Sheikh *et al* (2002). However, more improvement is required in the inclusion of interaction buckling.

Table 5.1 Comparison between Test Results and Finite Element Analysis Results

| Specimen | Eccentricity[1] (mm) | Test Results | | Predicted Results | | Test / Predicted |
|---|---|---|---|---|---|---|
| | | Peak Load (kN) | Buckling Mode | Peak Load (kN) | Buckling Mode | |
| **SSP1** | -10 | 1940 | Interaction Buckling | 2510 | Interaction Buckling | 0.77 |
| **SSP2** | 3 | 680 | Stiffener Tripping | 690 | Stiffener Tripping | 0.99 |
| **SSP3** | -5 | 1160 | Interaction Buckling | 1100 | Interaction Buckling | 1.06 |
| **SSP4** | -5 | 1890 | Interaction Buckling | 1980 | Interaction Buckling | 0.96 |
| | | | | | **Mean** | 0.95 |
| | | | | | **C.O.V** | 0.13 |

[1] Eccentricity measured from centroidal axis to location of loading (positive towards the flange).

Table 5.2 True Stresses and True Plastic Strains

| Measured Plate Thickness (mm) | Modulus of Elasticity E (MPa) | Yield Stress $\sigma_{ys}$ (MPa) | $\sigma_1$ (MPa) | $\varepsilon_{p1}$ | $\sigma_2$ (MPa) | $\varepsilon_{p2}$ | $\sigma_3$ (MPa) | $\varepsilon_{p3}$ | $\sigma_4$ (MPa) | $\varepsilon_{p4}$ | $\sigma_5$ (MPa) | $\varepsilon_{p5}$ |
|---|---|---|---|---|---|---|---|---|---|---|---|---|
| **3.00** | 206000 | 202 | 205 | 0.008 | 250 | 0.021 | 294 | 0.047 | 372 | 0.146 | 420 | 0.256 |
| **3.40** | 202000 | 285 | 290 | 0.023 | 336 | 0.048 | 388 | 0.096 | 440 | 0.211 | — | — |
| **4.80** | 202000 | 294 | 305 | 0.017 | 402 | 0.549 | 465 | 0.969 | 523 | 0.163 | 550 | 0.240 |
| **6.30** | 199000 | 331 | 335 | 0.020 | 418 | 0.050 | 490 | 0.090 | 548 | 0.145 | 587 | 0.217 |
| **7.90** | 196000 | 301 | 305 | 0.005 | 378 | 0.029 | 434 | 0.059 | 484 | 0.115 | 543 | 0.205 |
| **9.50** | 199000 | 407 | 410 | 0.018 | 464 | 0.049 | 512 | 0.092 | 570 | 0.175 | 588 | 0.233 |
| **12.7** | 204000 | 342 | 345 | 0.019 | 418 | 0.049 | 472 | 0.065 | 518 | 0.164 | 561 | 0.170 |

Table 5.3 Effect of Load Eccentricity on Load Carrying Capacity of SSP2 and SSP4

| Specimen | Eccentricity (mm) | Maximum Axial Load (kN) | Buckling Mode |
|---|---|---|---|
| **SSP2** | 0 | 1048 | Interaction Buckling |
| | 1 | 1134 | Interaction Buckling |
| | 1.25 | 993 | Stiffener Tripping |
| | 1.5 | 909 | |
| | 2 | 814 | |
| | 2.5 | 756 | |
| | 3 | 718 | |
| | 3.2 | 703 | |
| | 3.4* | 690 | |
| **SSP4** | -10 | 756 | Interaction Buckling |
| | -5 * | 1979 | Interaction Buckling |
| | 0 | 703 | Stiffener Tripping |
| | 5 | 718 | Stiffener Tripping |

* Test scenario

Table 5.4 Comparison between Prediction Equations and Test Results

| Test Specimen | DNV 2002 | | |
|---|---|---|---|
| | Predicted Load (kN) | Predicted Mode of Failure | $P_{Test}/P_{Predict}$ |
| SSP1 | 1817 | PI | 1.07 |
| SSP3 | 782 | PI | 1.48 |
| SSP4 | 1503 | PI | 1.26 |
| | | **Mean** | 1.27 |
| | | **C.O.V** | 0.16 |

| Test Specimen | API 2000 | | CSA-S136/CSA-S16 | |
|---|---|---|---|---|
| | Predicted Load (kN) | $P_{Test}/P_{Code}$ | Predicted Load (kN) | $P_{Test}/P_{Code}$ |
| SSP1 | 1388 | 1.40 | 1985 | 0.98 |
| SSP3 | 795 | 1.46 | 838 | 1.38 |
| SSP4 | 1488 | 1.27 | 1458 | 1.30 |
| | **Mean** | 1.38 | **Mean** | 1.22 |
| | **C.O.V** | 0.07 | **C.O.V** | 0.17 |

| | Test Specimen SSP2 | | |
|---|---|---|---|
| | Predicted Load (kN) | Predicted Mode of Failure | $P_{Test}/P_{Predict}$ |
| **DNV 2002** | 357 | ST | 1.90 |
| **API 2000** | 563 | — | 1.21 |
| **CSA-S136/CSA-S16** | 501 | — | 1.36 |
| | | **Mean** | 1.49 |
| | | **C.O.V** | 0.24 |

Note: PI – plate-induced overall buckling failure
ST – stiffener tripping failure

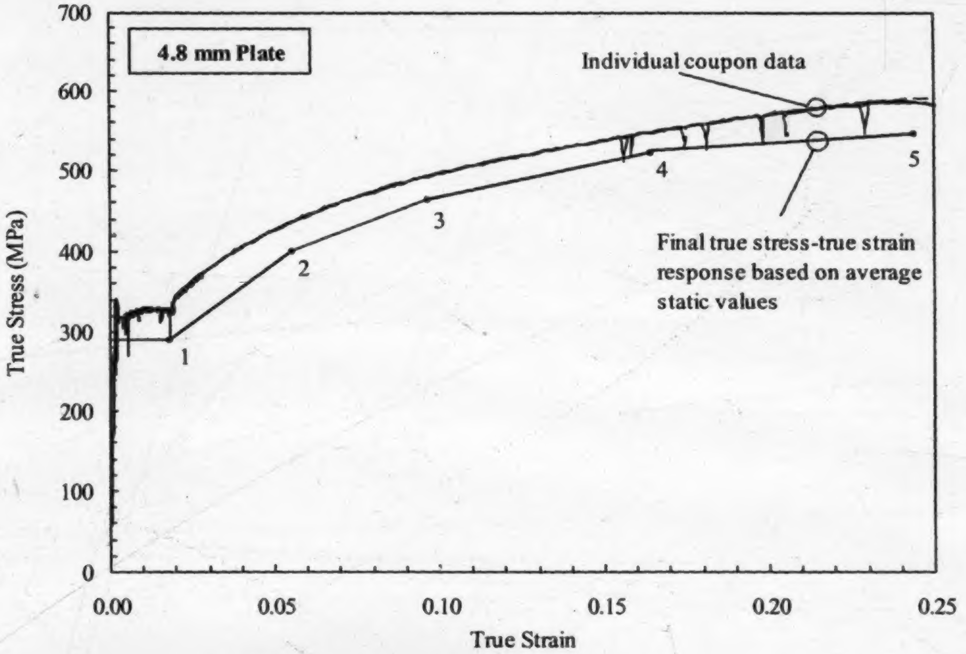

Figure 5.1 True Stress versus True Strain Curve for the 4.8 mm Plate

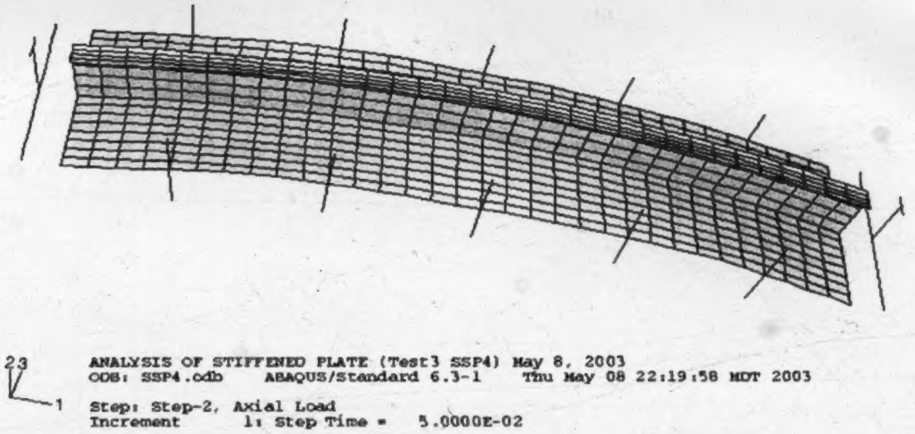

```
ANALYSIS OF STIFFENED PLATE (Test3 SSP4) May 8, 2003
ODB: SSP4.odb    ABAQUS/Standard 6.3-1    Thu May 08 22:19:58 MDT 2003

Step: Step-2, Axial Load
Increment      1: Step Time =   5.0000E-02
```

Figure 5.2 Finite Element Mesh with Initial Imperfections of Test Specimen SSP4 (imperfections magnified 200 times)

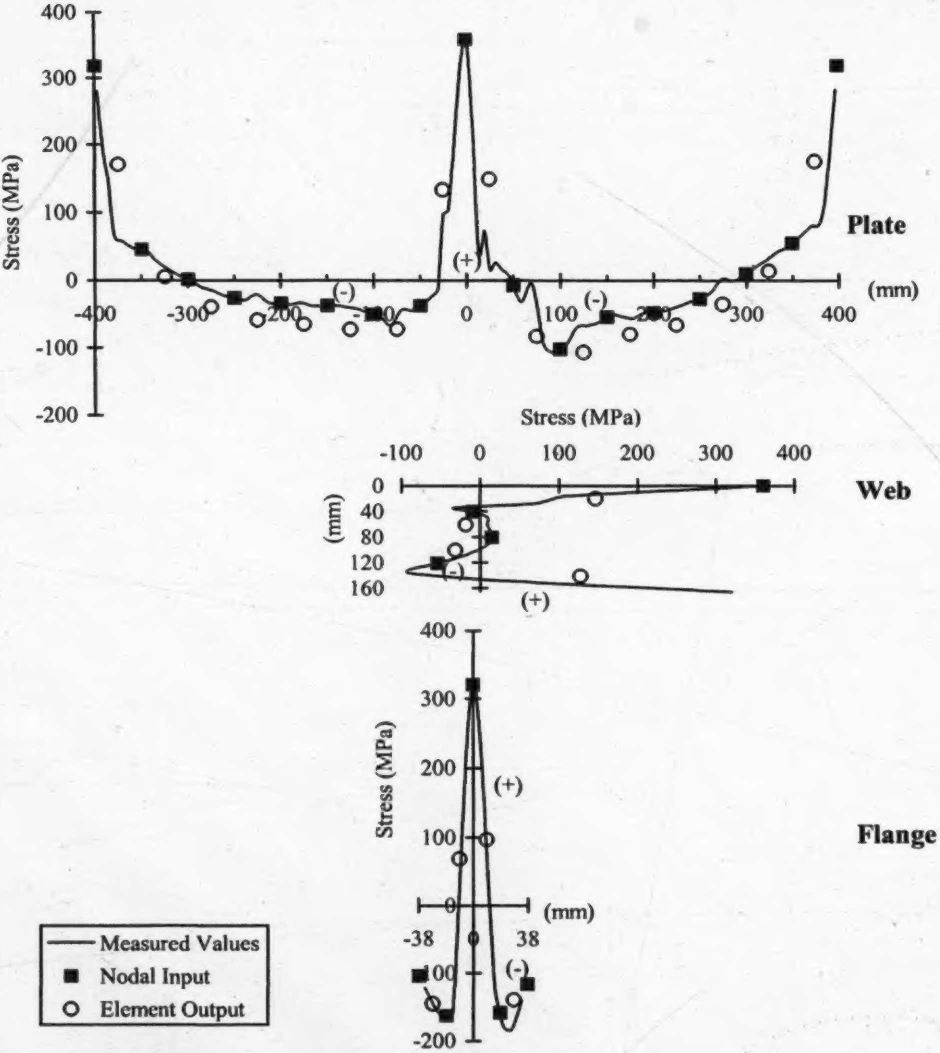

| | | $\left(\sigma_r / \sigma_y\right)$ |
|---|---|---|
| Maximum tensile residual stress | | |
| at flange-to-web weld = | 320 MPa | 1.1 |
| at plate-to-web weld = | 360 MPa | 1.1 |
| at plate edge = | 320 MPa | 0.94 |
| Average compression stress | | |
| in plate = | 41 MPa | 0.12 |
| in web = | 48 MPa | 0.16 |
| in flange = | 150 MPa | 0.51 |

Figure 5.3 Comparison between Measured and Modelled Residual Stresses for Specimen SSP1

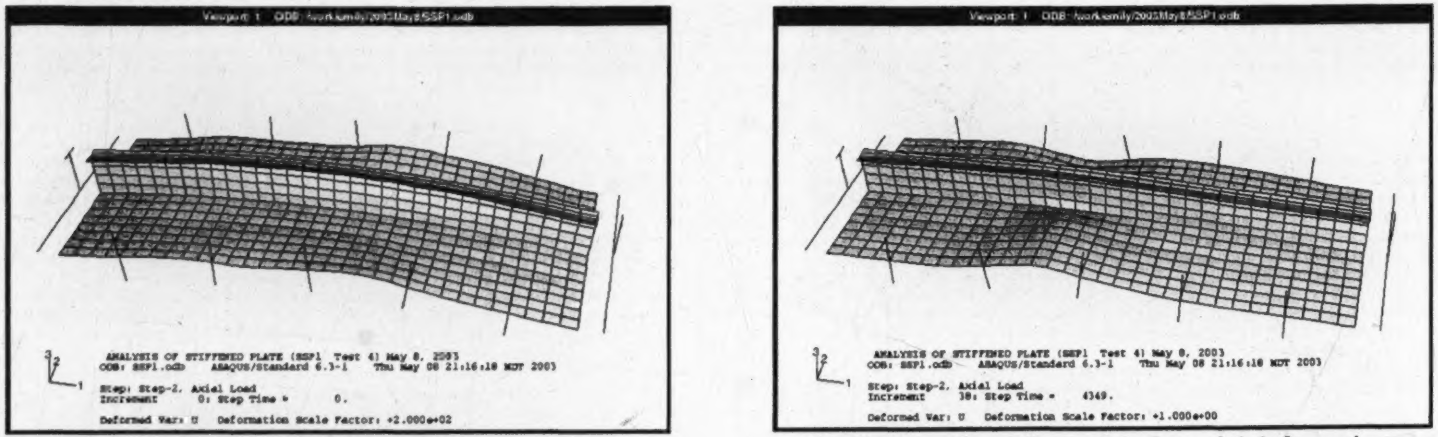

```
Viewport: 1   ODB: /work/emily/2003May8/SSP1.odb
ANALYSIS OF STIFFENED PLATE (SSP1  Test 4) May 8, 2003
ODB: SSP1.odb    ABAQUS/Standard 6.3-1    Thu May 08 21:16:18 MDT 2003

Step: Step-2, Axial Load
Increment      0: Step Time =       0.

Deformed Var: U   Deformation Scale Factor: +2.000e+02
```

(a) Plate configuration before loading
(displacements magnified 200 times)

```
Viewport: 1   ODB: /work/emily/2003May8/SSP1.odb
ANALYSIS OF STIFFENED PLATE (SSP1  Test 4) May 8, 2003
ODB: SSP1.odb    ABAQUS/Standard 6.3-1    Thu May 08 21:16:18 MDT 2003

Step: Step-2, Axial Load
Increment     38: Step Time =    4349.

Deformed Var: U   Deformation Scale Factor: +1.000e+00
```

(b) Plate configuration at 2.3 mm axial deformation

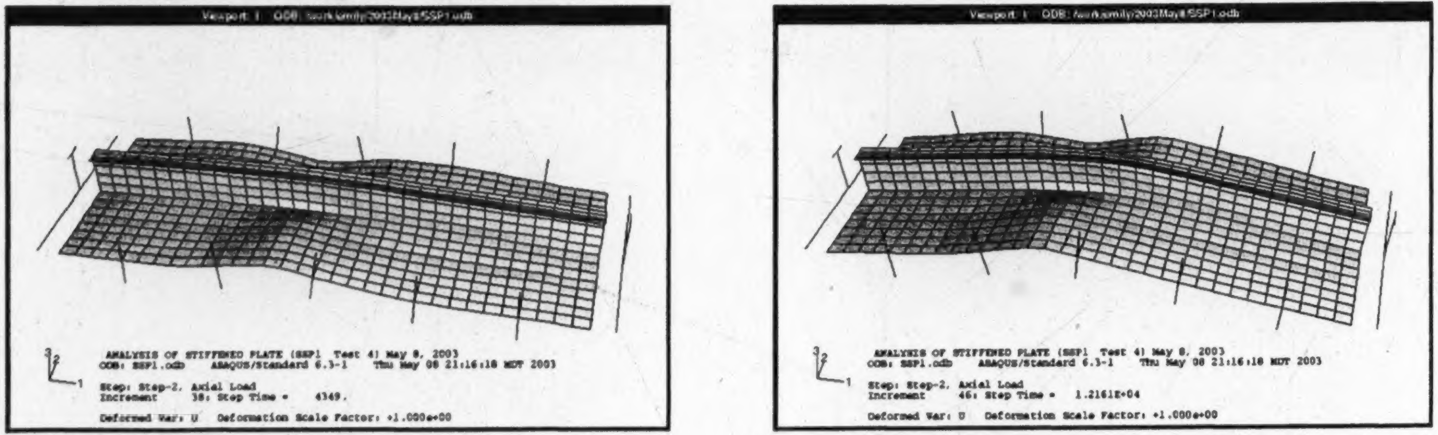

```
Viewport: 1   ODB: /work/emily/2003May8/SSP1.odb
ANALYSIS OF STIFFENED PLATE (SSP1  Test 4) May 8, 2003
ODB: SSP1.odb    ABAQUS/Standard 6.3-1    Thu May 08 21:16:18 MDT 2003

Step: Step-2, Axial Load
Increment     38: Step Time =    4349.

Deformed Var: U   Deformation Scale Factor: +1.000e+00
```

(c) Plate configuration at 9.4 mm axial deformation

```
Viewport: 1   ODB: /work/emily/2003May8/SSP1.odb
ANALYSIS OF STIFFENED PLATE (SSP1  Test 4) May 8, 2003
ODB: SSP1.odb    ABAQUS/Standard 6.3-1    Thu May 08 21:16:18 MDT 2003

Step: Step-2, Axial Load
Increment     46: Step Time =   1.2161E+04

Deformed Var: U   Deformation Scale Factor: +1.000e+00
```

(d) Plate configuration at 22 mm axial deformation

Figure 5.4 Deformed Shape of SSP1 at Various Stages of Loading

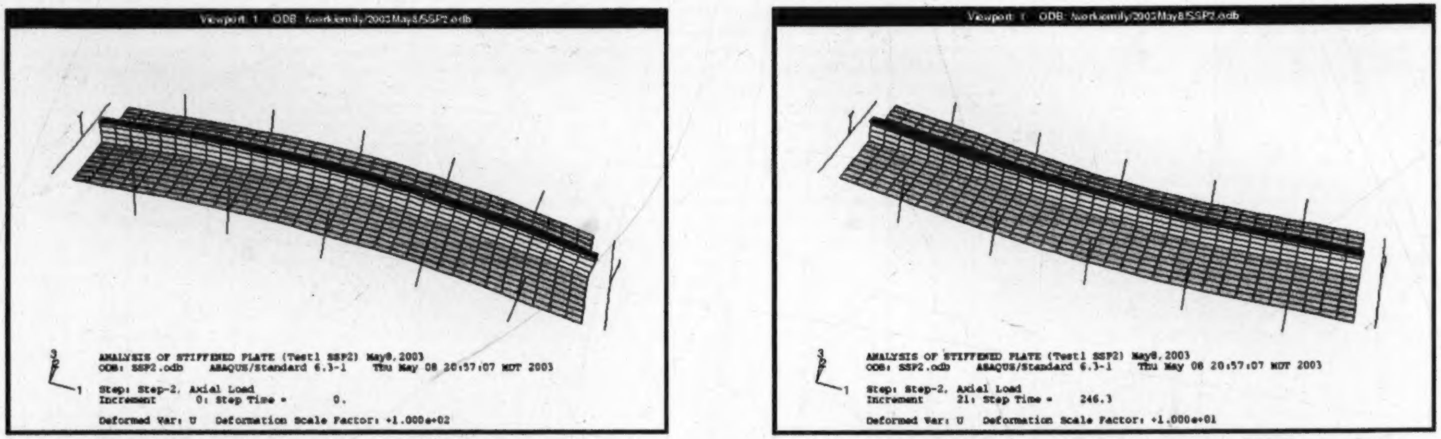

```
ANALYSIS OF STIFFENED PLATE (Test1 SSP2) May8,2003
ODB: SSP2.odb    ABAQUS/Standard 6.3-1    Thu May 08 20:57:07 MDT 2003

Step: Step-2, Axial Load
Increment      0: Step Time =        0.

Deformed Var: U   Deformation Scale Factor: +1.000e+02
```

```
ANALYSIS OF STIFFENED PLATE (Test1 SSP2) May8,2003
ODB: SSP2.odb    ABAQUS/Standard 6.3-1    Thu May 08 20:57:07 MDT 2003

Step: Step-2, Axial Load
Increment     21: Step Time =    246.3

Deformed Var: U   Deformation Scale Factor: +1.000e+01
```

(a) Plate configuration before loading
(displacements magnified 100 times)

(b) Plate configuration at 1.2 mm axial deformation
(displacements magnified 10 times)

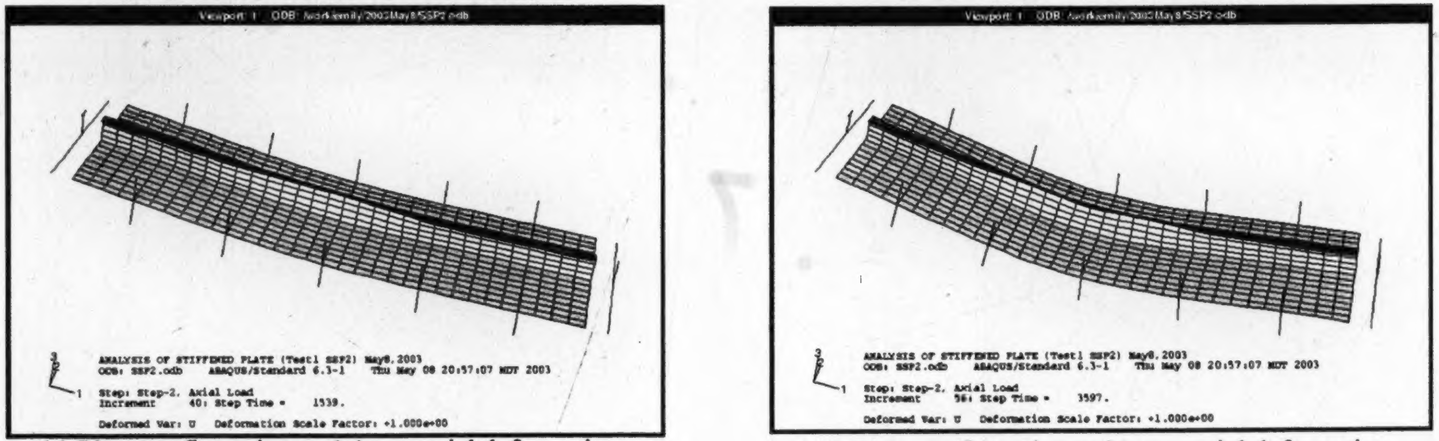

```
ANALYSIS OF STIFFENED PLATE (Test1 SSP2) May8,2003
ODB: SSP2.odb    ABAQUS/Standard 6.3-1    Thu May 08 20:57:07 MDT 2003

Step: Step-2, Axial Load
Increment     40: Step Time =     1539.

Deformed Var: U   Deformation Scale Factor: +1.000e+00
```

```
ANALYSIS OF STIFFENED PLATE (Test1 SSP2) May8,2003
ODB: SSP2.odb    ABAQUS/Standard 6.3-1    Thu May 08 20:57:07 MDT 2003

Step: Step-2, Axial Load
Increment     56: Step Time =     3597.

Deformed Var: U   Deformation Scale Factor: +1.000e+00
```

(c) Plate configuration at 4.4 mm axial deformation

(d) Plate configuration at 21 mm axial deformation

Figure 5.5 Deformed Shape of SSP2 at Various Stages of Loading

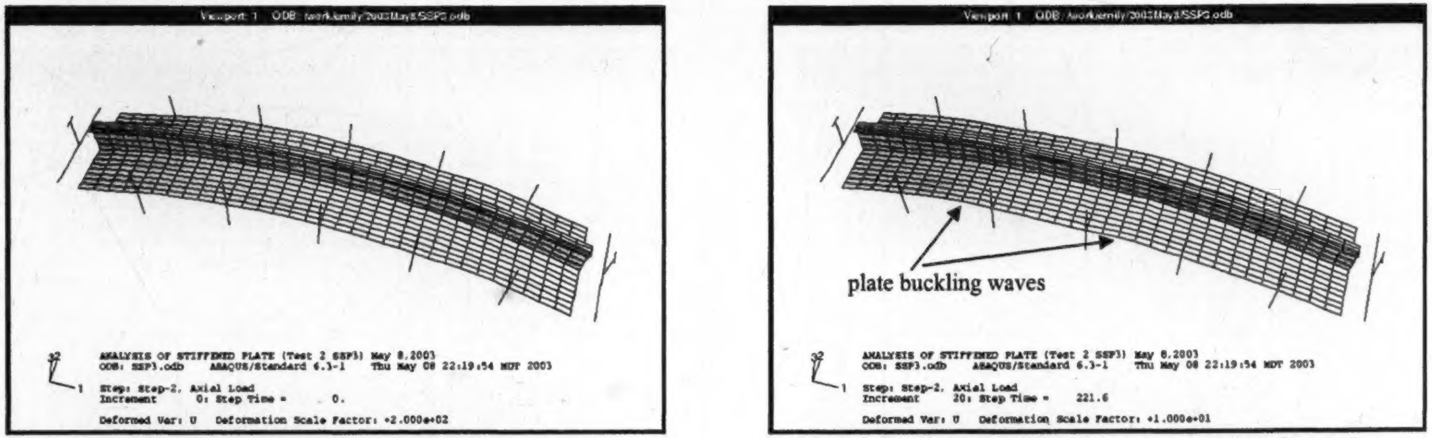
Viewport: 1   ODB: /work/emily/2003May8/SSP3.odb
Viewport: 1   ODB: /work/emily/2003May8/SSP3.odb
plate buckling waves
3
2
1

```
ANALYSIS OF STIFFENED PLATE (Test 2 SSP3) May 8,2003
ODB: SSP3.odb    ABAQUS/Standard 6.3-1    Thu May 08 22:19:54 MDT 2003

Step: Step-2, Axial Load
Increment      0: Step Time =       0.

Deformed Var: U   Deformation Scale Factor: +2.000e+02
```

(a) Plate configuration before loading
(displacements magnified 200 times)

```
ANALYSIS OF STIFFENED PLATE (Test 2 SSP3) May 8,2003
ODB: SSP3.odb    ABAQUS/Standard 6.3-1    Thu May 08 22:19:54 MDT 2003

Step: Step-2, Axial Load
Increment     20: Step Time =     221.6

Deformed Var: U   Deformation Scale Factor: +1.000e+01
```

(b) Plate configuration at 2.6 mm axial deformation
(displacements magnified 10 times)

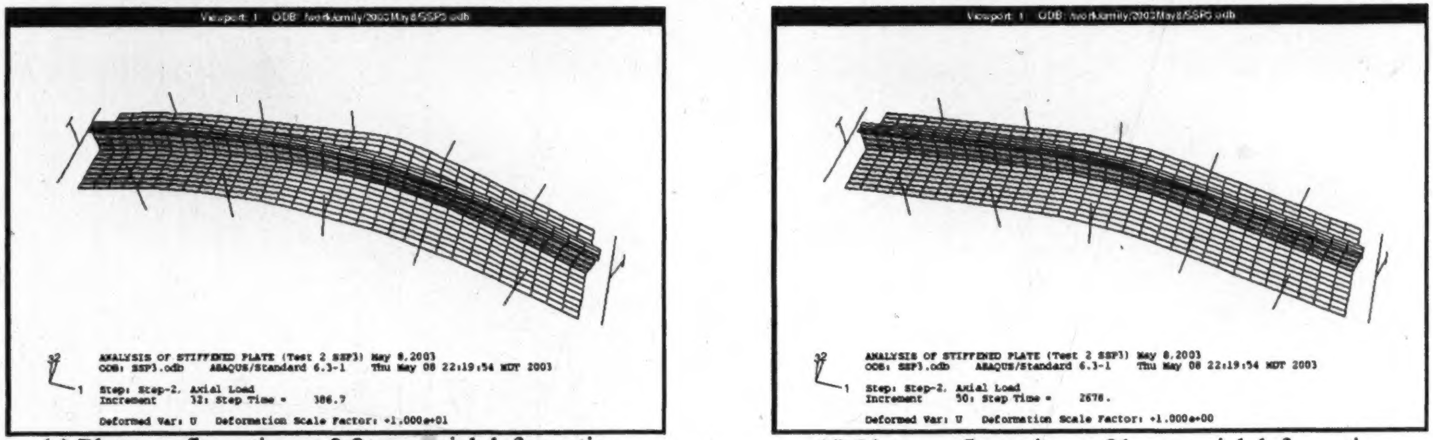
Viewport: 1   ODB: /work/emily/2003May8/SSP3.odb
Viewport: 1   ODB: /work/emily/2003May8/SSP3.odb
3
2
1

```
ANALYSIS OF STIFFENED PLATE (Test 2 SSP3) May 8,2003
ODB: SSP3.odb    ABAQUS/Standard 6.3-1    Thu May 08 22:19:54 MDT 2003

Step: Step-2, Axial Load
Increment     32: Step Time =     386.7

Deformed Var: U   Deformation Scale Factor: +1.000e+01
```

(c) Plate configuration at 2.8 mm axial deformation
(displacements magnified 10 times)

```
ANALYSIS OF STIFFENED PLATE (Test 2 SSP3) May 8,2003
ODB: SSP3.odb    ABAQUS/Standard 6.3-1    Thu May 08 22:19:54 MDT 2003

Step: Step-2, Axial Load
Increment     50: Step Time =     2678.

Deformed Var: U   Deformation Scale Factor: +1.000e+00
```

(d) Plate configuration at 21 mm axial deformation

Figure 5.6  Deformed Shape of SSP3 at Various Stages of Loading

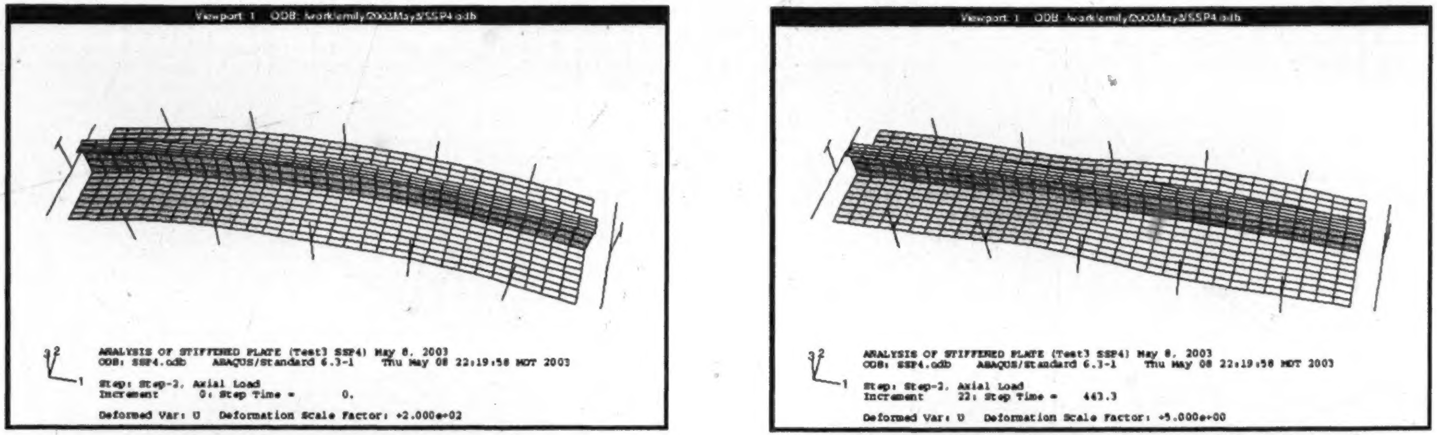
Viewport 1 ODB: /work/emily/2003May8/SSP4.odb
ANALYSIS OF STIFFENED PLATE (Test3 SSP4) May 8, 2003
ODB: SSP4.odb ABAQUS/Standard 6.3-1 Thu May 08 22:19:58 MDT 2003
Step: Step-2, Axial Load
Increment 0: Step Time = 0.
Deformed Var: U Deformation Scale Factor: +2.000e+02
Viewport 1 ODB: /work/emily/2003May8/SSP4.odb
ANALYSIS OF STIFFENED PLATE (Test3 SSP4) May 8, 2003
ODB: SSP4.odb ABAQUS/Standard 6.3-1 Thu May 08 22:19:58 MDT 2003
Step: Step-2, Axial Load
Increment 22: Step Time = 443.3
Deformed Var: U Deformation Scale Factor: +5.000e+00

(a) Plate configuration before loading
(displacements magnified 200 times)

(b) Plate configuration at 3.0 mm axial deformation
(displacements magnified 5 times)

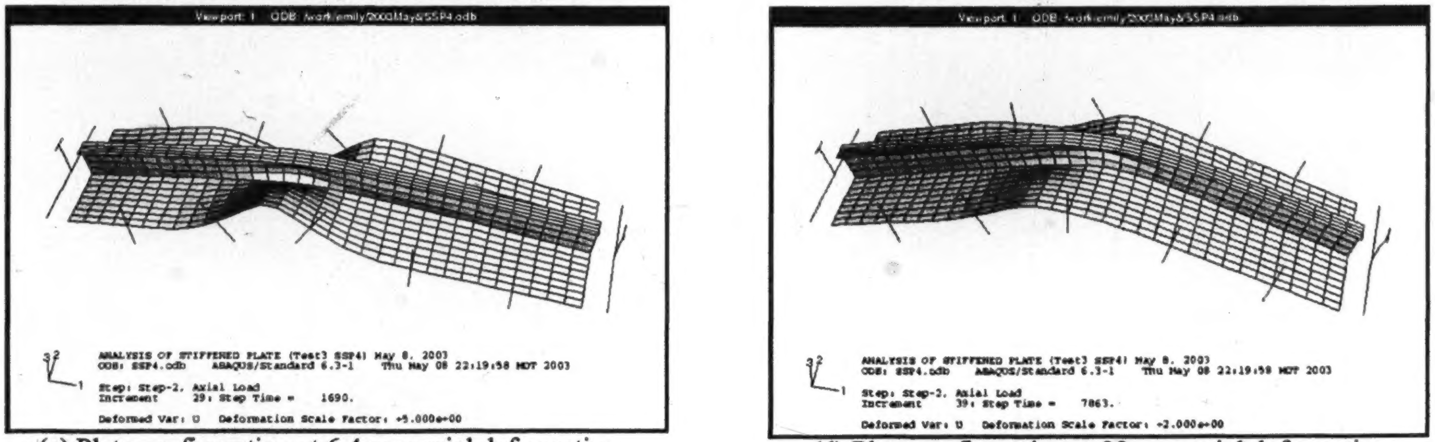
Viewport 1 ODB: /work/emily/2003May8/SSP4.odb
ANALYSIS OF STIFFENED PLATE (Test3 SSP4) May 8, 2003
ODB: SSP4.odb ABAQUS/Standard 6.3-1 Thu May 08 22:19:58 MDT 2003
Step: Step-2, Axial Load
Increment 29: Step Time = 1690.
Deformed Var: U Deformation Scale Factor: +5.000e+00
Viewport 1 ODB: /work/emily/2003May8/SSP4.odb
ANALYSIS OF STIFFENED PLATE (Test3 SSP4) May 8, 2003
ODB: SSP4.odb ABAQUS/Standard 6.3-1 Thu May 08 22:19:58 MDT 2003
Step: Step-2, Axial Load
Increment 39: Step Time = 7863.
Deformed Var: U Deformation Scale Factor: +2.000e+00

(c) Plate configuration at 6.4 mm axial deformation
(displacements magnified 5 times)

(d) Plate configuration at 22 mm axial deformation
(displacements magnified 2 times)

Figure 5.7 Deformed Shape of SSP4 at Various Stages of Loading

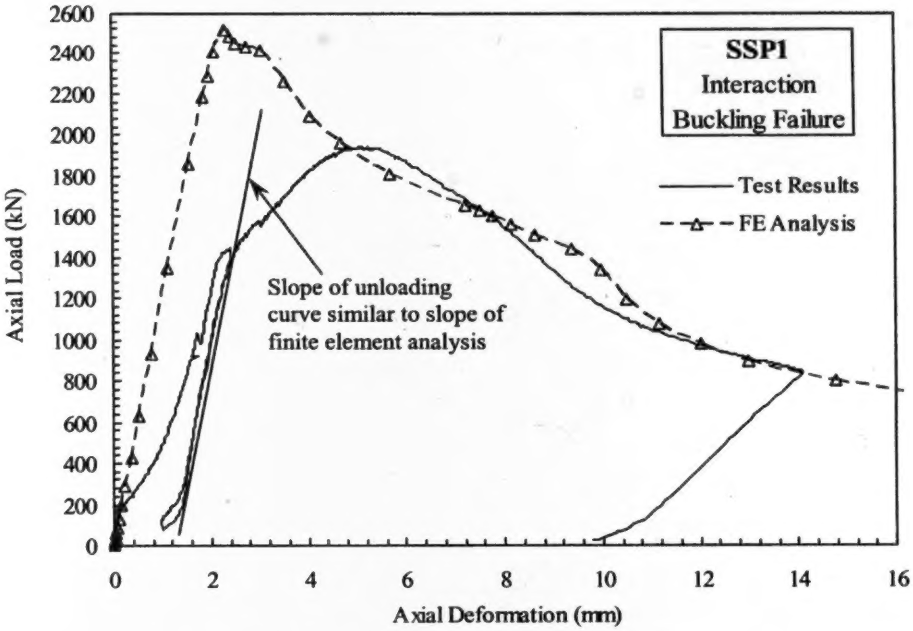

Figure 5.8 Axial Load versus Axial Deformation Curve for Specimen SSP1

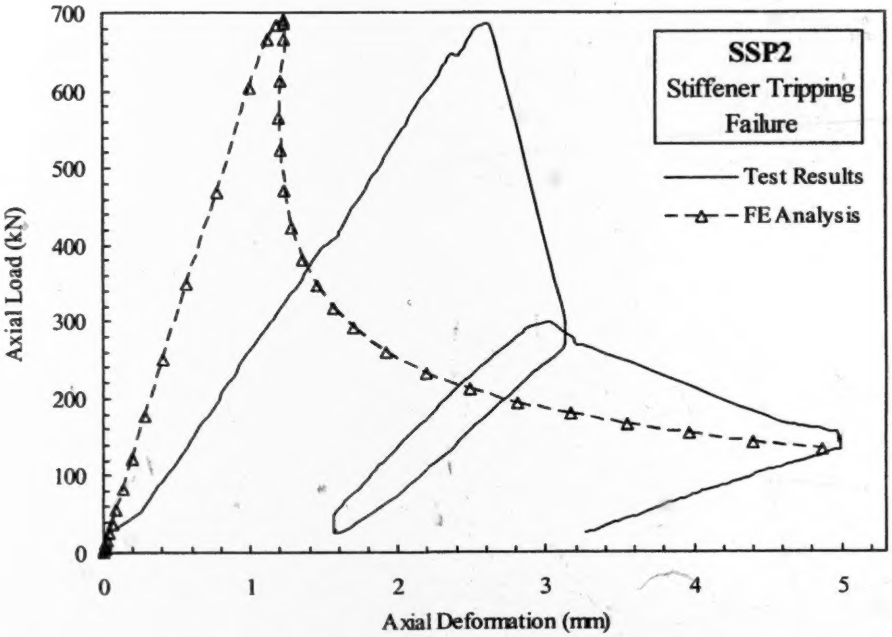

Figure 5.9 Axial Load versus Axial Deformation Curve for Specimen SSP2

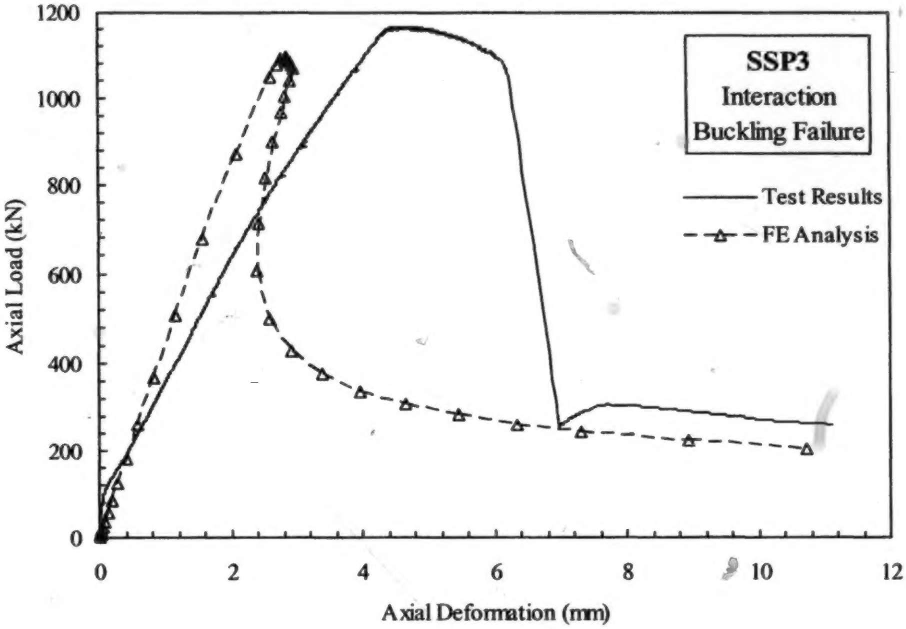

Figure 5.10 Axial Load versus Axial Deformation for Specimen SSP3

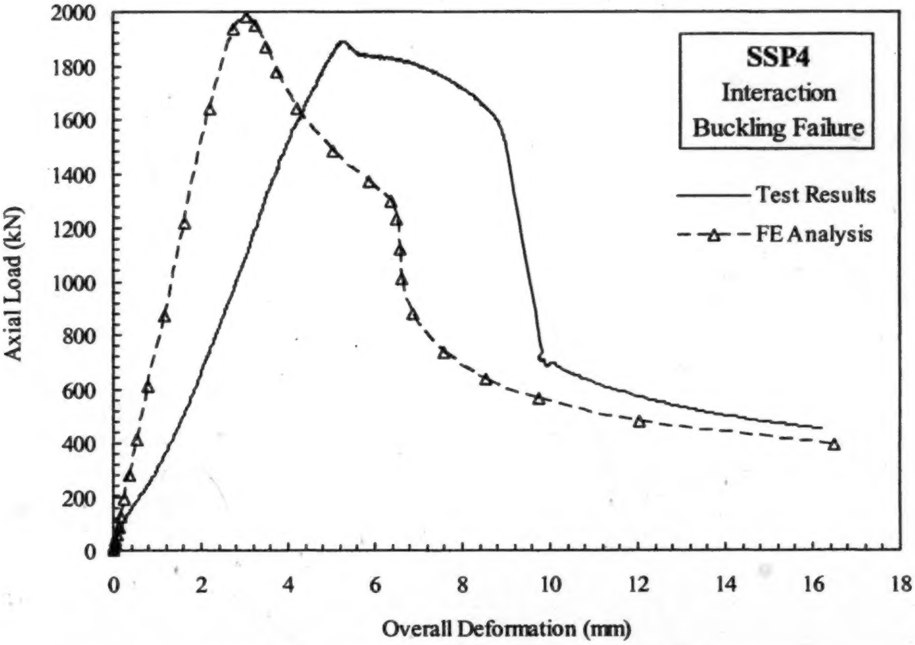

Figure 5.11 Axial Load versus Axial Deformation for Specimen SSP4

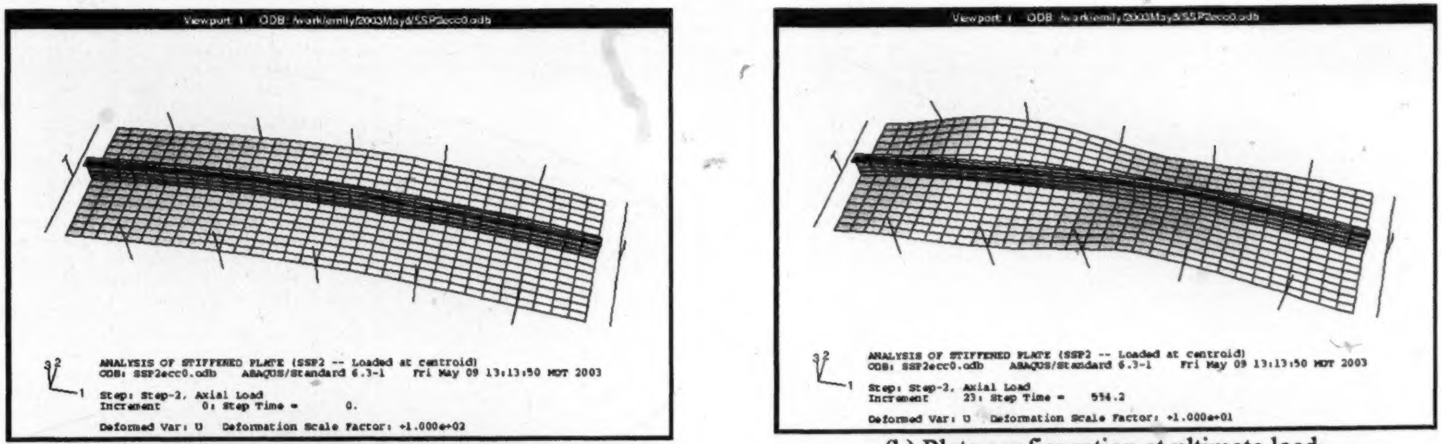

```
ANALYSIS OF STIFFENED PLATE (SSP2 -- Loaded at centroid)
ODB: SSP2ecc0.odb    ABAQUS/Standard 6.3-1    Fri May 09 13:13:50 MDT 2003

Step: Step-2, Axial Load
Increment      0: Step Time =        0.

Deformed Var: U   Deformation Scale Factor: +1.000e+02
```

```
ANALYSIS OF STIFFENED PLATE (SSP2 -- Loaded at centroid)
ODB: SSP2ecc0.odb    ABAQUS/Standard 6.3-1    Fri May 09 13:13:50 MDT 2003

Step: Step-2, Axial Load
Increment     23: Step Time =    534.2

Deformed Var: U   Deformation Scale Factor: +1.000e+01
```

(a) Plate configuration before loading
(displacements magnified 100 times)

(b) Plate configuration at ultimate load
(displacements magnified 10 times)

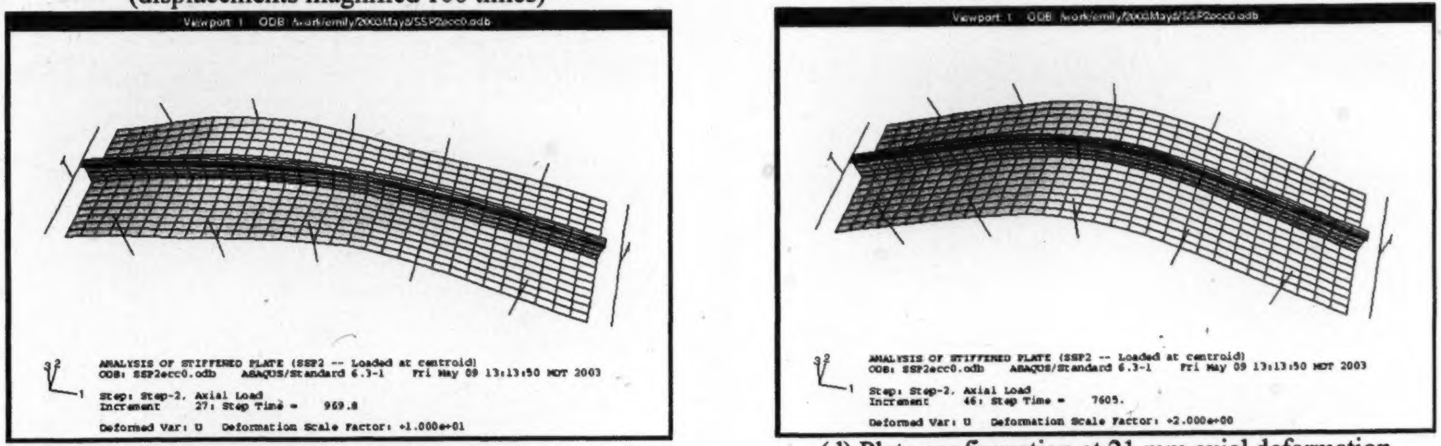

```
ANALYSIS OF STIFFENED PLATE (SSP2 -- Loaded at centroid)
ODB: SSP2ecc0.odb    ABAQUS/Standard 6.3-1    Fri May 09 13:13:50 MDT 2003

Step: Step-2, Axial Load
Increment     27: Step Time =    969.8

Deformed Var: U   Deformation Scale Factor: +1.000e+01
```

```
ANALYSIS OF STIFFENED PLATE (SSP2 -- Loaded at centroid)
ODB: SSP2ecc0.odb    ABAQUS/Standard 6.3-1    Fri May 09 13:13:50 MDT 2003

Step: Step-2, Axial Load
Increment     46: Step Time =    7605.

Deformed Var: U   Deformation Scale Factor: +2.000e+00
```

(c) Plate configuration at bottom of drop
(displacements magnified 10 times)

(d) Plate configuration at 21 mm axial deformation
(displacements magnified 2 times)

Figure 5.12 Deformed Shape of SSP2 at Various Stages of Loading (Load Applied at Centroid)

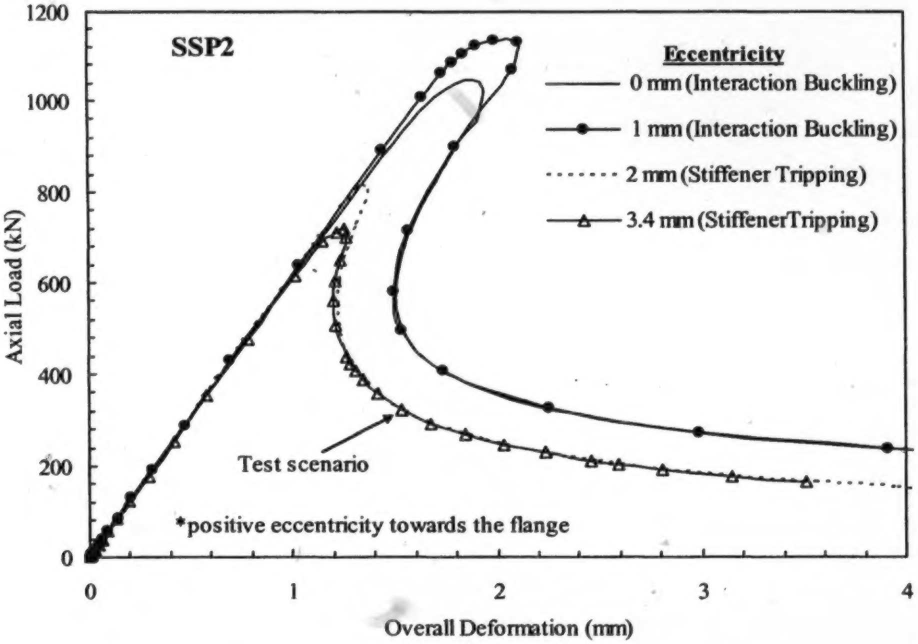

Figure 5.13 Effect of Load Eccentricity on the Behaviour of Specimen SSP2

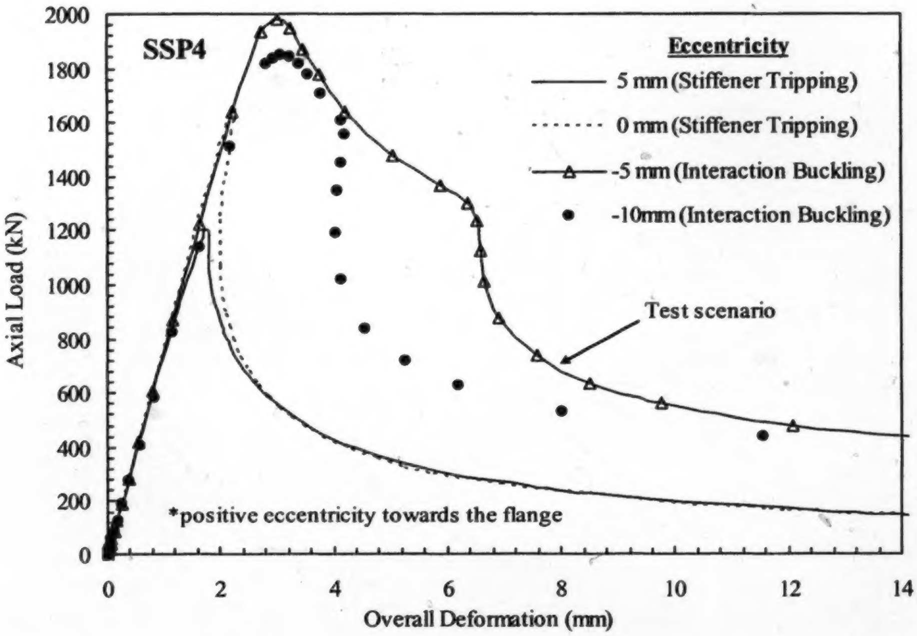

Figure 5.14 Effect of Load Eccentricity on the Behaviour of Specimen SSP4

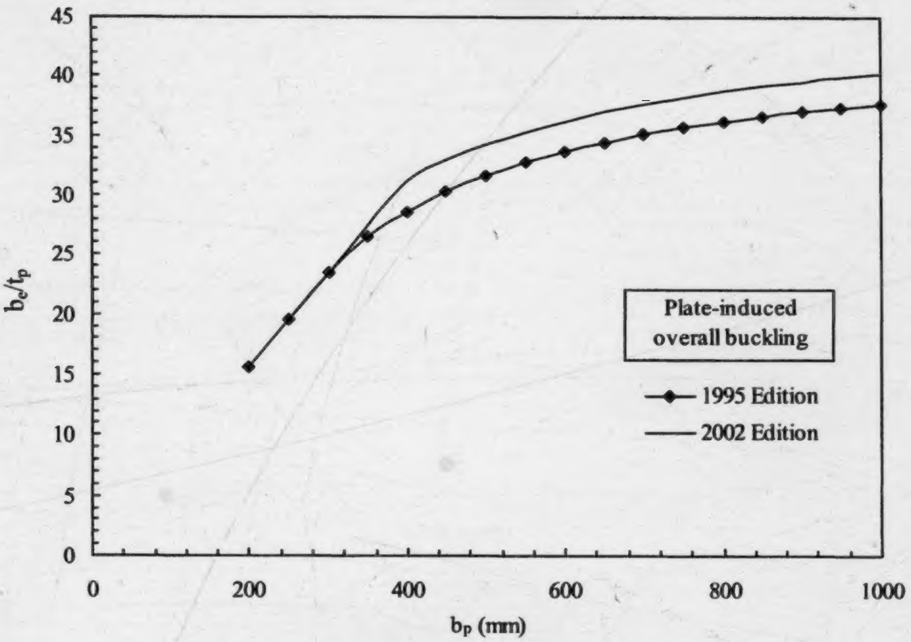

(a) Plate-induced Overall Buckling

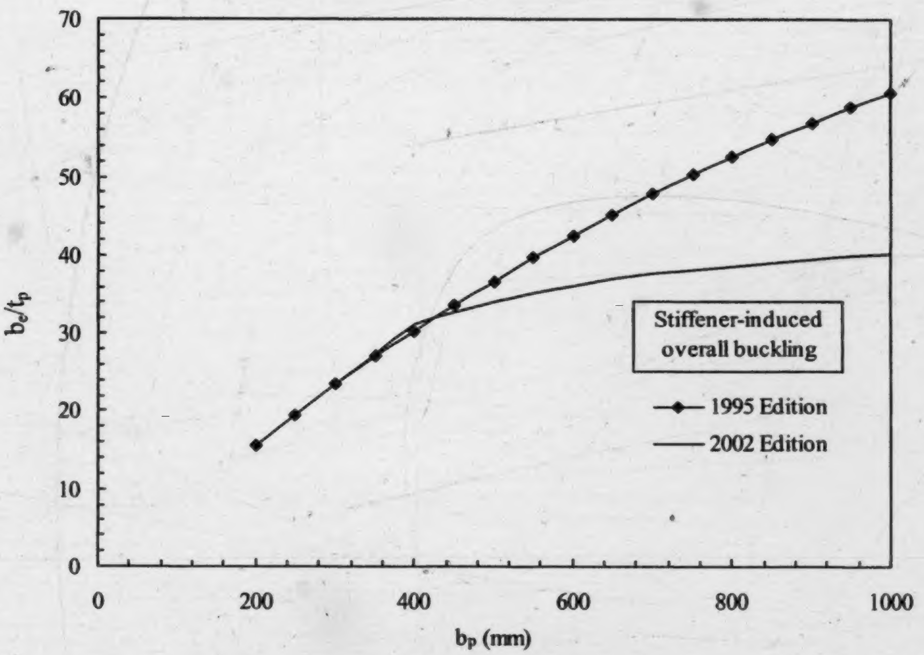

(b) Stiffener-induced Overall Buckling

Figure 5.15 Effective Width Comparisons between 1995 and 2002 Edition of DNV

# 6 Summary, Conclusions and Recommendations

## 6.1 Summary

A recent observation of the severe nature of interaction buckling of welded stiffened steel plates (Sheikh *et al.*, 2001) created the motivation for this study. Although extensive work has been done on the behaviour of stiffened steel plates, interaction buckling failure is not one of the largely recognized buckling behaviours. Stiffener tripping, plate buckling, stiffener-induced overall buckling and plate-induced overall buckling are more commonly addressed by design standards and guidelines. It is because interaction buckling is actually an interaction between two of the well-known buckling modes: plate-induced overall buckling and plate buckling. Its potential catastrophic behaviour similar to that of stiffener tripping causes a sudden drop in load carrying capacity in the post-buckling regime. This mode of failure was investigated in a numerical study performed by Sheikh *et al.* (2001). It was identified during an investigation of scale independent dimensionless variables (β-values) loaded under axial compression and combined axial compression and bending, but predominantly in the previous load case. Most common design guides, on the other hand, do not cover such a failure mode because it is not well recognized. Furthermore, the design guides that account for the mode of failure do not account for the severe nature of the failure mode. Therefore, a comprehensive testing program was carried out along with predictions from finite element modelling to further investigate the behaviour of stiffened steel plates failing by interaction buckling.

In order to study interaction buckling, a set of trial specimens was created following the work of Grondin *et al.* (1998) and the proposed range of β-values in Sheikh *et al.* (2001). A preliminary finite element analysis using the model developed by Grondin *et al.* (1998) was used to investigate these trial specimens and subsequently focus on those with preferred interaction buckling modes. The preliminary analysis model included the nominal dimensions of the trial specimens, assumed mechanical properties, "average" initial imperfections magnitude proposed by Smith *et al.* (1991), and residual stresses and distribution measured by Grondin *et al.* (1998). The analysis was conducted under uniaxial compression with five discrete restraints along each unloaded edge. Four built-up specimens were designed with each consisting of a longitudinal T-stiffener and a plate. Although the stiffened plates in the experimental program were full-scale specimens, they were of smaller scale than most stiffened plates encountered in practice.

Unlike the preliminary analysis approach, the test specimens were subjected to an eccentric compressive force. The compression test was conducted successfully with the restraint system developed by Grondin *et al.* (1998) to simulate edge continuity in a stiffened panel. During testing, axial shortening of the specimens along with the applied load was recorded for the development of the response diagrams. Additional responses were also examined throughout the test: the out-of-plane behaviour of the plate element, which reflects the plate buckling behaviour; in-plane and out-of-plane behaviour of the stiffener, which reflects the stiffener tripping behaviour; strain readings at the mid-span of the specimens to detect potential yielding of the cross-section; and end rotation to confirm the direction of the buckling behaviour. Prior to testing, initial imperfections were measured for all the specimens as well as an extensive measurement of longitudinal residual stresses on a duplicate specimen. Tension coupon tests were also performed to obtain the actual material properties of the stiffened plates. These ancillary tests helped tp refine the model for the finite element analysis.

Two failure modes were observed in the experimental program: interaction buckling and stiffener tripping. The existence of interaction buckling and the sudden loss of capacity resulting from it were confirmed from observation in three of the test specimens (SSP1, SSP3 and SSP4). The response diagrams of these test specimens also verified the work by Sheikh *et al.* (2001). The onset of plate buckling was typically observed just before the peak load while overall buckling was observed just before the sudden drop in load-carrying capacity. The plates exhibited a stable post-buckling behaviour for some displacement beyond the peak load, until abrupt loss in load carrying capacity. A different response was observed in the load versus axial deformation curve of SSP1. It shows that the plate buckling strength is much lower than the peak load, which is followed by a very gradual drop in load-carrying capacity. SSP1 has a higher $\beta_1$, making it more susceptible to plate buckling. The stiffener area in SSP1 is larger than SSP4, which allows the stiffened panel to carry much more load after plate buckling. The plate buckling phenomenon is more easily detected from a plot of load versus strain or out-of-plane deformation of the plate. The behaviour of SSP1 was so steady and stable that its failure cannot be identified as catastrophic.

Specimen SSP2 was intentionally designed to duplicate the most critical interaction buckling response found in Sheikh *et al.* (2001), which characterizes an interaction buckling behaviour where both plate buckling and overall buckling occur simultaneously. Unfortunately, SSP2 failed by stiffener tripping failure; its change in failure mode is attributed to the presence of eccentricity towards its stiffener.

In addition to the experimental program, a finite element analysis was carried out to predict the behaviour of the test specimens. The model was similar to the preliminary analysis model, but it incorporated the measured specimen dimensions, material properties, initial imperfection and residual stresses. The analyses were conducted at different load eccentricities as selected in the experimental program. The numerical model was verified by comparing the predicted failure mode and the predicted load versus displacement response against the response observed during testing. Two failure modes were observed in the analyses: interaction buckling and stiffener tripping, which were consistent with the corresponding buckling modes of the test specimens. The deformed shapes captured in the finite element analysis resembled the deformed pattern observed in the tests. Although the finite element model can adequately predict the failure mode and the buckling behaviour of test specimens, discrepancies were found in the displacements. The finite element model shows excellent agreement in the prediction of critical strength for three out of four test specimens but a relatively large difference in the strength for SSP1. The cause of such prediction for SSP1 is unknown. The finite element model predicted a more drastic reduction in capacity in the specimens that failed by interaction buckling.

A numerical investigation of the effect of load eccentricity indicated that the failure mode would shift from interaction buckling to stiffener tripping as the load moved towards the stiffener. Both the numerical and experimental investigations indicated high sensitivity to eccentricity. An eccentricity of 1.25 mm towards the stiffener was found to change the failure mode from interaction buckling to stiffener tripping for test specimen SSP2.

An assessment of DNV 2002, API 2000 and CSA-S136-01/S16-01 indicated that current practice is generally conservative in the prediction of the critical strength. DNV was capable of predicting the failure mode of the test specimens but predicted poorly the strength for stiffener tripping failure. Both API and S136/S16 were unable to predict the failure mode of stiffened steel plates because their design calculations do not provide the various failure modes similar to that of DNV. S136, however, accounts for interaction buckling. Although the API guideline provides the simplest approach, it does not give the most conservative estimate as compared to DNV. Even with the extra consideration for stiffener tripping, DNV did not provide a better solution in predicting the critical strength of stiffened steel plates.

## 6.2 Conclusions

The following conclusions can be drawn from the results of the work described above:

1. The existence of interaction buckling, characterized by plate buckling followed by plate-induced overall buckling was confirmed experimentally. This failure mode is potentially catastrophic with a sudden drop in load-carrying capacity and a substantial decrease in peak strength at the post-buckling regime.

2. The ability of designing stiffened plates with the proposed β-values was successful in duplicating an interaction buckling failure mode. Interaction

buckling was indeed affected primarily by the stiffener to plate area ratio ($\beta_5$) and by the plate transverse slenderness ratio ($\beta_1$) as proposed by Sheikh *et al.* (2001).

3. Plate buckling strength does not always take place at or near the peak load. It can occur before the peak load at as much as 72 % of the peak load. Overall buckling takes place just before the abrupt drop in load-carrying capacity or, infrequently, at the peak load. Therefore, the peak capacity is not associated to plate bucking and the sudden drop in load carrying capacity is not necessarily attributed to overall buckling. It is highly dependent on the redistribution of stresses within the cross-section. If the stiffener is stiff enough, higher capacity can be achieved after plate buckling. The stress within the member will redistribute from the plate to the stiffener, as in the case of specimen SSP1.

4. The failure mode of stiffened plate designed to fail by interaction buckling is sensitive to load eccentricity. A small eccentricity towards the stiffener would trigger stiffener tripping.

5. The finite element model was shown to be capable of predicting the failure mode and the critical strength of stiffened steel plates. The cause of the poor correlation between measured and predicted displacements is still unclear.

6. The examination of the current design guidelines showed that all three guidelines give conservative but unsatisfactory prediction on the critical strength of stiffened steel plates. The mean and coefficient of variation of the test-to-predicted ratio of DNV 2002, API 2000 and CSA-S136-01/S16-01 are 1.43 and 0.25; 1.34 and 0.09; and 1.26 and 0.15, respectively. Both DNV 2002 and CSA-S136-01/S16-01 account for interaction buckling failure but none account for the sudden loss of load carrying capacity. The guidelines also do not account for a hybrid section, therefore, assumptions are necessary as a designer uses the formulas. DNV is conservative in predicting the strength, but predicts well the failure mode of the test specimens. API has the simplest approach and S136/S16 gives the best mean

prediction. In general, there is no one method better than the others in the prediction for interaction buckling. And, it can be concluded that the guidelines are incapable to predict both the strength for interaction buckling and stiffener tripping for stiffened steel plates.

## 6.3 Recommendations

There were only four stiffened steel plates tested experimentally in this study, therefore, it is not sufficient to develop statistical analysis on interaction buckling. More physical tests are recommended to broaden the data for this failure behaviour.

Although the range of dimensionless variables that Sheikh *et al.* (2001) recommended are very successful in obtaining specimens failing by interaction buckling, there are still questions to be answered as to the cause of interaction buckling, the factor that controls the ductility of the stiffened steel plate and the factor that dominates the drastic behaviour in an interaction buckling failure. Hence, a future parametric study is recommended to verify the $\beta$-values recommended by Sheikh *et al.* (2001) and further explore the nature of interaction buckling.

As concluded in this study, stiffened steel plates are sensitive to load eccentricity. A slight eccentric load can cause a change in failure behaviour. Future analytical work is suggested to expand this issue and investigate the effect of eccentricities on failure modes and responses of stiffened steel plates.

The common design practices give poor predictions for the critical strength of interaction buckling failure and stiffener tripping. As such, there is a need to have these guidelines revisited for the stiffener tripping failure mode and to account for the catastrophic behaviour of interaction buckling failure. In addition, the design guidelines are limited to panels with uniform material properties. Therefore, it is necessary for the guidelines to clarify the material properties used in the proposed design calculations for a hybrid section.

# List of References

American Iron and Steel Institute (2002). The North American Specification for the Design of Cold-Formed Steel Members, December 2001 Edition.

American Petroleum Institute (2000). Bulletin on Design of Flat Plate Structures, API Bulletin 2V, Second Edition, September 2000, Washington, D.C.

American Society for Testing and Materials (2002). A370 Standard Test Methods and Definitions for Mechanical Testing of Steel Products. ASTM, Philadelphia, PA.

Aalberg, A., Langseth, M. and Larsen, P.K. (2001). Stiffened Aluminium Panels Subjected to Axial Compression, Thin-Walled Structures, Vol. 39, pp. 861-885.

Alagusundaramoorthy, P., Sundaravadivelu, R., Ganapathy, C. (1999). Experimental Study on Collapse Load of Stiffened Panels with Cutouts, Journal of Constructional Steel Research, Vol. 52, pp. 235-251.

ASCE-ASSHTO (1971). Journal of the structured division, Proceeding of the American society of Civil engineers, progress report on steel girder bridges April 1971 by the Subcommittee on Box Girders of the ASCE-ASSHTO Task Committee on Flexural Members.

Balaz, I. and Murray, N.M. (1992). A Comparison of Some Design Rules with Results from Tests on Longitudinally Stiffened Deck Plates of Box-Girders, Journal of Constructional Steel Research, Vol. 23, pp. 31-54.

Bedair, O.K. and Troitsky, M.S. (1997). A Study of the Fundamental Frequency Characteristics of Eccentrically and Concentrically Simply Supported Stiffened Plates, International Journal of Mechanical Science, Vol. 39, No. 11, pp. 1257-1272.

Bedair, O.K. (1997). Ultimate Compressive Strength of Orthogonally Stiffened Steel Plates (Discussion), Journal of Structural Engineer, August 1997, pp. 1116-1117.

Bedair, O.K. (1998). A Contribution to the Stability of Stiffened Plates under Uniform Compression, Computers and Structures, Vol. 66, No.5, pp. 535-570.

Bhat, S.U. and Wierzbicki, T. (1989). On the Plastic Tripping of Flatbar Stiffeners, Thin-Walled Structures, Vol. 7, No. 3-4, pp. 281-300.

Bonello, M.A. and Chryssanthopoulos, M.K. and Dowling, P.J. (1993). Ultimate Strength Design of Stiffened Plates under Axial Compression and Bending, Marine Structures, Vol. 6, pp. 533-552.

Brosowski, B. and Ghavami, K. (1996). Multi-Criteria Optimal Design of Stiffened Plates. Part 1. Choice of the Formula for the Buckling Load, Thin-Walled Structures, Vol. 24, pp. 353-369.

Budweg, H.L. and Shin, Y.S. (1987). Experimental studies on the tripping behaviour of Narrow T-stiffened Flat Plates Subjected to Hydrostatic Pressure and Underwater Shock, NASA Conference Publication. 2488, Washington, D.C, USA, pp. 61-95.

Canadian Standards Association (2001). CAN/CSA-S16-01—Limit States Design of Steel Structures, Canadian Standards Association, Rexdale, Ontario.

Carlsen, C.A. and Czujko, J. (1978). The Specification of Post-Welding Distortion Tolerances for Stiffened Plates in Compression, The Structural Engineer, Vol. 56A, No. 5, pp. 133-141.

Carlsen, C.A. (1980). A Parametric Study of Collapse of Stiffened Plates in Compression, The Structural Engineer, Vol. 58B, No. 2, pp.33-40

Chatterhee, S. and Dowling, P.J. (1976). The Design of Box Girder Compression Flanges, Paper from Steel Plated Structures, An International Symposium. Discussion can be found in Proceedings of the International Conference on Steel Plated Structures, July, pp. 196-228.

Chen,Q. (1993). Bending Strength of Longitudinally Stiffened Steel Cylinders. Structural Engineering Report No. 192, Department of Civil and Environmental Engineering, University of Alberta, Edmonton.

Chen, S.J. and Yang, K.C. (2002). Inelastic Behaviour of Orthotropic Steel Deck Stiffened by U-Shaped Stiffeners, Thin-Walled Structures, Vol. 40, pp. 537-553.

Danielson, D.A., Kihl, D.P., and, Hodges, D. H. (1990). Tripping of thin-walled plating stiffeners in axial compression. Thin-Walled Structures, Vol. 10, No. 2, pp. 121-142.

Det Norske Veritas (2002). Classification Notes No. 30.1, Buckling Strength Plated Structures, Det Norske Veritas, October 2002, Hovik, Norway.

Dubas, P. (1976). Plated Structures with Closed-Section Stiffeners, Steel Plated Structures, pp. 266-283.

Essa, H.S. and Kennedy, D.J.L. (1993). Distortional Buckling of Steel Beams, Structural Engineering Report No. 185, Department of Civil Engineering, University of Alberta, April.

Falco, S.A. and Ghavami, K. (2001). Vector Optimization of Stiffened Plates Subjected to Axial Compression Load Using the Canadian Norm, Third International Conference on Thin-Walled Structures, Thin-Walled Structures Advance and Developments, pp. 549-558.

Faulkner (1976). Compression Tests on Welded Eccentrically Stiffened Plate Panels, Steel Plated Structures - An International Symposium, pp. 581-617.

Fujii, K. (2002). Cyclic Behaviour of perforated stiffened plates under axial forces, Journal of structural engineering, pp.779-787.

Fujita, Y. and Yoshida, K. (1976). On Ultimate Collapse of Ship Structures – Research in Japan, International Conference on Steel Plated Structures, Imperial College, London, Steel Plated Structures, pp. 542-558.

Galambos, T.V. (1998). Guide to Stability Design Criteria for Metal Structures, Fifth Edition, John Wiley and Sons, Inc.

Ghavami, K. (1994). Experimental Study of Stiffened Plates in Compression up to Collapse, Journal of Constructional Steel Research, Vol. 28, pp. 197-221.

Graham, L.L. and Siragy, E.F. (2001). Stochastic Finite-Element Analysis for Elastic Buckling of Stiffened Panels, Journal of Engineering Mechanics, Vol. 127, No. 1, pp. 91-97.

Grondin, G Y., Chen Q., Elwi, A E. and Cheng, J.J.R. (1998). Stiffened Steel Plates under Compression and Bending, Journal of Constructional Steel Research, Vol. 45, No. 2, pp. 125-148.

Grondin, G.Y., Elwi, A.E. and Cheng, J.J.R. (1999). Buckling of Stiffened Steel Plates: a Parametric Study, Journal of Constructional Steel Research, Vol. 50, No. 2, pp. 151-175.

Horne, M.R. and Narayanan, R. (1976). The Strength of Straightened Welded Steel Stiffened Plates, The Structural Engineer, November, Vol. 54, No. 11, pp. 437-450.

Horne, M.R. and Narayanan, R. (1976). The Strength of Straightened Welded Steel Stiffened Plates, The Structural Engineer, November, Vol. 54, No. 11, pp. 437-450.

Hu, S.Z. (1993). A Finite Element Assessment of the Buckling Strength Equations of Stiffened Plates, In The Ship Strctures Symposium '93, Arlinton, VA, The Ship Structures Committee, pp. J1-J10.

Hu, S.Z., Chen, Q., Pegg, N. and Zimmerman, T.J.E. (1997). Ultimate Collapse Tests of Stiffened-Plate Ship Structural Units, Marine Structures, Vol. 10, No. 8, pp. 587-610.

Li, L.Y. and Bettess, P. (1997). Buckling of Stiffened Plates and Design of Stiffeners, International Journal of Pressure Vessels and Piping, Vol. 74, pp. 177-187.

Louca, L.A. and Harding, J.E. (1996). Torsional buckling of outstands in longitudinally stiffened panels, Thin-Walled Structures Vol. 24, No. 3, pp. 211-229.

Moolani, F.M. and Dowling, P.J. (1976). Ultimate Load Behaviour of Stiffened Plates in Compression, International Conference on Steel Plated Structures, Imperial College, London, pp. 51-88.

Murray, N.W. (1973). Buckling of Stiffened Panels Loaded Axially and in Bending, The Structural Engineer, Vol. 5, No. 8, pp. 285-301.

Murray, N.W. (1983). Ultimate Capacity of Stiffened Plates in Compression. In: Narayanan, R., editor; Plated Structures: Stability and Strength, Applied Science Publishers Ltd., London and New York, Chapter 5, pp. 135-163.

Narayanan, R. (1983). Plated Structures: Stability and Strength, Applied Science Publishers Ltd., London and New York.

Ostapenko, A. and Chu, P.C. (1986). Torsional Strength of Longitudinal in Marine Structures, Lehigh University Friz Engineering Laboratory Report No. 492.3.

Ostapenko, A. (1989). Tripping and Strength of Asymmetrical Plate Stiffeners, Proceedings of the Sessions Related to Steel Structures at Structural Congress '89, San Francisco, CA, USA, ASCE, New York, NY, USA, pp. 637-646.

Paik, J.K., Thayamballi, A.K., Kim, B.J., Wang, G., Shin, Y.S. and Liu, D. (2001). On Advanced Ultimate Limit State Design of Ship Stiffened Panels and Grillages, 2000 SNAME Annual Meeting.

Paik, J.K., Thayamballi, A.K. and Kim, B.J. (2001). Large Deflection Orthotropic Plate Approach to Develop Ultimate Strength Formulations for Stiffened Panels under Combined Biaxial Compression/Tension and Lateral Pressure, Thin-Walled Structures, Vol. 39, pp. 215-246.

Pan,Y.G. and Louca, L.A. (1999). Experimental and Numerical Studies on the Response of Stiffened Plates Subjected to Gas Explosions, Journal of Constructional Steel Research Vol. 52, pp.171-193.

Roik, K. (1976). Effective Breadth and Shear Lag in Plate Girder Bridges which Elastic and Elasto-plastic Material Behaviour, Steel Plated Structures, pp. 169-195.

Schafer, B.W. and Pekoz, T (1997). The Behavior and Design of Longitudinally Stiffened Thin-Walled Compression Elements, Thin-Walled Structures, Vol. 27, No. 1, pp. 65-78

Shanmugam, N.E. and Arockiasamy, M. (1996). Local Buckling of Stiffened Plates in Offshore Structures, Journal of Constructional Steel Research, Vol. 38, No. 1, pp. 41-60.

Sheikh, I.A., Elwi A.E. and Grondin G.Y. (2000). Buckling of Stiffened Steel Plates under Uniaxial Compression and Bending, 3rd Structural Specialty Conference of the CSCE, London, Ontario, June, pp. 21-28.

Sheikh, I.A., Grondin G.Y. and Elwi A.E. (2001). Stiffener Tripping in Stiffened Steel Plates, Structural Engineering Report No. 236, Department of Civil and Environmental Engineering, University of Alberta, April.

Sheikh, I.A., Grondin G.Y. and Elwi A.E. (2002). Stiffened Steel Plates under Uniaxial Compression, Journal of Constructional Steel Research, Vol. 58, pp. 1061-1080

Sheikh, I.A., Elwi, A.E. and Grondin, G.Y. (2003). Stiffened Steel Plates under Combined Compression and Bending, Journal of Constructional Steel Research, Vol. 59, pp. 911-930

Smith, C.S. (1975). Compressive Strength of Welded Steel Ship Grillages, Transactions of Research Institute Naval Architecture (RINA), Vol. 118, pp. 325-359.

Smith, C.S., Anderson, N., Chapman, J.C., Davidson, P.C., and Dowling, P.J. (1991). Strength of Stiffened Plating under Combined Compression and Lateral Pressure, Transactions of Research Institute Naval Architecture, Vol. 134, pp. 131-147.

Sridharan, S. and Zeggane, M. (2001). Stiffened Plates and Cylindrical Shells under Interactive Buckling, Finite Elements in Analysis and Design, Vol. 38, pp. 155-178.

Soares, C.G. and Gordo J.M. (1997). Design Methods for Stiffened Plates Under Predominantly Uniaxial Compression, Marine Structure, Vol. 10, No. 6, pp. 465-497.

Sun, G. and Williams, F.W. (1997). An Initial Post-Buckling Analysis for Prismatic Plate Assemblies under Axial Compression, International Journal of Solids Structures, Vol. 34, No. 28, pp. 3705-3725.

Tebedge, N., Alpsten, G.A. and Tall, L. (1971). Measurement of Residual Stresses – A Study of Methods. Fritz Engineering Laboratory Report No. 337.8, Department of Civil Engineering Lehigh University, Bethlehem, Pennsylvania.

Troitsky M.S. (1968). Orthotropic Bridges Theory and Design. The James F. Lincoln Arc Welding Foundtaion Cleveland, O.H.

Troitsky M.S. (1976). Stiffened Plates: Bending, Stability and Vibrations, Elsevier Scientific Publishing Company, Amsterdam, The Netherlands.

Von Karman, T., E.E. Sechler, and L. H. Donnell (1932). The Strength of Thin Plates in Compression, Transactions ASME, Vol. 54, APM 54-5.

Yu, W.W. (1990). Cold-Formed Steel Design. Second Edition, John Wiley and Sons, New York, N.Y.

Zha, Y.F. and Moan, T (2001). Ultimate Strength of Stiffened Aluminium Panels with Predominantly Torsional Failure Modes, Thin-Walled Structures, Vol. 39, pp. 631-648.

# Appendix A

# Ancillary Test Results

Table A.1 Tension Coupon Test Results

| Plate Designation | Coupon | Measured Plate Thickness (mm) | Modulus of Elasticity, E (MPa) | Static Yield Strength, $\sigma_{sy}$ (MPa) | Dynamic Yield Strength, $\sigma_{dy}$ (MPa) | Strain Hardening Modulus, $E_{sh}$ (MPa) | Static Ultimate Strength, $\sigma_{su}$ (MPa) | Dynamic Ultimate Strength, $\sigma_{du}$ (MPa) | Ultimate Strain (%) | Rupture Strain (%) |
|---|---|---|---|---|---|---|---|---|---|---|
| 11 GA | 1 | 3.0 | 202000 | 194 | 206 | 1360 | 301 | 323 | 24.8 | 46.8 |
| | 2 | 3.0 | 214000 | 185 | 208 | 1440 | — | 331 | 23.5 | — |
| | 3 | 3.0 | 203000 | 222 | 232 | 1360 | 332 | 353 | 24.5 | 46.8 |
| | Mean | 3.0 | 206000 | 200 | 215 | 1390 | 317 | 336 | 24.2 | 46.8 |
| 10 GA | 1 | 3.3 | 170000 | 286 | 301 | 1380 | 357 | 382 | 19.0 | 37.7 |
| | 2 | 3.4 | 204000 | 283 | 296 | 1390 | 355 | 378 | 19.1 | 40.3 |
| | 3 | 3.4 | 200000 | 284 | 297 | 1350 | 360 | 380 | 18.3 | 39.0 |
| | Mean | 3.4 | 191000 | 284 | 298 | 1380 | 357 | 380 | 18.8 | 39.0 |
| 3/16" | 1 | 4.8 | 204000 | 289 | 319 | 1780 | 439 | 468 | 22.3 | 33.2 |
| | 2 | 4.8 | 201000 | 306 | 319 | 1890 | 440 | 467 | 21.1 | 33.9 |
| | 3 | 4.8 | 201000 | 306 | 320 | 1990 | 443 | 467 | 23.1 | 34.4 |
| | Mean | 4.8 | 202000 | 300 | 319 | 1880 | 441 | 467 | 22.2 | 33.8 |
| 1/4" | 1 | 6.3 | 202000 | 329 | 346 | 2370 | 473 | 509 | 21.0 | 35.9 |
| | 2 | 6.3 | 196000 | 329 | 346 | 2410 | 479 | 510 | 20.6 | 34.5 |
| | 3 | 6.3 | 198000 | 331 | 346 | 2440 | 479 | 511 | 20.4 | 32.9 |
| | Mean | 6.3 | 199000 | 330 | 346 | 2410 | 477 | 510 | 20.7 | 34.4 |
| 5/16" | 1 | 7.9 | 195000 | 296 | 296 | 4340 | 440 | 469 | 19.3 | 40.0 |
| | 2 | 7.9 | 194000 | 294 | 293 | 4530 | 440 | 469 | 21.0 | 41.2 |
| | 3 | 7.9 | 200000 | 309 | 309 | 3840 | 439 | 468 | 19.6 | 39.6 |
| | Mean | 7.9 | 196000 | 287 | 299 | 4230 | 440 | 469 | 20.0 | 40.3 |
| 3/8" | 1 | 9.5 | 200000 | 403 | 417 | 1390 | 475 | 504 | 17.5 | 39.3 |
| | 2 | 9.5 | 201000 | 404 | 420 | 1410 | 479 | 507 | 18.3 | 38.7 |
| | 3 | 9.5 | 196000 | 400 | 419 | 1470 | 476 | 504 | 17.1 | 40.5 |
| | Mean | 9.5 | 199000 | 402 | 419 | 1420 | 476 | 505 | 17.7 | 39.5 |
| 1/2" | 1 | 12.7 | 201000 | 343 | 356 | 2110 | 473 | 500 | 16.8 | 42.5 |
| | 2 | 12.7 | 206000 | 341 | 354 | 2550 | 475 | 502 | — | 31.2 |
| | 3 | 12.7 | 204000 | 337 | 353 | 2410 | 476 | 500 | 18.7 | 44.0 |
| | Mean | 12.7 | 204000 | 340 | 354 | 2350 | 475 | 501 | 17.8 | 39.2 |

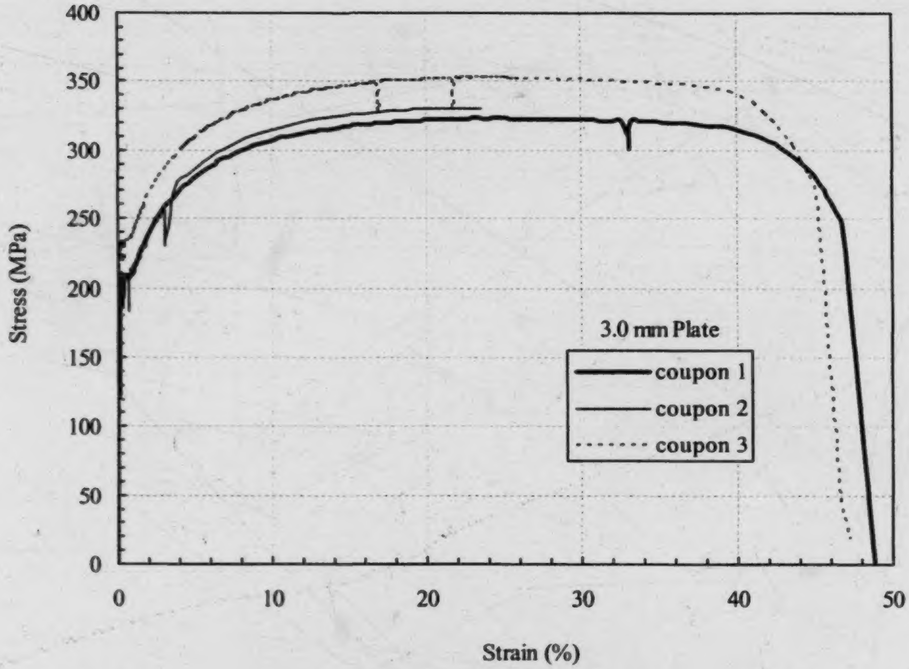

Figure A.1 Stress versus Strain Curves for the 3.0 mm Plate

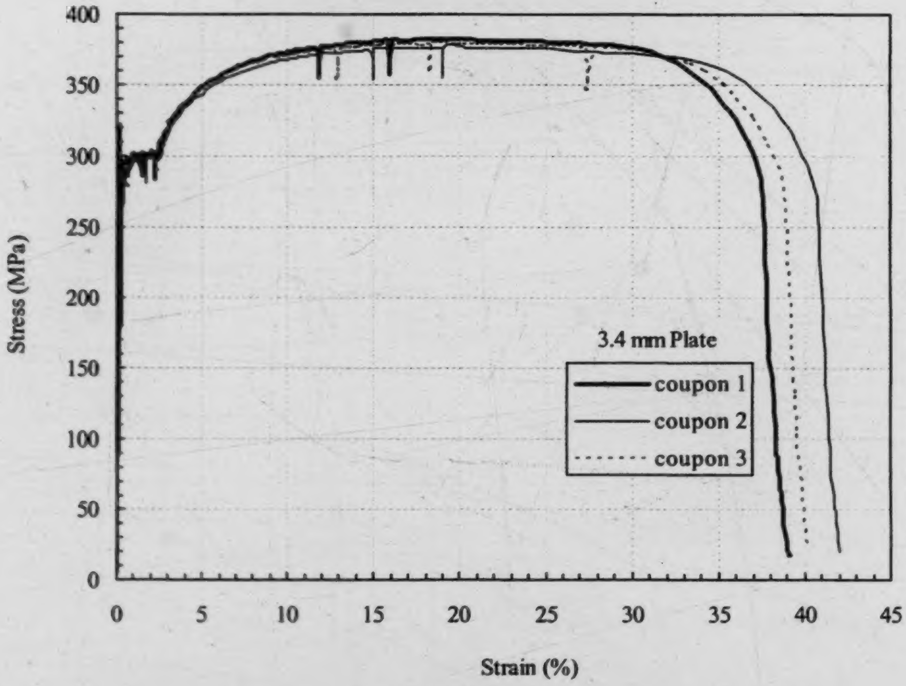

Figure A.2 Stress versus Strain Curves for the 3.4 mm Plate

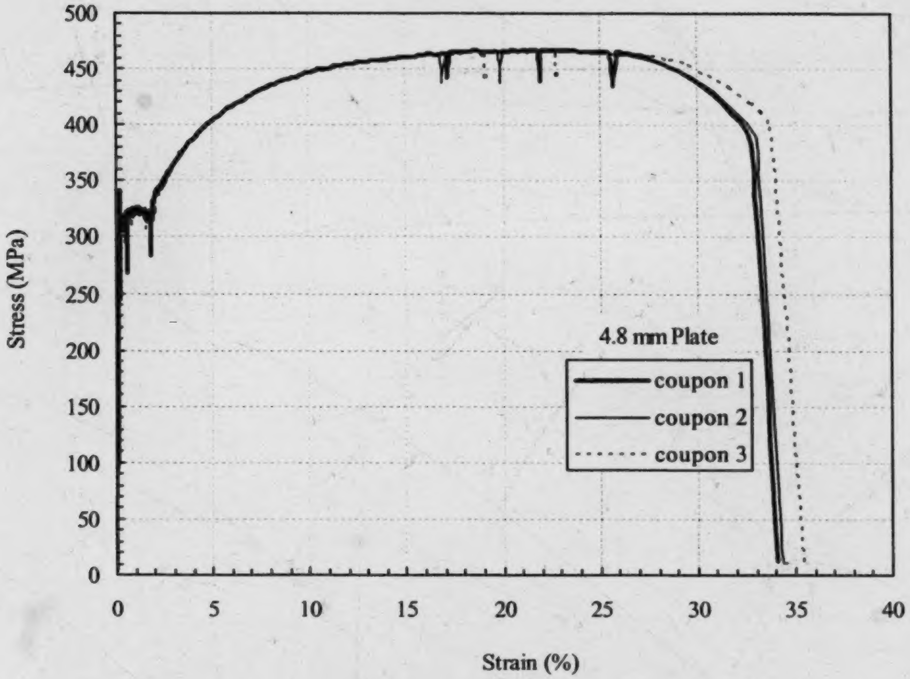

Figure A.3 Stress versus Strain Curves for the 4.8 mm Plate

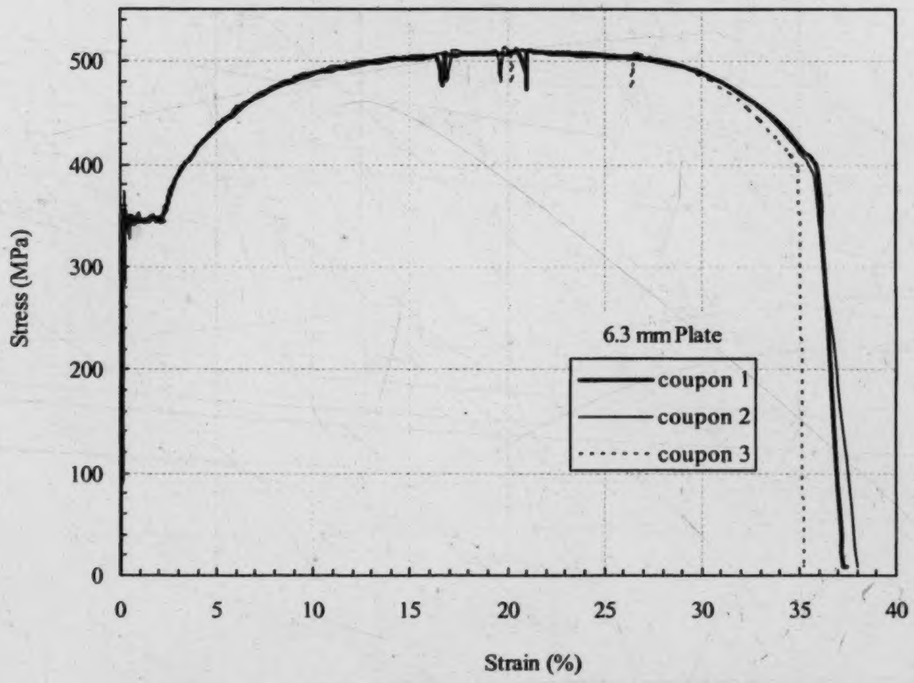

Figure A.4 Stress versus Strain Curves for the 6.3 mm Plate

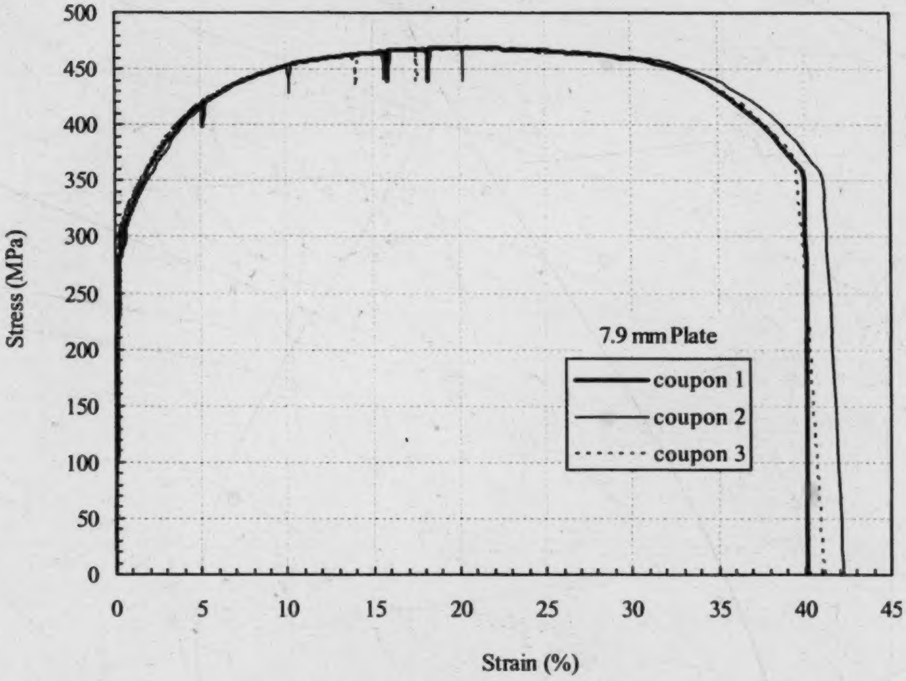

Figure A.5 Stress versus Strain Curves for the 7.9 mm Plate

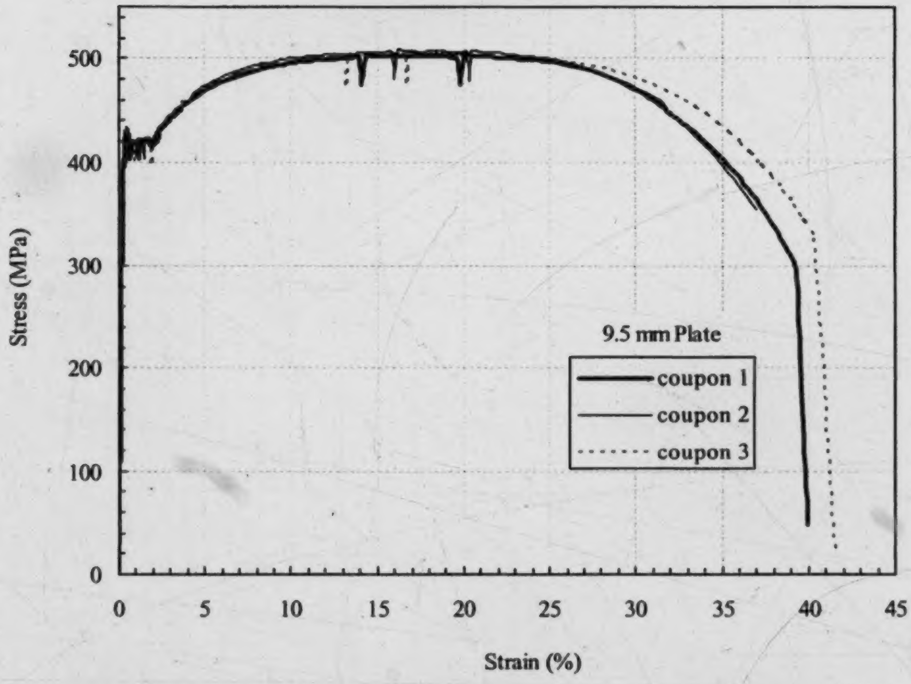

Figure A.6 Stress versus Strain Curves for the 9.5 mm Plate

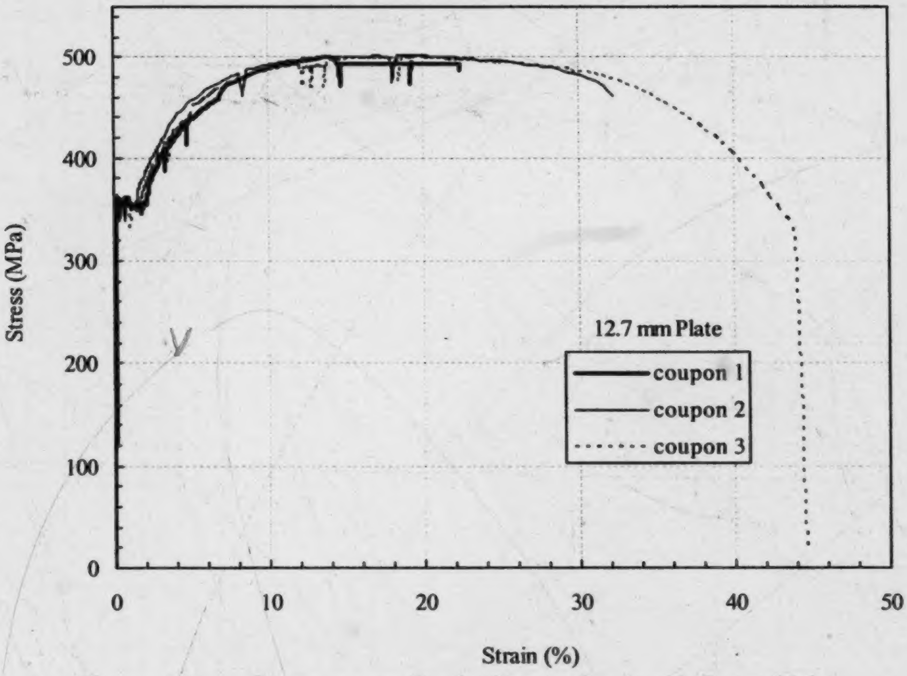

Figure A.7 Stress versus Strain Curves for the 12.7 mm Plate

# Appendix B

## Results of Initial Imperfection Measurements

## Initial Imperfection Measurements

The initial out-of-plane deflections of the test specimens were measured before testing. These measurements included the initial imperfections of the plate, web, and flange as presented in Tables B.1 to B.4. Since the initial imperfection measurements were not performed on the same grid layout as the finite element mesh, a mapping process based on an inverse distance weighted least squares method was carried out using the commercial software Surfer 8.0® Surface Mapping System. The adjusted results were used to develop models of the specimens for the finite element analysis. On top of the adjusted results, the program was capable of producing grid mesh of each specimen as shown in Figures B.1 to B.3.

Table B.1 Measured Initial Imperfection Data for Specimen SSP1

| Plate | | | | | | | | |
|---|---|---|---|---|---|---|---|---|
| **1-dir.** | **2-dir.** | **3-dir. (imperfection)** | **1-dir.** | **2-dir.** | **3-dir. (imperfection)** | **1-dir.** | **2-dir.** | **3-dir. (imperfection)** |
| -875 | 202 | 1.5 | -875 | -52.3 | 0.4 | -875 | 127.3 | -0.7 |
| -750 | 202 | 1.2 | -750 | -52.3 | 0.7 | -750 | 127.3 | -0.4 |
| -625 | 202 | 0.6 | -625 | -52.3 | 0.7 | -625 | 127.3 | 0.1 |
| -500 | 202 | 0.2 | -500 | -52.3 | 0.6 | -500 | 127.3 | 0.4 |
| -375 | 202 | 0.2 | -375 | -52.3 | 0.9 | -375 | 127.3 | 0.7 |
| -250 | 202 | 0.3 | -250 | -52.3 | 1.2 | -250 | 127.3 | 1.0 |
| -125 | 202 | -0.1 | -125 | -52.3 | 1.2 | -125 | 127.3 | 1.1 |
| 0 | 202 | -0.4 | 0 | -52.3 | 1.1 | 0 | 127.3 | 1.0 |
| 125 | 202 | -0.9 | 125 | -52.3 | 1.0 | 125 | 127.3 | 1.0 |
| 250 | 202 | -1.4 | 250 | -52.3 | 0.6 | 250 | 127.3 | 0.8 |
| 375 | 202 | -1.7 | 375 | -52.3 | 0.2 | 375 | 127.3 | 0.7 |
| 500 | 202 | -1.7 | 500 | -52.3 | 0.0 | 500 | 127.3 | 0.6 |
| 625 | 202 | -1.8 | 625 | -52.3 | 0.1 | 625 | 127.3 | 0.9 |
| 750 | 202 | -1.9 | 750 | -52.3 | 0.0 | 750 | 127.3 | 1.1 |
| 875 | 202 | -2.1 | 875 | -52.3 | -0.4 | 875 | 127.3 | 1.2 |
| -875 | 127 | -1.7 | -875 | 52.3 | -0.5 | -875 | 202.3 | -2.2 |
| -750 | 127 | -1.7 | -750 | 52.3 | 0.0 | -750 | 202.3 | -1.9 |
| -625 | 127 | -1.9 | -625 | 52.3 | 0.4 | -625 | 202.3 | -1.5 |
| -500 | 127 | -2.1 | -500 | 52.3 | 0.5 | -500 | 202.3 | -1.1 |
| -375 | 127 | -2.0 | -375 | 52.3 | 0.9 | -375 | 202.3 | -0.8 |
| -250 | 127 | -1.8 | -250 | 52.3 | 1.2 | -250 | 202.3 | -0.5 |
| -125 | 127 | -1.9 | -125 | 52.3 | 1.3 | -125 | 202.3 | -0.5 |
| 0 | 127 | -2.1 | 0 | 52.3 | 1.2 | 0 | 202.3 | -0.5 |
| 125 | 127 | -2.4 | 125 | 52.3 | 1.2 | 125 | 202.3 | -0.7 |
| 250 | 127 | -2.8 | 250 | 52.3 | 1.0 | 250 | 202.3 | -0.7 |
| 375 | 127 | -3.1 | 375 | 52.3 | 0.8 | 375 | 202.3 | -0.7 |
| 500 | 127 | -3.2 | 500 | 52.3 | 0.5 | 500 | 202.3 | -0.5 |
| 625 | 127 | -3.2 | 625 | 52.3 | 0.7 | 625 | 202.3 | -0.2 |
| 750 | 127 | -3.3 | 750 | 52.3 | 0.7 | 750 | 202.3 | 0.3 |
| 875 | 127 | -3.5 | 875 | 52.3 | 0.5 | 875 | 202.3 | 0.5 |

Note: All data in mm

Table B.1 Measured Initial Imperfection Data for Specimen SSP1 (con't)

| Flange | | | | | | | | |
|---|---|---|---|---|---|---|---|---|
| 1-dir. | 2-dir. | 3-dir. (imperfection) | 1-dir. | 2-dir. | 3-dir. (imperfection) | 1-dir. | 2-dir. | 3-dir. (imperfection) |
| -875 | -15 | 161.5 | -875 | 0 | 161.4 | -875 | 15 | 162.3 |
| -750 | -15 | 162.0 | -750 | 0 | 162.0 | -750 | 15 | 162.8 |
| -625 | -15 | 162.2 | -625 | 0 | 162.1 | -625 | 15 | 163.0 |
| -500 | -15 | 162.3 | -500 | 0 | 162.1 | -500 | 15 | 162.9 |
| -375 | -15 | 162.3 | -375 | 0 | 162.1 | -375 | 15 | 162.9 |
| -250 | -15 | 162.5 | -250 | 0 | 162.3 | -250 | 15 | 163.1 |
| -125 | -15 | 162.5 | -125 | 0 | 162.4 | -125 | 15 | 163.2 |
| 0 | -15 | 162.5 | 0 | 0 | 162.5 | 0 | 15 | 163.3 |
| 125 | -15 | 162.5 | 125 | 0 | 162.4 | 125 | 15 | 163.2 |
| 250 | -15 | 162.3 | 250 | 0 | 162.1 | 250 | 15 | 162.9 |
| 375 | -15 | 161.9 | 375 | 0 | 161.7 | 375 | 15 | 162.5 |
| 500 | -15 | 161.8 | 500 | 0 | 161.6 | 500 | 15 | 162.3 |
| 625 | -15 | 161.7 | 625 | 0 | 161.5 | 625 | 15 | 162.3 |
| 750 | -15 | 161.5 | 750 | 0 | 161.4 | 750 | 15 | 162.2 |
| 875 | -15 | 161.2 | 875 | 0 | 161.1 | 875 | 15 | 161.9 |

| Web | | | | | | | | |
|---|---|---|---|---|---|---|---|---|
| 1-dir. | 2-dir. (imperfection) | 3-dir. | 1-dir. | 2-dir. (imperfection) | 3-dir. | 1-dir. | 2-dir. (imperfection) | 3-dir. |
| -875 | 0.7 | 33.4 | -250 | -2.6 | 73.4 | 375 | -4.2 | 113.4 |
| -750 | 0.7 | 33.4 | -125 | -2.9 | 73.4 | 500 | -3.9 | 113.4 |
| -625 | 0.2 | 33.4 | 0 | -2.9 | 73.4 | 625 | -3.0 | 113.4 |
| -500 | -0.9 | 33.4 | 125 | -2.9 | 73.4 | 750 | -1.7 | 113.4 |
| -375 | -1.4 | 33.4 | 250 | -2.9 | 73.4 | 875 | -0.6 | 113.4 |
| -250 | -1.5 | 33.4 | 375 | -2.7 | 73.4 | -875 | -0.2 | 133.4 |
| -125 | -1.7 | 33.4 | 500 | -2.4 | 73.4 | -750 | -0.7 | 133.4 |
| 0 | -1.7 | 33.4 | 625 | -1.7 | 73.4 | -625 | -1.4 | 133.4 |
| 125 | -1.7 | 33.4 | 750 | -0.8 | 73.4 | -500 | -2.9 | 133.4 |
| 250 | -1.5 | 33.4 | 875 | -0.1 | 73.4 | -375 | -4.1 | 133.4 |
| 375 | -1.1 | 33.4 | -875 | -0.2 | 113.4 | -250 | -4.2 | 133.4 |
| 500 | -0.8 | 33.4 | -750 | -0.4 | 113.4 | -125 | -4.6 | 133.4 |
| 625 | -0.4 | 33.4 | -625 | -1.1 | 113.4 | 0 | -4.6 | 133.4 |
| 750 | 0.2 | 33.4 | -500 | -2.6 | 113.4 | 125 | -4.6 | 133.4 |
| 875 | 0.6 | 33.4 | -375 | -3.6 | 113.4 | 250 | -5.0 | 133.4 |
| -875 | 0.2 | 73.4 | -250 | -3.7 | 113.4 | 375 | -4.9 | 133.4 |
| -750 | 0.1 | 73.4 | -125 | -4.0 | 113.4 | 500 | -4.6 | 133.4 |
| -625 | -0.5 | 73.4 | 0 | -4.1 | 113.4 | 625 | -3.6 | 133.4 |
| -500 | -1.8 | 73.4 | 125 | -4.1 | 113.4 | 750 | -2.0 | 133.4 |
| -375 | -2.5 | 73.4 | 250 | -4.3 | 113.4 | 875 | -0.9 | 133.4 |

Note: All data in mm

Table B.2 Measured Initial Imperfection Data for Specimen SSP2

| Plate | | | | | | | | |
|---|---|---|---|---|---|---|---|---|
| **1-dir.** | **2-dir.** | **3-dir.** (imperfection) | **1-dir.** | **2-dir.** | **3-dir.** (imperfection) | **1-dir.** | **2-dir.** | **3-dir.** (imperfection) |
| -900 | -200 | -0.1 | -900 | -50 | 0.5 | -900 | 125 | 1.4 |
| -780 | -200 | 0.2 | -780 | -50 | 1.4 | -780 | 125 | 1.8 |
| -660 | -200 | 0.3 | -660 | -50 | 2.0 | -660 | 125 | 2.3 |
| -540 | -200 | 0.1 | -540 | -50 | 2.1 | -540 | 125 | 2.1 |
| -420 | -200 | -0.2 | -420 | -50 | 1.9 | -420 | 125 | 1.8 |
| -300 | -200 | -0.4 | -300 | -50 | 1.8 | -300 | 125 | 1.6 |
| -180 | -200 | -0.6 | -180 | -50 | 1.5 | -180 | 125 | 1.3 |
| -60 | -200 | -0.8 | -60 | -50 | 1.1 | -60 | 125 | 0.9 |
| 60 | -200 | -0.8 | 60 | -50 | 1.1 | 60 | 125 | 0.8 |
| 180 | -200 | -0.8 | 180 | -50 | 1.2 | 180 | 125 | 0.8 |
| 300 | -200 | -0.8 | 300 | -50 | 1.1 | 300 | 125 | 0.7 |
| 420 | -200 | -0.8 | 420 | -50 | 0.8 | 420 | 125 | 0.5 |
| 540 | -200 | -0.6 | 540 | -50 | 1.0 | 540 | 125 | 0.6 |
| 660 | -200 | -0.2 | 660 | -50 | 1.3 | 660 | 125 | 0.9 |
| 780 | -200 | 0.1 | 780 | -50 | 1.1 | 780 | 125 | 0.8 |
| 900 | -200 | -0.2 | 900 | -50 | 0.2 | 900 | 125 | 0.4 |
| -900 | -125 | -0.1 | -900 | 50 | 0.8 | -900 | 200 | 1.6 |
| -780 | -125 | 0.4 | -780 | 50 | 1.8 | -780 | 200 | 1.8 |
| -660 | -125 | 0.7 | -660 | 50 | 2.4 | -660 | 200 | 2.0 |
| -540 | -125 | 0.7 | -540 | 50 | 2.4 | -540 | 200 | 1.6 |
| -420 | -125 | 0.5 | -420 | 50 | 2.1 | -420 | 200 | 1.1 |
| -300 | -125 | 0.3 | -300 | 50 | 2.0 | -300 | 200 | 0.8 |
| -180 | -125 | 0.1 | -180 | 50 | 1.7 | -180 | 200 | 0.3 |
| -60 | -125 | -0.2 | -60 | 50 | 1.3 | -60 | 200 | -0.1 |
| 60 | -125 | -0.2 | 60 | 50 | 1.2 | 60 | 200 | -0.3 |
| 180 | -125 | -0.2 | 180 | 50 | 1.3 | 180 | 200 | -0.3 |
| 300 | -125 | -0.3 | 300 | 50 | 1.1 | 300 | 200 | -0.5 |
| 420 | -125 | -0.4 | 420 | 50 | 0.8 | 420 | 200 | -0.5 |
| 540 | -125 | -0.2 | 540 | 50 | 1.1 | 540 | 200 | -0.3 |
| 660 | -125 | 0.1 | 660 | 50 | 1.3 | 660 | 200 | -0.1 |
| 780 | -125 | 0.2 | 780 | 50 | 1.1 | 780 | 200 | 0.0 |
| 900 | -125 | -0.4 | 900 | 50 | 0.2 | 900 | 200 | -0.2 |

Note: All data in mm

Table B.2 Measured Initial Imperfection Data for Specimen SSP2 (con't)

| Flange | | | | | | | | |
|---|---|---|---|---|---|---|---|---|
| **1-dir.** | **2-dir.** | **3-dir.** **(imperfection)** | **1-dir.** | **2-dir.** | **3-dir.** **(imperfection)** | **1-dir.** | **2-dir.** | **3-dir.** **(imperfection)** |
| -900 | -15 | 95.4 | -900 | 0 | 95.3 | -900 | 15 | 96.0 |
| -780 | -15 | 96.8 | -780 | 0 | 96.6 | -780 | 15 | 97.4 |
| -660 | -15 | 97.4 | -660 | 0 | 97.3 | -660 | 15 | 98.3 |
| -540 | -15 | 97.4 | -540 | 0 | 97.4 | -540 | 15 | 98.4 |
| -420 | -15 | 97.2 | -420 | 0 | 97.2 | -420 | 15 | 98.3 |
| -300 | -15 | 97.1 | -300 | 0 | 97.0 | -300 | 15 | 98.0 |
| -180 | -15 | 97.0 | -180 | 0 | 96.8 | -180 | 15 | 97.6 |
| -60 | -15 | 96.8 | -60 | 0 | 96.6 | -60 | 15 | 97.3 |
| 60 | -15 | 96.6 | 60 | 0 | 96.3 | 60 | 15 | 97.1 |
| 180 | -15 | 96.7 | 180 | 0 | 96.5 | 180 | 15 | 97.3 |
| 300 | -15 | 96.5 | 300 | 0 | 96.5 | 300 | 15 | 97.4 |
| 420 | -15 | 96.6 | 420 | 0 | 96.5 | 420 | 15 | 97.5 |
| 540 | -15 | 96.7 | 540 | 0 | 96.5 | 540 | 15 | 97.3 |
| 660 | -15 | 97.0 | 660 | 0 | 96.7 | 660 | 15 | 97.4 |
| 780 | -15 | 96.7 | 780 | 0 | 96.6 | 780 | 15 | 97.4 |
| 900 | -15 | 95.6 | 900 | 0 | 95.6 | 900 | 15 | 96.5 |

| Web | | | | | | | | |
|---|---|---|---|---|---|---|---|---|
| **1-dir.** | **2-dir.** **(imperfection)** | **3-dir.** | **1-dir.** | **2-dir.** **(imperfection)** | **3-dir.** | **1-dir.** | **2-dir.** **(imperfection)** | **3-dir.** |
| -900 | 0.4 | 31.7 | -900 | 0.0 | 51.7 | -900 | -0.4 | 71.7 |
| -780 | 0.9 | 31.7 | -780 | 0.1 | 51.7 | -780 | -0.8 | 71.7 |
| -660 | 0.1 | 31.7 | -660 | -0.6 | 51.7 | -660 | -1.4 | 71.7 |
| -540 | -0.9 | 31.7 | -540 | -1.4 | 51.7 | -540 | -2.3 | 71.7 |
| -420 | -1.1 | 31.7 | -420 | -1.6 | 51.7 | -420 | -2.3 | 71.7 |
| -300 | -0.5 | 31.7 | -300 | -1.3 | 51.7 | -300 | -2.2 | 71.7 |
| -180 | -0.8 | 31.7 | -180 | -1.5 | 51.7 | -180 | -2.2 | 71.7 |
| -60 | -0.8 | 31.7 | -60 | -1.7 | 51.7 | -60 | -2.7 | 71.7 |
| 60 | -0.5 | 31.7 | 60 | -1.6 | 51.7 | 60 | -2.4 | 71.7 |
| 180 | -1.4 | 31.7 | 180 | -2.0 | 51.7 | 180 | -2.7 | 71.7 |
| 300 | -1.1 | 31.7 | 300 | -1.8 | 51.7 | 300 | -2.6 | 71.7 |
| 420 | -0.5 | 31.7 | 420 | -1.3 | 51.7 | 420 | -2.1 | 71.7 |
| 540 | -0.3 | 31.7 | 540 | -0.9 | 51.7 | 540 | -1.6 | 71.7 |
| 660 | 0.9 | 31.7 | 660 | 0.1 | 51.7 | 660 | -0.8 | 71.7 |
| 780 | 0.3 | 31.7 | 780 | -0.2 | 51.7 | 780 | -0.9 | 71.7 |
| 900 | 0.7 | 31.7 | 900 | 0.1 | 51.7 | 900 | -0.6 | 71.7 |

Note: All data in mm

Table B.3 Measured Initial Imperfection Data for Specimen SSP3

| Plate | | | | | | | | |
|---|---|---|---|---|---|---|---|---|
| **1-dir.** | **2-dir.** | **3-dir. (imperfection)** | **1-dir.** | **2-dir.** | **3-dir. (imperfection)** | **1-dir.** | **2-dir.** | **3-dir. (imperfection)** |
| -900 | -201.5 | 2.0 | -900 | -51.5 | 2.6 | -900 | 126.5 | 1.6 |
| -750 | -201.5 | 1.7 | -750 | -51.5 | 4.0 | -750 | 126.5 | 2.2 |
| -600 | -201.5 | 1.1 | -600 | -51.5 | 4.0 | -600 | 126.5 | 2.0 |
| -450 | -201.5 | 0.4 | -450 | -51.5 | 3.9 | -450 | 126.5 | 1.7 |
| -300 | -201.5 | -0.1 | -300 | -51.5 | 3.7 | -300 | 126.5 | 1.6 |
| -150 | -201.5 | -0.4 | -150 | -51.5 | 3.5 | -150 | 126.5 | 1.4 |
| 0 | -201.5 | -0.4 | 0 | -51.5 | 3.5 | 0 | 126.5 | 1.5 |
| 150 | -201.5 | 0.0 | 150 | -51.5 | 4.1 | 150 | 126.5 | 2.1 |
| 300 | -201.5 | 0.2 | 300 | -51.5 | 4.3 | 300 | 126.5 | 2.4 |
| 450 | -201.5 | 0.3 | 450 | -51.5 | 4.2 | 450 | 126.5 | 2.5 |
| 600 | -201.5 | 0.1 | 600 | -51.5 | 3.5 | 600 | 126.5 | 2.1 |
| 750 | -201.5 | 0.3 | 750 | -51.5 | 3.2 | 750 | 126.5 | 2.1 |
| 900 | -201.5 | 0.7 | 900 | -51.5 | 2.0 | 900 | 126.5 | 1.9 |
| -900 | -126.5 | 2.0 | -900 | 51.5 | 2.1 | -900 | 201.5 | 1.5 |
| -750 | -126.5 | 2.5 | -750 | 51.5 | 3.5 | -750 | 201.5 | 1.5 |
| -600 | -126.5 | 2.2 | -600 | 51.5 | 3.5 | -600 | 201.5 | 0.8 |
| -450 | -126.5 | 1.8 | -450 | 51.5 | 3.4 | -450 | 201.5 | 0.3 |
| -300 | -126.5 | 1.5 | -300 | 51.5 | 3.2 | -300 | 201.5 | 0.0 |
| -150 | -126.5 | 1.2 | -150 | 51.5 | 3.2 | -150 | 201.5 | -0.1 |
| 0 | -126.5 | 1.2 | 0 | 51.5 | 3.2 | 0 | 201.5 | 0.0 |
| 150 | -126.5 | 1.7 | 150 | 51.5 | 3.9 | 150 | 201.5 | 0.6 |
| 300 | -126.5 | 1.9 | 300 | 51.5 | 4.1 | 300 | 201.5 | 0.9 |
| 450 | -126.5 | 1.9 | 450 | 51.5 | 4.1 | 450 | 201.5 | 1.3 |
| 600 | -126.5 | 1.4 | 600 | 51.5 | 3.4 | 600 | 201.5 | 1.1 |
| 750 | -126.5 | 1.3 | 750 | 51.5 | 3.1 | 750 | 201.5 | 1.5 |
| 900 | -126.5 | 1.0 | 900 | 51.5 | 2.0 | 900 | 201.5 | 2.2 |

Note: All data in mm

Table B.3 Measured Initial Imperfection Data for Specimen SSP3 (con't)

| Flange | | | | | | | | |
|---|---|---|---|---|---|---|---|---|
| 1-dir. | 2-dir. | 3-dir. (imperfection) | 1-dir. | 2-dir. | 3-dir. (imperfection) | 1-dir. | 2-dir. | 3-dir. (imperfection) |
| -900 | -15 | 109.7 | -900 | 0 | 109.4 | -900 | 15 | 110.1 |
| -750 | -15 | 111.1 | -750 | 0 | 110.9 | -750 | 15 | 111.7 |
| -600 | -15 | 111.6 | -600 | 0 | 111.5 | -600 | 15 | 112.5 |
| -450 | -15 | 111.8 | -450 | 0 | 111.8 | -450 | 15 | 112.7 |
| -300 | -15 | 111.5 | -300 | 0 | 111.6 | -300 | 15 | 112.7 |
| -150 | -15 | 111.3 | -150 | 0 | 111.5 | -150 | 15 | 112.7 |
| 0 | -15 | 111.6 | 0 | 0 | 111.7 | 0 | 15 | 112.7 |
| 150 | -15 | 112.3 | 150 | 0 | 112.4 | 150 | 15 | 113.5 |
| 300 | -15 | 112.6 | 300 | 0 | 112.6 | 300 | 15 | 113.7 |
| 450 | -15 | 112.4 | 450 | 0 | 112.4 | 450 | 15 | 113.3 |
| 600 | -15 | 111.8 | 600 | 0 | 111.7 | 600 | 15 | 112.6 |
| 750 | -15 | 110.7 | 750 | 0 | 110.6 | 750 | 15 | 111.5 |
| 900 | -15 | 109.6 | 900 | 0 | 109.4 | 900 | 15 | 110.3 |

| Web | | | | | | | | |
|---|---|---|---|---|---|---|---|---|
| 1-dir. | 2-dir. (imperfection) | 3-dir. | 1-dir. | 2-dir. (imperfection) | 3-dir. | 1-dir. | 2-dir. (imperfection) | 3-dir. |
| -900 | 0.2 | 31.7 | -900 | -0.1 | 61.7 | -900 | -0.4 | 91.7 |
| -750 | 0.3 | 31.7 | -750 | -0.2 | 61.7 | -750 | -0.7 | 91.7 |
| -600 | 0.8 | 31.7 | -600 | 0.0 | 61.7 | -600 | -0.9 | 91.7 |
| -450 | 1.1 | 31.7 | -450 | 0.3 | 61.7 | -450 | -0.6 | 91.7 |
| -300 | -0.1 | 31.7 | -300 | -0.5 | 61.7 | -300 | -0.9 | 91.7 |
| -150 | -0.7 | 31.7 | -150 | -1.0 | 61.7 | -150 | -1.4 | 91.7 |
| 0 | -1.0 | 31.7 | 0 | -1.5 | 61.7 | 0 | -1.7 | 91.7 |
| 150 | -1.0 | 31.7 | 150 | -1.9 | 61.7 | 150 | -2.8 | 91.7 |
| 300 | 0.4 | 31.7 | 300 | -1.2 | 61.7 | 300 | -2.9 | 91.7 |
| 450 | 0.9 | 31.7 | 450 | -0.6 | 61.7 | 450 | -2.3 | 91.7 |
| 600 | 0.3 | 31.7 | 600 | -0.8 | 61.7 | 600 | -2.2 | 91.7 |
| 750 | 0.6 | 31.7 | 750 | -0.8 | 61.7 | 750 | -2.2 | 91.7 |
| 900 | 0.2 | 31.7 | 900 | -0.7 | 61.7 | 900 | -1.8 | 91.7 |

Note: All data in mm

Table B.4 Measured Initial Imperfection Data for Specimen SSP4

| Plate | | | | | | | | |
|---|---|---|---|---|---|---|---|---|
| **1-dir.** | **2-dir.** | **3-dir.** (imperfection) | **1-dir.** | **2-dir.** | **3-dir.** (imperfection) | **1-dir.** | **2-dir.** | **3-dir.** (imperfection) |
| -900 | -201.6 | 2.5 | -900 | -51.6 | 1.0 | -900 | 126.6 | -2.0 |
| -750 | -201.6 | 1.3 | -750 | -51.6 | 0.7 | -750 | 126.6 | -2.2 |
| -600 | -201.6 | 0.2 | -600 | -51.6 | 0.0 | -600 | 126.6 | -2.8 |
| -450 | -201.6 | -0.5 | -450 | -51.6 | -0.4 | -450 | 126.6 | -3.0 |
| -300 | -201.6 | -0.5 | -300 | -51.6 | 0.2 | -300 | 126.6 | -2.4 |
| -150 | -201.6 | -0.4 | -150 | -51.6 | 0.6 | -150 | 126.6 | -1.7 |
| 0 | -201.6 | -0.3 | 0 | -51.6 | 0.7 | 0 | 126.6 | -1.0 |
| 150 | -201.6 | -0.7 | 150 | -51.6 | 0.8 | 150 | 126.6 | -0.7 |
| 300 | -201.6 | -1.1 | 300 | -51.6 | 0.7 | 300 | 126.6 | -0.5 |
| 450 | -201.6 | -1.3 | 450 | -51.6 | 0.6 | 450 | 126.6 | -0.3 |
| 600 | -201.6 | -1.6 | 600 | -51.6 | 0.4 | 600 | 126.6 | -0.2 |
| 750 | -201.6 | -1.5 | 750 | -51.6 | 0.3 | 750 | 126.6 | 0.1 |
| 900 | -201.6 | -1.2 | 900 | -51.6 | 0.1 | 900 | 126.6 | 0.1 |
| -900 | -126.6 | 1.8 | -900 | 51.6 | -0.8 | -900 | 201.6 | -2.3 |
| -750 | -126.6 | 1.1 | -750 | 51.6 | -0.8 | -750 | 201.6 | -2.7 |
| -600 | -126.6 | 0.2 | -600 | 51.6 | -1.4 | -600 | 201.6 | -3.2 |
| -450 | -126.6 | -0.2 | -450 | 51.6 | -1.7 | -450 | 201.6 | -3.5 |
| -300 | -126.6 | 0.0 | -300 | 51.6 | -1.0 | -300 | 201.6 | -2.9 |
| -150 | -126.6 | 0.3 | -150 | 51.6 | -0.5 | -150 | 201.6 | -2.1 |
| 0 | -126.6 | 0.5 | 0 | 51.6 | 0.0 | 0 | 201.6 | -1.3 |
| 150 | -126.6 | 0.3 | 150 | 51.6 | 0.2 | 150 | 201.6 | -0.9 |
| 300 | -126.6 | 0.1 | 300 | 51.6 | 0.3 | 300 | 201.6 | -0.4 |
| 450 | -126.6 | -0.1 | 450 | 51.6 | 0.3 | 450 | 201.6 | 0.0 |
| 600 | -126.6 | -0.3 | 600 | 51.6 | 0.3 | 600 | 201.6 | 0.3 |
| 750 | -126.6 | -0.3 | 750 | 51.6 | 0.3 | 750 | 201.6 | 0.7 |
| 900 | -126.6 | -0.3 | 900 | 51.6 | 0.1 | 900 | 201.6 | 1.0 |

Note: All data in mm

Table B.4 Measured Initial Imperfection Data for Specimen SSP4 (con't)

| Flange | | | | | | | | |
|---|---|---|---|---|---|---|---|---|
| 1-dir. | 2-dir. | 3-dir. (imperfection) | 1-dir. | 2-dir. | 3-dir. (imperfection) | 1-dir. | 2-dir. | 3-dir. (imperfection) |
| -900 | -15 | 135.2 | -900 | 0 | 135.1 | -900 | 15 | 136.0 |
| -750 | -15 | 135.2 | -750 | 0 | 135.1 | -750 | 15 | 135.9 |
| -600 | -15 | 134.8 | -600 | 0 | 134.7 | -600 | 15 | 135.4 |
| -450 | -15 | 134.1 | -450 | 0 | 133.9 | -450 | 15 | 134.7 |
| -300 | -15 | 135.0 | -300 | 0 | 134.9 | -300 | 15 | 135.7 |
| -150 | -15 | 135.3 | -150 | 0 | 135.2 | -150 | 15 | 136.0 |
| 0 | -15 | 135.9 | 0 | 0 | 135.8 | 0 | 15 | 136.5 |
| 150 | -15 | 136.1 | 150 | 0 | 136.0 | 150 | 15 | 136.9 |
| 300 | -15 | 135.9 | 300 | 0 | 135.9 | 300 | 15 | 136.8 |
| 450 | -15 | 136.2 | 450 | 0 | 135.9 | 450 | 15 | 136.6 |
| 600 | -15 | 135.7 | 600 | 0 | 135.7 | 600 | 15 | 136.4 |
| 750 | -15 | 135.5 | 750 | 0 | 135.6 | 750 | 15 | 136.4 |
| 900 | -15 | 135.1 | 900 | 0 | 135.1 | 900 | 15 | 136.0 |

| Web | | | | | | | | |
|---|---|---|---|---|---|---|---|---|
| 1-dir. | 2-dir. (imperfection) | 3-dir. | 1-dir. | 2-dir. (imperfection) | 3-dir. | 1-dir. | 2-dir. (imperfection) | 3-dir. |
| -900 | 0.2 | 33.3 | -900 | 0.2 | 73.3 | -900 | 0.1 | 113.3 |
| -750 | -0.4 | 33.3 | -750 | -0.6 | 73.3 | -750 | -0.9 | 113.3 |
| -600 | 0.1 | 33.3 | -600 | -0.6 | 73.3 | -600 | -1.1 | 113.3 |
| -450 | 0.0 | 33.3 | -450 | -0.5 | 73.3 | -450 | -1.0 | 113.3 |
| -300 | -0.1 | 33.3 | -300 | -0.2 | 73.3 | -300 | -0.5 | 113.3 |
| -150 | -0.1 | 33.3 | -150 | 0.1 | 73.3 | -150 | 0.2 | 113.3 |
| 0 | -0.5 | 33.3 | 0 | -0.4 | 73.3 | 0 | 0.0 | 113.3 |
| 150 | -0.5 | 33.3 | 150 | -0.6 | 73.3 | 150 | -0.8 | 113.3 |
| 300 | 0.3 | 33.3 | 300 | 0.2 | 73.3 | 300 | 0.1 | 113.3 |
| 450 | 0.7 | 33.3 | 450 | 1.0 | 73.3 | 450 | 1.4 | 113.3 |
| 600 | 1.0 | 33.3 | 600 | 1.0 | 73.3 | 600 | 1.6 | 113.3 |
| 750 | 0.6 | 33.3 | 750 | 0.5 | 73.3 | 750 | 0.5 | 113.3 |
| 900 | 0.4 | 33.3 | 900 | 0.5 | 73.3 | 900 | 0.5 | 113.3 |

Note: All data in mm

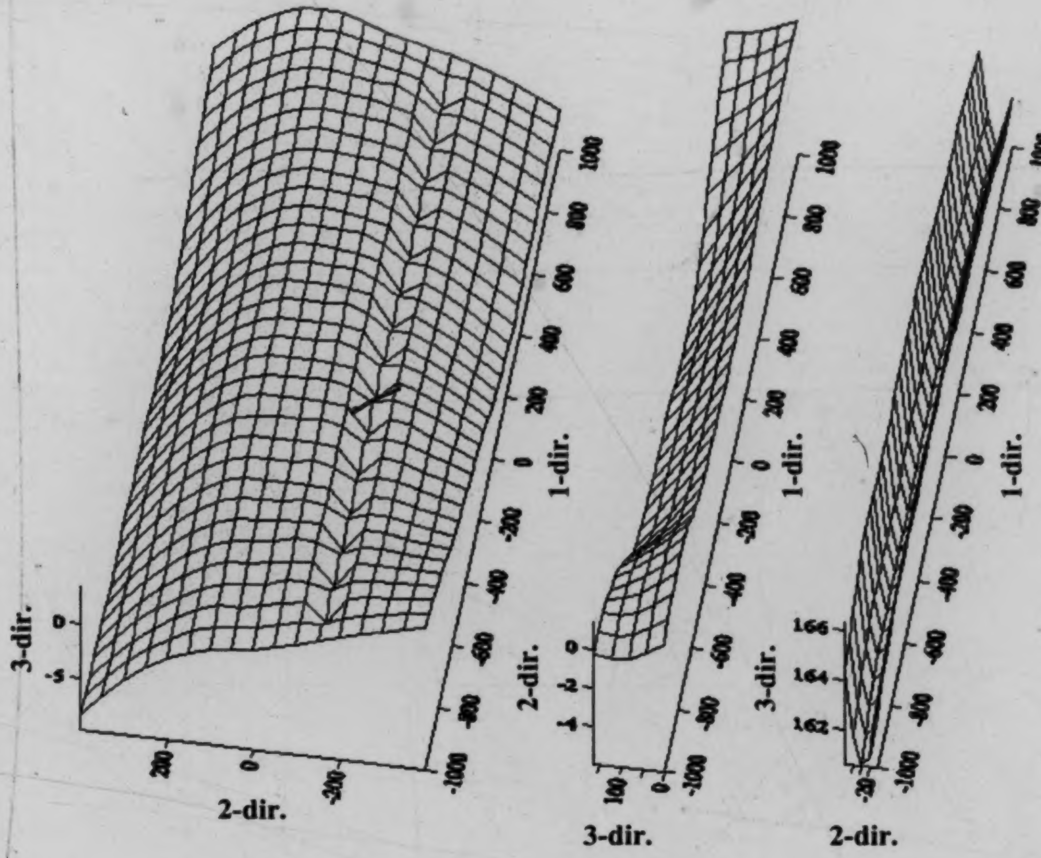

(a) Plate (b) Web (c) Flange

Figure B.1 Measured Initial Imperfections in SSP1

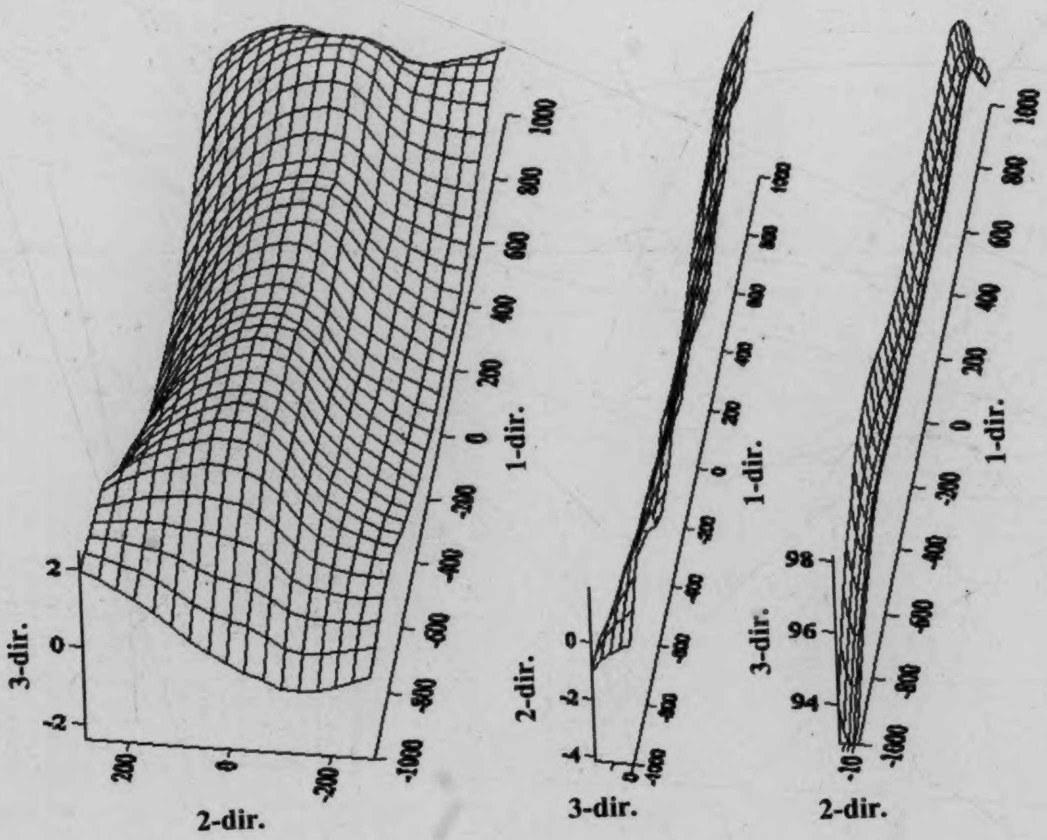

(a) Plate (b) Web (c) Flange

Figure B.2 Measured Initial Imperfections in SSP2

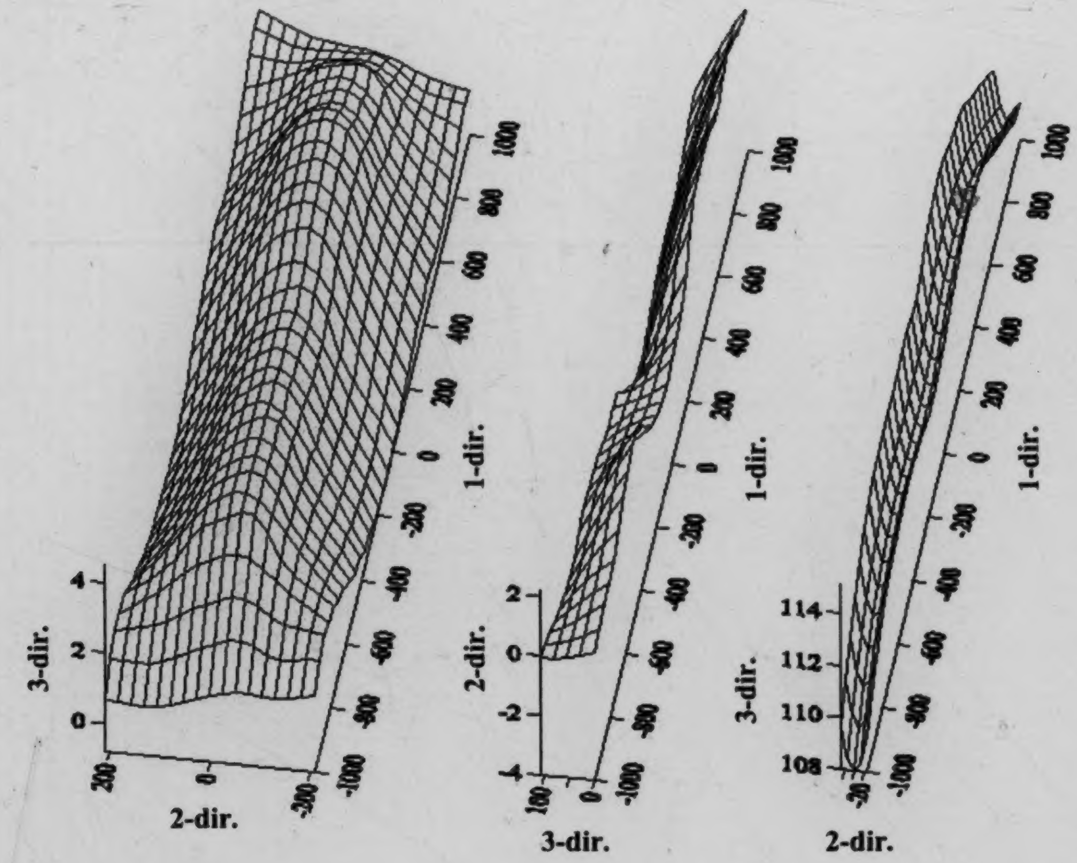

(a) Plate (b) Web (c) Flange

Figure B.3 Measured Initial Imperfections in SSP3

# Appendix C

## Experimental Strain Gauge Results

## Strain Gauge Results

Figure C.1 shows the location of the strain gauges that were used to monitor the strain deformation at the mid-span of the specimens during testing (Chapter 3). There were typically four strain gauges on the flange, two on the web and five on the plate. Only three strain gauges were mounted on the flange of SSP2 because of a sudden enlargement of the weld at the bottom left corner. Plots of axial load versus strain curves for each component of the specimens are shown in Figures C.2 to C.5. Compressive strains are plotted as negative.

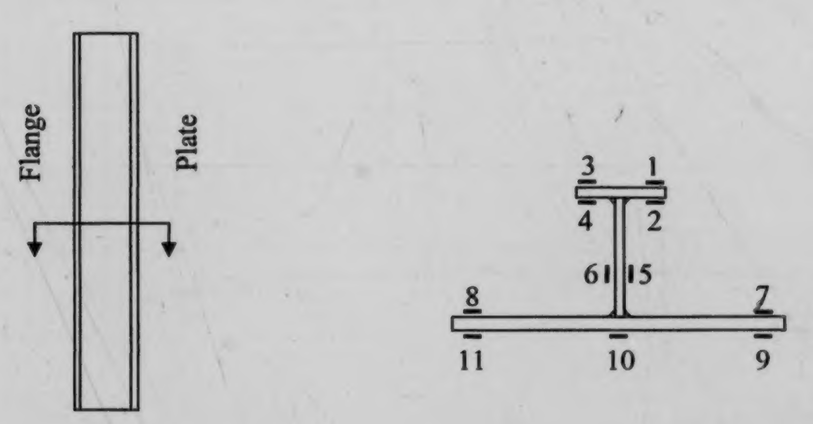

(Side View)

(Cross Section at Mid-span)

Figure C.1 Location of Strain Gauges on Test Specimen at Mid-span

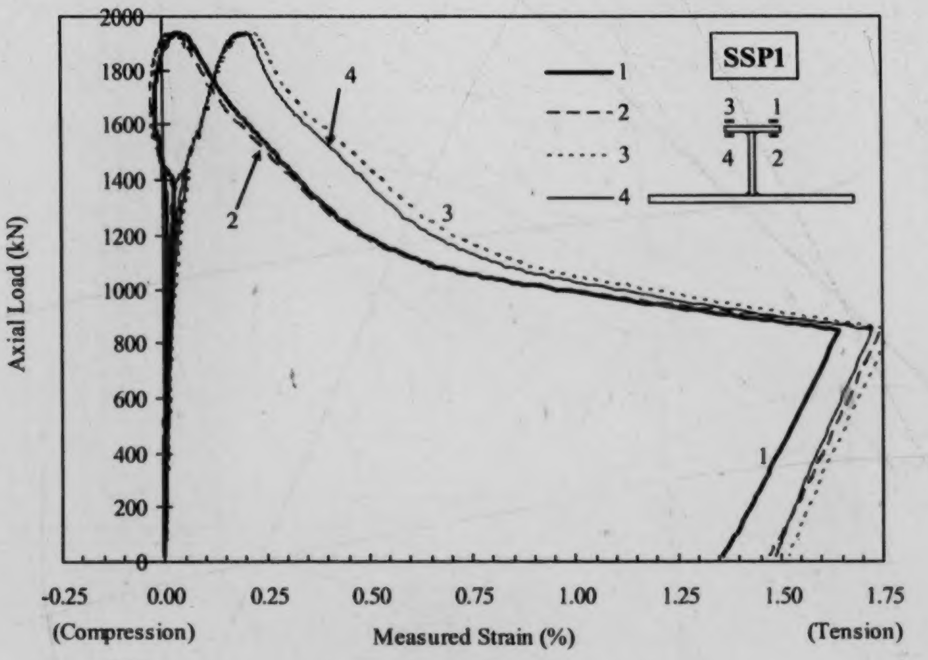

(a) Flange Measurement

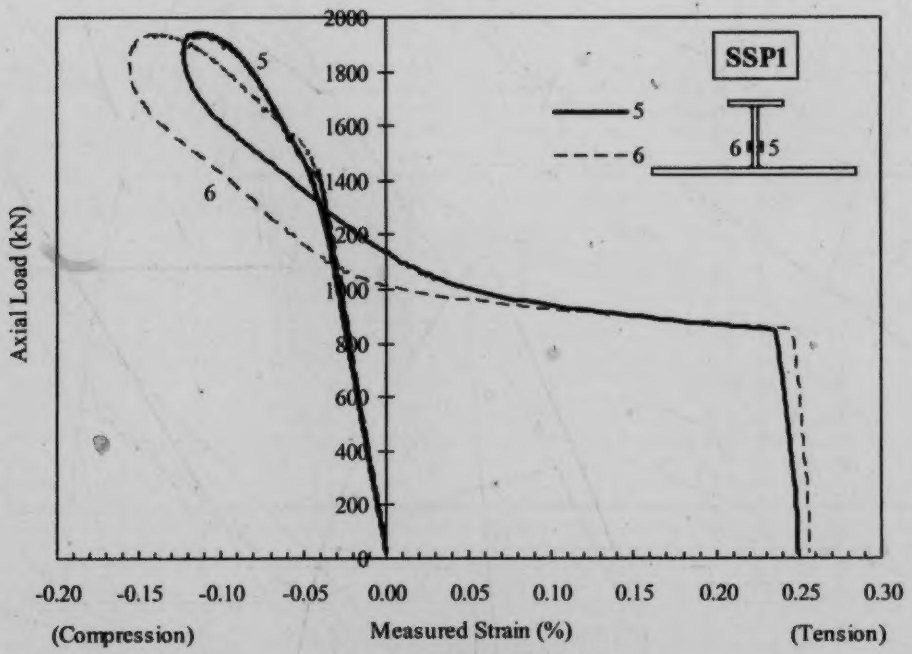

(b) Web Measurement

Figure C.2 Axial Load versus Strain Curve at Mid-span of SSP1

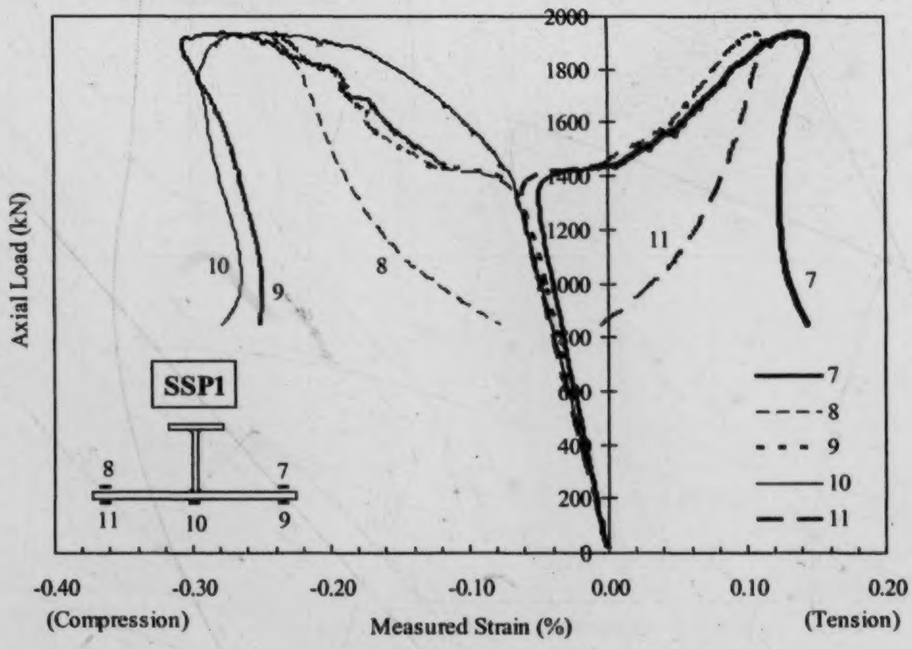

(c) Plate Measurement

Figure C.2 (Cont'd)

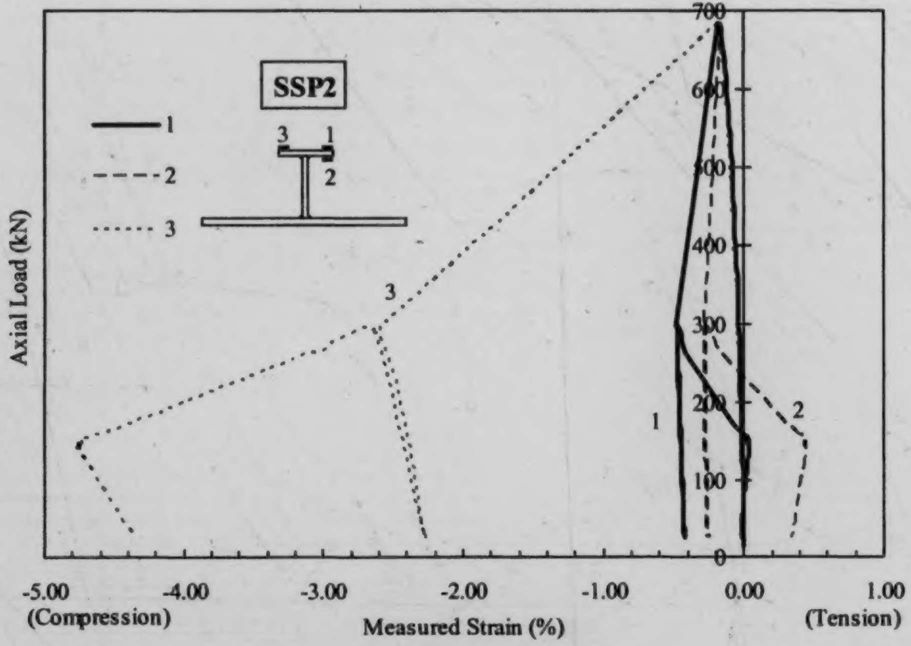

(a) Flange Measurement

Figure C.3 Axial Load versus Strain Curve at Mid-span of SSP2

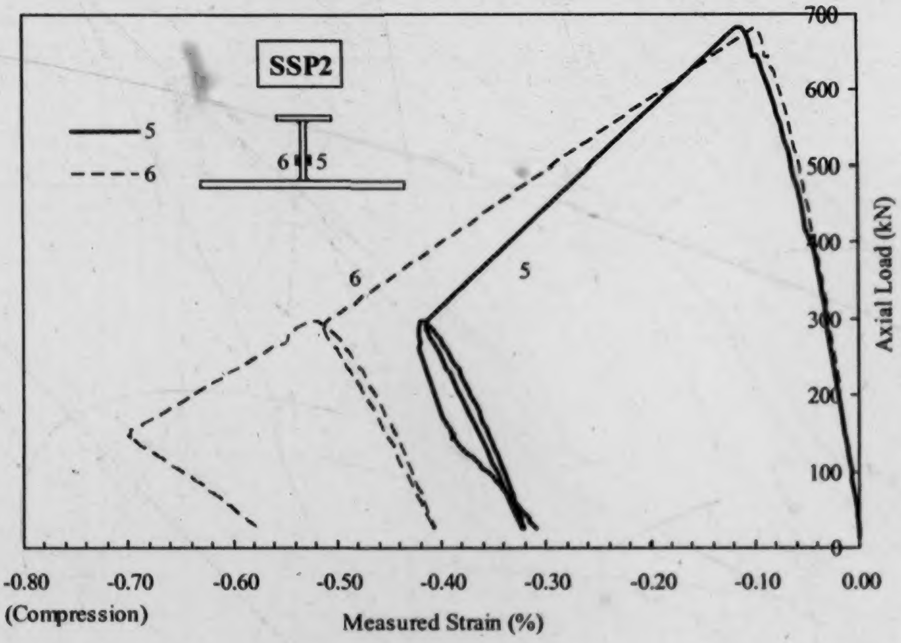

(b) Web Measurement

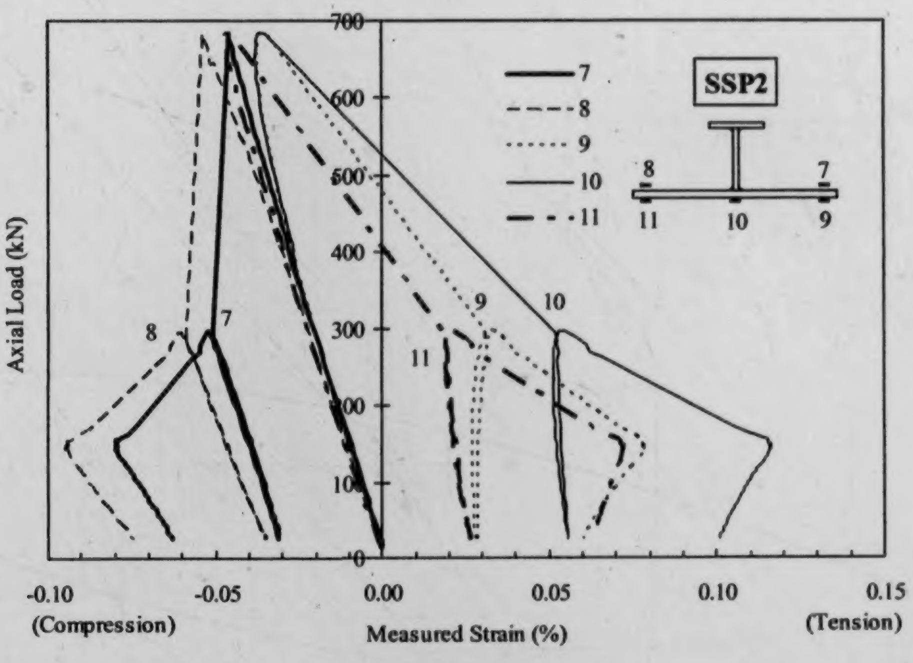

(c) Plate Measurement

Figure C.3 (Cont'd)

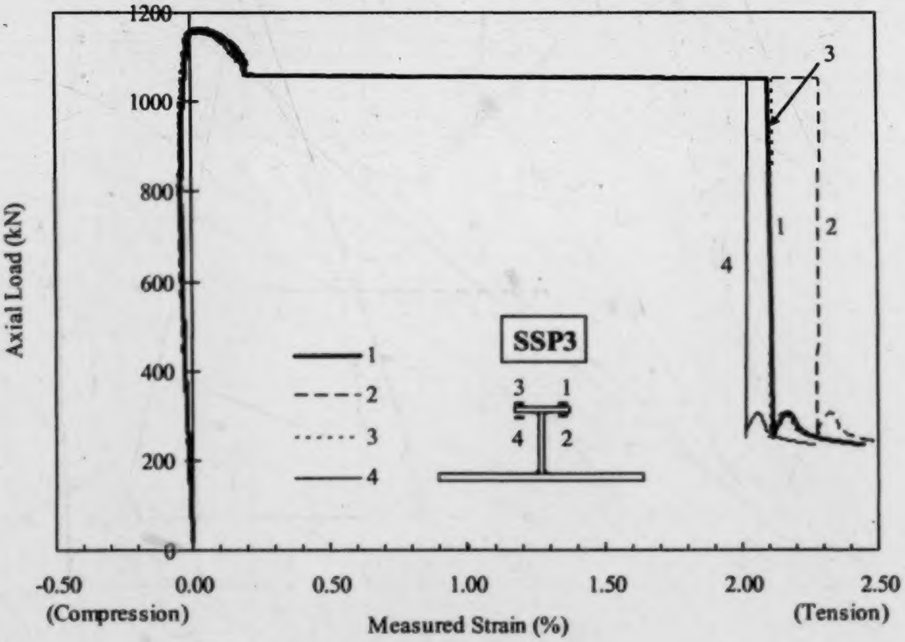

(a) Flange Measurement

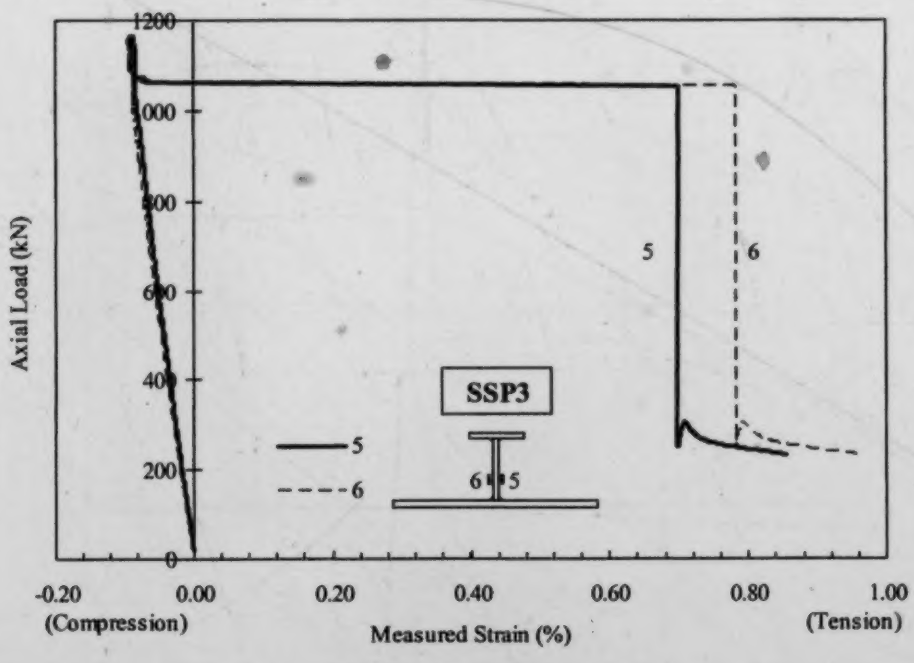

(b) Web Measurement

Figure C.4 Axial Load versus Strain Curve at Mid-span of SSP3

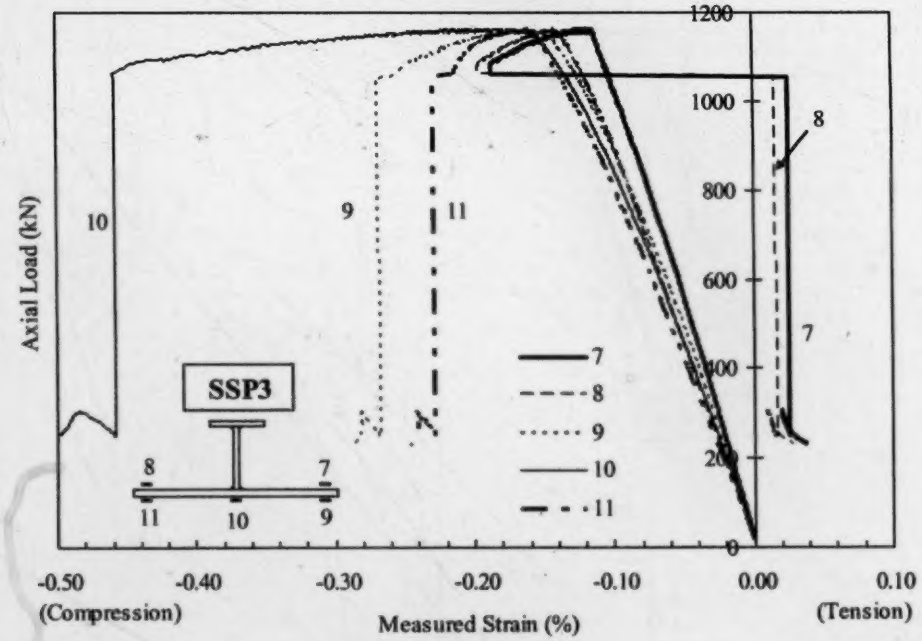

(c) Plate Measurement

Figure C.4 (Cont'd)

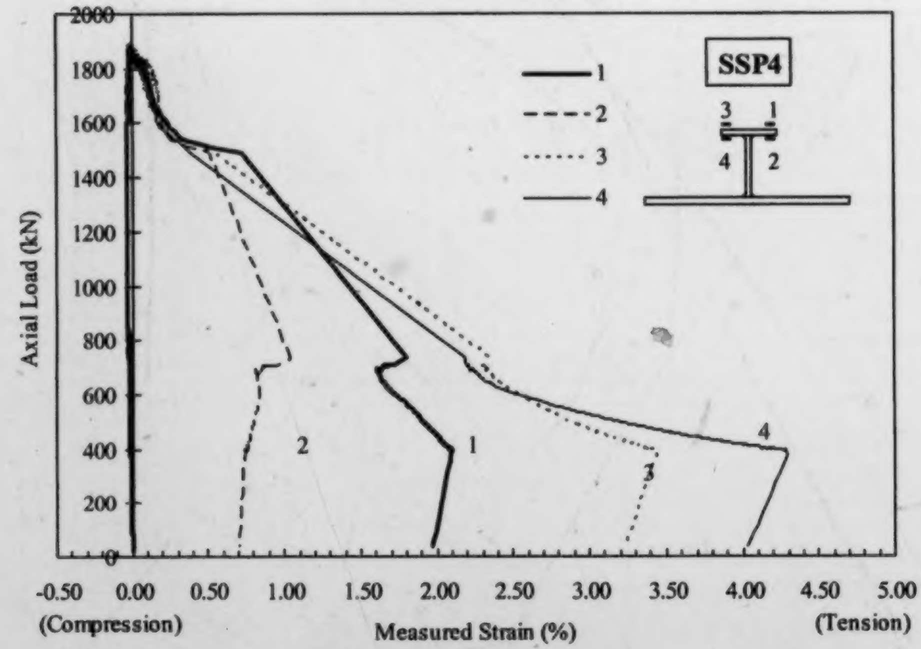

(a) Flange Measurement

Figure C.5 Axial Load versus Strain Curve at Mid-span of SSP4

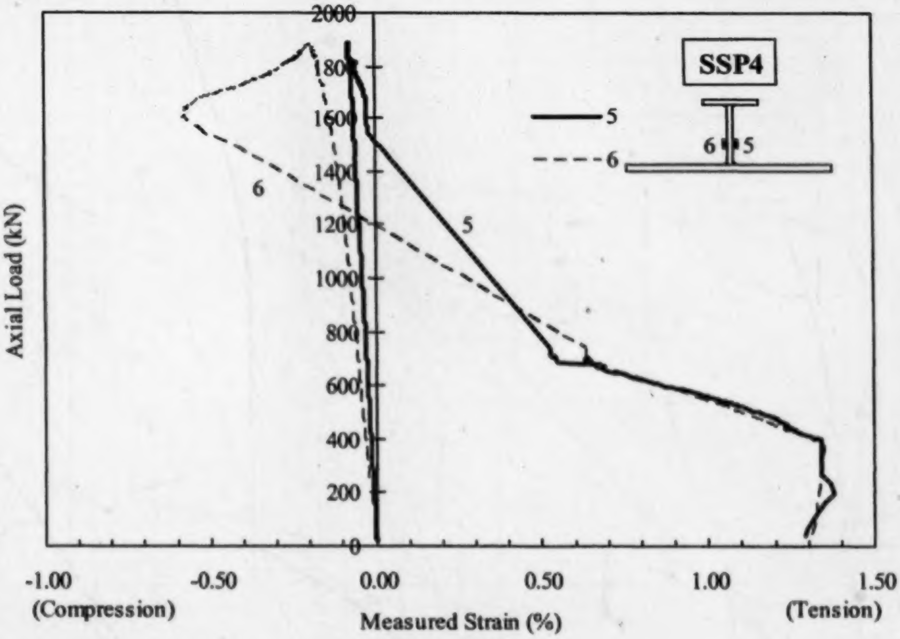

(b) Web Measurement

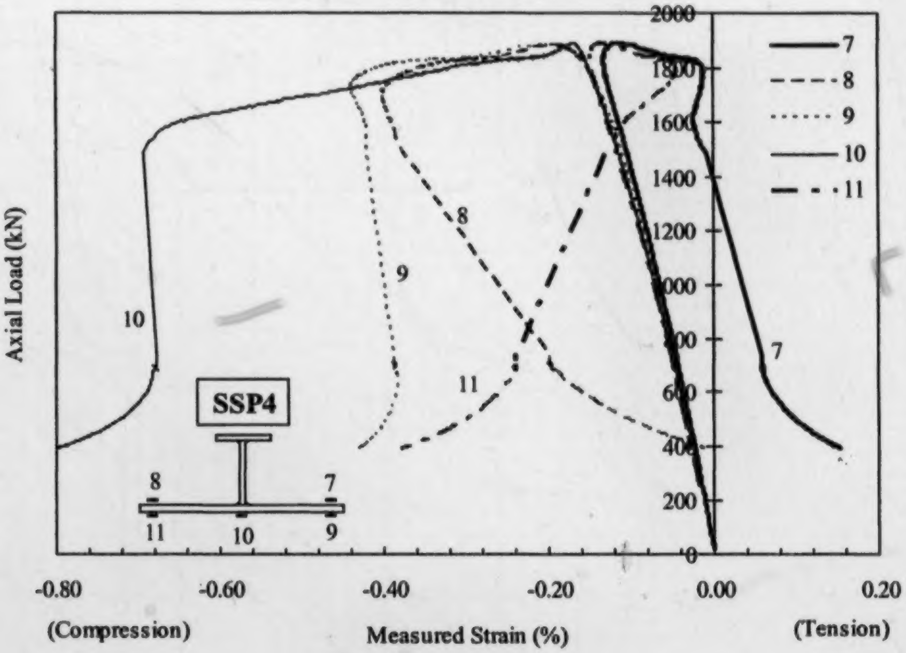

(c) Plate Measurement

Figure C.5 (Cont'd)

# Appendix D

## Measured Displacements

## Measured Displacements by Linear Variable Displacement Transformers (LVDTs)

Figure D.1 shows the location of the LVDTs that were used to monitor the buckling behaviour of the specimens during testing (see Chapter 3). Each LVDT was assigned a number as noted below.

LVDT data for the out-of-plane deformation (3-direction) of the plate are given in Figures D.2 to D.5. Positive readings correspond to deformation ($u_3$) away from the plate for all the specimens.

Although monitored, the in-plane and out-of-plane displacements (LVDTs 11 to 14) of the stiffeners are not reported in this study. Only minimal movements were observed in specimens that failed by interaction buckling mode. Because of the stiffener tripping failure mode, there were more in-plane deflections recorded for SSP2. However, the positions of LVDTs did not coincide with the location of the torsional buckling at the stiffener. Hence, the data collected can not contribute to the true deformation of stiffener tripping.

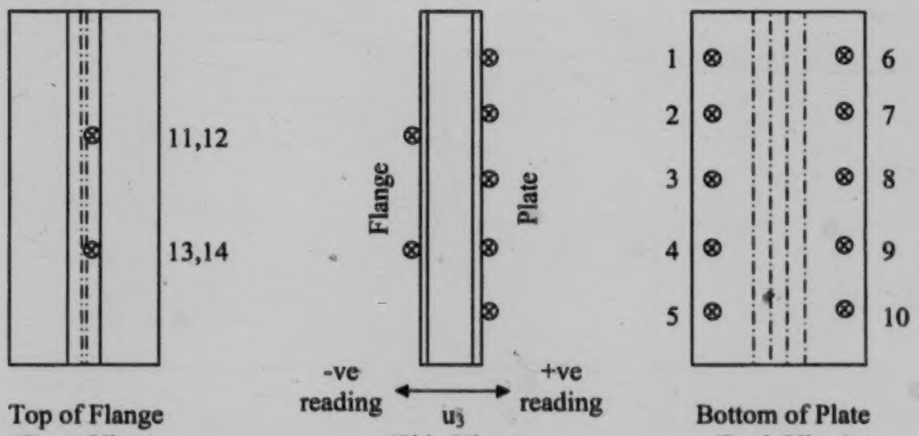

Top of Flange (Front View)

(Side View)

Bottom of Plate (Back View)

Figure D.1 Location of LVDT on Test Specimens

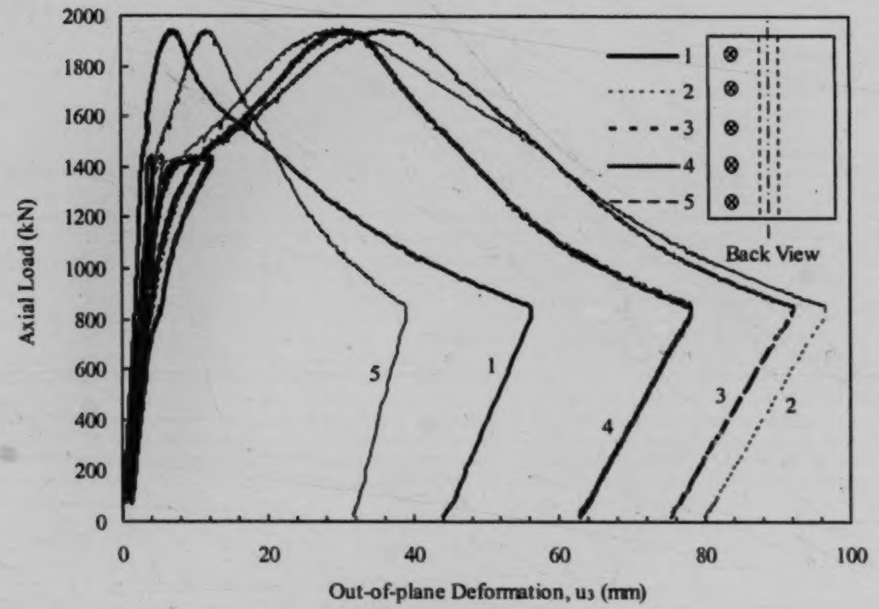

(a) West Side

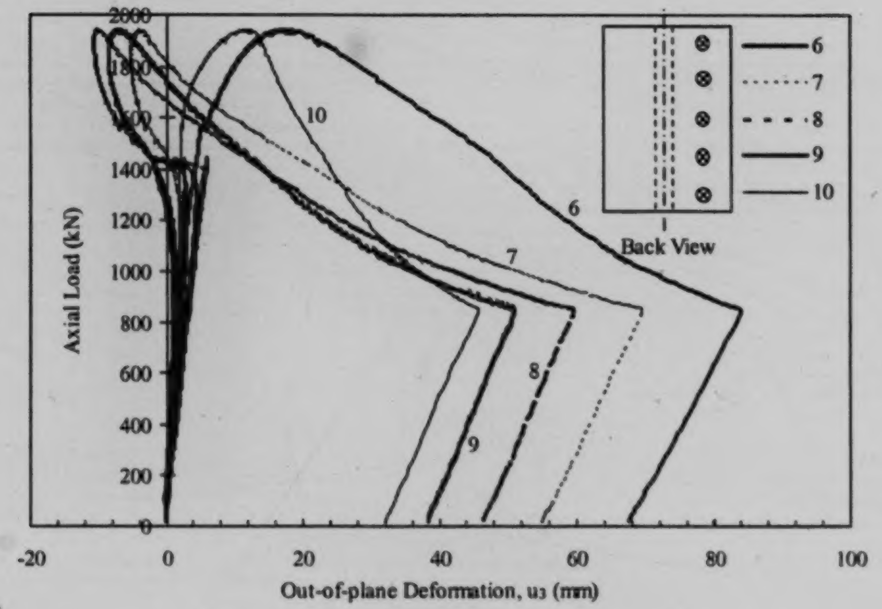

(b) East Side

Figure D.2 Out-of-plane deformations for the plate in SSP1

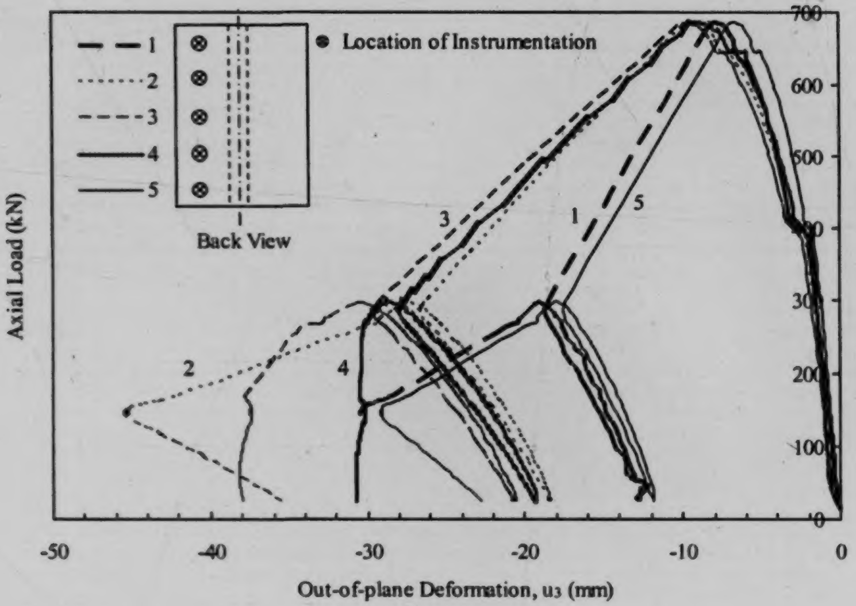

(a) West Side

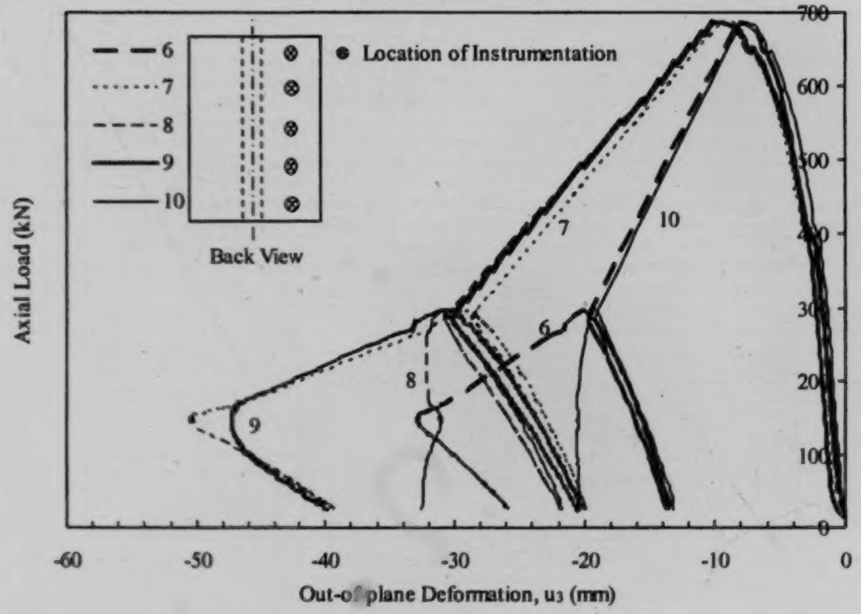

(b) East Side

Figure D.3 Out-of-plane deformations for the plate in SSP2

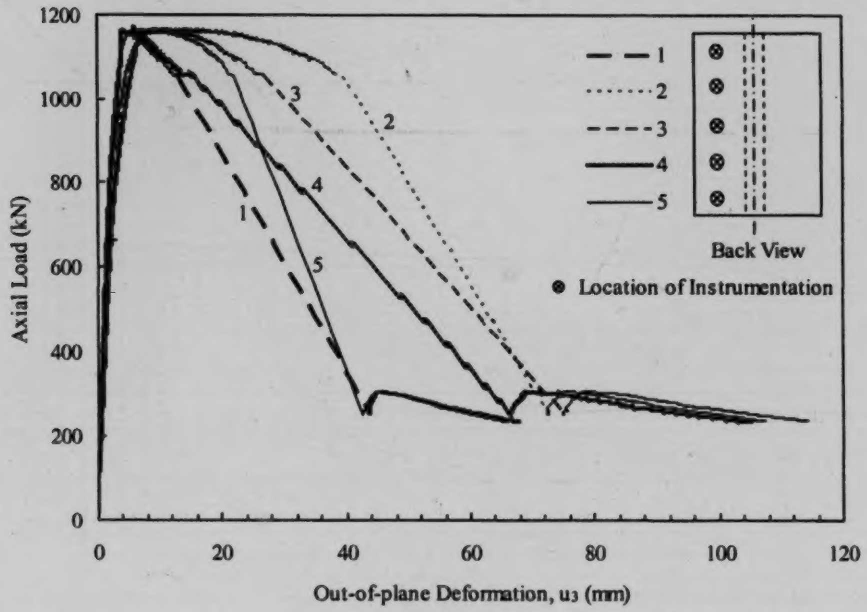

(a) West Side

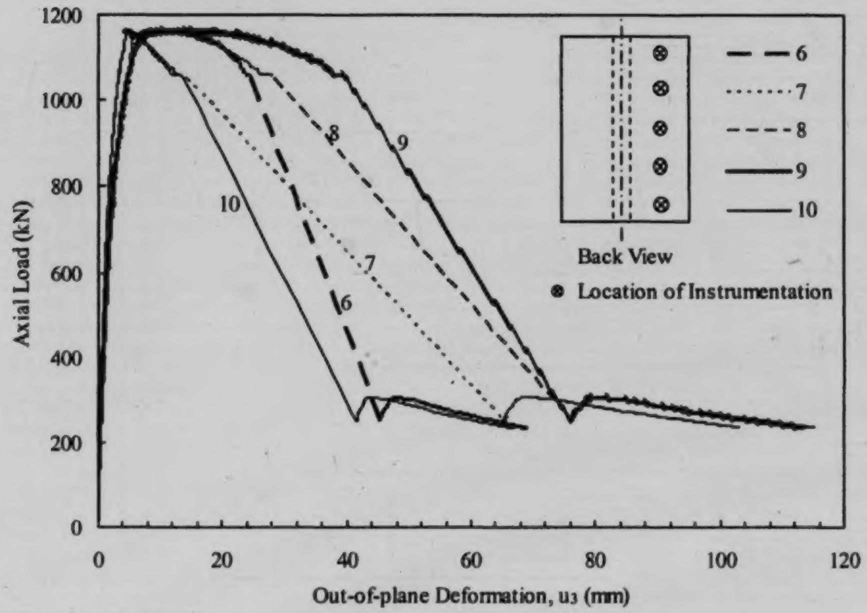

(b) East Side

Figure D.4 Out-of-plane deformations for the plate in SSP3

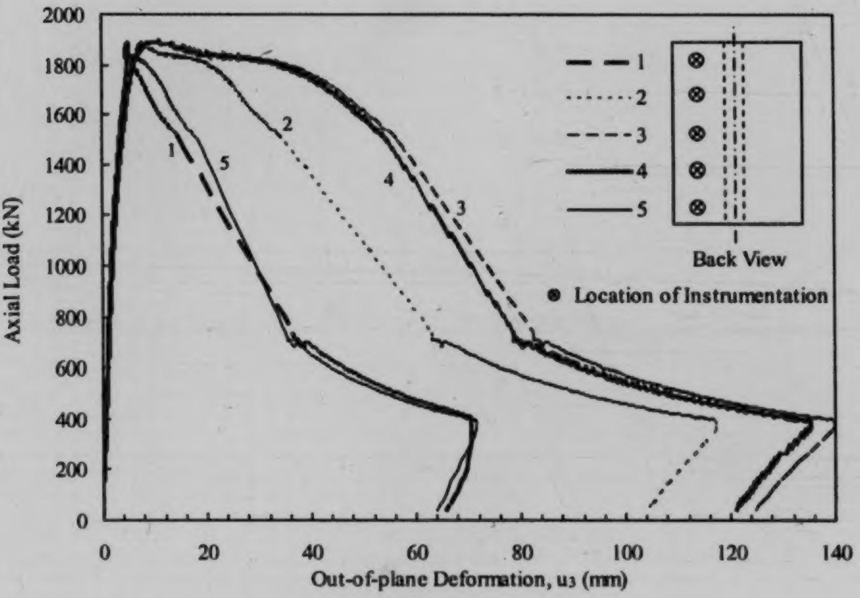

(a) West Side

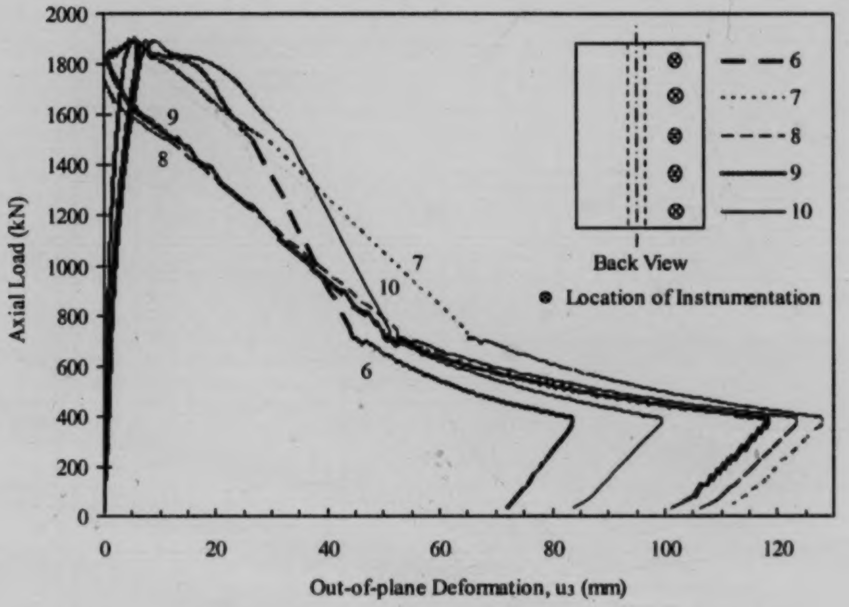

(b) East Side

Figure D.5 Out-of-plane deformations for the plate in SSP4

# Appendix E

## Summary and Recommendations of DNV-RP-C201, October 2002

## Summary and Recommendations of DNV-RP-C201, October 2002

The 2002 edition of DNV recommendations cover the design of panel buckling, stiffener buckling and local buckling of stiffener and girder flanges, webs and brackets for stiffened panels. Although the code deals with stiffened plate panels subjected to axial stress in two directions, shear stress and lateral load, only the section for uniaxial load is present in this study. The equations in Chapter 7 of the design guideline are simplified below to account for the uniaxial stress case only. Because the DNV guide does not consider member of hybrid sections, assumptions are made about the yield strength in the proposed formulas.

For the design of continuous plate with multiple stiffeners, DNV categorizes the calculations into lateral pressure on the plate side and lateral pressure on the stiffener side. Three types of failure modes are considered: plate-induced overall buckling, stiffener-induced overall buckling and stiffener tripping. Interaction buckling is accounted for by using a plate effective width for the calculations of the overall buckling capacity.

### Effective Plate Width

DNV adopts the effective width method to account for the loss of plate strength due to plate buckling under uniaxial compression. In order to account for the above, DNV calculates the effective width from a reduction factor, $C_{xs}$. This factor is determined from a ratio of the reduced plate slenderness, $\bar{\lambda}_p$, as follows:

$$\begin{aligned} C_{xs} &= \frac{\bar{\lambda}_p - 0.22}{\bar{\lambda}_p^2}, \quad if \quad \bar{\lambda}_p > 0.673 \\ &= 1.0, \qquad\qquad if \quad \bar{\lambda}_p \le 0.673 \end{aligned} \qquad \text{where } \bar{\lambda}_p = 0.525\frac{b_p}{t_p}\sqrt{\frac{f_{yp}}{E_p}} \qquad \text{(E-1)}$$

where $b_p$ is the plate width, $t_p$ is the plate thickness, $f_{yp}$ is the yield strength, and $E_p$ is Young's modulus of the plate. The effective plate width, $b_e$, for the stiffened plate is defined as,

$$b_e = C_{xs} b_p \tag{E-2}$$

Therefore, the effective cross-sectional area, $A_e$ becomes:

$$A_e = A_s + b_e t_p \tag{E-3}$$

**Lateral Pressure on the Plate Side**

The buckling capacity of stiffened plates failing by interaction buckling is obtained by conducting an overall buckling analysis on a section made up of a stiffener and an effective plate. The effective width of the stiffened plate is calculated using Equation (E-2) and it is incorporated in the following calculations. DNV proposes the following interaction buckling equation for stiffened plates with lateral pressure on the plate side:

$$\frac{N_{Sd}}{N_{kp,Rd}} + \frac{N_{Sd}\ z^*}{M_{p,Rd}\left(1 - \frac{N_{Sd}}{N_E}\right)} \leq 1.0 \tag{E-4}$$

where

$N_{Sd}$ = design axial load

$N_{kp,Rd}$ = design plate-induced axial buckling resistance

$z^*$ = moment arm

$M_{p,Rd}$ = design bending moment resistance

$N_E$ = effective Euler buckling load

In order to evaluate the prediction from the DNV recommendation, the applied load from the experimental results replaces the design axial load, $N_{Sd}$ in the above equation.

The design plate-induced axial buckling resistance, $N_{kp,Rd}$, is defined as:

$$N_{kp,Rd} = A_e f_k \tag{E-5}$$

where $A_e$ is the effective area and $f_k$ is the inelastic bucking stress which is obtained from the following column curve:

$$f_k = f_{yp} \qquad when\ \bar{\lambda} \le 0.2$$

$$f_k = f_{yp}\left[\frac{1+\mu+\bar{\lambda}^2-\sqrt{\left(1+\mu+\bar{\lambda}^2\right)^2-4\bar{\lambda}^2}}{2\bar{\lambda}^2}\right] \qquad when\ \bar{\lambda} > 0.2 \qquad \text{(E-6)}$$

where the column slenderness parameter, $\bar{\lambda}$ is the square root of the yield strength of the plate, $f_{yp}$ , over the Euler buckling strength, $f_E$.

$$\bar{\lambda} = \sqrt{\frac{f_{yp}}{f_E}} \qquad \text{where} \quad f_E = \frac{\pi^2 E_p I_e}{A_e l^2} \qquad \text{(E-7)}$$

In which, $I_e$ is the moment of inertia of the effective cross-section. It is unclear in the guideline what material properties to use for a built-up hybrid sections. Therefore, to be conservative, it is assumed here that the yield strength and modulus of elasticity of the plate applies, i.e. $f_{yp}$ and $E_p$ for pressure on the plate side.

The geometric coefficient, $\mu$, used in Equation (E-6) is expressed as

$$\mu = \left(0.34 + 0.08\frac{z_p}{i_e}\right)\left(\bar{\lambda} - 0.2\right) \qquad \text{(E-8)}$$

where $i_e$ is the radius of gyration of the effective cross-section and $z_p$ is the distance from the centroid of the effective cross-section to the extreme fibre on the plate side.

In the second term of the interaction buckling equation (Equation E-4), $z^*$ is the distance from the centroid of the effective cross-section to the working point of the axial force, taken as positive towards the plate.

The design bending moment resistance on the plate side of the structural member, $M_{p,Rd}$ is,

$$M_{p,Rd} = \frac{I_e}{z_p} f_{yp} \tag{E-9}$$

The denominator of the second term of Equation (E-4) accounts for the second-order effects due to the axial load acting on a deformed member. It is determined from the effective Euler buckling load,

$$N_E = \frac{\pi^2 E_p I_e}{l^2} = f_E A_e \tag{E-10}$$

**Lateral Pressure on the Stiffener Side**

The calculation for the buckling strength of the plate loaded on the stiffener side is similar to that for the pressure on the plate side. DNV considers both the stiffener-induced overall buckling and stiffener tripping failure modes in this section. The interaction buckling equation proposed for lateral pressure on the stiffener side is:

$$\frac{N_{Sd}}{N_{ks,Rd}} - \frac{N_{Sd}\ z^*}{M_{s2,Rd}\left(1 - \frac{N_{Sd}}{N_E}\right)} \leq 1.0 \tag{E-11}$$

where

$N_{ks,Rd}$ = stiffener induced overall buckling

$M_{s2,Rd}$ = bending moment resistance on the stiffener side

The stiffener induced overall buckling resistance, $N_{ks,Rd}$ is expressed as,

$$N_{ks,Rd} = A_e f_k \tag{E-12}$$

where $f_k$ can be obtained from Equations (E-6) to (E-8) except that $z_t$ is used in Equation (E-8), where $z_t$ is the distance from the centroid of the effective cross-section to the extreme fibre on the stiffener side. Again it is unclear what material properties should be used in the above equation. Since the member is loaded on the stiffener side, the flange is susceptible to much of the load. Thus, the yield strength and modulus of elasticity of the flange, i.e. $f_{yf}$ and $E_f$, are used here.

In order to differentiate between stiffener-induced overall buckling and stiffener tripping, DNV limits the characteristic strength, $f_r$, of the stiffened steel plate based on the value of the reduced torsional slenderness, $\bar{\lambda}_T$, as follows:

*if* $\bar{\lambda}_T \leq 0.6$, $f_r = f_{yf}$, stiffener-induced overall buckling governs.

*if* $\bar{\lambda}_T > 0.6$, $f_r = f_T$, stiffener tripping governs

where

$$\bar{\lambda}_T = \sqrt{\frac{f_{yf}}{f_{ET}}} \qquad \text{(E-13)}$$

The torsional buckling strength, $f_T$, is obtained from a three-part calculation. The guideline first reduces the elastic buckling capacity of simply supported plate to account for yielding. This is used to calculate a coefficient of the amount of support from the plate to the stiffener. The torsional elastic buckling strength, $f_{ET}$, will then be determined from this coefficient, *β*, and the geometry of the stiffener. The value of *β* is depended on the ratio of the applied axial stress over the reduced Euler's buckling capacity. In order to obtain the capacity of the stiffened steel plate, $\beta = 1.0$. Thus,

$$f_{ET} = \frac{A_w + \left(\frac{t_f}{t_w}\right)^2 A_f}{A_w + 3A_f} G \left(\frac{t_w}{h_w}\right)^2 + \frac{\pi^2 E_f I_z}{\left(\frac{A_w}{3} + A_f\right) l_T^2} \qquad \text{(E-14)}$$

where

$t_w$ = thickness of the web

$t_f$ = thickness of the flange

$A_w$ = area of the web

$A_f$ = area of the flange

G = modulus of rigidity of steel = 77 GPa

$l_T$ = $l$, the length of the test specimen since there is no additional tripping brackets providing lateral supports to the stiffener.

$I_z$ = moment of inertia of the stiffeners about the centroidal axis normal to the plane of the plate.

Given the value of $\bar{\lambda}_T$, the final torsional buckling strength can then be calculated from the following expressions:

$$f_T = f_{yf} \qquad when\ \bar{\lambda}_T \le 0.6$$

$$f_T = f_{yf}\left[\frac{1+\mu+\bar{\lambda}_T^2-\sqrt{\left(1+\mu+\bar{\lambda}_T^2\right)^2-4\bar{\lambda}_T^2}}{2\bar{\lambda}_T^2}\right] \qquad when\ \bar{\lambda}_T > 0.6 \qquad \text{(E-15)}$$

where

$$\mu = 0.35\left(\bar{\lambda}_T - 0.6\right) \qquad \text{(E-16)}$$

The bending moment resistance on the stiffener side of the structural member is used in the second term of the Equation (E-11).

$$M_{s2,Rd} = \frac{I_e}{z_t} f_r \qquad \text{(E-17)}$$

In addition, the value of z* is negative because the stiffened plate is loaded on the stiffener side.